Contributions to Classic Control Strategies and Application to Industrial Facilities

Ph.D. in Computer Science

UNIVERSIDAD DE ALMERÍA

Ángeles Hoyo Sánchez

Contributions to Classic Control Strategies and Application to Industrial Facilities

Contribuciones a Estrategias de Control Clásico y Aplicación a Plantas Industriales

A thesis submitted to the Department of Computer Science and
the International PhD School of the University of Almería
for the degree of Doctor of Philosophy in Computer Science (RD 99/11)

Author
Ángeles Hoyo Sánchez

Supervisors
Dr. José Luis Guzmán Sánchez
Dr. José Carlos Moreno Úbeda

Almería, September 2023

A mis padres, Ángeles y Félix,
a mis hermanos, Gregorio e Irene,
y a mis amigos.

———-

To my parents, Ángeles and Félix,
to my siblings, Gregorio and Irene,
and to my friends.

Agradecimientos

En primer lugar, quiero expresar mi agradecimiento a mis directores, José Luis Guzmán y José Carlos Moreno, por vuestra dedicación, paciencia, confianza y motivación. Desde mis primeros años como estudiante de ingeniería, fuisteis una fuente constante de inspiración y despertasteis en mí la pasión por el control automático. Aprecio enormemente vuestro apoyo tanto científico como creativo durante el desarrollo de esta tesis, así como todos vuestros consejos, los cuales guardaré siempre. Me considero afortunada de haber contado con vuestra guía y que hayáis sido un referente para mí durante esta etapa.

Asimismo, quiero expresar mi gratitud hacia todos mis compañeros del Grupo de Investigación de Automática, Robótica y Mecatrónica por su disposición a brindar ayuda y por el ambiente colaborativo que se respira en nuestro equipo. Ha sido un verdadero placer compartir momentos tanto laborales como fuera de la universidad, contar con vuestra compañía y compartir el día a día juntos. Vuestra presencia ha enriquecido mi experiencia y ha contribuido a hacer de este proceso un viaje emocionante y enriquecedor.

Me gustaría también mencionar a algunos de ellos por los recuerdos y experiencias que siempre atesoraré:

A José Luis Guzmán y José Carlos Moreno, gracias de nuevo por vuestro apoyo inquebrantable a lo largo de este recorrido. Vuestra positividad y entusiasmo han sido contagiosos, y estoy agradecida por haberos tenido como referentes durante todos estos años. A Manuel Berenguel y Francisco Rodríguez por todos los trabajos en los que hemos colaborado y por ser grandes referentes para mí. A María del Mar Castilla, Malena Caparroz, Marta Leal y Marina Martínez por formar parte del grupo ARM Women. Sois inspiración, no solo para mí, sino para todas las nuevas generaciones que lleguen a la Universidad. A mis compañeros Juan Diego Gil, Jerónimo Ramos, Enrique Rodríguez y Manolo Muñoz que me disteis la bienvenida con los brazos abiertos cuando comencé esta etapa. A mis compañeros Francisco Mañas y Francisco García, por todos los momentos compartidos en la estancia en Lund. A mis compañeros de despacho, Igor Mendes y Fernando Cañadas, por hacer de esta última etapa de rutina la más divertida de

todos estos años. A Pablo Otálora, José González, Rubén González y Juan Miguel Serrano, por todos esos momentos compartidos dentro y sobre todo, fuera de la Universidad. A Jorge Sánchez, José Luis Torres, José Domingo Álvarez, José Luis Blanco y Antonio Giménez por las actividades en las que hemos colaborado estos años. Me siento afortunada de haber coincidido con vosotros y estoy agradecida por las relaciones que hemos creado. Cada uno de vosotros habéis desempeñado un papel importante en este camino, y siempre llevaré estos recuerdos dentro de mí.

Tampoco puedo olvidar al Departamento de Automática y Control de la Universidad de Lund (Suecia), que me acogió durante tres meses como estudiante doctoral. Especialmente, quisiera dar las gracias al profesor Tore Hägglund, por guiarme durante la estancia. Tus observaciones, ideas y colaboraciones en esta tesis y tu hospitalidad en Lund han tenido y tendrán un gran impacto en mi carrera. Me siento afortunada de haber compartido esos tres meses contigo trabajando juntos y compartiendo Fikas. Igualmente, he de agradecer a todos los compañeros que conocí en el departamento, que me enseñaron qué era el Innebandy e hicieron de la estancia una experiencia que no olvidaré.

Finalmente, quisiera dar las gracias a mis amigos, que son como hermanos, y a mi familia, por permitirme disfrutar de su compañía en todo este tiempo; especialmente a mi madre Ángeles, mis hermanos Gregorio e Irene y mi padre Félix. Sois quienes realmente habéis estado cerca de mí todos estos años, apoyándome desinteresadamente. Me habéis animado en los momentos más duros y compartido los de mayor felicidad. Todo esto habría sido imposible sin vosotros. Gracias de corazón por todos los momentos compartidos.

Muchas gracias a todos,
Ángeles

Acknowledgements

First and foremost, I would like to express my gratitude to my supervisors, José Luis Guzmán and José Carlos Moreno, for their dedication, patience, trust, and motivation. Since my early years as an engineering student, you have been a constant source of inspiration, incentivizing my passion for automatic control. I especially appreciate your scientific and creative support throughout the development of this thesis, as well as all your valuable advice, which I will cherish forever. I consider myself lucky to have had your advice and to have you as a role model in this phase of my life. Likewise, I would like to thank all my Automatic, Robotics, and Mechatronics Research Group colleagues for your continued willingness to help and for the collaborative atmosphere that our team has. It has been a true pleasure to share work-related and non-academic moments. Your presence has enriched my journey and made this process exciting and fulfilling.

I would also like to mention some individuals for the memories and experiences that I will always cherish:

To José Luis Guzmán and José Carlos Moreno, thank you for your unwavering support throughout this journey. Your positivity and enthusiasm have been contagious. I am grateful to have had you as my mentors all these years. To Manuel Berenguel and Francisco Rodríguez for our collaborative work and for being great role models to me. To María del Mar Castilla, Malena Caparroz, Marta Leal and Marina Martínez, for being part of the ARM Women group. You are an inspiration, not only to me but to all the new generations entering the university. To my colleagues Juan Diego Gil, Jerónimo Ramos, Enrique Rodríguez, and Manolo Muñoz, that welcomed me when I first started this journey with open arms. To my colleagues Francisco Mañas and Francisco Garía, for all the shared moments during our stay in Lund. To my office mates, Igor Mendes and Fernando Cañadas, for making this last routine stage the most enjoyable of all these years. To Pablo Otálora, José González, Rubén González, and Juan Miguel Serrano, for all the shared moments inside and outside the university. To Jorge Sánchez, José Luis Torres, José Domingo Álvarez, José Luis Blanco, and Antonio Giménez, For all the collaboration we have worked on throughout the years. I consider myself blessed to have crossed paths with such

incredible individuals, and I am grateful for the relationships we have built. Each of you has played an essential role in this journey, and I will always carry these memories with me.

I also want to give a special mention to the Department of Automatic Control at Lund University (Sweden), which welcomed me as a doctoral student for three months. Especially, I want to thank Professor Tore Hägglund for guiding me throughout my stay. Your observations, ideas and collaborations on this thesis, and your hospitality in Lund have had and will continue to have a great impact on my career. I feel fortunate to have spent those three months working with you and sharing Fika's moments. Likewise, I must express my gratitude to all the colleagues I met at the department, who introduced me to Innebandy and made the stay an unforgettable experience.

Finally, I would like to thank my friends, who are like siblings to me, and to my family, for allowing me to enjoy their company all this time. I would especially like to thank my mother, Ángeles, my siblings, Gregorio and Irene, and my father, Félix. You have been truly by my side all these years, supporting me selflessly, encouraging me during the most challenging moments, and sharing the happiest ones. All of this would not have been possible without you. A heartfelt thanks for all the shared moments.

Thank you very much to all of you,
Ángeles

Resumen

Durante décadas, las técnicas clásicas de control se han utilizado ampliamente en diversas industrias para garantizar el funcionamiento estable y eficiente de sistemas dinámicos. Estas técnicas, que son el fundamento de la teoría de control, desempeñan un papel vital en el funcionamiento de numerosos procesos y sistemas. Se basan en modelos matemáticos que describen la dinámica del sistema y buscan manipular las variables de entrada para controlar su comportamiento. Operan según los principios del control por retroalimentación, monitoreando continuamente la salida del sistema y comparándola con un valor de referencia deseado. Cualquier desviación entre las salidas reales y deseadas desencadena ajustes en la acción de control, llevando el sistema de vuelta a su estado deseado. Estas técnicas clásicas de control a menudo se basan en algoritmos bien establecidos, como el control Proporcional, Integral y Derivativo (PID), que sigue siendo uno de los métodos más ampliamente utilizados en la industria. El control PID logra un equilibrio entre estabilidad, capacidad de respuesta y precisión en estado estacionario, lo que lo hace adecuado para una amplia gama de aplicaciones.

En el campo del control automático, los procesos industriales plantean desafíos únicos debido a su inherente complejidad. Los sistemas que se encuentran en plantas de fabricación, procesos químicos, redes eléctricas y redes de transporte exhiben interacciones intrincadas, no linealidades, incertidumbres y dinámicas variables en el tiempo. Estas complejidades surgen de varios factores. En primer lugar, la escala misma de estos sistemas presenta dificultades en el modelado, análisis y diseño del control. Por otro lado, los procesos industriales a menudo involucran numerosos componentes interconectados, subsistemas y variables, lo que dificulta capturar con precisión su dinámica. Además, estos sistemas operan en tiempo real, lo que requiere respuestas de control rápidas y precisas ante cambios en las condiciones de operación y ante la aparición de perturbaciones.

La estructura de control típica en la industria se basa en un control jerárquico, teniendo un control óptimo de alto nivel, y un control de bajo nivel basado en estrategias clásicas de control. Actualmente, la mayoría de las contribuciones de control automático en investigación tienden a derivar a resultados teóricos y enfocados a estrategias de control basadas en nuevas

Resumen

tecnologías, como *Machine Learning* o *Deep Learning*. Sin embargo, las clásicas son las más afianzadas en la industria y, debido a esta tendencia en la investigación, durante los últimos años se han ido reduciendo paulatinamente las contribuciones que estudian y mejoran estas estrategias clásicas, dando por hecho que está todo resuelto y bien establecido. Sin embargo, existen todavía muchos problemas por resolver y mejoras que proponer en las estrategias de control clásicas y que son fundamentales para que los objetivos definidos por las capas más altas puedan llevarse a cabo de forma satisfactoria. Es aquí donde surge la motivación del desarrollo de esta tesis. Por un lado, aportar contribuciones a las estrategias de control clásicas basadas en PID, rechazo a perturbaciones con el control por adelanto o el control en cascada. Por otro lado, con el fin de demostrar estas estrategias en el sector industrial, se propone la aplicación de algunas de ellas para resolver el problema de control de diferentes procesos industriales.

Esta tesis aporta varias contribuciones a las estrategias de control clásicas basadas en control PID, rechazo de perturbaciones con control por adelanto y control en cascada. Adicionalmente, con el fin de demostrar estas estrategias en el sector industrial, se propone su aplicación para el control de las variables más importantes en diferentes procesos industriales.

En primer lugar, se proponen diferentes contribuciones a las estrategias de control clásicas. De este modo, se han estudiado sistemas con incertidumbre en el modelo y sometidos a perturbaciones, para los que se diseña un controlador robusto basado en una estructura de control clásica. La principal aportación ha consistido en modificar los límites originales de la metodología Quantitative Feedback Theory (QFT) para el problema de regulación en un esquema de control por adelanto y diseñar un controlador PI robusto que tenga en cuenta esas incertidumbres. Se demuestra en simulación cómo mejora el rendimiento del controlador en el rechazo a las perturbaciones del sistema. También se ha estudiado el efecto de las perturbaciones medibles en un control en cascada clásico. Se ha realizado un análisis sobre cómo implementar el control por adelanto junto con el cascada basado en lo que dicta la literatura. Basándose en ese estudio, se ha propuesto una solución compuesta por dos controladores por adelanto estáticos que en paralelo aplicados tanto al lazo externo como al interno que mejora el rendimiento del sistema, tanto en términos de su salida como de la señal de control. Se demuestra su viabilidad con múltiples ejemplos en simulación. Por último, se ha estudiado en detalle el problema de saturación en el rechazo a perturbaciones medibles mediante un control por adelanto clásico. En este sentido, se aporta una regla de sintonía sencilla de la ganancia del controlador por adelanto que permite modificarla cuando el sistema entra en saturación. Con este cambio el rechazo a la perturbación se realiza de forma más rápida mejorando el rendimiento a la salida del sistema. Se demuestra su validación mediante la aplicación a múltiples sistemas en simulación y además, se implementa de forma satisfactoria en una plataforma de control de temperatura.

En segundo lugar, se han utilizado varias plantas experimentales para evaluar las aplicaciones y estrategias de control desarrolladas. Tres contribuciones han sido desarrolladas para el control y simulación de las variables más importantes en el crecimiento de las microalgas en un reactor *raceway* a escala industrial, haciendo uso de la planta industrial ubicada en las instalaciones del Instituto Andaluz de Investigación y Formación Agraria y Pesquera (IFAPA), cerca de la Universidad de Almería. Concretamente se ha desarrollado una herramienta para simular la producción de microalgas en fotobiorreactores industriales de tipo *raceway*. En ella se pueden modificar múltiples factores del modelo para simular diferentes escenarios. Por ejemplo, la cepa, el diseño físico del reactor, la estación del año en la que simula el modelo o la estrategia de control que se desea implementar. También se ha resuelto el problema de control de pH haciendo

uso de distintas estrategias de control, concretamente un controlador predictivo y un controlador robusto basado en QFT. Este último se ha implementado en la planta capturando la gran incertidumbre del modelo de crecimiento, obteniendo resultados satisfactorios. Por otro lado, se ha implementado con éxito un controlador robusto combinado con la técnica de linealización mediante retroalimentación para el control de temperatura de un invernadero. Un invernadero situado en la Estación Experimental "Las Palmerillas" de Fundación Cajamar (El Ejido, Almería) ha servido como planta de ensayo para la implementación del controlador propuesto, obteniendo resultados satisfactorios.

Las reflexiones finales de esta tesis concluyen que, si bien las técnicas avanzadas de control y los enfoques de aprendizaje automático están ganando popularidad en el control industrial, las estrategias clásicas de control siguen siendo esenciales y continúan siendo utilizadas ampliamente en instalaciones industriales complejas. Estas estrategias proporcionan una base sólida para el diseño, operación y mantenimiento de sistemas de control, asegurando un rendimiento estable y eficiente en entornos industriales complejos, y como se demuestra en esta tesis, aún siguen teniendo margen de mejora.

Palabras clave: PID, control por adelanto, control en cascada, linealización por realimentación, control predictivo lineal, teoría de la realimentación cuantitativa, anti-windup, invernadero, reactor raceway de microalgas, TCLab.

Abstract

For decades, classic control techniques have been extensively employed across process industry to ensure the stable and efficient operation of dynamic systems. These conventional control methods, which serve as the basis of control theory, have played a vital role performing numerous processes and systems. These techniques rely on mathematical models that describe the dynamics of the system and aim to manipulate input variables to control its behavior. They operate on the principles of feedback control, continuously monitoring the system's output and comparing it to a desired reference value. Any deviation between the actual and desired outputs triggers adjustments in the control action, bringing the system back to its desired state. Classic control techniques often rely on well-established algorithms, such as Proportional, Integral, and Derivative (PID) control, which remains one of the most widely used methods in the industry. PID control strikes a balance between stability, responsiveness, and steady-state accuracy, making it suitable for a wide range of applications.

In the field of automatic control, industrial processes have unique challenges due to their inherent complexity. Systems found in manufacturing plants, chemical processes, power grids, and transportation networks exhibit intricate interactions, nonlinearities, uncertainties, and time-varying dynamics. These complexities stem from various factors. Firstly, the large scale of these systems presents difficulties in modeling, analysis, and control design. Moreover, industrial processes often involve numerous interconnected components, subsystems, and variables, making it challenging to accurately capture their dynamics. Additionally, these systems operate in real-time, necessitating prompt and accurate control responses to changing operating conditions in the presence of disturbances.

The typical control structure in the industry is based on hierarchical control, with high-level optimal control layers based on economic or safety objectives and low-level control layers based on classical control strategies. Currently, most automatic control research contributions focus on theoretical results and control strategies based on new technologies such as Machine Learning or Deep Learning. However, classical control strategies are the most established in the industry, and due to this research trend, there has been a gradual reduction in contributions that

study and improve these classical strategies, assuming that all the research is already done and well-established. Nevertheless, there are still many open problems to solve and improvements to propose in classical control strategies, which are essential for achieving objectives defined by higher-level layers. These are the reasons that have motivated the development of this thesis.

This thesis provides various contributions to classical control strategies based on PID control, disturbance rejection with feedforward control, and cascade control. Additionally, in order to demonstrate these strategies in the industrial sector, their application to solve the control problem in different industrial processes is proposed.

Firstly, different contributions to classical control strategies are proposed. Systems with model uncertainties and subjected to disturbances have been studied, for which a robust controller based on a classical feedforward control structure has been designed. The main contribution lies in modifying the original limits of the Quantitative Feedback Theory (QFT) methodology for the regulation problem with feedforward control and designing a robust PI controller that considers the uncertainties. Simulation results demonstrate an improved controller performance in rejecting system disturbances. The effect of measurable disturbances on classical cascade control has also been studied. Based on literature guidelines, an analysis has been conducted on how to implement feedforward control together with cascade control. From this study, a solution composed of two static feedforward controllers applied in parallel to both the outer and inner loops has been proposed, improving the system's output and control signal performance. Its feasibility has been demonstrated through multiple simulation examples. Lastly, the saturation problem in rejecting measurable disturbances using classical feedforward control has been examined in detail. A simple tuning rule for the feedforward controller gain has been provided, allowing for modification when the system becomes saturated. This modification enables faster disturbance rejection, improving the system's output performance. Its validation has been demonstrated through the application of multiple systems in simulation, and it has also been successfully implemented in a temperature control platform.

Secondly, several control applications and strategies, including one developed in this thesis, have been tested in various experimental plants. Firstly, three contributions have been developed for modeling and controlling the most important variables in microalgae growth. An industrial-scale raceway reactor located at the Instituto Andaluz de Investigación y Formación Agraria y Pesquera (IFAPA) facilities close to the University of Almería has been used as an industrial plant. Specifically, a tool has been developed to simulate the production of microalgae in industrial-scale raceway photobioreactors. Multiple factors of the model can be modified to simulate different scenarios, such as the strain, physical design of the reactor, time of year for the simulation, or the desired control strategy. The pH control of the microalgae growth has also been addressed using different control strategies, specifically a linear predictive controller and a robust controller based on QFT. The latter has been implemented in the real plant, capturing the significant uncertainty in the process model and achieving satisfactory results. Furthermore, a robust controller combined with a feedback linearization technique has been successfully implemented for a greenhouse temperature control. The greenhouse located at the experimental center "Las Palmerillas" Cajamar Foundation (El Ejido, Almería) has served as the testing plant for the proposed controller, yielding satisfactory results.

The final reflections of this thesis conclude that while advanced control techniques and artificial intelligence approaches are gaining popularity nowadays, classic control strategies

remain essential and continue to be widely used in complex industrial facilities. They provide a solid foundation for control system design, operation, and maintenance, ensuring stable and efficient performance in challenging industrial environments. In this thesis, it is demonstrated that there are still many open research problems around classic control techniques.

Keywords: PID, feedforward, cascade control, feedback linearization, model predictive control, quantitative feedback theory, anti-windup, greenhouse, microalgae raceway reactor, TCLab.

Contents

Contents

List of Figures

List of Tables

Acronyms

Acronym	Description
ARM	Automática, Robótica y Mecatrónica
AW	Anti-windup
CARIMA	Controlled AutoRegresive Integrated Moving Average
CC	Cascade Control
FF	FeedForward
FL	Feedback Linearization
FOPDT	First Order Plus Dead Time
IAE	Integral Absolute Error
IFAC	International Federation of Automatic Control
IFAPA	Instituto Andaluz de Investigación y Formación Agraria y Pesquera
GPC	Generalized Predictive Control
GUI	Graphical User Interface
JCR	Journal Citation Reports
MIMO	Multiple Inputs Multiple Outputs
MPC	Model Predictive Control
NLP	Non Linear Programming
NP	Nichols Plane
PAR	Photosynthetically Active Radiation
PhD	Doctor of Philosophy
PID	Proportional Integral Derivative
QFT	Quantitative Feedback Theory
SCADA	Supervisory Control and Data Acquisition

Acronyms

SCI	Sum of Control Increments
SISO	Single Input Single Output
STEM	Science, Technology, Engineering and Mathematics
TCLab	APMonitor Temperature Control Lab

Nomenclature

Symbols	Description
A	Reactor surface (m^2)
A_s	Surfac in contact with the environment in the TCLab
α, β, φ	Tunning parameters
$\alpha_{h,i}$	Factor relating the current passing through transistor i to the heat produced
b_s, c_s	Set-point weights
c_p	Specific heat capacity
C	Controller transfer function
$C_{a,s}$	Soil surface area (m^2)
C_{aoc}	Greenhouses air's short wave absorption coefficient (-)
C_b	Biomass concentration $(g\,L^{-1})$
C_{cn-cv}	Conduction and convection in the cover heat coefficient $(W m^{-2} K^{-1})$
C_{cv}	Greenhouse air-soil surface convection coefficient $(W m^{-2} K^{-1})$
$C_{d,a}$	Air density $(Kg m^{-3})$
C_{et}	Evapotranspiration constant $(J kg^{-1})$
C_f	Conversion factor $(J kg^{-1} \mathrm{K}^{-1})$
C_g	Gravity constant $(m s^{-2})$
C_p	Specific heat capacity of the culture $(J kg^{-1o}C^{-1})$
$C_{sh,a}$	Air specific heat $(J kg^{-1} \mathrm{K}^{-1})$
$C_{v,d}$	Ventilation discharge coefficient (-)
$C_{v,l-l}$	Length of lateral vents (m)
$C_{v,l-r}$	Length of roof vents (m)
$C_{v,s}$	Air volume inside the greenhouse (m^3)

Nomenclature

Symbols	Description
$C_{v,w-l}$	Width of lateral vents (m)
$C_{v,w-r}$	Width of roof vents (m)
$C_{ven,h}$	Ventilation effective height (m)
$C_{ven,w}$	Ventilation wind effect coefficient (-)
$[CO_2^*]$	Equilibrium concentration with gas phase for carbon dioxide $(mol\ m^{-3})$
$[C_T]$	Total inorganic carbon concentration $(mol\ m^{-3})$
$[C_T]_m$	Total inorganic carbon in the medium $(mol\ m^{-3})$
d	Disturbance
DO	Dissolved Oxygen $(\%)$
δ	Weighting factor for future tracking errors
δ_{di}	Disturbance rejection at the plant input limit specification in QFT
δ_{do}	Disturbance rejection at the plant output limit specification in QFT
Δ	$(1 - z^{-1}$, or plant increment $\Delta P)$
$e,\ e(t)$	Error variable $e = r - y$, and error variable at time t
E_t	Evapotranspiration $(Kg\,s^{-1}m^{-2})$
ϵ_h	Emissivity
ε	Gadrient of a function
ε_s	Gas hold-up $(-)$
F	Prefilter transfer function
G	Constrains matrix for GPC design
h	Culture depth (m)
H	Sensor dynamic transfer function
I	Identity matrix
I_{av}	Solar average irradiance $(\mu E\,m^{-2}s^{-1})$
I_k	Solar irradiance $(\mu E\,m^{-2}s^{-1})$
I_0	Solar incident radiation $(\mu E\,m^{-2}s^{-1})$
J	Function to minimize in predictive control
K_a	Biomass light attenuation $(m^2\,g^{-1})$
K_d	Disturbance model static gain
K_{ff}	Feedforward gain
K_i	Static gain of process i
$K_{laCO_{2c}}$	Volumetric coefficient for carbon dioxide into the channel (s^{-1})
$K_{laO_{2c}}$	Volumetric coefficient for oxygen into the channel (s^{-1})
K_p	PID proportional gain
K_u	Process model static gain
L_d	Disturbance model dead time
$L_f\varepsilon$	Lie derivative of ε respect to f
L_g	Lie derivative of g
L_i	Dead time of process i

L_u	Process model dead time
L_0	Nominal open-loop transfer function
λ	Closed loop time constant for Lambda method
Λ	Weighting factor for control effort
m	Mass of the heater
m_f	Form parameter
M_{CO_2}	Molecular weight of the carbon dioxide ($g\ mol^{-1}$)
M_{O_2}	Molecular weight of the oxygen ($g\ mol^{-1}$)
n	Form exponent (-)
n_l	Number of lateral vents (-)
n_r	Number of roof vents (-)
N	Receding horizon
N_u	Control horizon
N_1	Lower value of prediction horizon
N_2	Upper value of prediction horizon
$\aleph$	Filter derivative value
$[O_2]$	Dissolved oxygen concentration (%)
$[O_2^*]$	Equilibrium concentration with gas phase for oxygen ($mol\ m^{-3}$)
$[O_2]_m$	Total dissolved oxygen in the medium ($mol\ m^{-3}$)
P	Process transfer function
pH	Culture pH
P_0	Nominal plant
$P_{rs,o}(t)$	Outside solar radiation (Wm^{-2})
$P_{t,o}(t)$	Outside temperature (K)
$P_{ws,o}(t)$	Wind speed (m s^{-1})
PO_2	Oxygen photosynthesis rate ($Kg_{O_2}\ kg^{-1}s^{-1}$)
PCO_2	Carbon dioxide photosynthesis rate ($Kg_{O_2}\ kg^{-1}s^{-1}$)
$PO_{2,max}$	Oxygen maximum photosynthesis rate ($Kg_{CO_2}\ kg^{-1}s^{-1}$)
$\overline{PO_2(DO)}$	Dissolved Oxygen effect on the oxygen productivity (-)
$\overline{PO_2(pH)}$	pH effect on the oxygen productivity (-)
$\overline{PO_2(X_r)}$	Temperature effect on the oxygen productivity (-)
$\mathcal{P}$	Family of plants
$\mathcal{P}^*$	Representative plants of $\mathcal{P}$ for design stage
Q	Heat flow (W)
Q_i	Heat dissipated by heater i
Q_{ac}	Accumulated heat in the greenhouse air (Wm^{-2})
Q_{cn-cv}	Heat transfer by convection and conduction in the cover between the outside and the inside air (Wm^{-2})
$Q_{cv,cal}$	Convection heat transfer with the pipes heating system (Wm^{-2})
$Q_{cv,ss}$	Ground surface convection heat transfer (Wm^{-2})

Nomenclature

Q_{liq}	Volumetric flow rate of the liquid ($m^3 s^{-1}$)
Q_m	Volumetric flow rate of the medium ($m^3 s^{-1}$)
Q_s	Solar radiation absorbed by the greenhouse air ($W m^{-2}$)
$Q_{t,c}$	Latent heating produced by the crop transpiration ($W m^{-2}$)
Q_v	Input and output exchange due to natural ventilation ($W m^{-2}$)
$r, \ r(t)$	Reference variable, and reference variable at time t
r_d	Relative degree
R_s	Saturation ratio
R_T	Time constant ratio
RO_2	Respiration coefficient for dissolved oxygen ($mg \ L^{-1}$)
ρ	Density of the culture ($kg m^{-3}$)
s	Complex variable used in Laplace transform
S, R	Closed loop polynomial in GPC design
S_{lim}	Stability limit specification in QFT
σ_h	Stefan-Boltzmann constant
t	Time
t_0	Initial time
t_f	Final time
T_d	Disturbance model time constant
T_i	Time constant of process i
T_m	Sample time
T_p	Time constant for the pole
T_{pl}	T-polynomial in GPC design
T_{dy}	Closed loop transfer function from input d to output y
T_t	Anti-windup tracking time
T_u	Process model time constant
T_{uy}	Closed loop transfer function from input u to output y
T_z	Time constant for the zero
$\top$	Transpose
τ_i	PID integral time
τ_d	PID derivative time
$u, \ u(t)$	Input variable, and input variable at time t
u_{limit}	Control signal limit value
u_{max}, u_{min}	Maximum and minimum values of the control signal
u_{peak}	Control signal peak value
u_{sat}	Control signal saturated
u_0	Control signal initial value
U	Laplace transform of the control signal
$U_{ven}(t)$	Vent opening control signal (^{o})

v	Virtual control signal in feedback linearization technique
v_r	Raceway reactor constant velocity (ms^{-1})
V_s	Volume of each section (m^3)
$V_{t,c}$	Short wave transmission coefficient based on the cover transmission coefficient, whitening and the shader mesh state (-)
$V_{v,a-l}$	Areas of the sidewall ventilation openings (m^2)
$V_{v,a-r}$	Areas of the roof ventilation openings (m^2)
w	Raceway reactor width
ω_i	Specific frequency value
Ω	Set of frequencies
$X_{h,i}$	TCLab heater i temperature
X_r	Raceway reactor temperature
$X_{t,a}(t)$	Air temperature (K)
$X_{t,ss}(t)$	Soil surface temperature (K)
X_∞	Environment temperature (^oC)
$\xi(z^{-1})$	Characteristic polynomial of GPC design
ϕ_l	Leakage by infiltration when vents are closed flux $(m^3 s^{-1})$
$\phi_v(t)$	Ventilation flow $(m^3 s^{-1})$
Φ	Convertible function for feedback linearization
ψ	Coordinates in feedback linearization
$y, \ y(t)$	Output variable, and ouput variable at time t
Y_{b/O_2}	Biomass yield coefficient (kg)
z^{-1}	Backward shift operator

Contributions to Classic Control Strategies and Application to Industrial Facilities

1. Introduction

In this introductory chapter, Section 1.1 offers a brief description of the current concerns in the classic control strategies and their application in the industry. Section 1.2 presents the main topics treated in this thesis. Section 1.3 sketches out the rest of the chapters, Section 1.4 summarizes all the publications developed during this thesis, and Section 1.5 contains the personal and scientific achievements derived during the doctoral period.

1.1 Background and Motivation

Control theory has witnessed significant advancements over the years, with the development of new algorithms, techniques, and solutions. There has been a growing focus on advanced control techniques in control systems, while classic control techniques have received less attention in recent literature. For example, integrating machine learning techniques in control systems has emerged [16]. Data-driven control methods leverage large datasets and algorithms to learn system dynamics, identify optimal control strategies, and adapt to changing environments. Reinforcement learning, neural networks, and deep learning techniques have been explored extensively recently [70, 76, 91, 122, 127].

Several reviews have studied the implementation of these new control strategies in the industry and have concluded that, despite the significant research interest in all these new control techniques, the industry is hesitant to adopt them. Instead, they prefer to stick to classical control strategies that have been proven to be effective. For example, in [16], the authors state that the research field has recently expanded to include new areas incorporating Machine Learning applications. However, it is uncertain whether this trend will continue, as it has been seen in other fields where initial interest quickly diminished. One possible reason for this is the use of cutting-edge algorithms that may be appealing to academics but lack practicality for industrial practitioners. It emphasizes the importance of striking a balance between novelty and industrial applicability. To gain acceptance, relying on established and well-understood techniques may be more beneficial than complex and novel ones, which could potentially have a negative impact.

Therefore, while the appeal of advanced control techniques captivates researchers, it is crucial to recognize the enduring significance of classic control techniques. As cited by Abramovitch in [2]: *"When the media and the public discuss such topics as self-driving vehicles and automated drones, the buzzwords used are all about machine learning (ML) and artificial intelligence (AI), with little mention of the "measure–compare–adjust–measure" loops that permeate and enable such systems."*, he emphasizes the significance of applying and teaching fundamental control principles, underscoring their essential role as a base for emerging fields such as artificial intelligence.

These classic control strategies form the foundation of hierarchical control systems widely implemented in industry, where different control layers interact to achieve system objectives. They are the basis of the lower layer of the hierarchical control system, and their adequate performance will ensure the upper layer's control objectives. Classical control strategies, rooted in well-established theories such as Proportional, Integral, and Derivative (PID) control [1, 135], feedforward control (FF), cascade control (CC), feedback linearization (FL) or model predictive control (MPC), have stood the test of time and proven their effectiveness in a wide range of control scenarios. For example, in [19], the authors state that, based on an extensive literature survey, the PID controller has become the most widely used controller in various application domains because of its simple structure and easy implementation. They study how to automatically tune the PID parameters, concluding that tuning PID controllers would be a large research area.

Numerous studies have highlighted the significance of addressing load disturbances in the process industry, particularly emphasizing the widespread use of feedforward control as a main solution. In [77], a comprehensive review of feedforward control algorithms in industrial applications. The authors present the characteristics and application domains of the most representative feedforward control algorithms and some benchmarks in industrial processes. In [37], a summary of a set of new simple tuning rules that have been obtained, providing considerable improvements in the control system performance and a short history of feedforward control is presented.

Moreover, several studies have researched the application and effectiveness of cascade control in the industry. In [104], various series cascade control strategies for stable, integrating, and unstable process models are briefly reviewed, and suitable tuning strategies are recommended. Cascade control is widely used in industry, and authors emphasize the significant advantages of this control strategy, including improved process stability, enhanced control accuracy, faster response to disturbances, and better handling of complex and nonlinear systems. Besides, they provide insights into selecting appropriate process variables, tuning methods for cascade control loops, and integrating other classic control algorithms for optimal performance.

Furthermore, classic control techniques remain immensely important in the industrial landscape [136]. They are indispensable in ensuring critical systems security and efficient operation across diverse sectors. Industrial systems have challenges in modelling, analysis, and control system design. They often involve numerous interconnected components, subsystems, and variables, making it challenging to accurately capture their dynamics. In this sense, classical control strategies have a long history of successful application in diverse industries. The wealth of knowledge and experience accumulated over the years has led to a deep understanding of the strengths and limitations, making them a reliable choice for many industrial applications [134]. However, as industrial systems become more complex and dynamic, there is a need to improve and tailor classical control strategies to meet specific requirements.

Due to the industry increasing complexity, uncertainties are an inherent part of the industrial process. They can arise from various sources, such as parameter variations, disturbances, measurement errors, and model mismatches, and reveal that uncertainty can significantly affect the accuracy and performance of modelling and control systems, leading to a suboptimal operation, reduced efficiency, and increased risks. In literature, several studies have researched the effects of uncertainty on modelling and control in various industrial sectors. Authors in [108] aim that managing uncertainties in industrial systems is a daily challenge to ensure improved design, robust operation, accountable performance, and responsive risk control. Understanding the challenges of uncertainty and exploring strategies to enhance modelling and control techniques in the presence of uncertainties is important. To deal with these uncertainties, robust control techniques must be applied. In [31], the author thoroughly covers the fundamentals of the Quantitative Feedback Theory (QFT) robust control technique, as well as practical control solutions for unstable, time-delay, non-minimum phase or distributed parameter systems, plants with large model uncertainty, high-performance specifications, nonlinear components, multi-input multi-output characteristics or asymmetric topologies.

In summary, despite the increased interest in advanced control techniques and the relative lack of attention given to classic control techniques in recent literature, there is still an extensive scope for exploration and advancement in this field. The belief that everything has been accomplished with classic control techniques is misguided, and further research and development are crucial. It is important to recognize their significance and invest in the continued study and refinement of classic control techniques to ensure the advancement and success of control systems in the industry. By delving into the theoretical foundations, refining implementation methodologies, and exploring novel applications, it is possible to unlock new potentials and enhance the effectiveness of these techniques.

This thesis is driven by the motivation to address unresolved challenges within classical control schemes, emphasizing their importance and applicability in industry. By applying these strategies to different experimental plants, this research aims to provide practical evidence of their effectiveness, contributing to the advancement of control theory and practice.

1.2 Main Topics and Contributions of The Thesis

This section briefly overviews the main topics studied and the contributions developed throughout the thesis. It exposes the different contributions of classical control strategies and their subsequent application in experimental plants.

1.2.1 Contribution on Classic Control Strategies

As mentioned before, classic control methods persistently hold significance in industrial applications despite modern control technique advancements [65]. They offer robust and reliable control solutions that are comprehensively understood and have a long history of successful implementation. Moreover, they are relatively straightforward to implement within industrial settings, require minimal computational resources, and can integrate into existing control systems. Their simplicity also facilitates understanding, maintenance, and system upgrades.

Based on this fact, the control strategy extensively studied in this thesis, which proposes modifications to unresolved issues, is based on classical control loops with PID controllers

subjected to disturbances [1, 18, 135]. The PID controller is a well-established and widely understood control technique with extensive research and practical experience, extensively used in various industries. Based on the understanding that most industrial processes are affected by disturbances, the control scheme applied throughout the thesis for the regulation problem is feedforward control. This control strategy aims to improve system performance by compensating for load disturbances in the system before they affect the output [38]. While there is extensive literature on disturbance rejection, there are still unresolved issues, such as saturation in feed-forward control schemes, uncertainty in the plant and disturbance models, or the rejection of measurable disturbances in cascade control schemes.

In this regard, this thesis presents three solutions to the abovementioned problems. The first contribution focuses on studying the presence of uncertainty in the regulation problem of systems subjected to measurable disturbances. In this context, the strategy involves designing a robust PID controller using QFT, modifying the original limits, and considering the uncertainties inherent in the system [114].

On the other hand, a solution for the saturation problem is provided for feedforward control. Some limitations have not been thoroughly studied for feedforward control, such as the saturation of the control signal upon the arrival of the disturbance. When this happens, the power of the feedforward control is compromised, resulting in a deteriorated performance at the output. Hence, the other significant contribution proposes a tuning rule for the gain of the feedforward controller upon the arrival of the measurable disturbance based on the saturation limit, peak value, and steady-state value of the control signal. The improvement in output performance is demonstrated through various simulations and experimental examples.

Finally, the rejection of disturbances using feedforward control in cascade control schemes has been examined. This control strategy involves utilizing multiple control loops, where the output of one control loop serves as the set-point or reference for another control loop. Its main utility lies in enhancing disturbance rejection in the inner loop and stability by isolating the effects of disturbances and changes in the inner loop from the outer loop [69]. However, the literature has not extensively developed the study of applying feedforward control for disturbance rejection affecting the outer loop. Therefore, the contribution focuses on implementing two static feedforward controllers that enter both the inner and outer loops. For tuning the gain of the feedforward controller that enters the inner loop, a simple rule is proposed based on the parameters of both loop and disturbance models.

Overall, this thesis addresses the issues mentioned before by studying the presence of uncertainty in regulation problems, proposing a tuning rule for feedforward control saturation, and exploring the application of feedforward control in cascade control schemes. These contributions aim to improve control system performance, enhance disturbance rejection capabilities, and contribute to the advancement of classical control strategies in industrial applications.

1.2.2 Application on Experimental Facilities

The implementation of automatic control systems has revolutionized the management and optimization of industrial processes, playing a vital role in their efficient operation. These systems are specifically designed to monitor and control key parameters such as temperature, pressure, flow rate, and level, ensuring optimal performance and reliability. With advancements in automation and control technologies, the significance of automatic control in industrial facili-

ties has become increasingly evident. The primary objective of automatic control is to enhance efficiency, productivity, and safety in industrial operations. By continuously monitoring and adjusting parameters in real-time, these control systems enable precise and accurate regulation. They ensure that processes operate at optimal set-points, minimizing energy consumption and waste generation. This not only results in significant cost savings but also contributes to environmental sustainability, making industries more competitive in the dynamic market of today. In this thesis, three different facilities have been used to implement some of the control techniques and solutions defined in the document.

Several control techniques have been implemented in a raceway microalgae photobioreactor. Extensive research has been conducted on raceway photobioreactors to facilitate large-scale cultivation of microalgae in an industrial setting. Today, these reactors are widely recognized as the preferred technology for industrial microalgae cultivation due to their scalability and practicality. The appeal of raceway reactors lies in their relatively low initial investment costs compared to alternative technologies like tubular photobioreactors, which necessitate more intricate infrastructure and equipment. Additionally, raceway reactors offer other notable advantages, including straightforward operation and minimal maintenance expenses. In this way, three contributions have been developed and implemented in a real raceway reactor located in Almería, Spain. A linear predictive controller was integrated into the model, enabling precise anticipation of system behavior. Furthermore, a robust controller was developed to ensure stability and reliable performance, with testing conducted both in simulation and in an actual industrial plant. Lastly, an interactive tool was created to streamline the implementation of control strategies, enhance comprehension of the intricate photobioreactor model, and provide comprehensive training for researchers and plant operators alike.

A greenhouse facility has also been used in this thesis. Greenhouses play a crucial role in modern agriculture by creating an environment that enables the cultivation of crops throughout the year, regardless of external weather conditions. One of the key factors that directly influence plant growth and productivity in a greenhouse is temperature control. A combination of the feedback linearization control technique and QFT is used to address the challenging issue of controlling the complex non-linear climate. By incorporating feedback linearization and leveraging the principles of QFT, the aim is to effectively tackle the intricacies associated with controlling non-linear climate dynamics.

Furthermore, temperature control is essential in various industries as it directly affects manufacturing processes' quality, safety, and efficiency. Maintaining precise temperature levels is crucial for successfully operating and optimizing industrial systems. A temperature control lab system has also been used as a benchmark problem to implement some of the new control solutions developed in this thesis.

1.3 PhD Outline

The purpose of this document is to provide an overview of the key elements covered in the thesis. The focus is primarily on the contributions made in the thesis, but there are also brief explanations of general concepts included to facilitate understanding for the reader. The chapters are structured in the following manner:

- Chapter 2 is devoted to summarizing the main concepts and facilities involved in the thesis. First, a comprehensive overview of the classic control schemes used in this thesis is presented. Feedback control, PID control, feedforward control, cascade control, General Predictive Control (GPC), feedback linearization, and QFT are explained in detail. Second, a wide description of the industrial facilities in which the control strategies have been implemented is provided (the greenhouse, microalgae raceway photobioreactor, and temperature platform, together with a description of the corresponding dynamic models).

- Chapter 3 studies three solutions for different classical control schemes in the presence of measurable disturbances. Section 3.1 introduces a robust solution based on QFT for the feedforward control scheme. This approach combines PI control with feedforward compensators to effectively handle process uncertainties. In Section 3.2, a novel design rule is proposed to improve the response of a classical feedforward control scheme when saturation occurs due to disturbances. Finally, Section 3.3 presents a dual feedforward scheme for a cascade control scheme, considering measurable disturbances at the output.

- Chapter 4 presents the implementation of the classic control techniques on industrial facilities. In Section 4.1, three contributions are focused on the application of control strategies to the raceway reactors. The implementation of a linear predictive controller in simulation is first discussed. Also, the design and implementation of a robust controller is addressed, where experimental results are presented. Lastly, an interactive tool is introduced with the aim of simplifying the implementation of control strategies, improving comprehension of the intricate photobioreactor model, and providing training opportunities for researchers and plant operators. In Section 4.2, a combination of the feedback linearization control technique and QFT is applied. This approach is utilized to effectively handle the complex nonlinearities involved in a greenhouse temperature control problem. Finally, the new control approach presented in this thesis to deal with saturation problems in feedforward control scheme is evaluated in a lab-scale temperature system in Section 4.3.

- Finally, some conclusions and future research works are presented in Chapter 5.

1.4 Publications and Other Contributions

The research work of this thesis is supported by the publications listed below, where the name of the Ph.D. candidate and author of this thesis has been highlighted in bold font. She also took part in three other local conferences on the occasion of the Annual Meeting of the Ph.D. Program in Informatics of the University of Almería, in which the progress of research work is periodically shared among the members of the Department of Informatics and the academic community.

1.4.1 Scientific Journals

Hoyo, Á., Moreno, J. C., Guzmán, J. L., and Rodríguez, F., "Robust QFT-based feedback linearization controller of the greenhouse diurnal temperature using natural ventilation", *IEEE Access*, vol. 7, pp. 64148-64161, 2019. Impact factor in 2019 (JCR): 3.745. Journal Rank in Category in 2019 (JCR): 35/156 (Q1) in Computer Science, Information Systems; 61/266 (Q2) in Environmental Sciences. Reference: [62].

Hoyo, Á., Rodríguez-Miranda, E. Guzmán, J. L., Acién, F. G., Berenguel, M., and Moreno, J. C., "A computer-based tool to simulate raceway photobioreactors for design, operation and control purposes", *Computers & Chemical Engineering*, vol. 156, pp. 107572, 2022. Impact factor in 2022 (JCR): 4.3. Journal Rank in Category in 2022 (JCR): 42/112 (Q2) in Computer Science, Interdisciplinary Applications; 44/143 (Q2) in Engineering, Chemical. Reference: [63].

Hoyo, Á., Guzmán, J. L., Moreno, J. C., and Baños, A., "Robust pH control in a raceway photobioreactor", *Revista Iberoamericana de Automática e Informática industrial*, vol. 19, no. 3, pp. 274-283, 2022. Impact factor in 2022 (JCR): 1.500. Journal Rank in Category in 2022 (JCR): 55/65 (Q4) in Automation & Control Systems; 28/30 (Q4) in Robotics. Reference: [55].

Hoyo, Á., Hägglund, T., Guzmán, J. L., and Moreno, J. C., "A practical solution to the saturation problem in feedforward control for measurable disturbances", *Control Engineering Practice*, 2023, **(submitted to the journal and under review)**. Impact factor in 2022 (JCR): 4.9. Journal Rank in Category in 2022 (JCR): 18/65 (Q2) in Automation & Control Systems; 70/276 (Q2) in Engineering, Electrical & Electronic. Reference: [58].

Hoyo, Á., Guzmán, J. L., Moreno, J. C., and Hägglund, T., "Double feedforward compensation for cascade control schemes", 2023, **(submitted)**. Reference: [59].

Barceló-Villalobos, M., **Hoyo, Á.**, Rodríguez-Miranda, E., Guzmán, J. L., and Acién, F. G., "A new control strategy to improve the mass transfer capacity and reduce air injection costs in raceway reactors", *New Biotechnology*, vol. 70, pp. 49-56, 2022. Impact factor in 2022 (JCR): 1.44. Journal Rank in Category in 2022 (JCR): 10/79 (Q1) in Biochemical Research Methods; 29/159 (Q1) in Biotechnology & applied Microbiology. Reference: [8].

1.4.2 International Conferences

Hoyo, Á., Guzmán, J. L., and Berenguel, M., "Use of the benchmark for PID control in engineering studies at the University of Almería", in *3rd IFAC Conference on Advances in PID Control*, Ghent, Belgium, 2018. Reference: [53].

Hoyo, Á., Moreno, J. C., Guzmán, J. L., and Hägglund, T., "Robust QFT-based PI controller for a feedforward control scheme", in *3rd IFAC Conference on Advances in PID Control*, Ghent, Belgium, 2018. Reference: [61].

Hoyo, Á., Guzmán, J. L., Acién, F. G., Berenguel, M., and Moreno, J. C., "A graphical tool to simulate raceway photoreactors", in *IWA Conference on Algas Technologies and Stabilization Ponds for Wastewater Treatment and Resource Recovery (IWAlgae)*, Valladolid, España, 2019. Reference: [52].

Leal, M., **Hoyo, Á.**, Guzmán, J. L., and Hägglund, T., "Double back-calculation approach to deal with input saturation in cascade control problems", in *International Conference on Automatic Control and Sof-Computing (CONTROLO)*, Bragança, Portugal, Julio, 2020. Reference: [72].

Guzmán, J. L., Mañas, F., **Hoyo, Á.**, Ramos-Teodoro, J., and Donaire, J. G., "Use of TCLab kits for control engineering curricula at the University of Almería", in *13th IFAC Symposium on Advances in Control Education (ACE)*, Hamburg, Germany, 2022. Reference: [35].

Hoyo, Á., Mañas-Álvarez, F. J., Rodríguez-Miranda, E., Gil, J. D. and Castilla, M., and Guzmán, J. L., "Bringing Automatics and Robotics closer to pre-university students", in *13th IFAC Symposium on Advances in Control Education (ACE)*, Hamburg, Germany, 2022. Reference: [60].

1.4.3 National Conferences

Hoyo, Á., Guzmán, J. L., and Moreno, J. C., "Control robusto de procesos industriales no lineales con compensación de perturbaciones", in *Proceedings of the XVI CEA Symposium on Control Engineering*, Almería, Spain, 2018, (in Spanish). Reference: [54].

Hoyo, Á., Guzmán, J. L., Moreno, J. C., and Berenguel M., "Control robusto con QFT del pH de un fotobiorreactor industrial", in *XXXVIII Jornadas de Automática*, Gijón, España, 2017. Reference: [57].

Hoyo, Á., Guzmán, J. L., Moreno, J. C. and Berenguel M., " Control predictivo lineal del pH en un fotobiorreactor raceway", in *XL Jornadas de Automática*, Ferrol, España, 2019. Reference: [56].

Hoyo, Á., García-Mañas, F., Ramos-Teodoro, J., Sánchez-Molina, J. A., Guzmán, J. L., and Rodríguez, F., " Uso del paradigma Take-Home Labs para la enseñanza del control automático en estudios de ingeniería", in *XLII Jornadas de Automática*, Coruña, España, 2021. Reference: [56].

1.4.4 Local Conferences

Hoyo, Á., "Un simulador para la enseñanza de la producción de microalgas en fotobioreacotores raceway", in *En el camino de la investigación educativa: Encuentro de investigación del alumnado 2019 (EIDA 2019)*, Almería, Spain, 2019. Reference: [47].

Hoyo, Á., "Contribuciones de control robusto para sistemas sometidos a perturbaciones", in *Proceedings of the II Annual Meeting of the PhD Programme in Informatics of the University of Almería*, Almería, Spain, 2019, (in Spanish). Reference: [46].

Hoyo, Á., "Contribuciones de control robusto para sistemas sometidos a perturbaciones", in *Proceedings of the III Annual Meeting of the PhD Programme in Informatics of the University of Almería*, Almería, Spain, 2020, (in Spanish). Reference: [48].

Hoyo, Á., "Contribuciones de control robusto para sistemas sometidos a perturbaciones", in *Proceedings of the IV Annual Meeting of the PhD Programme in Informatics of the University of Almería*, Almería, Spain, 2021, (in Spanish). Reference: [49].

Hoyo, Á., "Contribuciones de control robusto para sistemas sometidos a perturbaciones", in *Proceedings of the V Annual Meeting of the PhD Programme in Informatics of the University of Almería*, Almería, Spain, 2022, (in Spanish). Reference: [50].

Hoyo, Á., "Contribuciones de control robusto para sistemas sometidos a perturbaciones", in *Proceedings of the VI Annual Meeting of the PhD Programme in Informatics of the University of Almería*, Almería, Spain, 2023, (in Spanish). Reference: [51].

1.4.5 Intellectual Property Registration

During the development of the doctoral thesis, two intellectual property registrations have been made in the Junta de Andalucía:

- *"Herramienta gráfica para la simulación de reactores raceway"*. No: 04 / 2021 / 4183. 2021. [52].

- *"Herramienta SCADA para en Control y Supervisión de las instalaciones del proyecto Sabana"*. No: 04 / 2021 / 4178. 2021.

1.5 Other Research, Teaching and Educational Activities

Regarding the rest of the milestones that evidence the acquisition of competencies needed for the world of research, there are two which have been key: one is the three-month stay (01/09/2022-30/11/2022) at the Department of Systems and Automatics of Lund University (Lund, Sweden), within the Research Group by Tore Hägglund, which satisfies one of the requirements to receive the Acknowledgement of International Ph.D.; the other corresponds to the three research projects and the research contract in which the doctoral student has collaborated (see the next subsection), as they provided a solid background in planning research.

Attending to educational and teaching involvement, the Ph.D. candidate has been engaged in five editions of the European Researchers' Night (from 2018 to 2022), one of the actions funded by the Marie Skłodowska-Curie program; five of the European Robotics Week (from 2018 to 2022); six of the First Lego League (from 2018 to 2023); and several other activities under educational programs of the University of Almería. Meanwhile, she has been giving lectures in the subjects listed below and acted as a co-supervisor in one Bachelor's thesis [71]:

- Industrial Informatics and Robotics, 118 hours, Computer Science Engineering Degree.

- Industrial Automation, 57 hours, Industrial Electronics Engineering Degree.

- Machine Control and Electric Drives, 4 hours, Industrial Electrical Engineering Degree.

1.5.1 Collaboration in Scientific Outreach Workshops for Girls

The doctoral student has been involved in several scientific outreach workshops during these years, aiming to bring science closer to young people. Many of these workshops have focused on motivating young girls and encouraging them to pursue STEM careers:

- Participation in the "Campus Tecnológico Para Chicas" program. University of Almería. July 2018-2022.

- Participation in the "Talleres para jóvenes programadoras" program. University of Almería. February 2018 and 2019.

- Participation in the "11 de Febrero - Día de la mujer y la niña en la Ciencia" program. 2018-2022.

- Participation in the "Ciencia y Tecnología en femenino" program. Almería. 2018.

- Participation in the "Girls in Control" workshop at the 59th Conference on Decision and Control. December 2020.

- Participation in the "I Jornadas Mujer y Automática" (Women and Automation Conference) organized by the Spanish Committee of Automation, conducting scientific outreach activities. April 2021.

1.5.2 Collaboration in Research Projects and Contracts

- UAL2020-TEP-A1991, Agricultural Collaborative Robot Inside the IoT I. University of Almería through FEDER funds granted by the Ministry of University, Research, and Innovation. Chief/Principal Investigator: Antonio Giménez Fernández and José Carlos Moreno Úbeda (University of Almería). 2021-2023. 29.200 €.

- PY20_00767, Agricultural Collaborative Robot Inside the IoT II. University of Almería through FEDER funds granted by the Ministry of University, Research, and Innovation. Chief/Principal Investigator: Antonio Giménez Fernández (University of Almería). 2021-2023. 78.500 €.

- 21_22_1_29C, Analysis and evaluation of the use of the Take-Home Labs paradigm for teaching automatic control in engineering studies. Call for the Creation of Innovation Groups and Good Teaching Practices. University of Almería. Chief/Principal Investigator: Francisco de Asís Rodríguez Díaz (University of Almería). 2021-2022. 1.200 €.

- PID2020-112709RB-C21, Hybrid control and optimization of a sustainable biorefinery for the industrial production of microalgae (HYCO2BIO). National Plan Project. Ministry of Science and Innovation. Chief/Principal Investigator: José Luis Guzmán Sánchez and José Carlos Moreno Úbeda (University of Almería). 178.000 €.

- DPI201784259-C2-1-R, Modelling and Control of the integrated process for microalgae production and wastewater treatment using industrial reactors (CALRESI). National Plan Project. Ministry of Economy and Competitiveness. Chief/Principal Investigator: José Luis Guzmán Sánchez (University of Almería). 2018-2021. 147.200 €.

- DPI2014-55932-C2-1-R, Control and optimization of biomass production using microalgae as a renewable energy source (PROBIOREN). National Plan Project. Ministry of Economy and Competitiveness. Chief/Principal Investigator: José Luis Guzmán Sánchez (University of Almería). 2015-2018. 123.000 €.

- 101060991 REALM, Horizon Europe – the Framework Programme for Research and Innovation. Chief/Principal Investigator: José Luis Guzmán Sánchez (University of Almería). 2021-2027. 515.000 €.

1.5.3 Awards

The doctoral candidate has received the following awards during the period of the doctoral thesis:

- Young Author Award for the article "Robust QFT-based PI controller for a feedforward control scheme" at the 3rd IFAC Conference on Advances in Proportional-Integral-Derivative Control in Ghent, Belgium, 2018 [61].

- IX edition of the "Implicación Social en las Universidades Públicas de Andalucía" Award. Graduate Category. Foro de Consejos Sociales de Universidades Públicas de Andalucía, 2019.

2. Material and Methods

Classic control strategies play a vital role in the industrial sector, offering valuable solutions for achieving stable and efficient operation of various systems [65]. Despite the advancements in modern control techniques, classic control strategies continue to hold significant importance in various industries [106]. They are considered standard practices in the industry and are trusted by professionals. They have been widely adopted in manufacturing, power generation, chemical processing, and automation industries for decades.

Classic control techniques are based on feedback control that involves continuously comparing the output or response of a system to a desired reference value or setpoint and using the resulting error signal to adjust the control input. The key idea behind feedback control is to utilize information about the system's performance to make corrective adjustments and drive the system toward the desired state. Classical control methods often employ well-established algorithms, such as PID, cascade, or feedforward control for measurable disturbances [1, 18, 135].

In this context, this chapter provides a brief summary of the different control schemes, such as feedback, feedforward, cascade control, GPC, Feedback Linearization, and QFT, in Section 2.1. In Section 2.2, all the industrial facilities used in this thesis and their models where these control techniques have been implemented are exposed. These facilities are a greenhouse, a photobioreactor, and a temperature platform (TCLab).

2.1 Automatic Control

Automatic Control is a highly complex field of engineering that cannot be easily summarized in a few words. It encompasses various disciplines and requires a multidisciplinary approach. Generally, it can be defined as utilizing various techniques to meet particular problem specifications autonomously. The breadth and scope of this field were acknowledged by Rufus Oldenburger in 1978 when he commented on the name and extensive nature of Automatic Control. He believed that the term encompassed all systems, as every system involves variables,

and the focus lies in maintaining these variables at constant or desired values. This concept applies to diverse biological, economic, political, and engineering systems, even if they do not incorporate explicit automatic control devices [12, 40].

The origins of Automatic Control can be traced back to ancient Greece with the development of water clocks and float regulators around 300 B.C. However, it is commonly associated with the 18th century when centrifugal governors were developed and applied to wind and water mills. James Watt's governor, a significant invention during that time, is often regarded as a symbol of Automatic Control [6]. Over the years, Automatic Control has continued to advance, becoming pervasive in modern life, with applications in cars, industries, multimedia devices, mobile phones, hospitals, and practically every device used by people today.

The fundamental concept that lies at the core of Automatic Control is feedback, which has a significant impact on this fascinating field. As mentioned earlier, the objective of Automatic Control is to meet particular problem specifications by maintaining a set of variables at a desired value or within a predetermined range. Feedback plays a crucial role in achieving this objective by providing a mechanism to correct the disparity between desired and actual performance. While the idea of feedback can be traced back thousands of years, it is commonly attributed to the early 1920s when significant advancements were made in the signal amplification field. In his work on the signal amplification problem, H.S. Black employed high-gain amplifiers by feeding back a portion of the output signal to reduce distortion caused by noise [17]. Similarly, during that period, N. Minorsky conducted a comprehensive analysis in position control systems and formulated a control law now known as three-term PID control [12]. Since those early days, feedback features have been extensively analyzed and studied, with the scheme shown in Figure 2.1 serving as a common reference point for research and analysis [1].
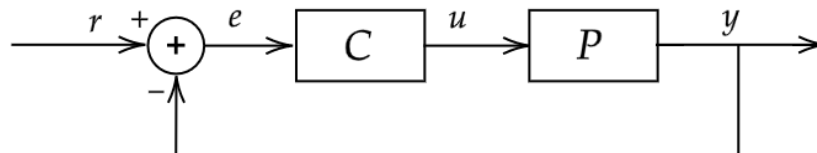
Figure 2.1. Feedback basic block scheme.

The system under consideration consists of two main components: the process P and the controller C. These components are represented as boxes, with arrows indicating the causal relationship between inputs and outputs. The process, influenced by the manipulated variable u (also known as the control signal), has a single input. This signal represents the actuator, typically a valve or a motor, which facilitates the impact of the control variable on the process. The process variable y, on the other hand, is the output of the process and is measured by a sensor. In this context, the set point or reference value r represents the desired value of the process variable. The control error e is the difference between the set point and the process variable [1].

Various controllers have been employed to leverage the beneficial properties of feedback. Among them, the PID controller stands out as the most widely used form of feedback control. It has found applications in diverse environments and processes, undergoing modifications to its original form, developing new tuning rules, and exploring its limitations. Presently, typical

PID controllers or their variants are utilized to control most industrial processes. However, the need for more advanced control techniques has emerged due to industrial competition, stringent performance requirements, and the presence of complex and challenging-to-control processes. A comprehensive overview of this evolution can be found in references [1] and [121]. The control strategies employed in this thesis include PID control, cascade control, feedforward control, feedback linearization, GPC, QFT, and their combinations. This section provides a brief description of these control techniques.

2.1.1 PID Control

This section provides an introduction to PID control. PID controller is by far the most common control algorithm. PID controllers have long been the dominant choice in industrial applications, with estimates suggesting that over 90% of controllers used in the industry are of the PID type [1]. These controllers are widely employed in the process industries, serving as the foundation for advanced control algorithms and strategies. Despite the advancements in control theory, PID controllers remain the go-to solution for addressing a wide range of control problems. They are accessible to users with varying levels of control knowledge. In practice, PID controllers often operate as PI controllers, omitting the derivative action. However, there are scenarios where incorporating derivative action can lead to significant improvements [1, 135].

Various forms of PID controllers exist, with the following equation representing the standard form:

$$u(t) = K_p \left(e(t) + \frac{1}{\tau_i} \int_0^t e(\tau)d\tau + \tau_d \frac{de(t)}{dt} \right) \tag{2.1}$$

where the control error $e = r - y$, as shown in Figure 2.1 represents the difference between the reference signal and the measured output. In the basic PID controller, the proportional gain is denoted as K_p, the integral time as τ_i, and the derivative time as τ_d. In the Laplace domain, the controller is represented as:

$$C(s) = K_p \left(1 + \frac{1}{\tau_i s} + \tau_d s \right) \tag{2.2}$$

Over time, various modifications have been made to the elementary PID controller, resulting in different representations. These modifications mainly focus on how set-points are handled and how signals are filtered. One such modification is the PID with set-point weighting, which offers a more flexible structure. This variant of the PID controller is characterized by

$$u(t) = K_p \left(e_p(t) + \frac{1}{\tau_i} \int_0^t e(\tau)d\tau + \tau_d \frac{de_d(t)}{dt} \right) \tag{2.3}$$

where $e_p = b_s r - y$ and $e_d = c_s r - y$, with b_s and c_s being the set-point weights. Thus, by tuning the parameters b_s and c_s, different behaviors of the PID controller can be achieved to handle reference tracking.

Another approach to representing the PID controller involves incorporating filters with the derivative term to mitigate the impact of high-frequency noise on the control signal. Typically, the derivative term is filtered using a first-order filter, or the ideal derivative can be combined with a second-order filtering of the measured signal. The transfer function of a PID controller with a filtered derivative can be expressed as:

$$C(s) = K_p \left(1 + \frac{1}{s\tau_i} + \frac{s\tau_d}{1 + s\tau_d/\aleph} \right) \tag{2.4}$$

with $C(\infty) = K_p(1 + \aleph)$ representing the high-frequency gain, parameter $\aleph$ can be utilized to minimize fluctuations in the control signal.

In practical scenarios, most physical processes face various constraints due to factors such as physical limitations, safety requirements, or performance criteria. Anti-windup schemes are commonly implemented in PID controllers to prevent integrator windup when the actuator saturates. These schemes ensure that the system remains unaffected as long as saturation is not active. However, when saturation occurs, the integral term in the controller is adjusted until the system exits the saturation limit.
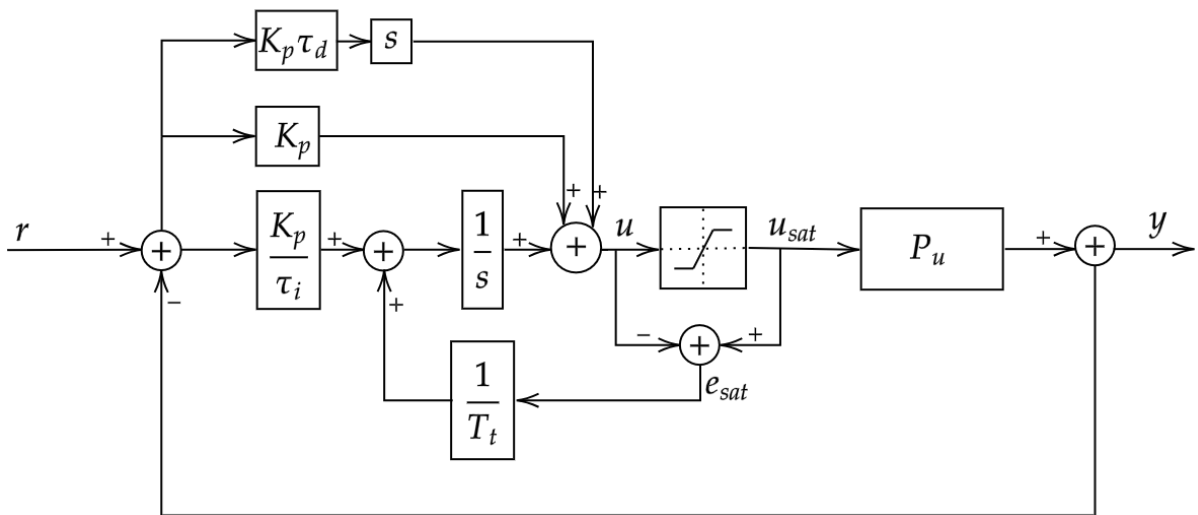
Figure 2.2. PID anti-windup scheme.

The back-calculation anti-windup method is one of the most common anti-windup methods (see Figure 2.2), and here the integrator is dynamically changed with a tracking time constant T_t when the control signal saturates [1]. In the literature, the selection of the tracking time constant is a problem that still needs to be solved. However, there are some proposals about how to tune it. It is recommended to set the tracking time constant in the interval $0 \leq T_t \leq \tau_i$ [117].

In some contributions of the thesis, the controller $C(s)$ is a PI controller with a transfer function defined in Equation (2.2), with $\tau_d = 0$. The Lambda tuning method has been considered along the document. This method has been selected because it is commonly used in the process industry [131]. It allows to achieve a first-order closed-loop transfer function for the process. In this method, the tuning parameter, denoted by λ, determines the location of the closed-loop pole, thereby establishing the desired closed-loop time constant. So the PI controller parameters are given by (2.5) [25]. Notice that other tuning methods could be considered without affecting the methodology presented in this thesis.

$$K_p = \frac{T_u}{K_u(\lambda + L_u)} \qquad \tau_i = T_u \tag{2.5}$$

2.1.2 Cascade Control

Load disturbance rejection is a critical aspect of process control applications. Implementing a cascade control system is often considered to enhance performance in dealing with unmeasured load disturbances. By incorporating an additional sensor, the fast dynamics of the process can be separated from the slow dynamics. This separation allows for the practical rejection of disturbances [135].
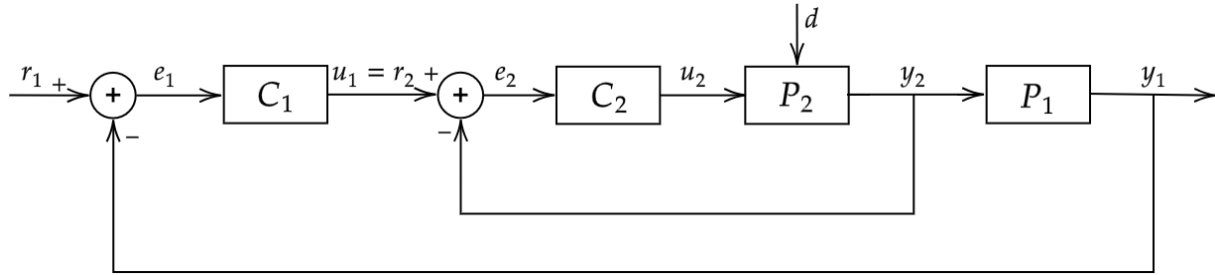
Figure 2.3. Cascade control scheme.

Figure 2.3 illustrates a typical configuration of a series cascade control system. This thesis will focus on two nested loops for simplicity, but the concept can be extended to include more loops if needed. The process transfer function is represented by $P(s) = P_2(s)P_1(s)$, where y_1 is the primary output and y_2 is the secondary output. The secondary controller, $C_2(s)$, controls y_2, while the primary controller, $C_1(s)$, controls y_1. It is worth noting that the primary controller's output signal serves as the secondary controller's set-point. Similarly, the inner loop is commonly referred to as the secondary loop, while the outer loop is called the primary loop.

The cascade control system is effective because it takes advantage of the separation between the slow dynamics represented by $P_1(s)$ and the fast dynamics represented by $P_2(s)$. This allows efficient compensation of disturbances that affect the secondary loop before they significantly impact the main process output, y_1. Another advantage of the cascade control system is that the inner loop can effectively address the presence of non-linearities in $P_2(s)$.

The effectiveness of cascade control is particularly noticeable when disturbances affect the inner loop and when the secondary sensor is strategically placed to separate the fast dynamics of the process from the slower dynamics [69]. However, when the secondary process exhibits significant dead time or has a non-minimum phase, cascade control may not be generally beneficial, considering the additional cost associated with the secondary sensor and controller. Another advantage is that nonlinearities in the process within the inner loop are handled within that loop, removing them from the more critical outer loop. Hence, the parameters of the overall control system should be carefully chosen to achieve a tight tuning of the inner loop concerning the outer loop. It is worth noting that having an integrator in the inner loop is not strictly necessary since the outer loop can ensure zero steady-state error.

Typically, the overall cascade control system is designed by initially tuning the secondary controller while keeping the primary loop in manual mode. This tuning process is based on the secondary process transfer function. Subsequently, the primary controller is tuned using the closed-loop transfer function of the secondary loop in conjunction with the primary process transfer function. This approach ensures that the dominant dynamics are accounted for due to the

tight tuning of the secondary loop. It should be noted that the design of a cascade control system is sequential, which can make it more time-consuming compared to designing a traditional single-loop controller. Therefore, there is a need for automatic tuning functionalities that can simultaneously tune both controllers [135].

2.1.3 Feedforward Control

Control schemes with measurable disturbances compensation are well-known in the process industry [38]. The combination of feedforward and feedback control, as shown in Figure 2.4, can significantly improve control performance when the system is affected by a measurable disturbance that impacts the system output. In an ideal situation, this control scheme can eliminate the effect of the disturbance. However, even with some modelling errors or inversion problems, the feedforward control still reduces the impact of the disturbance on the plant output.
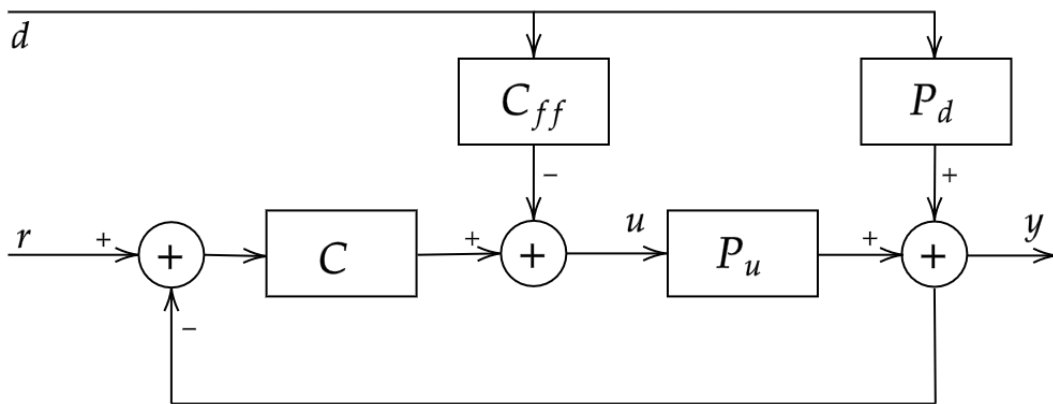
Figure 2.4. Feedforward control classic scheme.

The diagram is composed of the process model $P_u(s)$, the controller $C(s)$, the reference r, the process output y and the control signal u. There is also a measurable load disturbance d, and the model $P_d(s)$ describes the dynamics between this disturbance and the process output. The objective of the feedforward control $C_{ff}(s)$ is to compensate for the disturbance d at the system output y.

From the block diagram in Figure 2.4, the closed-loop transfer function relating the process output with the disturbance is given by:

$$T_{dy}(s) = \frac{P_d(s) - C_{ff}(s)P_u(s)}{1 + P_u(s)C(s)} \tag{2.6}$$

where a perfect elimination of the load disturbance is obtained when:

$$C_{ff}(s) = \frac{P_d(s)}{P_u(s)} \tag{2.7}$$

In this thesis, it is assumed that the two process transfer functions can be approximated by first-order systems with time delays (FOPDT), which is a classical choice in the process industry [90]. They are defined in Equation (2.8), where K_u and K_d are the static gains, T_u and T_d are the time constants, and L_u and L_d are the time delays.

$$P_u(s) = \frac{K_u}{T_u s + 1} e^{-L_u s} , \quad P_d(s) = \frac{K_d}{T_d s + 1} e^{-L_d s} \tag{2.8}$$

There are, of course, processes that are not well described by these transfer functions, but for process control applications, this structure is normally suitable, and it has become the standard model structure. In this thesis, the controller $C(s)$ is a PID controller with a transfer function defined in Equation (2.1).

Four possible feedforward structures, denoted as C_{ff}, can be considered:

Static gain: $\qquad\qquad\qquad C_{ff}(s) = K_{ff}$

Static gain with time delay: $\quad C_{ff}(s) = K_{ff} e^{-sL_{ff}}$

Lead-lag: $\qquad\qquad\qquad C_{ff}(s) = K_{ff} \dfrac{1 + sT_z}{1 + sT_p}$

Lead-lag with time delay: $\quad C_{ff}(s) = K_{ff} \dfrac{1 + sT_z}{1 + sT_p} e^{-sL_{ff}}$

where substituting the parameters from Equation (2.8) in Equation (2.7), $K_{ff} = K_d/K_u$, $T_z = T_u$, $T_p = T_d$ and $L_{ff} = L_d - L_u$, the lead-lag feedforward compensator becomes:

$$C_{ff}(s) = \frac{K_d}{K_u} \frac{1 + sT_u}{1 + sT_d} e^{-s(L_d - L_u)} \tag{2.9}$$

Implementing (2.9), a perfect feedforward compensation is applied. Nevertheless, if $L_d < L_u$, the optimal parameters give a non-causal feedforward compensator since L_{ff} becomes negative. This means that perfect feedforward is not possible in this case, and $L_{ff} = 0$ must be used. It is common to just have a static feedforward compensator in this case:

$$C_{ff}(s) = K_{ff} = \frac{K_d}{K_u} \tag{2.10}$$

where the effect of the disturbance in steady state is eliminated.

Other alternatives have been studied in the literature when implementing the ideal compensator is unreliable. The tuning rule that takes the delay inversion problem into account presented in [36] has been used along the thesis. This rule is based on setting the feedforward gain and time constant T_p in order to reduce the overshoot in the process output and minimize the IAE value. The compensator parameters are calculated as follows:

1. First, set $T_z = T_u$ and $L_{ff} = \max(0, L_d - L_u)$.

2. Then, T_p is calculated as:

$$T_p = \begin{cases} T_d & L_u - L_d \leq 0 \\ T_d - \dfrac{L_u - L_d}{1.7} & 0 < L_u - L_d < 1.7T_d \\ 0 & L_u - L_d \geq 1.7T_d \end{cases} \tag{2.11}$$

3. Finally, the compensator gain is determined as:

$$K_{ff} = \frac{K_d}{K_u} - \frac{K}{\tau_i} IE \qquad (2.12)$$

where:

$$IE = \begin{cases} K_d(T_u - T_d + T_p - T_z) & L_d \geq L_u \\ K_d(L_u - L_d + T_u - T_d + T_p - T_z) & L_d < L_u \end{cases}$$

2.1.4 Feedback Linearization

The fundamental idea of the linear feedback linearization technique [107] is to treat nonlinear systems as linear ones through algebraic transformations and feedback, as shown in Figure 2.5.
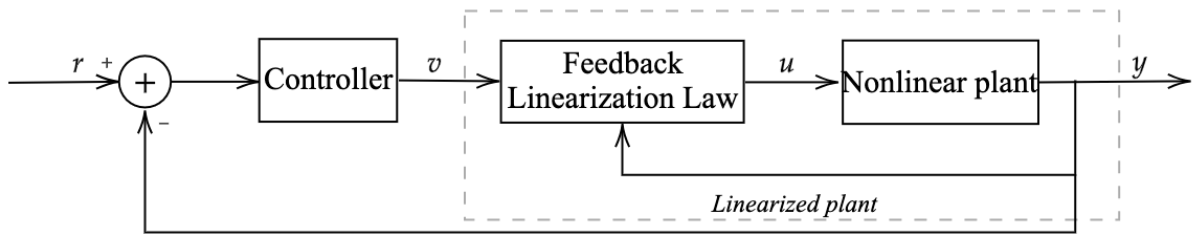
Figure 2.5. Feedback linearization classic scheme.

It taking into account that the gradient of a function $\varepsilon(x)$ (defined on a subset U of $\mathbb{R}^n$) is denoted as $d\varepsilon(x)$ and defined as an n-dimensional vector, where the i element is the partial derivative of ε concerning x_i, with $i = 1, 2, ..., n$:

$$d\varepsilon(x) = \left(\frac{\partial \varepsilon}{\partial x_1}, \frac{\partial \varepsilon}{\partial x_2}, ... \frac{\partial \varepsilon}{\partial x_n} \right) \qquad (2.13)$$

The function $L_f \varepsilon$ is defined as the Lie derivative of ε with respect to f and is given by:

$$d\varepsilon(x) = \frac{\partial \varepsilon}{\partial x} f(x) = \sum_n^{i=1} \frac{\partial \varepsilon}{\partial x_i} f_i(x) \qquad (2.14)$$

The resulting function from Equation (2.14) can also be applied to another function $g(x)$ as following:

$$L_g L_f \varepsilon(x) = \frac{\partial (L_f \varepsilon)}{\partial x} g(x) \qquad (2.15)$$

If ε is k times differentiable with respect to f, the function $L_f^k \varepsilon(x)$ satisfies the following recursion:

$$L_f^k \varepsilon(x) = \frac{\partial (L_f^{k-1} \varepsilon)}{\partial x} g(x) \qquad (2.16)$$

On the other hand, considering a nonlinear system with a single input u and an output y, in the form of:

$$x = f(x) + g(x)u \tag{2.17}$$

$$y = h(x)$$

The relative degree, r_d, of the system, around an operating point x^o is defined as the number of times that $y(t)$ needs to be differentiated at time $t = t^o$ to obtain $u(t^o)$. The relative degree of a system of the form in Equation (2.17) is determined by the following conditions:

$$L_g L_f^k h(x) = 0 \ \forall x \text{ around } x^o \text{ and } k < r_d - 1 \tag{2.18}$$

$$L_g L_f^{r_d - 1} h(x^o) \neq 0$$

The final goal of the feedback linearization technique is to perform a coordinate transformation of the nonlinear system such that the resulting system becomes linear in which a linear control can be applied. For this purpose, it is necessary that a convertible function $\Phi_i : \mathbb{R}^n \to \mathbb{R}^n$ exists in a region of the state spaces, such that $\Phi^{-1}(\Phi(x)) = x$ holds. That is to say, a diffeomorphism should exist globally (across the entire space defined by x) or locally (in the neighborhood of a given point). Starting from the system defined in Equation (2.17), it is possible to define Φ as a set of functions that define a coordinate transformation around x^o, given by:

$$\Phi(x) = \begin{bmatrix} \Phi_1(x) \\ \Phi_2(x) \\ . \\ . \\ \Phi_m(x) \end{bmatrix} = \begin{bmatrix} h(x) \\ L_f(x) \\ . \\ . \\ L_f^{r_d - 1} h(x) \end{bmatrix} \tag{2.19}$$

being

$$r_d \leq n.$$

The new coordinates, ψ, will be:

$$\psi_i = \Phi_i(x) L_f^{i-1} h(x) \ \ 1 \leq i \leq n. \tag{2.20}$$

Assuming $r_d = n$, which means a relative degree equal to the dimension of the state space of the system, the system from Equation (2.17) in state space for the coordinates ψ can be obtained as follows:

$$\frac{\partial \psi_i}{dt} = \frac{\partial \Phi}{\partial x} \frac{dx}{dt} = L_f h(x(t)) = \Phi_{i-1} = z_{i-1} \ \forall i < r_d$$

$$\frac{d\psi_{rd}}{dt} = \frac{\partial L_f^{r_d - 1} h(x)}{\partial x} (f(x(t)) + g(x(t))u)$$

$$L_f^{r_d} h(x(t)) + L_g L_f^{r_r - 1} h(x(t)) u(t) \ if \ i = r_d. \tag{2.21}$$

Asigning:

$$a(\psi) = L_g L_f^{r_d - 1} h(x(t)) = L_g L_f^{r_d} - 1 h(\Phi^{-1} h(\Phi^{-1}(t))) \tag{2.22}$$

$$b(\psi) = L_f^{r_d} h(c(t)) = L_f^{r_d} h(\Phi^{-1}(t))$$

The system in Equation (2.21) could be resumed in:

$$\dot{\psi}_i = \psi_{i-1}(t) \text{ if } i < r_d$$

$$\dot{\psi}_{rd} = b(\psi) + a(\psi u) \text{ if } i = r_d.$$

(2.23)

Choosing the control law in the coordinate space as follows ψ:

$$u = \frac{1}{\partial(\psi)}(-b(\psi) + v),$$

(2.24)

the closed-loop system in state space will be formed by the set:

$$\dot{\psi}_i = \psi_{i-1}(t) \text{ if } i < r_d$$

(2.25)

$$\dot{\psi}_{rd} = v \text{ if } i = r_d.$$

(2.26)

For a nonlinear system of the form in Equation (2.17), the output η in the new state space will be $\eta = h(\Phi^{-1})$. Therefore, the control law from Equation (2.24) in the coordinate space x will be:

$$u = \frac{1}{L_g L_f^{n-1} h(x)} - L_f^n h(x) + v$$

(2.27)

2.1.5 General Predictive Control

Model Predictive Control (MPC) is a control technique that belongs to a family of control methods aiming to optimize a specific criterion by utilizing a predictive model of the system's behavior to calculate a sequence of future control actions. MPC offers the flexibility to incorporate various models, objective functions, and constraints, making it suitable for addressing a wide range of operational requirements encountered in industrial processes. It combines optimal, stochastic, multivariable, and constrained control with time-delayed processes to effectively handle time-domain control problems [22, 79, 115]. MPC is particularly appealing to process control operators with limited control knowledge, as its concepts are intuitive, and tuning is relatively straightforward.

MPC offers the capability to control a wide range of processes, including those with simple dynamics, long delay times, non-minimum phase zeros, or unstable dynamics. It also provides a straightforward extension to multivariable plants and inherent compensation for dead time. Additionally, MPC naturally incorporates feedforward control to handle measured disturbances effectively. Dealing with constraints and tracking signals is simple and can be systematically integrated during the controller design. A nonlinear programming (NLP) problem arises for nonlinear constrained systems, although analytical solutions can be found in exceptional cases [126]. Without constraints, the controller for linear systems is a linear control law. However, a quadratic programming (QP) problem must be solved when constraints are present. MPC follows the strategy depicted in Figure 2.6 and adopts the structure shown in Figure 2.7. Among the various predictive control algorithms, GPC [23] is one of the most popular ones and the one used in this thesis.

GPC uses an internal model to generate future plant behavior predictions. The predictive control methodology relies on a controlled autoregressive integrated moving average model (CARIMA) [23]. This model takes the form of a polynomial equation involving input sequence $u(t)$, output sequence $y(t)$, time delay d, and zero-mean white noise $\epsilon(t)$. The polynomials
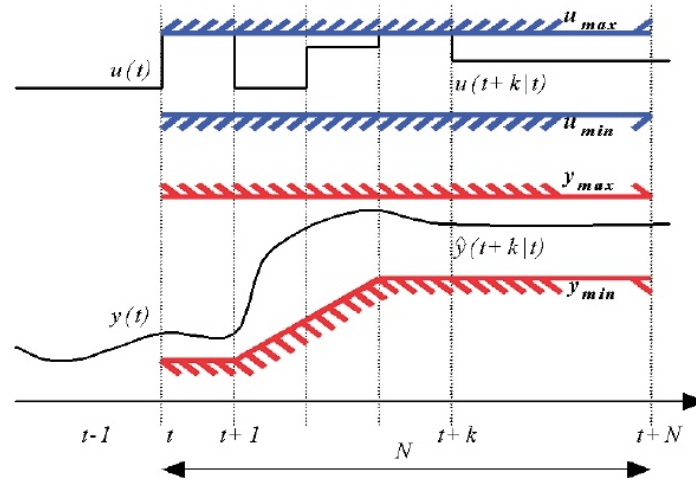
Figure 2.6. MPC strategy.
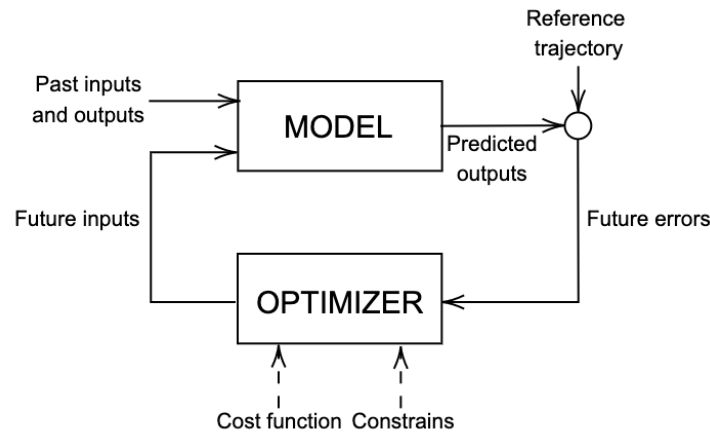
Figure 2.7. Basic MPC structure.

$A(z^{-1})$, $B(z^{-1})$, and $T(z^{-1})$ are expressed in terms of the backward shift operator z^{-1}, and they represent the dynamics of the system:

$$A(z^{-1})y(t) = z^{-d}B(z^{-1})u(t-1) + T_{pl}(z^{-1})\frac{\epsilon(t)}{\Delta} \tag{2.28}$$

$$A(z^{-1}) = 1 + a_1 z^{-1} + a_2 z^{-1} + \cdots + a_{n_a} z^{-n_a} \tag{2.29}$$

$$B(z^{-1}) = b_0 + b_1 z^{-1} + b_2 z^{-1} + \cdots + b_{n_b} z^{-n_b} \tag{2.30}$$

$$T_{pl}(z^{-1}) = 1 + t_1 z^{-1} + t_2 z^{-1} + \cdots + t_{n_t} z^{-n_t} \tag{2.31}$$

The choice of this model aims to achieve offset-free closed-loop behavior while accounting for non-stationary disturbances. The polynomial $T_{pl}(z^-1)$ is typically set to 1 in GPC formulations. To improve robustness, the $T_{pl} - polynomial$ is utilized as a design element, acting as a filter to attenuate prediction errors caused by high-frequency unmodeled dynamics and unmeasured load disturbances. Without modelling errors, the $T_{pl} - polynomial$ primarily affects disturbance rejection without significantly impacting the algorithm's set-point tracking capability. Consequently, T_{pl} can be adjusted as a design parameter to enhance robust stability [22, 115].

The GPC algorithm employs a quadratic cost function that considers the discrepancy between the predicted trajectory, a predefined reference, and the control effort. The cost function is expressed as follows:

$$J = E\left\{\sum_{j=N_1}^{N_2} \delta(j)[\hat{y}(t+j|t) - r(t+j)]^2 + \sum_{j=1}^{N_u} \Lambda(j)[\Delta u(t+j-1)]^2\right\} \quad (2.32)$$

where E represents the expectation, $\hat{y}(t+j|t)$ denotes an optimal prediction sequence of the system output based on available data up to time t, $\Delta u(t+j-1)]^2$ represents a sequence of future control increments derived from minimizing the cost function, N_1 and N_2 correspond to the minimum and maximum prediction horizons, N_u is the control horizon, and the weighting sequences $\delta(j)$ and $\Lambda(j)$ are used to penalize future tracking errors and control efforts, respectively. The prediction horizons, control horizons, and weighting sequences are design parameters that can be adjusted to fine-tune the controller. The reference trajectory $r(t+j)$ can be either the set-point or a smooth approximation starting from the system output $y(t)$ current value and gradually converging towards the known reference using a first-order system.

The control increments computed by the GPC approach are determined by minimizing the quadratic function from Equation (2.32) given by:

$$J = \delta(y-r)^\top (y-r) + \Lambda \Delta u^\top \Delta u \quad (2.33)$$

The sequence of future predictions consists of both the free and forced responses, expressed as:

$$y = G\Delta u + f \quad (2.34)$$

where matrix G contains the coefficients of the system's open-loop step response and f includes terms that depend on present and past plant outputs and past inputs. The optimization process is performed by substituting the sequence of future outputs (2.34) into the cost function (2.33) to determine the optimal control increments that minimize the specified quadratic cost:

$$J = \frac{1}{2}\Delta u^\top H \Delta u + b^\top \Delta u + f_0 \quad (2.35)$$

with $\delta(j) = \delta$, $\Lambda(j) = \Lambda$, $H = 2(\delta G^\top G + \Lambda I)$, $b^\top = 2\delta(f-r)^\top G$, $f_0 = \delta(f-r)^\top(f-r)$. The optimum solution without constraints is linear and given by:

$$\Delta u = -H^{-1}b$$

When constraints are considered, a linear solution is unavailable, and the problem becomes a quadratic programming task. A quadratic cost function with linear inequality and equality constraints is used, expressed as $\Delta u \leq c$ and $\Delta u = a$ for the control increment Δu. The specific constraints considered are outlined in Table 2.1 [22]. In this table, Γ represents an $N - dimensional$ vector ($N = N_2 - N_1$ being the length of the receding horizon) with all elements equal to one, Υ is an $N \times N$ lower triangular matrix with all elements equal to one, and T_m denotes the sampling time.

Variable	Lineal Constraint
Control signal amplitude $u_{min} \leq u(t) \leq u_{max} \; \forall t$	$\Gamma u_{min} \leq \Upsilon \Delta u + u(t-1)\Gamma \leq \Gamma \, u_{max}$
Control signal increment $\Delta u_{min} \leq u(t) - u(t-1) \leq \Delta u_{max} \forall t$	$\Gamma \Delta u_{min} \leq \Delta u \leq \Gamma \Delta u_{max}$
Output signal amplitude $y_{min}(t) \leq y(t) \leq y_{max}(t)$	$\Gamma \, y_{min} \leq G \Delta u + f \leq \Gamma \, y_{max}$
Envelope constraints $y_{min}(t) \leq y(t) \leq y_{max}(t)$	$G \Delta u \leq y_{max} - f, \; y_{max} = [y_{max}(t+1) \cdots$ $\cdots y_{max}(t+N)]$ $G \Delta u \leq y_{min} - f, \; y_{min} = [y_{min}(t+1) \cdots$ $\cdots y_{min}(t+N)]$
Output overshoot $y(t+j) \leq \gamma r(t) j = N_{o1}, \cdots, N_{o2}$	$G \Delta u \leq \Gamma \gamma r(t) - f$
Output monotone behavior $y(t+j) \leq y(t+j+1) \; if \; y(t) < r(t)$ $y(t+j) \geq y(t+j+1) \; if \; y(t) > r(t)$	$G \Delta u + f \leq \left[\frac{0^\top}{G'} \right] \Delta u + \left[\frac{y(t)}{f'} \right]$ G' and f' are the result of eliminating the first row of G and f.
Limit inverse response $y(t+j) \leq y(t) \; if \; y(t) > r(t)$ $y(t+j) \geq y(t) \; if \; y(t) < r(t)$	$G \Delta u \geq \Gamma y(t) - f$
Final state $y(t+N+1) \cdots y(t+N+m_t) = r$	$y_m = [y(t+N+1), \cdots, y(t+N+m_t)]^\top$ $y_m = G_m \Delta u + f_m, G_m \Delta u = w_m - f_m$
Output integral $T_m \sum_{j=t+1}^{j=t+N_i} y(t+j) = I$	$[y(t+1) \cdots y(t+N_i)]^T \Gamma = G_i \Delta u + f_i \geq I$

Table 2.1. GPC constraints list.

2.1.6 Quantitative Feedback Theory

Most control strategies are based on a mathematical model that simulates the dynamic behavior of the processes to be controlled, which is used for designing the controller. Therefore, the effectiveness of a control system largely depends on how well this mathematical model represents the real process dynamics. In the field of automatic control, the most commonly used models for design purposes are deterministic models, which do not account for possible errors or modelling uncertainties. However, in some cases, these models may not provide sufficient information to control a system properly, needing the use of robust control techniques that consider uncertainties during the design phase.

In this context, industrial processes can be highly complex to accurately describe by a mathematical model, leading to modelling errors [114]. Thus, any mathematical model will inherently have uncertainties or modelling errors to some extent. To efficiently design an appropriate controller, it is necessary to have information about potential sources of uncertainty and evaluate their effects on the overall system behavior.

The field of application for robust control contains all problems characterized by considering model uncertainties that a fixed linear time-invariant controller can tolerate. In robust control, the technique that considers uncertainties most accurately during the design phase is the QFT methodology [114]. QFT is a powerful design technique that allows for achieving performance and stability tolerances over a range of uncertain plants. It is a frequency-domain-based design methodology that uses the Nichols chart to achieve the desired robust design over a specific region of plant uncertainty. The objective is to design a compensator $C(s)$ and a prefilter $F(s)$ (if necessary), as shown in Figure 2.8, such that the performance and stability specifications are met for a family of plants $\mathcal{P}(s)$. This family can be considered as a set of plants $P(s)$ with parametric uncertainty (although QFT also supports non-parametric uncertainty), such as described by Equation (2.36).
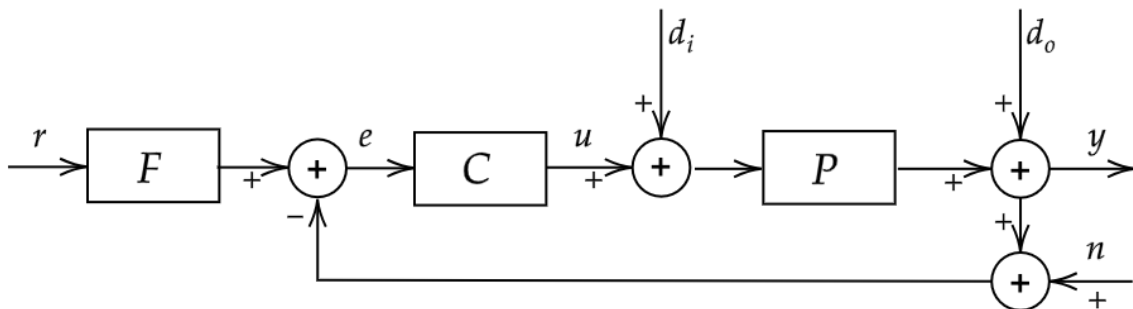
Figure 2.8. Two-degree-of-freedom feedback system.

$$\mathcal{P}(s) = \Big\{ \kappa \frac{\mathcal{P}_{i=1}^{n_r}(s + \ell_i)\mathcal{P}_{j=1}^{m_r}(s^2 + 2\beta_j\omega_{0j} + \omega_{0j}^2)}{s^{N_r}\mathcal{P}_{r=1}^{a_r}(s + \zeta_r)\mathcal{P}_{s=1}^{b_r}(s^2 + 2\beta_s\omega_{0s} + \omega_{0s}^2)} : \qquad (2.36)$$
$$\kappa \in [\kappa_{min},\ \kappa_{max}],\ \ell_i \in [\ell_{i,min},\ \ell_{i,max}],\ \zeta_r \in [\zeta_{r,min},\ \zeta_{r,max}],$$
$$\beta_j \in [\beta_{j,min},\ \beta_{j,max}],\ \omega_{0j} \in [\omega_{0j,min},\ \omega_{0j,max}],$$
$$\beta_s \in [\beta_{s,min},\ \beta_{s,max}],\ \omega_{0s} \in [\omega_{0s,min},\ \omega_{0s,max}],$$
$$n_r + m_r < a_r + b_r + N_r \Big\}$$

The QFT technique uses plant uncertainty and a set of specifications as quantitative information. The two-degree-of-freedom compensator $\{F, C\}$ (hereafter, the variable s will be omitted when necessary for clarity) must be designed so that plant behavior variations due to uncertainty are within a specific tolerance margin in a closed loop. A typical QFT design consists of the following steps:

1. *Specifications definition.* The model of the plant with uncertainty is obtained, and a set of design frequencies is selected based on the system's bandwidth, $\Omega = \omega_1, \omega_2, ..., \omega_k$. Specifications for stability, tracking, input and output disturbances, noise, and control effort are defined for each frequency, and the nominal plant P_0 is selected.

2. *Templates calculation.* Quantitative information about the uncertainties is represented by a set of points on the Nichols chart. This set of points is called templates and graphically defines the uncertainty for each design frequency ω. Figure 2.9 shows an example of a system given by the transfer function $P_u(s) = K_u/s(s + a)$, with $K_u \in [1, 10]$ and $a \in [1, 10]$ for the frequency set $\Omega = \{0.5, 1, 2, 38, 15, 30, 60, 90, 120, 180\}rad/s$.

3. *QFT boundaries calculation*. The specifications set in the first step are transformed for each frequency ω into prohibited regions on the Nichols chart for the transfer function $L_0(j\omega) = C(j\omega)P_0(j\omega)$. These regions are defined by limits called boundaries. Each specification is translated to each frequency as a different boundary, so each set of boundaries for a particular frequency is dealt with to obtain a single prohibited zone for that frequency. Figure 2.10 shows the L_0 design for the previous example.

4. *Controller design (loop shaping)*. This step involves designing the controller such that the transfer function $L_0(j\omega) = C(j\omega)P_0(j\omega)$ satisfies the calculated "boundaries" from the previous step.

5. *Pre-filter synthesis*. The filter $F(s)$ is designed so that the closed-loop transfer function from the reference to the output satisfies the design specifications for reference tracking. Therefore, the variations of the closed-loop system must be within the desired range, as shown in Figure 2.11.

6. *Validation of the design*. Finally, the closed-loop control system is validated to ensure it satisfies all the specifications given in the first step for the entire set of plants and frequencies within the bandwidth.
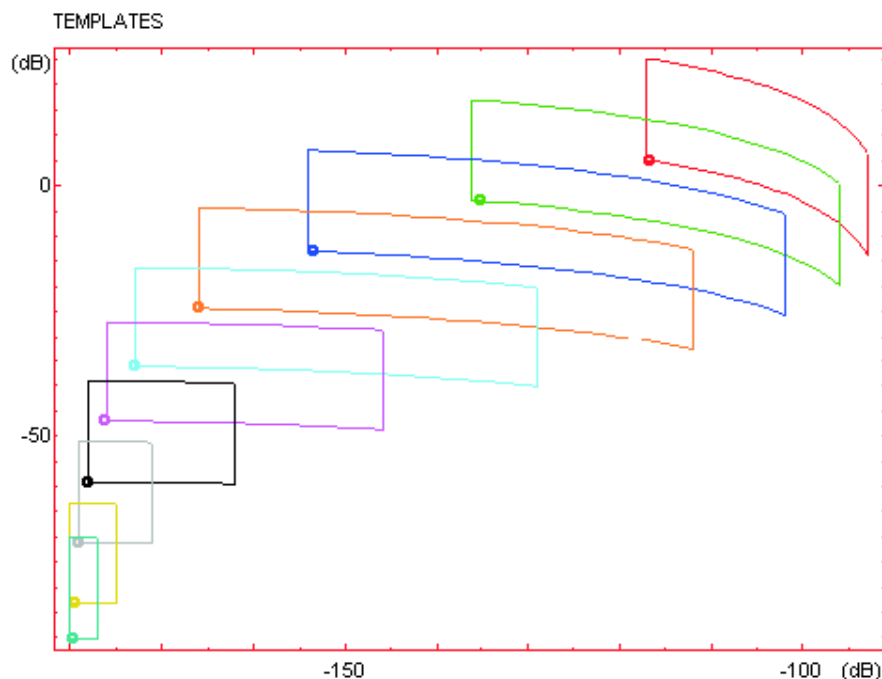

Figure 2.9. QFT templates calculation.

Time domain specifications

The closed-loop specifications for the system in Figure 2.8 are defined in terms of the input or the output. Both must be bounded to ensure the uncertain system operates within a specific range. For example:
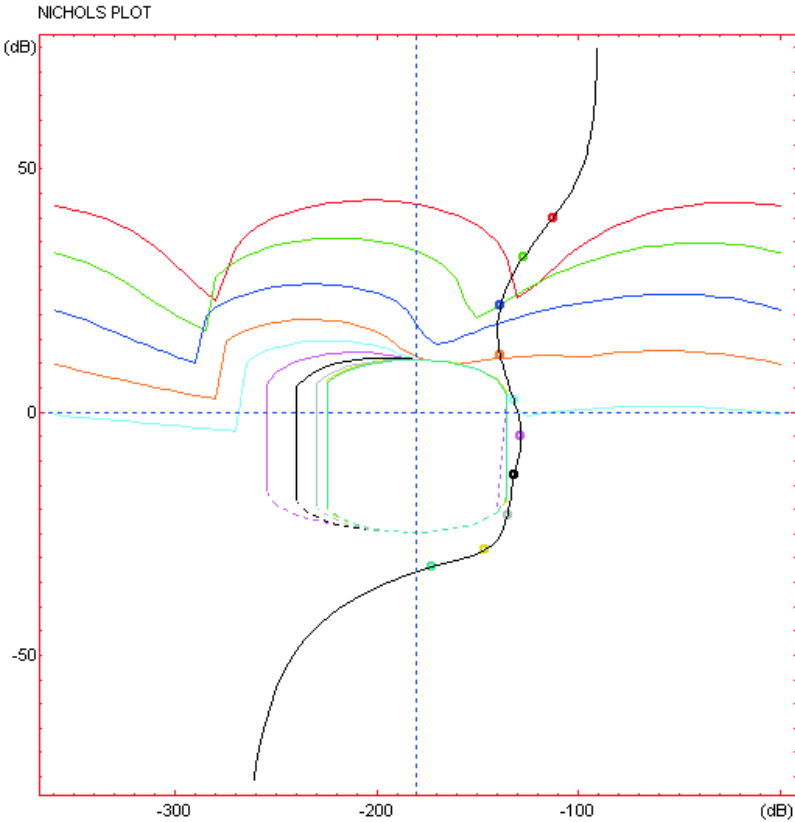
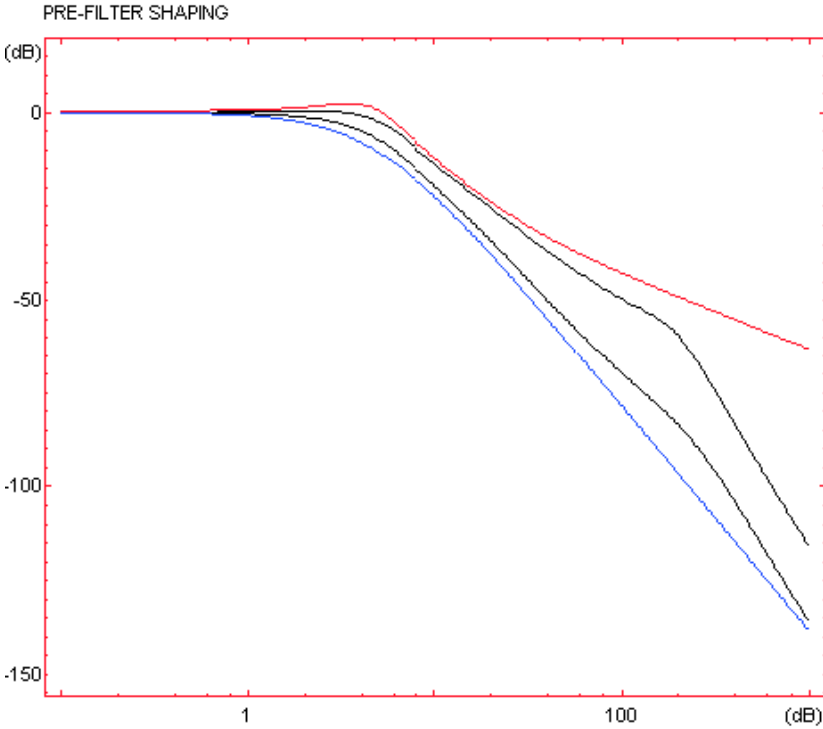Figure 2.10. QFT boundaries calculation.

Figure 2.11. QFT filter adjustment.

1. In a regulation problem, the objective is to have the system output close to 0 or a specific operating point. In this case, the time domain specifications should be defined with operating regions where the goal is to have the plant output close to 0 or the specific operating point (Figures 2.12a and 2.12b).

2. In a tracking problem, the plant output should follow the input reference with specific characteristics within the time domain. Figure 2.12c shows an example of the specific region where the system output should remain.

Frequency domain specifications

The closed-loop specifications for the system in Figure 2.8 are typically defined in terms of inequalities in the closed-loop transfer function of the system, as shown in Equations (2.37)-(2.42).

1. Disturbances rejection at the plant output:

$$\left| \frac{y}{d_0} \right| = \left| \frac{1}{1 + P(j\omega)C(j\omega)} \right| \leq \delta_{do}(\omega) \; \forall \; \omega > 0, \; \forall \; P \in \mathcal{P} \qquad (2.37)$$

2. Disturbances rejection at the plant input:

$$\left| \frac{y}{d_i} \right| = \left| \frac{P(j\omega)}{1 + P(j\omega)C(j\omega)} \right| \leq \delta_{di}(\omega) \; \forall \; \omega > 0, \; \forall \; P \in \mathcal{P} \qquad (2.38)$$

3. Stability:

$$\left| \frac{y}{rF} \right| = \left| \frac{P(j\omega)C(j\omega)}{1 + P(j\omega)C(j\omega)} \right| \leq S_{lim} \; \forall \; \omega > 0, \; \forall \; P \in \mathcal{P} \qquad (2.39)$$

4. Tracking:

$$B_l(\omega) \leq \left| \frac{y}{r} \right| = \left| \frac{F(j\omega)P(j\omega)C(j\omega)}{1 + P(j\omega)C(j\omega)} \right| \leq B_u(\omega) \; \forall \; \omega > 0, \; \forall \; P \in \mathcal{P} \qquad (2.40)$$

5. Noise rejection:

$$\left| \frac{y}{n} \right| = \left| \frac{P(j\omega)C(j\omega)}{1 + P(j\omega)C(j\omega)} \right| \leq \delta_n(\omega) \; \forall \; \omega > 0, \; \forall \; P \in \mathcal{P} \qquad (2.41)$$

6. Control effort:

$$\left| \frac{u}{n} \right| = \left| \frac{C(j\omega)}{1 + P(j\omega)C(j\omega)} \right| \leq \delta_{ce}(\omega) \; \forall \; \omega > 0, \; \forall \; P \in \mathcal{P} \qquad (2.42)$$

For the specifications given in equations (2.37), (2.38), and (2.40), small arbitrarily chosen specifications can be achieved by designing the controller C such that $|C(j\omega)| \rightarrow \infty$. Therefore, with a slight deviation from the operating point due to some disturbance and sensitivity close to zero, the control system becomes more independent of the plant uncertainty. To achieve an increase in $|C(j\omega)|$, it is necessary to increase the cutoff frequency (the frequency in rad/s at which the magnitude of the open-loop transfer function $L_0(j\omega) = P_0(j\omega)C(j\omega)$ is 0 dB in the system). Therefore, to achieve small arbitrary specifications, increasing the system's bandwidth is necessary. In this context, the control effort is defined from the noise sensor input n to the control signal u.
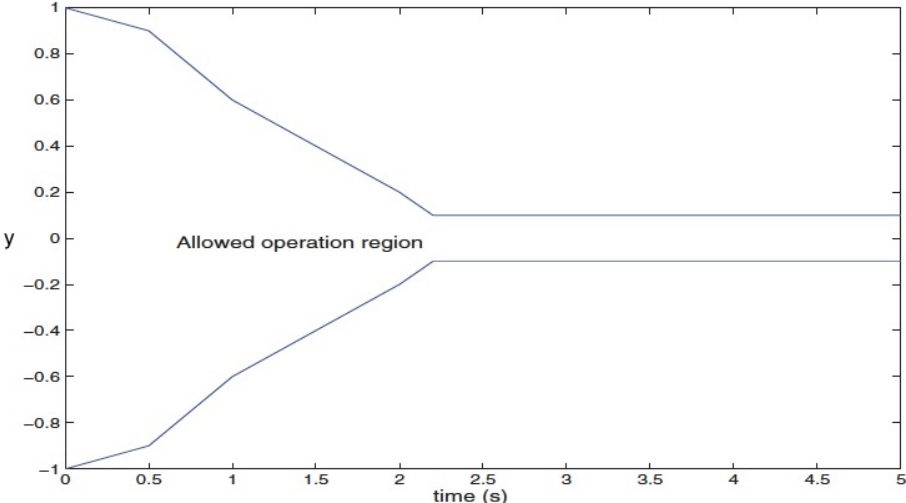
(a) Regulation problem.
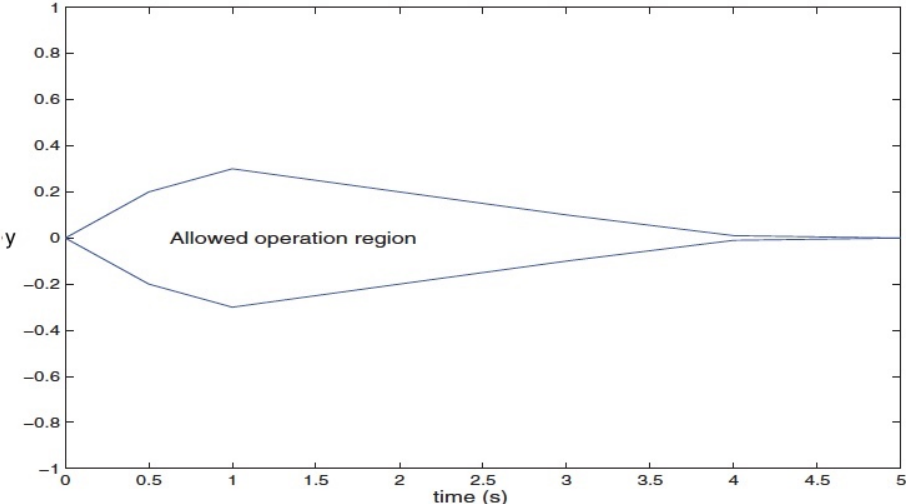
(b) Regulation problem for other initial conditions.
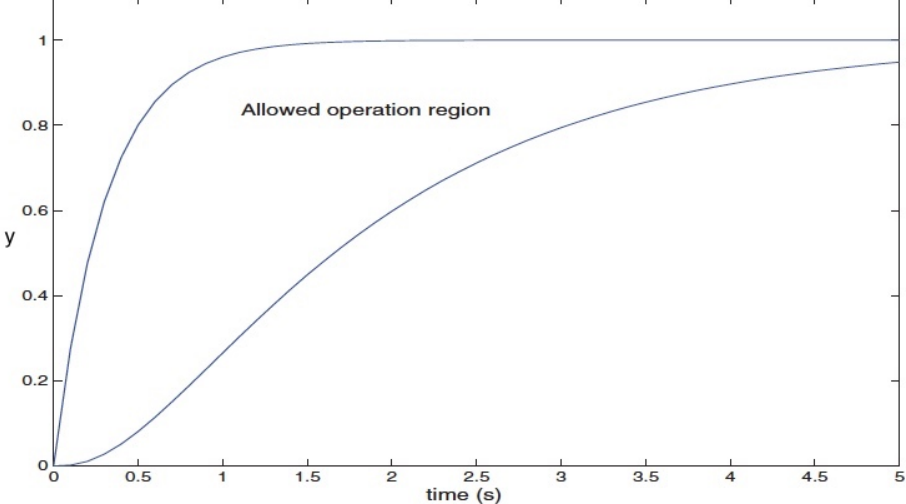
(c) Tracking problem.

Figure 2.12. Time domain specifications examples.

On the other hand, increasing the value of the controller $|C(j\omega)|$ poses a problem in terms of the control effort and sensor specification for disturbance rejection, as increasing the bandwidth will make the sensor noise affect the system more. A balance must be achieved among all the specifications. The stability specification is related to the relative stability margins: phase margin and gain margin.

Translation of specifications from the time domain to the frequency domain

As mentioned earlier, the design in QFT is conducted in the frequency domain, so it is necessary to transfer the specifications defined in the time domain to the frequency domain. One way to do this, for example, for tracking problems, is by assuming a model of the closed-loop transfer function between the reference signal r and the output signal y, denoted as $T_{ry}(s)$, and searching for parameter values that satisfy the limits defined in the time domain for the system's output.

As an example, a first-order system given by $P_u(s) = K_u/(s + a)$ is considered. When the reference signal $r(t)$ is a unit step function, the system's output is defined as $y(t) = (K_u/a)(1 - e^{-at})$. Therefore, to achieve $y(t) = r(t)$ for a sufficiently long time t, the value of K_u must be set to $K_u = a$. For a first-order model, $T_u = 1/a = a/\omega_b$ represents the time constant. Generally, a higher bandwidth leads to a faster response to the system's output.

Controller design

The goal is to design a two-degree-of-freedom controller $\{F, C\}$ as shown in Figure 2.8 in order to satisfy all the previously defined specifications and achieve closed-loop stability for the entire plant P in $\mathcal{P}$. The specifications are translated from the time domain to the frequency domain using circles in the Nyquist Chart, which define the allowed regions for the function $L_0(j\omega) = P_0(j\omega)C(j\omega)$. The allowed region is the exterior of the circles in equations (2.37)-(2.41) and the interior for equation (2.42). Combining the allowed regions generated for all specifications of each function L_0 corresponding to each plant P in $\mathcal{P}$, a set of constraints is obtained at each frequency ω for the controller C. The boundaries of these regions, represented in the Nichols Chart, are called boundaries. These frequency-domain limits can be formulated for both the controller C and the function $L_0(j\omega) = P_0(j\omega)C(j\omega)$ for any nominal plant P_0.

2.2 Experimental Facilities

This section presents the different experimental plants used in this thesis. Each plant is described in detail, including its characteristics and modelling approach. Furthermore, various control strategies have been implemented and tested in each plant, aiming to optimize the plant's performance and achieve the desired objectives. The details of these control strategies will be thoroughly discussed in Chapter 4, highlighting their effectiveness and applicability to specific industrial contexts. By analyzing and comparing the results obtained from different plants, valuable insights and recommendations can be drawn, contributing to improve control systems in industrial facilities.

2.2.1 Raceway Reactors for Microalgae Production

Raceway photobioreactors have been studied since 1950 with the aim of providing a solution for the industrial-scale cultivation of microalgae. Nowadays, due to their scalability and feasibil-

ity, they are considered the most suitable technology for the industrial cultivation of microalgae. The popularity of raceway reactors stems from their low initial investment cost compared to other technologies, such as tubular photobioreactors, which require more complex structures and equipment. Other relevant advantages of raceway reactors include their simplicity of operation and low maintenance costs.

There are mainly two types of reactors: closed tubular and open raceway. The most commonly used are raceway reactors, mainly due to their lower initial investment cost than tubular reactors, which require more complex structures and equipment. Raceway photobioreactors have been studied since the 1950s to provide a solution for large-scale microalgae cultivation. Today, due to their scalability and feasibility, they are considered the most suitable technology for large-scale microalgae cultivation. Other relevant advantages of raceway reactors are their simplicity of operation and low maintenance costs [137]. Numerous studies have focused on the optimal selection of design and configuration of raceway photobioreactors to ensure optimal conditions for microalgae growth. Currently, numerous designs of photobioreactors vary slightly from the original design proposed by Oswald and Golueke [94], who suggested the optimal growth conditions [101].

Several studies have focused on the optimal selection of design and configuration for raceway photobioreactors to ensure optimal growth conditions for microalgae. Currently, various designs of raceway photobioreactors differ slightly from the original design proposed by Oswald and Golueke [95], which ensures optimal growth conditions. Despite the abundance of reactor structure designs, the core work remains the same, and a multitude of similar factors must be achieved to obtain the desired biomass production, all of which are related to variables that influence the growth process [101]. The three main parts of a raceway reactor are the loop, the sump and the paddle wheels, as shown in Figure 2.13.
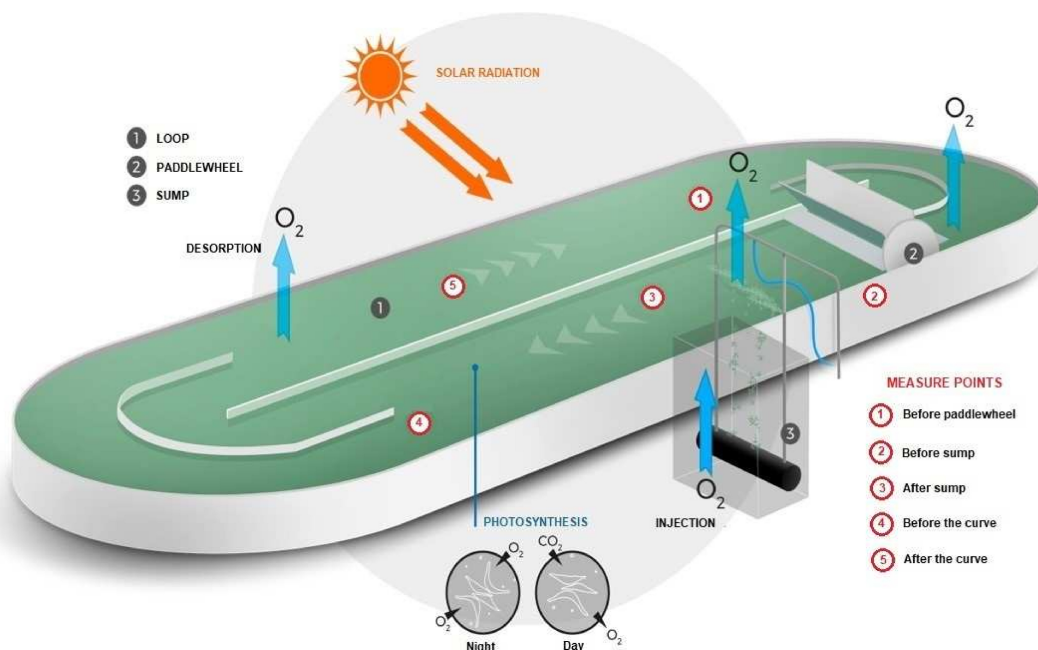

Figure 2.13. Raceway recator scheme.

These biological systems exhibit complex dynamics that pose challenges in modelling and control [64]. In recent years, various biological models of microalgae have been developed. In [15], a model captures the effect of temperature and light on microalgae growth, thus predicting its productivity. In [119], a microalgae-bacteria model is developed and validated based on the respiration and photosynthesis ratios in wastewater treatment processes with microalgae. Similarly, in [7], photosynthetic efficiency is improved by optimizing the light and dark regimes to which the cells are exposed. Furthermore, models based on first principles have also been developed, as shown in [27]. In [113], a new temperature model is obtained that determines the evolution of the culture temperature based on reactor design and external conditions, which was used for indirect temperature control in [32].

As indicated in [24], the most important variables affecting microalgae growth are medium temperature, solar radiation, pH, and dissolved oxygen. Additionally, the photosynthetic response of microalgae to solar radiation depends on many other variables, making the system highly complex [28]. For raceway reactors, the system's architecture generally determines the requirements for solar radiation incidence and temperature operating conditions. Therefore, the variables to be controlled in this type of reactor are pH and dissolved oxygen. Both variables have a highly dynamic nature dependent on the photosynthesis process, and it is necessary to maintain them close to desired operating points [102]. Between these two variables, pH is the most crucial variable to control as it directly influences proper photosynthesis. This variable exhibits strongly nonlinear dynamics, affected by CO_2 injection into the medium and CO_2 consumption during photosynthesis. CO_2 plays a vital role in the final biomass production of microalgae, as approximately half of the biomass consists of carbon. The demand for CO_2 in raceway reactors can be met in various ways and is mainly characterized by the source of CO_2 used. Carbon dioxide can be obtained from the atmosphere, supplied as a pure gas, or provided through flue gas. In the first case, growth is carbon-limited, as only 5% of the required carbon for the culture is directly transferred from the atmosphere. On the other hand, the most effective transfer yield is obtained from pure carbon dioxide.

The microalgae raceway reactor used in this thesis is located at the IFAPA center, close to the University of Almería, Spain (Figure 2.14). It is composed of two 50 m long and 1 m wide channels connected by a U-shaped bend, providing a total surface of 100 m^2. As recommended by [83], the reactor is operated at a constant liquid height of 0.15 m in order to reduce dark zones. The total reactor volume is 15 m^3. The reactor flow is driven by a paddlewheel made up of 8 aluminum blades of 1.5 m diameter, controlled by an electric motor. Its speed is set at 2 m/s. Carbonation is carried out in a sump of 1 m depth, 0.65 m length, and 1 m width. It is located at 1.8 m downstream of the paddlewheel. The microalgae strain used for the experiments in this thesis corresponds to *Scenedesmus almeriensis*. This type of microalgae is characterized by a high growth rate, withstanding temperatures of up to 45 °C, and pH values ranging from 7 to 10. Optimum growth conditions are 30 °C and a pH value around 8.

Model Description

The dynamic models for microalgae production in raceway reactors from [15, 28, 64, 113, 119] are combined and implemented as the kernel of the tool developed in this thesis and described in Chapter 4. The models consider fluid-dynamic, mass transfer and biological phenomena taking place in the reactor. Notice that all these models were properly validated using real data at an industrial scale in previous works.

Figure 2.14. Microalgae raceway reactor located at the IFAPA center, close to the University of Almería.

Regarding the biological model, oxygen production is directly related to biomass production. The model can be represented by (2.43).

$$PO_2 = PO_2(I_{av}) \cdot \overline{PO_2(X_r)} \cdot \overline{PO_2(pH)} \cdot \overline{PO_2(DO)} \tag{2.43}$$

The oxygen productivity is composed by four terms: photosynthesis rate $PO_2(I_{av})$, temperature effect $\overline{PO_2(X_r)}$, pH effect $\overline{PO_2(pH)}$ and dissolved oxygen effect $\overline{PO_2(DO)}$. The photosynthesis rate term is a quantitative factor that represents the oxygen production per unit of biomass and time $[kg_{O_2} \; kg^{-1} \; s^{-1}]$, whereas the rest of the terms are dimensionless and normalized factors with values between 0 and 1.

The photosynthesis rate is defined in Equation (2.44) as the oxygen production rate per biomass unit. It is calculated as a function of the following microalgae strains biological parameters: maximum photosynthesis rate under culture conditions $P_{O_2,max}$ $[kg \, O_2 \, kg^{-1}s^{-1}]$, the form exponent $n \, [-]$, the minimum light need by microalgae to achieve maximum photosynthesis I_k $[\mu \, \mathrm{E} \, \mathrm{m}^{-2} \, \mathrm{s}^{-1}]$ and the average irradiance, I_{av} $[\mu \, \mathrm{E} \, \mathrm{m}^{-2} \, \mathrm{s}^{-1}]$. The average irradiance integrates the local irradiance values alongside culture depth over the total volume of the culture in the reactor, and it is calculated according to Equation (2.45). The equation is based on the incident radiation I_0 $[\mu E \, m^{-2} \, s^{-1}]$ on the total surface of the reactor, the biomass concentration C_b $[g \, L^{-1}]$, the biomass light attenuation K_a $[m^2 \, g^{-1}]$ and the culture depth $h \, [m]$. Notice that the biomass concentration varies with time, t, and position along the reactor channel, x.

$$PO_2(I_{av}) = \frac{P_{O_2,max} I_{av}^n}{I_k^n + I_{av}^n} \tag{2.44}$$

$$I_{av}(t,x) = \frac{I_0(t)}{K_a C_b(t,x) h} \left(1 - e^{-K_a C_b(t,x) h} \right) \tag{2.45}$$

In Equation (2.43), a cardinal model is used where the values of the variable only exist on a range between the maximum and minimum tolerable values, with a Gaussian form [84, 85]. According to this model, the contribution to oxygen productivity from temperature and pH variables is defined by Equations (2.46) and (2.47), respectively. The temperature term $\overline{PO_2(X_r)}$ depends on the maximum $X_{r,max}$, minimum $X_{r,min}$, optimal $X_{r,opt}$ temperatures for the selected strain and on the current culture temperature, X_r. In the same way, the term for pH $\overline{PO_2(pH)}$ depends on the maximum pH_{max}, minimum pH_{min}, optimal pH_{opt} of the selected strain and the current pH value. For the dissolved oxygen term, a model considering inhibition by product [24] is used, as shown in (2.48). It depends on the actual dissolved oxygen value DO, the maximum $DO_{2,max}$ for the selected strain, and on a form parameter m_f.

$$\overline{PO_2(X_r)} = \frac{(X_r - X_{r,max})}{(X_{r,opt} - X_{r,min})} \cdot$$
$$\cdot \frac{(X_r - X_{r,min})^2}{\left((X_{r,opt} - X_{r,min})(X_r - X_{r,opt}) - (X_{r,opt} - X_{r,max})(X_{r,opt} + X_{r,min} - 2X_r)\right)} \tag{2.46}$$

$$\overline{PO_2(pH)} = \frac{(pH - pH_{max})}{(pH_{opt} - pH_{min})} \cdot$$
$$\cdot \frac{(pH - pH_{min})^2}{\left((pH_{opt} - pH_{min})(pH - pH_{opt}) - (pH_{opt} - pH_{max})(pH_{opt} + pH_{min} - 2pH)\right)} \tag{2.47}$$

$$\overline{PO_2(DO)} = 1 - \left(\frac{DO}{DO_{max}}\right)^{m_f} \tag{2.48}$$

The temperature model implemented in the software was developed in [113]. Equation (2.49) shows the thermal balance in the reactor.

$$\frac{dX_r}{dt} = \frac{Q_{irradiance} + Q_{radiation} + Q_{evaporation} + Q_{convection} + Q_{inlet} - Q_{outlet}}{h \cdot A \cdot C_p \cdot \rho} \tag{2.49}$$

The temperature of the culture in the reactor X_r $[^{\circ}C]$ depends on the heat flow from sunlight $Q_{irradiance}$ $[W]$, the heat flow from long-wave radiation $Q_{radiation}$ $[W]$, the convection heat flow $Q_{convection}$ $[W]$, the heat flow between the reactor and the layer under it through the conduction process $Q_{conduction}$ $[W]$, the heat added when the medium is supplied to the reactor Q_{inlet} $[W]$, the heat subtracted when the medium is removed from the reactor Q_{outlet} $[W]$, the culture depth h $[m]$, the reactor surface A $[m^2]$, the specific heat capacity of the culture C_p $[J\,kg^{-1}\,^{\circ}C^{-1}]$, and the density of the culture ρ $[kg\,m^{-3}]$. A detailed description of this model can be found in [113].

Regarding the engineering model, the reactor is divided into two main parts: channel and sump. Constant velocity v_r $[m\,s^{-1}]$ and liquid height h $[m]$ is assumed, so the volumetric flow rate of the liquid Q_{liq} $[m^3\,s^{-1}]$ is defined as the multiplication of the cross-sectional area of the channel and velocity (where w represents the reactor width). Mass balances have been applied to each reactor section in liquid and in gas phases. In this paper, for the sake of simplicity, only mass balances in the liquid phase are presented (Equations (2.50)-(2.55)). Mass balances in the gas phase are described in [28].

Chapter 2. Material and Methods

In the liquid phase, three main components are taken into account: biomass concentration $C_b \, [kg \, m^{-3}]$, dissolved oxygen $[O_2] \, [\%]$ and total inorganic carbon concentration $[C_T] \, [mol \, m^{-3}]$. For each section of the reactor, mass balances with these three components are defined.

For the channel, the proposed balances are shown in Equations (2.50) to (2.52). The oxygen mass transfer is a function of the volumetric coefficient for oxygen into the channel $K_{laO_{2c}} \, [s^{-1}]$ and the logarithmic driving force. The carbon dioxide mass transfer is calculated in the same way, using instead the volumetric mass transfer for carbon dioxide into the channel $K_{laCO_{2c}} \, [s^{-1}]$. The variables used in these equations are: the oxygen photosynthesis rate $P_{O_2} \, [kgO_2 \, kg^{-1} \, s^{-1}]$, the carbon dioxide photosynthesis rate $P_{CO_2} \, [kgCO_2 \, kg^{-1} \, s^{-1}]$, the biomass yield coefficient $Y_{b/O_2} \, [kg]$, the molecular weight of the oxygen $M_{O_2} \, [g \, mol^{-1}]$, carbon dioxide $M_{CO_2} \, [g \, mol^{-1}]$, the equilibrium concentration with gas phase for oxygen $[O_2^*] \, [mol \, m^{-3}]$ and the equilibrium concentration with gas phase for dioxide carbon $[CO_2^*] \, [mol \, m^{-3}]$.

$$\frac{\partial C_b(t,x)}{\partial t} = -whv_r \frac{\partial C_b(t,x)}{\partial x} + whP_{O_2}(t,x)C_b(t,x)Y_{b/O_2} \tag{2.50}$$

$$wh\frac{\partial [O_2](t,x)}{\partial t} = -whv_r \frac{\partial [O_2](t,x)}{\partial x} +$$
$$+ wh\frac{P_{O_2}(t,x)C_b(t,x)}{M_{O_2}} + whK_{laO_{2c}}([O_2^*](t,x) - [O_2(t,x)]) \tag{2.51}$$

$$wh\frac{\partial [C_T](t,x)}{\partial t} = -whv_r \frac{\partial [C_T](t,x)}{\partial x} +$$
$$+ wh\frac{P_{CO_2}(t,x)C_b(t,x)}{M_{CO_2}} + whK_{laCO_{2c}}([CO_2^*](t,x) - [CO_2(t,x)]) \tag{2.52}$$

Analogous mass balances are applied to the sump, where the air and carbon dioxide are injected. Equations (2.53) to (2.55) show the corresponding balances. In these equations, the volume of each section $V_s \, [m^3]$ is corrected by a gas hold-up (ε_s) to determine the right liquid volume in each section. The terms of the volumetric flow rate of the liquid $Q_{liq} \, [m^3 \, s^{-1}]$ and the volumetric flow rate of culture medium $Q_m \, [m^3 \, s^{-1}]$ are also included. The constants included in this equation are, the dissolved oxygen $[O_2]_m \, [mol \, m^{-3}]$ and the total inorganic carbon in the medium $[C_T]_m \, [mol \, m^{-3}]$.

$$\frac{dC_{b,out}(t)}{dt} = -\frac{Q_{liq}}{V_s(1 - \varepsilon_s(t))}(C_{b,out}(t) - C_{b,in}(t)) +$$
$$+ P_{O_2}(t)C_{b,in}(t)Y_{b/O_2} - \frac{Q_m}{V_s(1 - \varepsilon_s(t))}C_{b,out}(t) \tag{2.53}$$

$$\frac{d[O_2]_{out}(t)}{dt} = -\frac{Q_{liq}}{V_s(1 - \varepsilon_s(t))}([O_2]_{out} - [O_2]_{in}(t)) + \frac{P_{O_2}(t)C_{b,out}(t)}{M_{O_2}} +$$
$$+ K_{laO_{2s}}([O_2^*](t) - [O_2](t)_{lm}) + \frac{Q_m}{Vs(1 - \varepsilon_s(t))}([O_2]_m - [O_2]_{out}(t)) \tag{2.54}$$

$$\frac{d[C_T]_{out}(t)}{dt} = -\frac{Q_{liq}}{V_s(1 - \varepsilon_s(t))}([C_T]_{out}(t) - [C_T]_{in}(t)) + \frac{P_{CO_2}(t)C_{b,out}(t)}{M_{CO_2}} +$$

$$+ K_{laCO_{2s}}([CO_2^*](t) - [CO_2](t)_{lm}) + \frac{Q_m}{Vs(1 - \varepsilon_s(t))}([C_T]_m - [C_T]_{out}(t)) \quad (2.55)$$

2.2.2 Greenhouse

A greenhouse is an enclosed structure where the variables that affect the growth and development of crops can be manipulated. The growth of a crop is primarily determined by the climatic variables of its environment and the amount of water and fertilizers applied through irrigation. Therefore, proper management of these variables allows for control over crop growth. That is why a greenhouse is ideal for cultivation, as it provides a closed environment where these variables (ventilation, heating, shading system, water and fertilizer supply, etc.) can be manipulated to achieve optimal plant growth and development. However, achieving the optimal conditions for climatic variables and fertigation comes with economic costs regarding energy, water, and fertilizers. Therefore, from an economic perspective, the goal is not necessarily to maximize production but to maximize profit, which is the difference between the income from selling the final product and its associated costs. Other objectives, such as quality or water use efficiency, can also be considered in maximizing the overall benefit [111].

The diversity of elements that compose a greenhouse and their interrelationships make it a highly complex system where energy, mass, and information are dynamically present in different magnitudes. The crop is the main element and is subject to the influence of various variables, such as climate variations (temperature, humidity, photosynthetically active radiation (PAR)), and carbon dioxide (CO_2 levels), nutrition (water and nutrients), biological factors (pests, diseases, viruses, bacteria), and crop management practices (pruning, pesticides). These variables interact with each other with a high degree of complexity, requiring their identification and modelling as subsystems. Therefore, it is necessary to have an adequate greenhouse model (usually dynamic) that represents all these interactions and allows for its operation. The greenhouse structure, the crop's type and condition, the actuators' effect, and external climatic conditions all affect the behavior of the greenhouse.

The following variables are considered the most important for addressing the climate control problem (see Figure 2.15):

- Controlled variables: These variables are directly related to the crop growth. On one hand, there are climate variables such as PAR radiation, internal temperature, and CO_2 concentration. Relative humidity can be controlled using CO_2 since it is directly related to the crop's absorption of CO_2. On the other hand, there are fertilization variables such as water supply, pH, and electrical conductivity.

- Disturbances: These variables affect the system but cannot be controlled. In this case, they include external climate conditions (temperature, relative humidity, solar radiation, rainfall, wind direction, and speed), medium transpiration (dependent on the crop's state), and greenhouse structural variables (structure, soil, etc.).

- Control variables: These variables are used to compensate for the effects of disturbances and set-point changes in the system, and they are directly related to the actuators within the process. The commonly used actuators include natural ventilation, heating, humidification systems, and CO_2 injection.
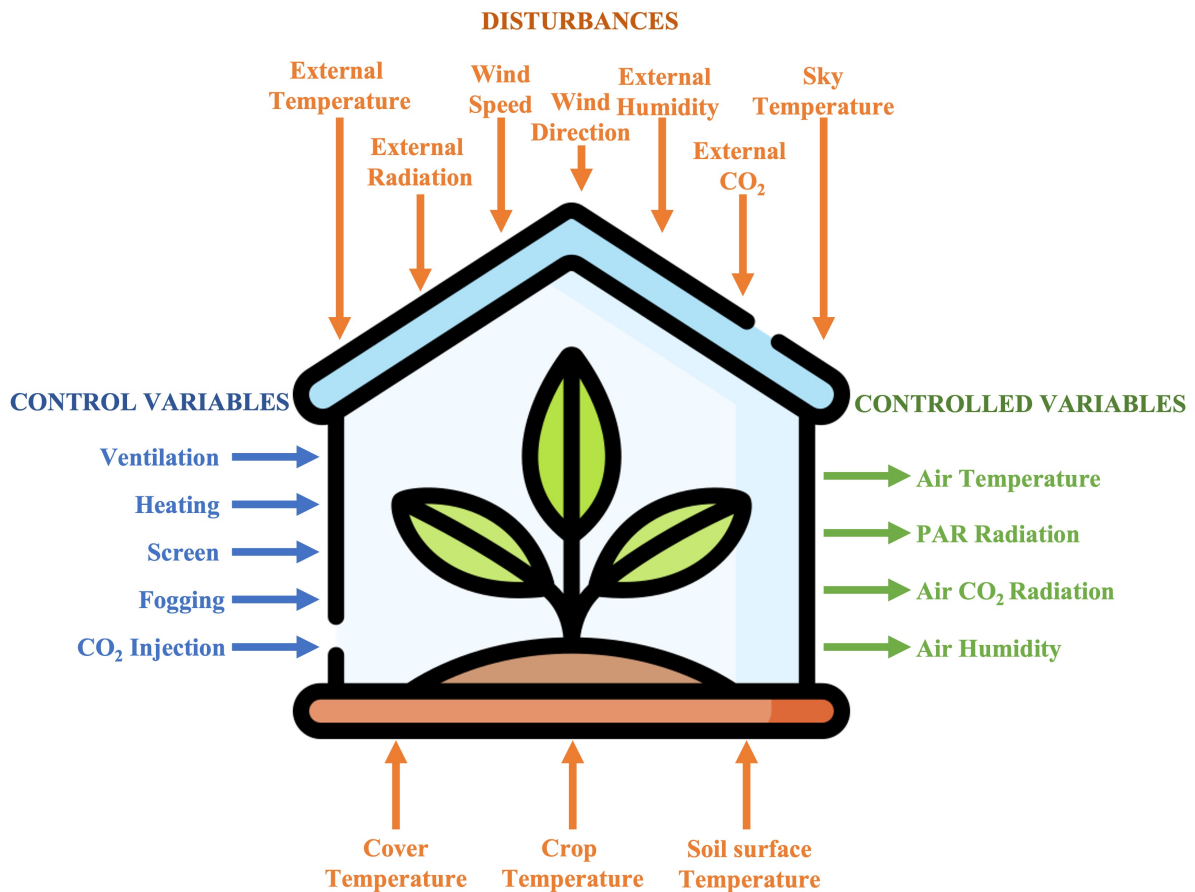

Figure 2.15. Greenhouse climate control problem.

All the processes that happen inside and outside the greenhouse have a strong relationship between them. The inside diurnal temperature varies by convective air exchange between the outside and inside [21]. This exchange rate, coupled with CO_2 taken by the crop during photosynthesis, determines the concentration of CO_2 in the greenhouse. When the photosynthetic rates are higher, the concentration of CO_2 falls below the atmospheric, producing a growth deficit that is increased when the crop reaches its maximum development [111]. Furthermore, the photosynthesis rate indirectly affects the humidity content because when the leaves stomata are opened to capture the CO_2, the plant emits water vapor through the transpiration process, increasing the humidity inside the greenhouse. This released vapor can be reduced, and the concentration of CO_2 is increased by ventilation [129].

Inside the greenhouse, the crop growth is influenced by PAR radiation, temperature, and CO_2 level. Under diurnal conditions, PAR radiation and temperature influence the process of plant photosynthesis. In particular, temperature influences the speed of sugar production by photosynthesis, and a higher radiation level implies a higher temperature. Thus, radiation and temperature have to be in balance, and it is necessary to maintain the temperature at a

level optimal for the photosynthesis process. The diurnal temperature control problem is the refrigeration of the greenhouse air using natural ventilation to reach the optimal temperature. The air exchange and flow inside the greenhouse are determined by natural ventilation as a consequence of the difference between inside and outside temperatures. The objective of the control system is to maintain the inside temperature close to an optimal level [111], having a direct effect on crop growth. This is the control problem treated in this thesis.

The parral greenhouse used in this work is located at The Cajamar Foundation (El Ejido, Almería, South-East Spain) (Figure 2.16).

Figure 2.16. Greenhouse facilities used for the experiences performed in this thesis.

The structure of the greenhouse, the type and state of the crop, the effect of the actuators, and the outlet environmental conditions affect the dynamic behavior of the greenhouse climate (see Figure 2.15). The material that covers the greenhouse is a polyethylene film of 200 μm thickness, installed on a galvanized steel structure. The actuators are a hinged roof window with a maximum opening angle of $45°$ and a lateral window with a length of 37 m and an opening of $45°$.

The greenhouse has a great variety of sensors to obtain data. Soil temperature is measured using semiconductor sensors at different depths (just below the surface layer of the soil and 50 mm deep) and on both sides of the mulch. Eight semiconductor contact sensors have been installed along the cover to measure the outside temperature. The temperature of the air and the relative humidity inside the greenhouse are measured through thermosensitive and capacitive sensors, respectively, positioned in the upper part of the crop. Outside the greenhouse, a meteorological station has been installed at a height of 6 m to measure temperature, relative humidity, global radiation, photosynthetic radiation (PAR), rain, and wind speed and direction.

Chapter 2. Material and Methods

Model Description

In order to describe the indoor climate greenhouse model, the following hypothesis are assumed:

- The state variable for the system is the air temperature, $X_{t,a}$, and it is also considered the controlled variable.

- There are three external elements that interact with the greenhouse: outside air, floor surface, and the crop.

- Exogenous variables and disturbances affecting the system and considered as environmental conditions are the outdoor air temperature, $P_{t,o}$, wind speed $P_{ws,o}$, outdoor global radiation, $P_{rs,o}$ and ground surface temperature, $X_{t,ss}$.

- System control input is ventilation position U_{ven}.

- Air is not inert to solar radiation.

- There is no reflection.

- Air physical characteristics, such as density or specific heat, are constant with temperature and time.

Thus, according to the previous statements, the accumulated heat on the greenhouse air is given by the following balance equation [111]. Notice that references to t variable have been deleted in equations in order to obtain more compact expressions:

$$Q_{ac} = Q_s + Q_{cv,ss} + Q_{cv,cal} - Q_{cn-cv} - Q_v - Q_{t,c} \tag{2.56}$$

where Q_{ac} is the accumulated heat in the greenhouse air, Q_s is the solar radiation absorbed by the greenhouse air, $Q_{cv,ss}$ is the heat transfer by convection and conduction in the cover between the outside and the inside air, $Q_{cv,cal}$ is the convection heat transfer with the pipes heating system, Q_{cn-cv} is the convection and conduction heat transfer between the input and output greenhouse air, Q_v is the heat transfer to the outside air due to ventilation and infiltration losses, and $Q_{t,c}$ is the latent heating produced by the crop transpiration.

Expressing the accumulated heat in the greenhouse as the variation of inside air temperature $X_{t,a}$ with respect to time, it results in:

$$C_{sh,a} C_{d,a} \frac{C_{v,s}}{C_{a,s}} \frac{dX_{t,a}}{dt} = Q_s + Q_{cv,ss} - Q_{cn-cv} - Q_v - Q_{t,c} \tag{2.57}$$

where $C_{sh,a}$ is the air specific heat, $C_{d,a}$ is air density, $C_{v,s}$ is air volume, $C_{a,s}$ is the surface ground area, and where $Q_{cv,cal}$ is zero due to the heating system is turned off.

Then, according to the results obtained in Equation [111] for the balances presented in (2.57), and considering that in this paper only the diurnal dynamics is considered ($Q_{cv,cal} = 0$), the following greenhouse temperature simplified model is obtained:

$$C_{sh,a}C_{d,a}\frac{C_{v,s}}{C_{a,s}}\frac{dX_{t,a}}{dt} = C_{aoc}V_{t,c}P_{rs,o} + C_{cv}(X_{t,ss} - X_{t,a}) - C_{cn-cv}(X_{t,a} - P_{t,o}) -$$

$$- \frac{C_{d,a}C_{sh,a}}{C_{a,s}}\phi_v(X_{t,a} - P_{t,o}) - E_t(C_{et} - C_f X_{t,a}) \tag{2.58}$$

where C_{aoc} is the greenhouse air short wave absorption coefficient, $V_{t,c}$ is the short wave transmission coefficient based on the cover transmission coefficient, whitening, and the shader mesh, C_{cv} is the greenhouse air-soil surface convection coefficient, ϕ_v is the ventilation flow, C_{et} is the evapotranspiration constant, C_f is the conversion factor and E_t is the crop evapotranspiration which is obtained based on the crop state and climate variables such as greenhouse air humidity and net radiation. The ventilation flow is represented by:

$$\phi_v = \left[\left(\frac{V_{v,a-l}V_{v,a-r}}{\sqrt{V_{v,a-l}^2 + V_{v,a-r}^2}} \right)^2 \left(2C_g C_{ven,h}\frac{X_{t,a} - P_{t,o}}{X_{t,a} + P_{t,o}} \right) \right.$$

$$\left. + \left(\frac{V_{v,a-l} + V_{v,a-r}}{2} \right)^2 C_{ven,w}P_{ws,o}^2 \right]^{0.5} C_{v,d} + \phi_l \tag{2.59}$$

with

$$V_{v,a-l} = C_{v,l-l}C_{v,w-l}U_{ven}n_l \tag{2.60}$$

$$V_{v,a-r} = 2C_{v,l-r}C_{v,w-r}\sin\left(\frac{U_{ven}}{2}\right)n_r \tag{2.61}$$

where $V_{v,a-l}$ and $V_{v,a-r}$ are the areas of the sidewall and roof ventilation openings respectively, C_g is the gravity constant, $C_{vent,h}$ is the ventilation effective height, $C_{vent,w}$ is the ventilation wind effect coefficient, $C_{v,d}$ is the ventilation discharge coefficient and ϕ_l is the leakage by infiltration when vents are closed flux. $C_{v,l-l}$ and $C_{v,l-r}$ are the length of the lateral and roof vents respectively, $C_{v,w-l}$ and $C_{v,w-r}$ are the width of lateral and roof vents respectively, and n_l and n_r is the number of lateral and roof vents respectively. The evaporation process in soil surface has been neglected due to the greenhouse being mulched [111].

Variable U_{ven} is the vent opening (control signal) and represents the aperture value for both lateral and roof windows. Thus, the model presented in Equation (2.58) allows to describe the evolution of the diurnal greenhouse temperature (process output) based on the vent opening (control signal) and the process disturbances. Notice that this nonlinear model has been calibrated and validated in previous works with a goodness of fit over 90% [105, 111]. This model was used in this thesis to develop a robust feedback linearization approach as presented in Chapter 4.

2.2.3 TCLab

This section summarizes a commercial example of a pocket-sized device called APMonitor Temperature Control Lab, abbreviated to TCLab [5]. TCLab (see Figure 2.17) is a low-cost portable device intended as an educational tool for model identification and testing of control strategies. The TCLab kit is a multi-variable system consisting of two heaters (transistors), whose temperatures need to be controlled and two thermal sensors (thermistors). Its compact size and being an Arduino-based device make TCLab an easy-to-use kit for control engineering students. Over the last years, TCLab has been proven to be a suitable tool in different university courses, as described below [35, 60].
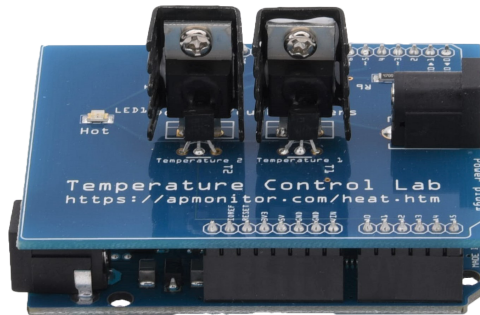
Figure 2.17. Picture of a TCLab kit [5].

TCLab's control objective is to make its transistors reach a certain temperature by varying the current passing through them. Each sensor-actuator pair is attached to a sink, in permanent contact, and glued with a thermochromic material (as shown in Figure 2.17). Both sensors and actuators are connected to an Arduino board, as depicted in Figure 2.18.

Figure 2.18. TCLab connections diagram [5]. Black "A" indicates actuators, blue "C" indicates connection, and green "S" indicates sensors.

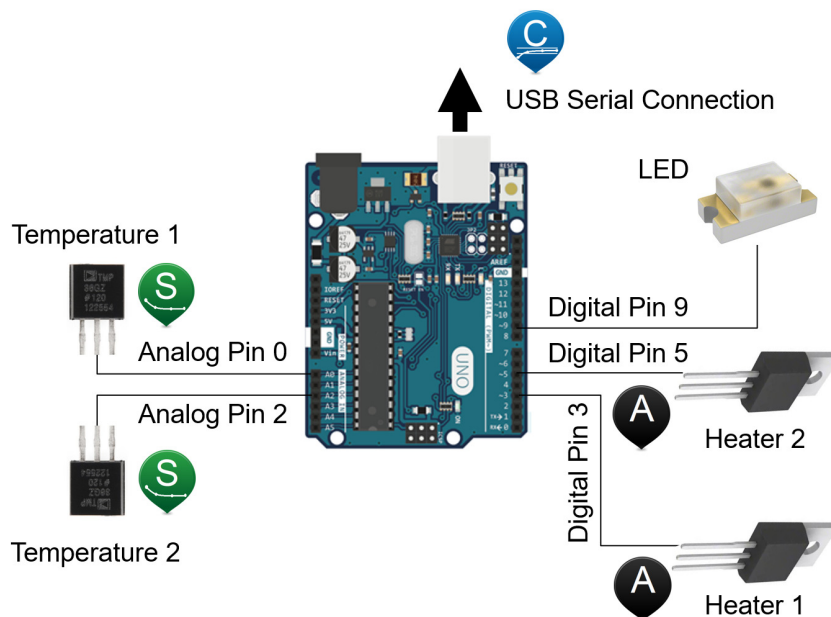The USB connector is used to transfer code from a personal computer to the microcontroller, allowing students to program any control strategy that they need to implement. Although Arduino uses its own language, which is similar to C++, it is possible to program Arduino with other high-level languages, such as Python, Matlab® or Simulink®, thanks to the available libraries from different developers. This is the case for the activities carried out in this thesis, for which all the programming is done in either Matlab® or Simulink®.

In order to work with TCLab, a basic thermal model that considers the main physical phenomena is used. The broad approach of considering a multi-variable system yields an expression for each of the transistors, as stated in (2.62) and (2.63):

$$mc_p\frac{dX_{h,1}}{dt} = U_hA_c(X_\infty - X_{h,1}) + \epsilon_h\sigma_hA_c(X_\infty^4 - X_{h,1}^4) + Q_{C12} + Q_{R12} + \alpha_{h,1}Q_1 \quad (2.62)$$

$$mc_p\frac{dX_{h,2}}{dt} = U_hA_c(X_\infty - X_{h,2}) + \epsilon_h\sigma_hA_c(X_\infty^4 - X_{h,2}^4) - Q_{C12} - Q_{R12} + \alpha_{h,2}Q_2 \quad (2.63)$$

where m is the mass of the transistor-thermistor-sink assembly (from now on, "heater"), c_p is its specific heat capacity, A_c is the surface in contact with the environment, U_h is the overall heat transfer coefficient , X_∞ is the environment temperature, ϵ_h is the emissivity, σ_h is the Stefan-Boltzmann constant, α_i is a factor that relates the current passing through transistor i to the heat produced, $X_{h,i}$ is the temperature of heater i, Q_i is the heat dissipated by heater i, $Q_{C12} = U_hA_s(X_{h,2} - X_{h,1})$ is the convective heat transfer from heater 1 to heater 2, $Q_{R12} = \epsilon_h\sigma_hA_s(X_{h,2}^4 - X_{h,1}^4)$ is the radiative heat transfer from heater 1 to heater 2, and A_s is the surface area between heaters.

3. Contributions to Classic Control Strategies

Most industrial processes are affected by load disturbances. A regulation problem is classically known as the design of a feedback controller to reduce the effects of load disturbances in the process output. However, if the disturbance can be measured, it can be accounted for in advance to help the feedback controller reject it. The most common solution to reject measurable load disturbances is feedforward control [37, 77, 120, 123]. It is commonly used in process industry. It is implemented in most distributed control systems to improve the control performance in applications such as distillation columns [92], power plants [138] or microalgae cultures, among many other examples [4].

Feedforward control provides the ability to take control actions before the disturbance affects the process output. The ideal compensator is formed as the dynamics between the disturbance and the process output divided by the dynamics between the control signal and the process output, with the reversed sign. If this feedforward compensator is used, the effects of the load disturbance can be removed completely from the process output. However, it is normally not possible to implement and apply this ideal feedforward compensator since it results from a division between two process transfer functions. Thus, the compensator may be non-causal (having a negative delay), non-proper (having more zeros than poles), or unstable. Another reason is that the compensator may require so large control signal actions that the control signal becomes saturated.

In recent years, research results dealing with the design of tuning rules to improve feedforward control when perfect cancellation is not realizable have been presented [37, 38, 41, 109, 110]. This research has mainly been focused on the delay inversion problem leading to non-causal compensators. In this thesis, another problem that makes the ideal compensator non-realizable is treated, namely the fact that feedforward control signals often become saturated.

In the adjustment and design of feedforward control, ideal linear models of both the plant and disturbance are used. In industry, process models can be complex, and often the parameters may have uncertainty because of modelling approximation for control design proposes. Therefore, by employing robust control strategies such as QFT [114], attempts are made to compensate for the

differences between the model used in feedforward control and the actual plant and disturbance models.

Similarly, due to the complexity of industrial processes, it is sometimes necessary to combine different control strategies to achieve the best process performance. In this regard, strategies such as cascade control are widely used and implemented [135]. Since they can also be subject to disturbances, it is necessary to combine them with feedforward control and, therefore, develop solutions to address these issues.

This chapter provides three solutions for classical control schemes that deal with measurable disturbances. In Section 3.1, a QFT-based robust solution is presented for the feedforward control scheme, where PI control is combined with feedforward compensators, considering the uncertainties of the processes. Section 3.2 proposes a new design rule to improve the response when saturation occurs in a classical feedforward control scheme due to a disturbance effect. Lastly, in Section 3.3, a dual feedforward scheme is proposed for a cascade control scheme subjected to measurable disturbances at the process output.

3.1 Robust QFT-Based PI Controller for a Feedforward Control Scheme

Usually, when feedforward is calculated, nominal models are used, and the robustness case is not studied. Notice that when uncertainties are considered, the feedforward control scheme deteriorates even for the perfect cancellation case. In that case, the cancellation of the feedforward is not perfect, and the closed-loop specifications may not be fulfilled when the system deviates from the nominal conditions [36]. Thus, it is interesting to analyze this situation and propose robust solutions for this problem.

There are only a few works in literature where the robustness of the feedforward control scheme has been studied. In [36], the robustness of the feedback control with feedforward compensator was analyzed with respect to uncertainties in the process gain and approximated high-order dynamics. It was demonstrated that the variability of the process model parameters affects the response of the PID controller with the feedforward compensation. The authors in [4] presented a robust design solution for feedforward controllers when the available dynamic models include estimated limits for the uncertainties. A model-based design and tuning procedure is proposed to account for model uncertainties. It is derived that the feedforward and the feedback controllers should be tuned simultaneously for efficient disturbance rejection. This idea has been used later in other works. For instance, in [133], a sequential tuning of feedforward controllers within an IMC control structure is proposed. In that work, the compensator is defined as the invertible part of the quotient plus a tunable filter which is chosen to minimize the interaction between both controllers. Furthermore, in [109], a robust design methodology for simultaneously tuning both feedforward and feedback controllers is presented. Disturbance rejection performance condition is expressed as a degradation band above a desired shape. Finally, in [26], QFT was used to design robust feedback and feedforward controllers. New QFT bounds were obtained for the design stage, and it was the first time that the feedback was linked to the existence of a feedforward controller in QFT.

The aim of the contribution is to propose a QFT-based robust solution for the classical feedforward control scheme (see Figure 2.4) presented in this thesis, where PI control is combined

with feedforward compensators [61]. The idea consists in moving the uncertainties effect to bounds in the QFT specifications and then designing a robust PI controller. The main contribution is based on modifying the original boundaries of the QFT methodology for the regulation problem and designing a robust PI controller to account for the uncertainties. Notice that the feedforward compensator is not designed from a robust point view since its effect is moved to the QFT specifications.

3.1.1 Preliminaries

The feedforward control scheme used in this work is shown in Figure 2.4. It consists of a feedback controller $C(s)$, a process $P_u(s)$, a set-point signal r, a control signal u, and a process output y. The disturbance d, which is measurable, influences the feedback loop as shown in the figure. The transfer function between the load d and the output y is $P_d(s)$. The feedforward compensator $C_{ff}(s)$ feeds the disturbance d, and its output is added to the feedback control signal.

A PI controller is considered as feedback regulator $C(s)$, defined in Equation (2.2), with $\tau_d = 0$. The models of the process $P_u(s)$ and the disturbance $P_d(s)$ are described by first-order transfer functions without time delay, as shown in Equation (2.8), where the gains and the time constants in both cases, K_u, T_u for the process and K_d, T_d for the disturbance, are the parameters that bring the uncertainty to the system as described below. Notice that in this contribution, the free-delay case is considered the first approach to the robust problem. However, the solution can easily be extended to the time delay case. The proposed feedforward compensator is given by the Equation (2.9).

3.1.2 Robustness Analysis and Design

Such as described in Section 2.1.3, the feedforward element is commonly used as a lead-lag compensator described by Equation (2.9). Usually, it is calculated from models in Equation (2.8), assuming that there is no uncertainty [36]. Notice that for the nominal case, and if there are no inversion problems, the disturbance effect can be totally canceled.

In this contribution, uncertainties in gain and time constant are assumed in the process transfer functions P_u and P_d to perform a robustness analysis of the classical feedforward control design. Thus, now a set of plants given by the following equations is defined:

$$P_u(s) \in \mathcal{P} = \left\{ \frac{K_u}{1 + T_u s}, \text{ with } K_u \in [K_{u,low}, K_{u,high}], \ T_u \in [T_{u,low}, T_{u,high}] \right\} \tag{3.1}$$

$$P_d(s) \in \mathcal{P} = \left\{ \frac{K_d}{1 + T_d s}, \text{ with } K_d \in [K_{d,low}, K_{d,high}], \ T_d \in [T_{d,low}, T_{d,high}] \right\} \tag{3.2}$$

$$P_u^0(s) = \frac{K_u^0}{T_u^0 s + 1} \tag{3.3}$$

$$P_d^0(s) = \frac{K_d^0}{T_d^0 s + 1} \tag{3.4}$$

where P_u^0 and P_d^0 are the nominal plants.

The first issue to be analyzed is to observe how the use of the feedforward control scheme and the presence of uncertainties affect the system specifications in the regulation control problem. The closed-loop transfer function from disturbance to system output is defined as:

$$T_{dy}(s) = \frac{P_{dg}(s)}{1 + C(s)P_u(s)} \tag{3.5}$$

where P_{dg} is given by the following equation:

$$P_{dg}(s) = C_{ff}(s)P_u(s) + P_d(s) \tag{3.6}$$

Notice that $C_{ff} = 0$ represents the classical regulation problem.

When P_u and P_d are uncertain, and QFT is used to design the feedback regulator, the specification for the robust regulation problem is given, from Equation (2.37), as:

$$\left| \frac{1}{1 + C(j\omega)P_u(j\omega)} \right|_{dB} \leq \delta_{dB}(\omega) - |P_{dg}(j\omega)|_{dB} = \gamma_r(\omega) \tag{3.7}$$

for all plants $P_u, P_d \in \mathcal{P}$, and where γ_r is the new specification bound.

Therefore, it can be observed how the feedforward compensator and the uncertainties affect the bound in the specification problem. Thus, according to Equations (2.37) and (3.7), there are two different ways to account for the robust control problem:

- The first one would be to use Equation (3.7) and follow the classical robust design with QFT. In this case, the specification bound γ_r depends on the uncertainties and the feedforward compensator present in $P_{dg}(j\omega)$. Then, the minimum value of γ_r for all plants $P_u, P_d \in \mathcal{P}$, must be considered as specification. Once this minimum bound is calculated, classical QFT is used to obtain the resulting controller. However, a very conservative solution will be obtained since the specification bound is computed for the worst possible case.

- A second solution to this problem is to consider the specification from Equation (2.37) and to modify the boundary calculation in QFT. So, new boundaries are obtained considering the presence of the feedforward compensator and then a robust controller is obtained based on these new limits. This is the new solution proposed in this contribution and presented in the following.

First, the nominal plants $P_u^0(s)$ and $P_d^0(s)$ are selected, and the nominal feedforward compensator is calculated using the rules proposed in [36]. That is, $K_{ff} = K_d^0/K_u^0$, $T_p = T_d^0$ and $T_z = T_u^0$.

Then, the algorithm proposed in [86] to compute classical boundaries in QFT is modified in order to include a new kind of boundary that assures the satisfaction of specification in Equation (2.37) when $C_{ff} \neq 0$. It is important to remember the concept of crossection defined in [86]. Fixed a phase in Nichols Plane (NP) (and the frequency ω for which the boundary is being computed), the crossection is a function of the magnitude of the nominal open-loop transfer function $L_0 = CP_u^0$, that provides a value of interest, the value of $Max|T_{dy}(j\omega)|_{dB}$ in this contribution. Obviously, the location of $L_0(j\omega)$ in the NP depends on the value of $C(j\omega)$ because P_u^0 is fixed.
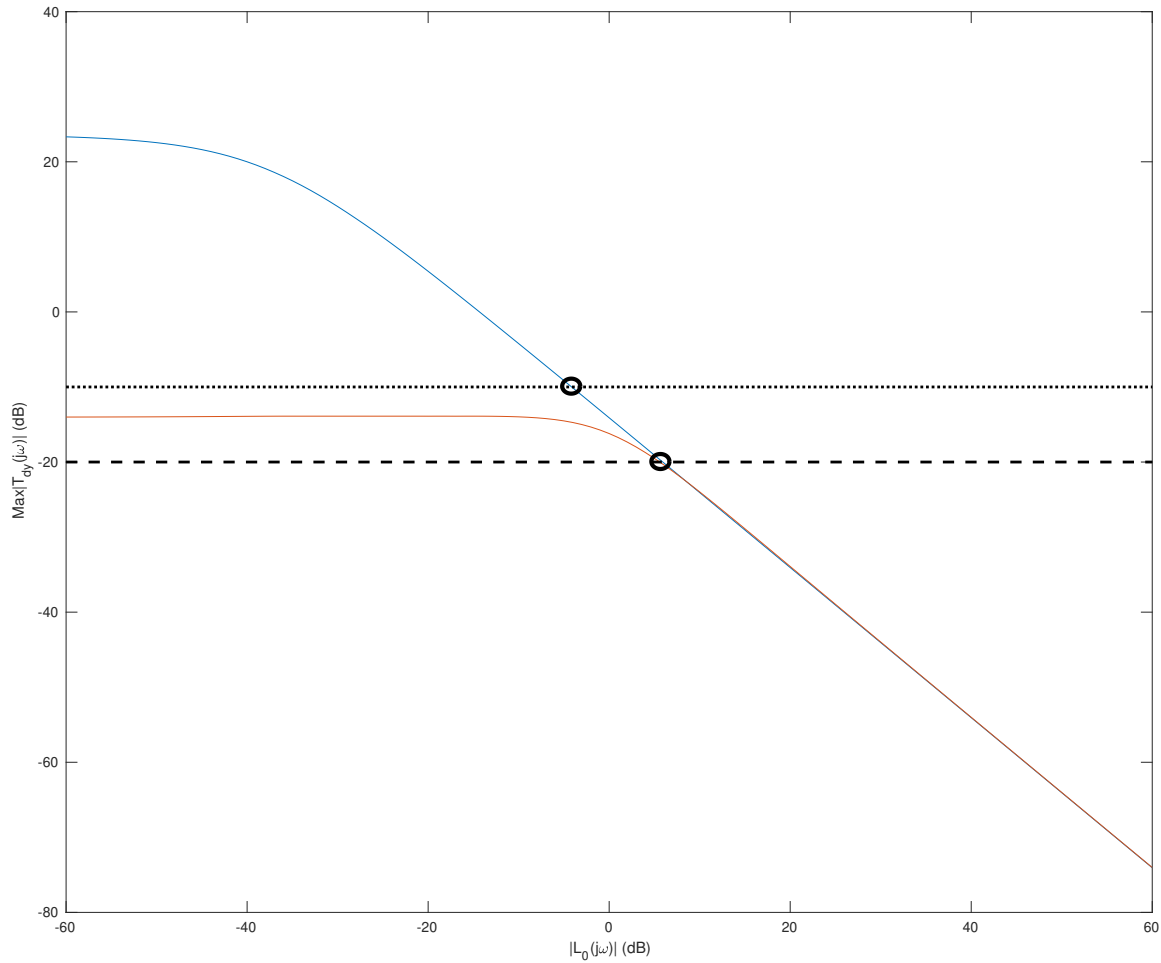
Figure 3.1. Crossections for the regulation problem for $C_{ff} = 0$ (red) and for $C_{ff} \neq 0$ (blue) for $\omega = 1$ rad/s and $phase(L_0(j\omega)) = -100$ degrees. Two specifications are shown, for $\delta_{dB} = -20$ (- -) and $\delta_{dB} = -10$ (-·).

Figure 3.1 shows an example of crossection for the regulation problem for the cases with and without feedforward compensator and for $\omega = 1$ rad/s and phase$(L_0(j\omega)) = -100$ degrees. In this figure, two different specifications are shown for $\delta_{dB} = -20$ and $\delta_{dB} = -10$, respectively. It can be observed how, for specifications where $\delta_{dB} < -20$, both cases are equal for this frequency. See for instance, the case where both solutions cut the specification of $\delta_{dB} = -20$ at the value of 5.66 dB. However, for specifications with $\delta_{dB} \geq -20$ both solutions are different. This means that different boundaries will be obtained for both cases, and thus, different control designs must be done. For instance, for the specification of $\delta_{dB} = -10$, the case where $C_{ff} = 0$ does not cut the limit, while the case with $C_{ff} \neq 0$ cuts the specification bound at the value of -4.19 dB. Thus, a more restrictive solution is given for the case when the feedforward is included in the control scheme. This result indicates that the use of the feedforward compensator can affect the control problem negatively when modelling errors appear in the system. This fact can better be seen in Figure 3.2. This figure shows the boundaries for the specification of $\delta_{dB} = -10$. As observed, the boundary is open when $C_{ff} \neq 0$ and closed when $C_{ff} = 0$, thus being the first one much more restrictive. However, it is interesting to see how, for the zone around (-180°, 0 dB), the boundary for $C_{ff} \neq 0$ is smaller and thus less restrictive. In any case, this is usually protected by the stability boundaries, and thus it is not an important advantage.
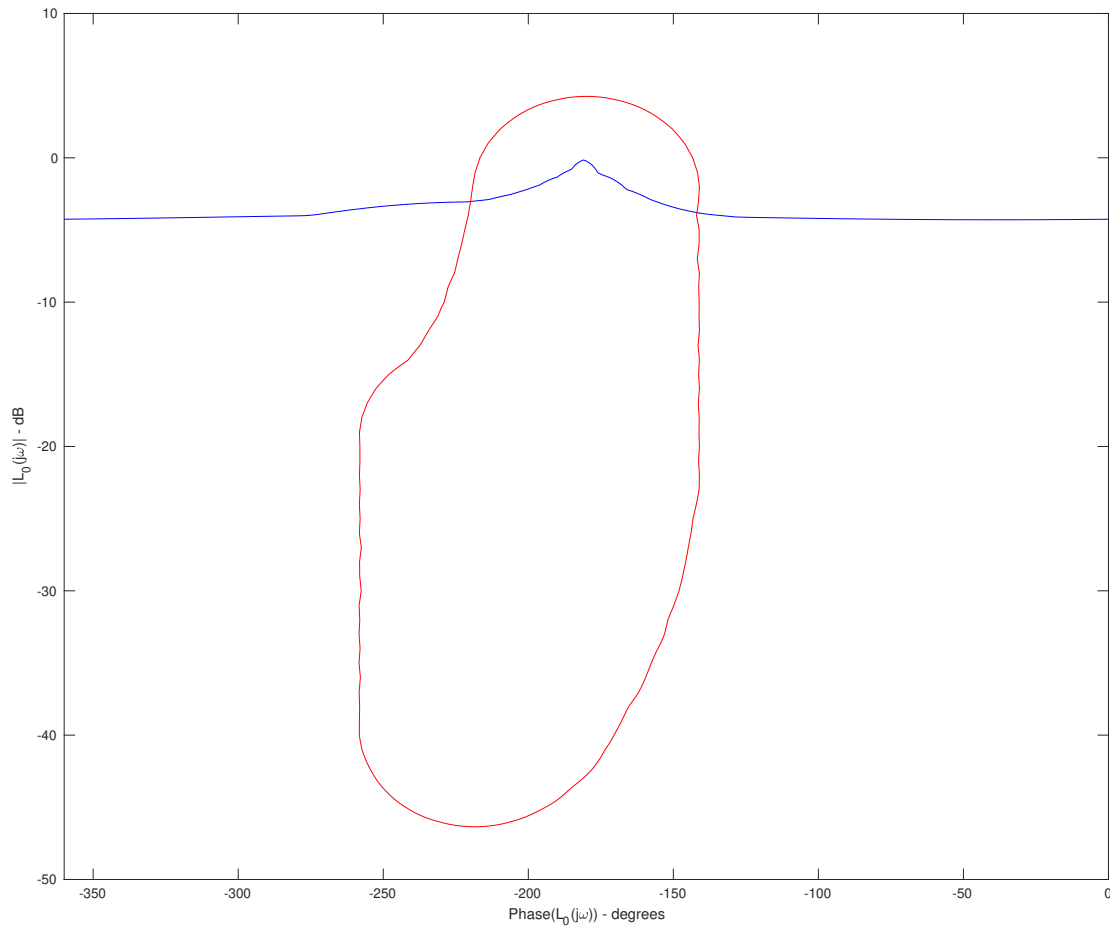
Figure 3.2. Boundary comparisons for the regulation problem for $C_{ff} = 0$ (red) and for $C_{ff} \neq 0$ (blue) for $\omega = 1$ rad/s and for the specification $\delta_{dB} = -10$.

Thus, it is concluded that QFT can be used as a robust control design method when a feedforward control scheme is considered to account for the uncertainties in the process. However, the presence of the feedforward compensator affects to the calculation of the classical boundaries in QFT, and new specifications must be fulfilled during the controller design stage as shown in the following section with numerical examples.

3.1.3 Numerical Example

This section presents a numerical example to demonstrate the contributions described in the previous section. Let's assume the following models for the process:

$$P_u(s) \in \mathcal{P} = \left\{ \frac{K_u}{1 + T_u s}, \ \ \text{with} \ \ K_u \in [1, \ 10], \ \ T_u \in [1, 10] \right\} \tag{3.8}$$

and

$$P_d(s) \in \mathcal{P} = \left\{ \frac{K_d}{1 + T_d s}, \ \ \text{with} \ \ K_d \in [3, \ 7], \ \ T_d \in [11, 15] \right\} \tag{3.9}$$

with nominal models P_u^0 given by $K_u^0 = 1$ and $T_u^0 = 10$ and P_d^0 given by $K_d^0 = 3$ and $T_d^0 = 11$.

Such as commented in the previous section, there are two possible solutions to the problem based on considering the specifications as shown in Equations (2.37) or (3.7). The following subsections show the analysis and results for both cases.

Classical Solution

One solution for the problem would be to use the specification of the problem according to Equation (3.7) for the worst case and then use the classical stages for QFT with classical boundaries.

Figure 3.3 shows different values for the γ_r function defined by Equation (3.7) for all the plants in $\mathcal{P}$. The curve represented by asterisks shows the case when $C_{ff} = 0$, and the rest of the curves are all γ_r values when $C_{ff} \neq 0$. Is is assumed that $\delta_{dB} = -40dB$. Thus, it is observed how for this nominal choice, there are many cases of uncertainty where the presence of the feedforward compensator results in a more restrictive specification (a more aggressive controller will be required) since they are below the case when $C_{ff} = 0$. Therefore, this result indicates that, in this case, the selection of the nominal plant cannot be made arbitrarily. It would be necessary to obtain the nominal plant that gives the maximum value of γ_r for all possible combinations.
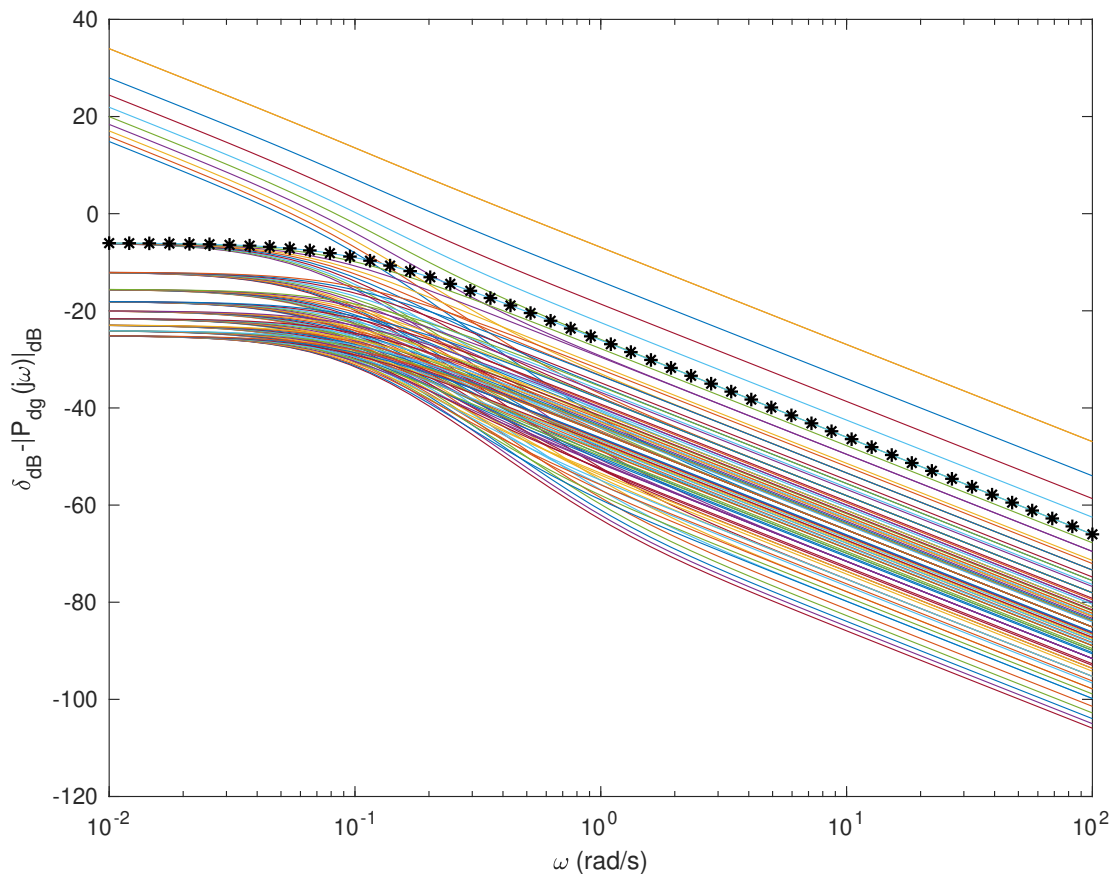

Figure 3.3. Right side of Equation (3.7) with $C_{ff} = 0$ (*) and with $C_{ff} \neq 0$ (-) for nominal models P_u^0 given by $K_u^0 = 1$ and $T_u^0 = 10$ and P_d^0 given by $K_d^0 = 3$ and $T_d^0 = 11$.

If this is performed for this example, the results presented in Figure 3.4 are obtained for the best case. That is, it is the selection of the nominal models that give the less restrictive γ_r values. This solution has been obtained for the nominal models P_u^0 given by $K_u^0 = 10$ and $T_u^0 = 1$ and

P_d^0 given by $K_d^0 = 3$ and $T_d^0 = 11$. It can be seen that when $C_{ff} \neq 0$ all γ_r functions are greater than or equal to the γ_r function corresponding to $C_{ff} = 0$. Then, the function that must be used as the specification in Equation (3.7) is given by $\gamma_r(\omega) = \delta_{dB} - |P_d(j\omega)|_{dB}$, which is the same specification as when the feedforward term is not considered. If any other value for nominal used to compute C_{ff} is chosen, some γ_r functions will be located below the line with asterisks in the Figure 3.4 as shown in the case of Figure 3.3. Thus, the specification would be more restrictive, and a more demanding feedback controller will be necessary in order to ensure the specifications.
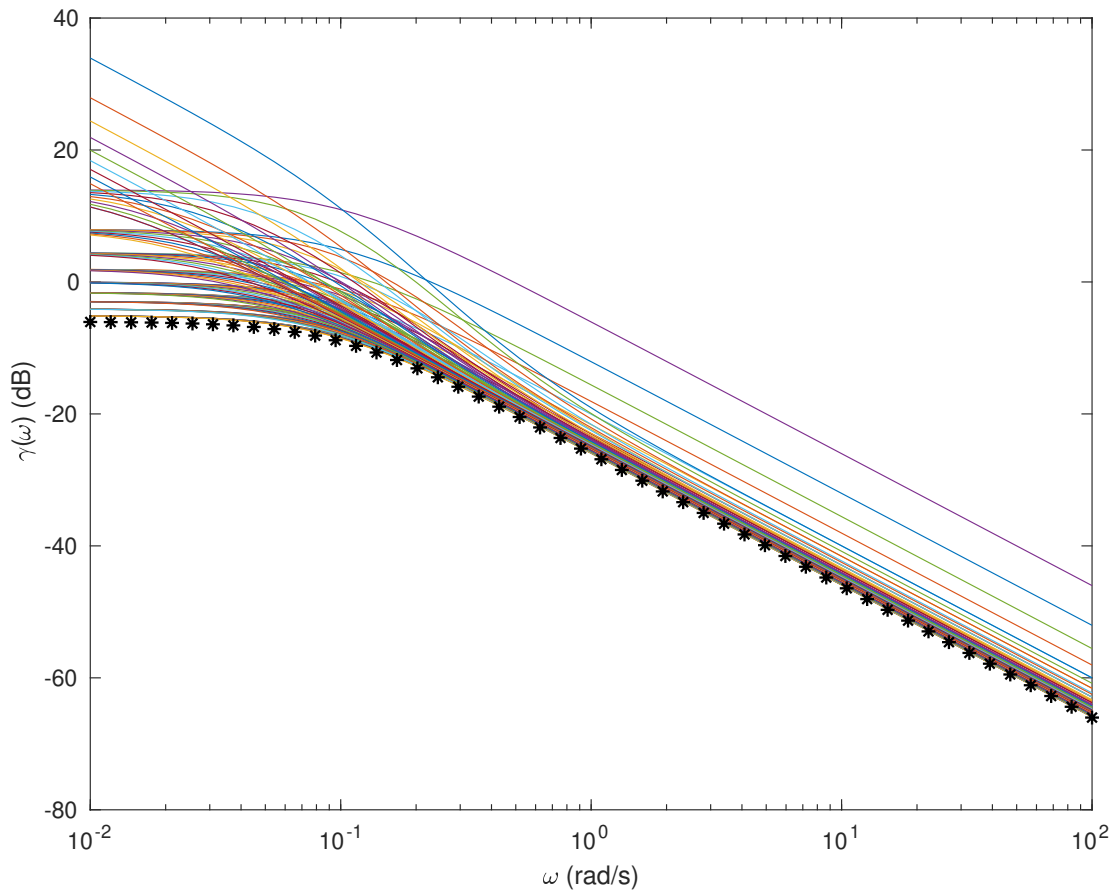

Figure 3.4. Right side of Equation (3.7) with $C_{ff} = 0$ (*) and with $C_{ff} \neq 0$ (-) for nominal models P_u^0 given by $K_u^0 = 10$ and $T_u^0 = 1$ and P_d^0 given by $K_d^0 = 3$ and $T_d^0 = 11$.

Hence, it is concluded that when the specification from Equation (3.7) is considered, the same specification as the case when $C_{ff} = 0$ can be used for the robust control problem.

New Solution

In this case, the specification (2.37) is considered, and the new solution described above is used for this example.

Then, classical stability specifications in QFT and the new kind of disturbance rejection specifications, including the feedforward element, are taken into account. A phase margin greater than or equal to 45 degrees for the whole uncertainty set is used as stability specification. So, this specification on the closed-loop transfer function is given by:

$$\left| \frac{C(j\omega)P_u(j\omega)}{1 + C(j\omega)P_u(j\omega)} \right| \leq 2.32dB \,\forall\, \omega > 0 \tag{3.10}$$

On the other hand, a disturbance rejection specification is given by $\delta_{dB} = -40dB$ is assumed. The set of design frequencies chosen is $\Omega = \{0.1, 1, 10, 100\}$ rad/s.

Figure 3.5 shows the templates for the set of design frequencies and for the set of plants from Equation (3.8). Figure 3.6 shows the stability bounds, all of which are closed boundaries, and the disturbance rejection bounds, all open boundaries, for the same set of frequencies. A nominal open-loop transfer function shaped fulfilling all the boundaries is drawn, given by a PI controller with $K_p = 400$ and $\tau_i = 100$. The parameters used for the C_{ff} element are $T_z = 10$, $T_p = 11$, and $K_{ff} = 3$.

Figures 3.7 and 3.8 show that the control system satisfies all the specifications from a frequency domain point of view.

Finally, Figures 3.9 and 3.10 show the results in the time domain for the proposed robust control approach presented in this contribution and for the nominal control design presented in [36], respectively. It can be observed how for the proposed case, the disturbance is almost rejected beside the uncertainties with an important performance improvement with respect to the nominal case in Figure 3.10. Moreover, this result is achieved with very similar control effort as shown in the controller output signal of both figures.
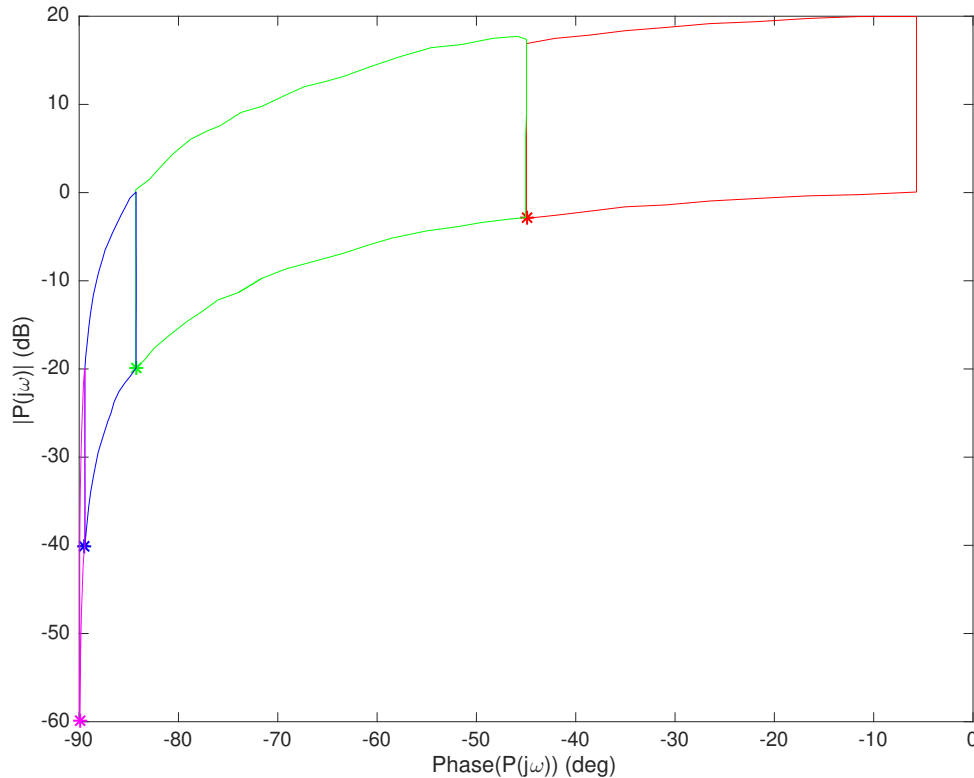

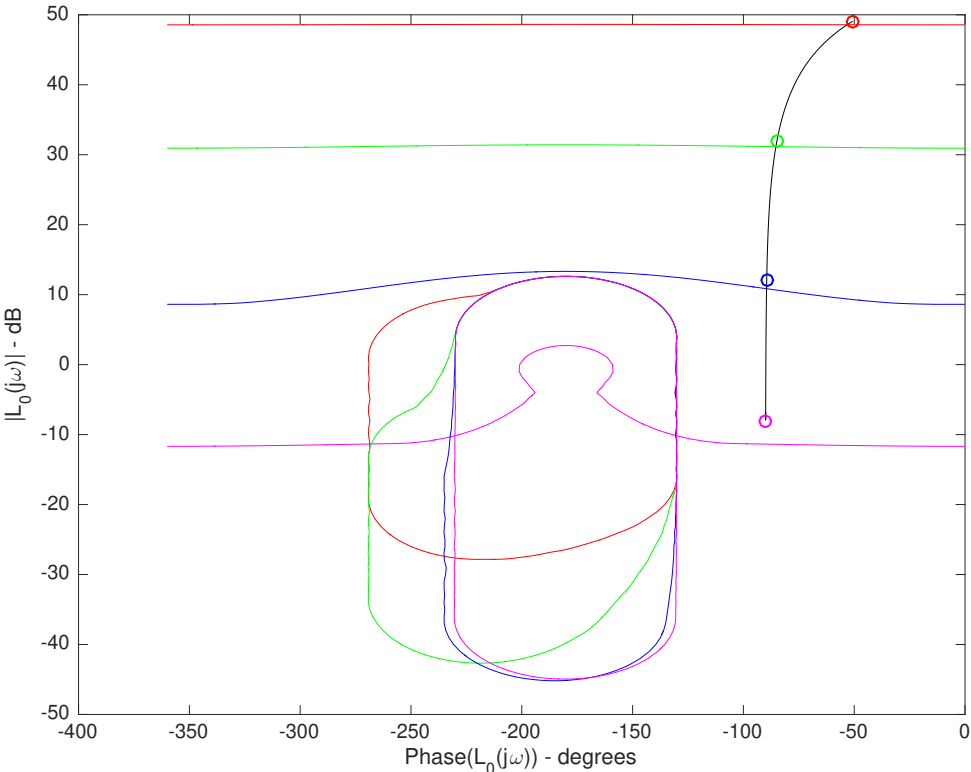Figure 3.5. Templates for $\omega \in \{0.1, 1, 10, 100\}$ rad/s.

Figure 3.6. Nominal open-loop shaping and stability and disturbance on output rejection bounds taking the FF element into account.
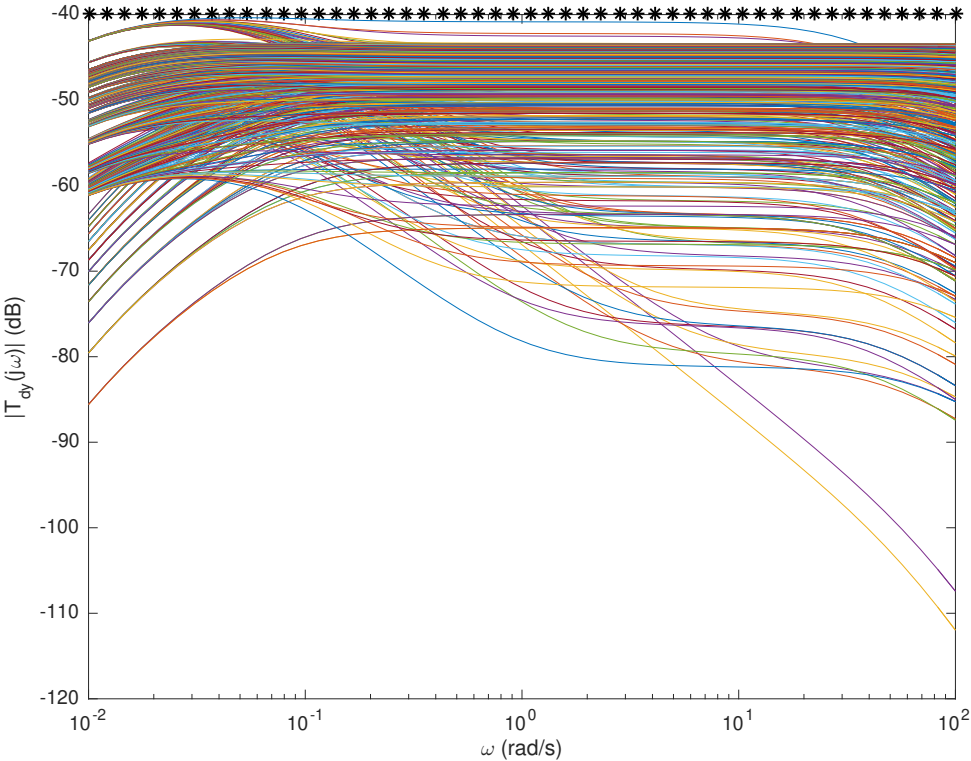

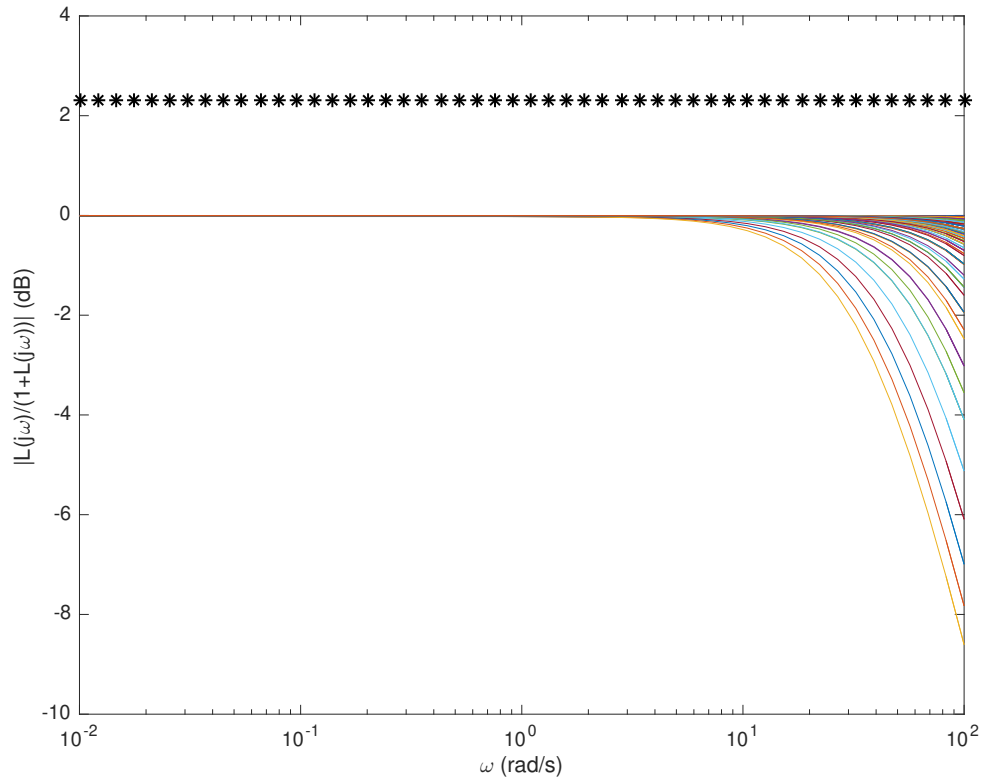Figure 3.7. $T_{dy}(j\omega)$ transfer functions and specification.

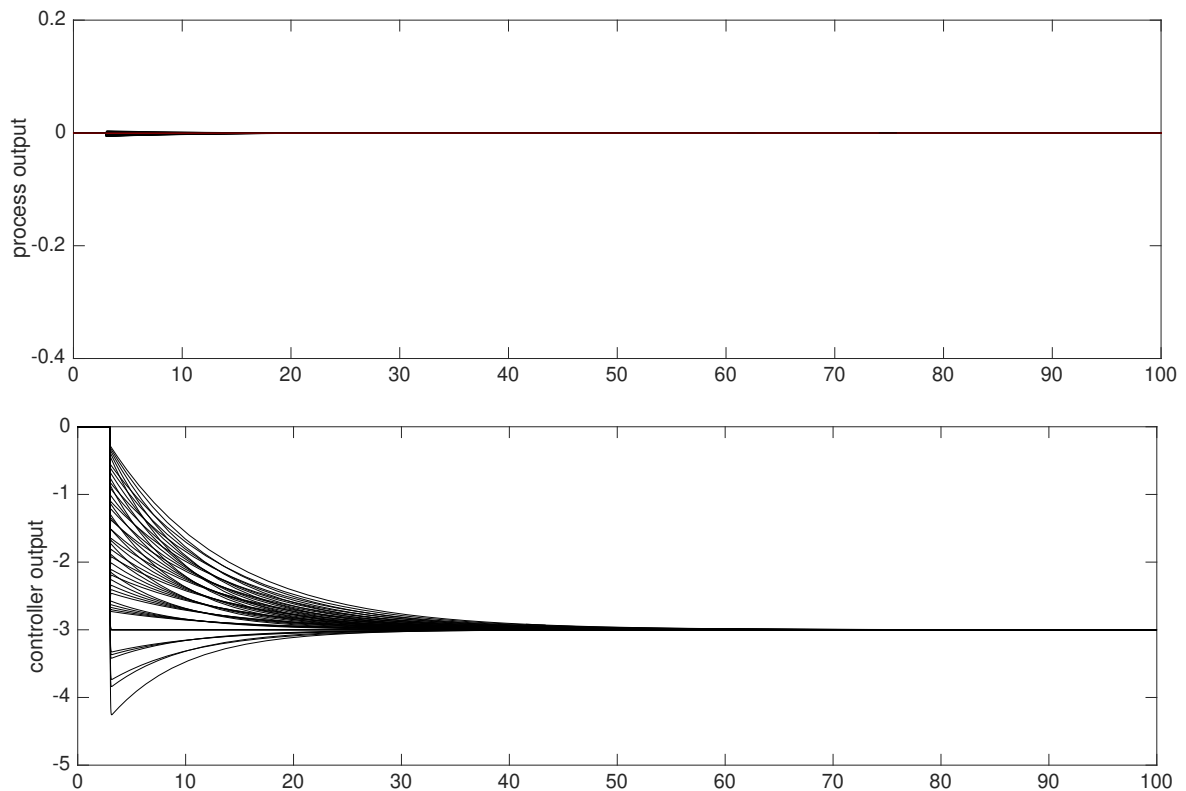Figure 3.8. $T_{dj}(j\omega)$ transfer functions and specification.

Figure 3.9. Time domain simulations for the proposed robust control design. A unitary step disturbance was included at time $t = 3$ seconds.
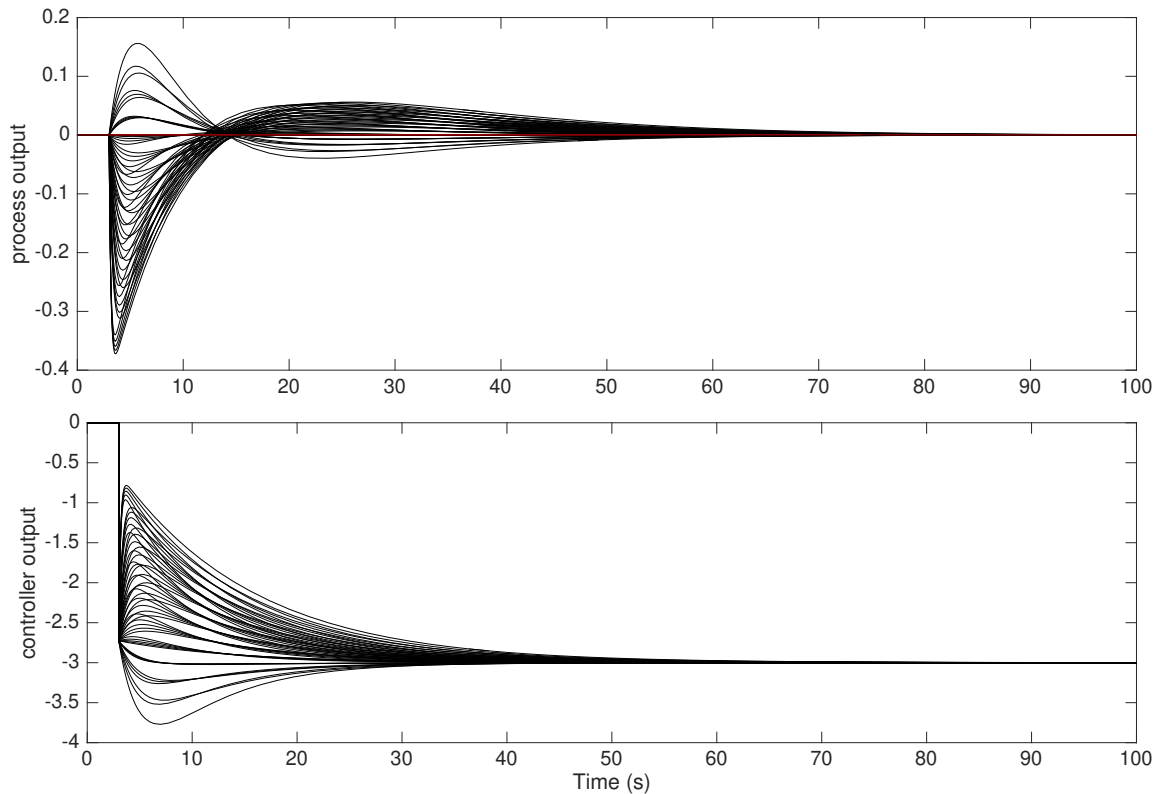
Figure 3.10. Time domain simulations for nominal control design [36]. A unitary step disturbance was included at time $t = 3$ seconds.

3.1.4   Conclusions

This contribution has analyzed the classical feedforward control scheme for measured disturbances for the case when uncertainties are considered. QFT has been used as a robust control design method. It was shown that the presence of the feedforward compensator changes the classical QFT specification for the regulation problem. This modification leads to two different solutions. The first one consists in using the same specification as the case when the feedforward is not considered, and classical QFT boundaries for the control design process are calculated. This approach would result in very conservative results, and the presence of the feedforward compensator would not give remarkable advantages. The second solution is based on modifying the boundaries of the regulation problem with QFT to include the presence of the feedforward controller. In this case, new boundaries were obtained, and the QFT method was used to design a robust PI controller to account for uncertainties in obtaining promising results.

This contribution was presented and obtained the Young Author Award for the article "Robust QFT-based PI controller for a feedforward control scheme" at the 3rd IFAC Conference on Advances in Proportional-Integral-Derivative Control in Ghent, Belgium, 2018 [61].

3.2 A Practical Solution to the Saturation Problem in Feedforward Control for Measurable Disturbances

The potential of feedforward control is based on the possibility of taking large control signal actions at sudden load disturbance changes. However, sometimes the system actuators are unable to reach these large control signal values, and saturation problems may appear. When it happens, the power of the feedforward control is reduced. It is obvious that control signal saturation limits the capacity of the controller, but in this thesis, it is shown that the saturation problem is aggravated by the anti-windup function that is enabled when the control signal is saturated.

A controller with integral action must have an anti-windup function to prevent the integral term from winding up when the control signal saturates [1, 128]. The back-calculation anti-windup scheme is one of the most common schemes. When the control signal saturates, the back-calculation method changes the integral term dynamically with a tracking time constant [80]. In this thesis, it is shown that this change of the integral action may cause sluggish load disturbance responses, and this is the opposite of the intention for adding feedforward action to the feedback controller.

To overcome this problem, it is suggested to reduce the gain of the feedforward compensator during periods of control signal saturation. A method to calculate this gain reduction is presented, and several simulation examples show that this idea will result in a great performance improvement in these cases. The proposed algorithm is tested on a lab-scale temperature control system to demonstrate noticeable practical capabilities, and experimental results presented in Chapter 4.

3.2.1 Problem Statement

Figure 3.11 shows a blocks diagram of the classical feedback control scheme to deal with the rejection of load disturbances. The diagram is composed of the process model $P_u(s)$, the controller $C(s)$, considering the control signal saturation block, the reference r, the process output y, the control signal u, and the output from the control signal saturated u_{sat}. There is also a measurable load disturbance d, and the model $P_d(s)$ describes the dynamics between this disturbance and the process output.
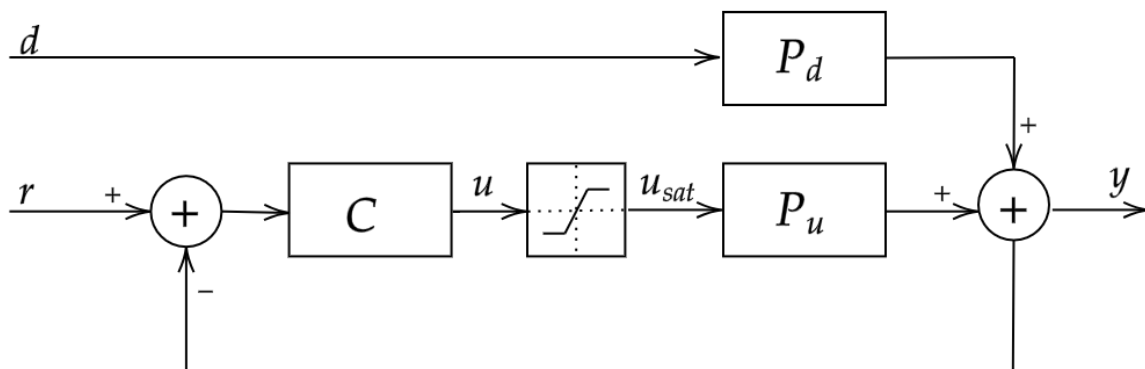

Figure 3.11. Feedback control scheme with control signal saturation.

It is assumed that the two process transfer functions can be approximated by a FOPDT, defined in Equation (2.8). K_u and K_d are the static gains, T_u and T_d are the time constants, and L_u and L_d are the time delays.

Since d in Figure 3.11 is measurable, feedforward can be used to improve the load disturbance rejection. Figure 3.12 shows a block diagram where a feedforward compensator $C_{ff}(s)$, that takes disturbance d as input and subtracts its output from the feedback control signal, has been added to the feedback loop. The difference between the control signal given by the controller (u), and the one saturated (u_{sat}), is $e_{sat} = u - u_{sat}$.
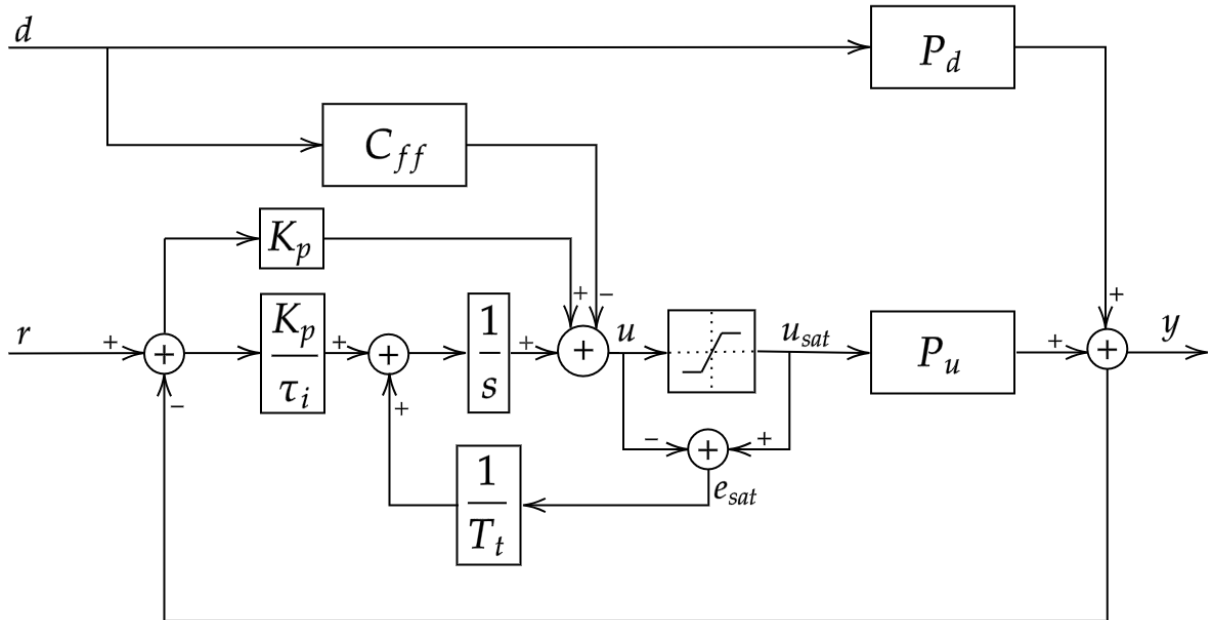

Figure 3.12. Feedback control loop complemented with feedforward and anti-windup.

From the block diagram in Figure 3.12, one can see that when the control signal is not saturated, the closed-loop transfer function relating the process output with the disturbance signal is given by

$$T_{dy}(s) = \frac{P_d(s) - C_{ff}(s)P_u(s)}{1 + P_u(s)C(s)} \qquad (3.11)$$

where perfect elimination of the load disturbance is obtained if Equation (2.7) is applied.

As commented previously, this ideal compensator is, unfortunately, normally not realizable, see [36]. The most common reason is the delay inversion problem that arises when the delay in $P_u(s)$ is longer than the delay in $P_d(s)$. Other reasons may be that the compensator becomes unstable or gets derivative action or that the control signal becomes saturated. In this contribution, only the delay inversion and control signal saturation problems are treated.

As described in Chapter 2, in industry, the feedforward compensator $C_{ff}(s)$ is often just a static gain, but a significant improvement can often be made when the following lead-lag structure is used, see [37]. The structure that will be treated in this section is defined in Equation (2.9).

The saturation problem in the control loop arises when the control variable u exceeds the limits of the actuator. If it happens, the actuator will stay within these limits for a period of time in spite of changes in the error signal. Due to this, it is necessary to implement an anti-windup

technique in order to avoid the windup of the integral term of the controller. In Figure 3.12, the back-calculation anti-windup method is implemented. This is one of the most common anti-windup methods, and here the integrator is dynamically changed with a tracking time constant T_t when the control signal saturates [1]. The tracking constant choice $T_t = 0.3T_i$ has been used in this thesis for all the examples in order to normalize the results, but of course, other tuning choices can be made.
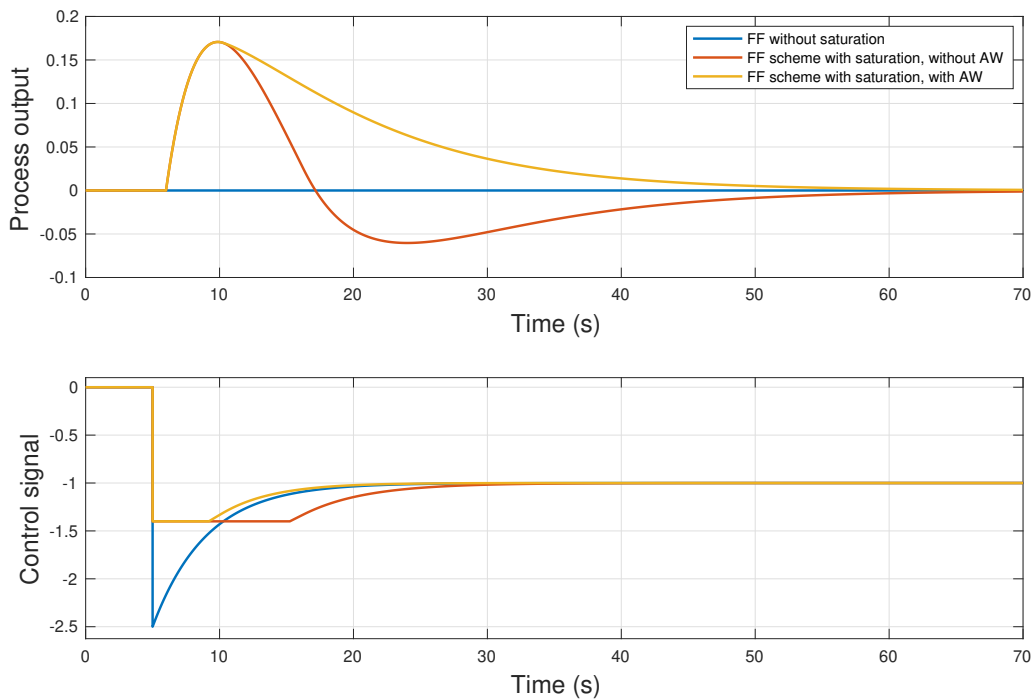

Figure 3.13. Comparison of different implementations for control at saturation problem.

Figure 3.13 shows an example to present a performance comparison between different cases for the control problem in the presence of saturation. The process model parameters are $K_u = K_d = 1,\ L_u = L_d = 1,\ T_u = 10, T_d = 4$, and the PI controller has been designed with the Lambda method, where $\lambda = 0.2T_u$. The controller parameters are $K_p = 3.3,\ \tau_i = 10$. The control signal is limited between ± 1.4. The figure shows responses to a step load disturbance with magnitude $d = 1$ at time $t = 5s$. Notice that the reference signal, r, will be equal to 0 in order to show better the disturbance rejection response. This choice for the reference signal will be used for the rest of the examples in this contribution.

In Figure 3.13, it can be observed that in the case of feedforward without saturation, a perfect cancellation of the disturbance d is obtained. It can also be seen that this perfect cancellation requires a significant peak in the control signal at the time when the disturbance arrives. However, if the control signal saturates, the ideal feedforward is no longer realizable. The case when the anti-windup is not included shows a large overshoot in the process output and a long saturation time. This is because the windup of the integral term occurs. In the third case, the anti-windup function is enabled. With this implementation, it can be seen that there is no overshoot in the process output, and the anti-windup helps the controller leave the saturation earlier. However, it can also be seen that the response is sluggish. The reason is that the anti-windup function has

caused a significant increase of the integral term to counteract the desired large negative peak of the control signal because of the feedforward action. The sluggish response is caused by the slow recovery of this term.

Therefore, it can be observed that the performance of the process output is highly affected due to the control signal saturation and the anti-windup function. So, the goal of this thesis contribution has been to find a method to improve the process output performance by reducing this bad influence of the anti-windup function on the feedforward action. For this purpose, the Integral Absolute Error (IAE) has been considered as a metric to quantify the control system performance, as presented in the next section.
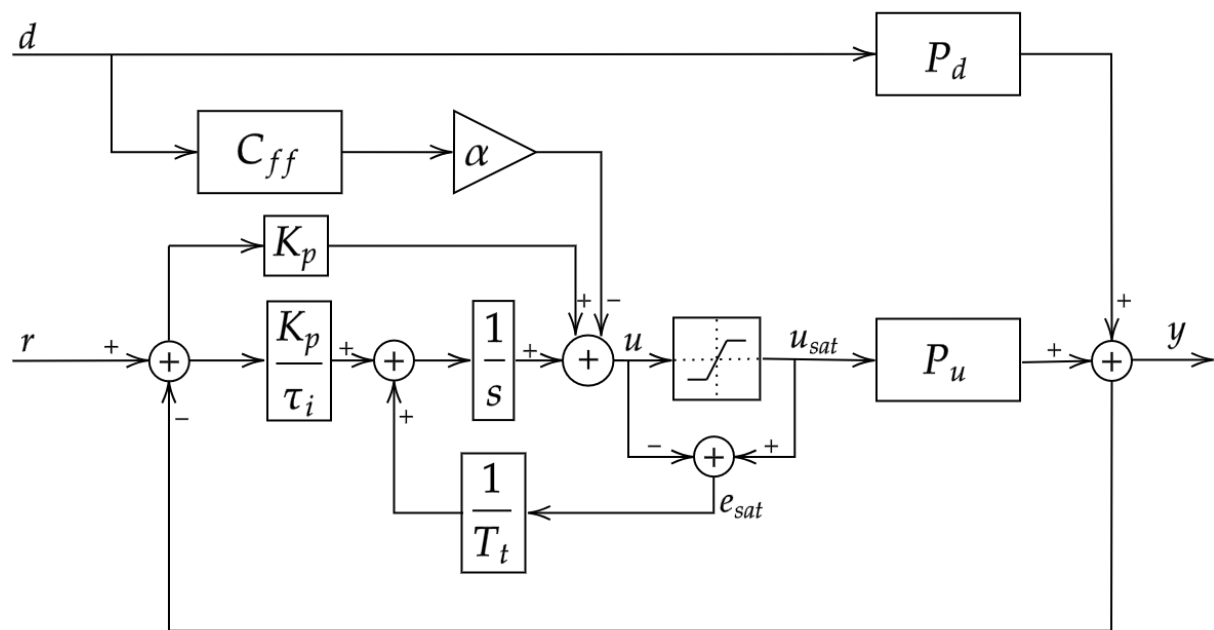
3.2.2 Proposed Method

Figure 3.14. Feedforward and anti-windup scheme with the new gain-reduction factor α.

Thus, according to the discussion in the previous section, the sluggish response when the feedforward control signal is saturated is caused by the anti-windup function. So, a natural remedy would have been to modify this function in some way. This is, however, not an option since the anti-windup function is there to prohibit windup for many other reasons than the saturation caused by the feedforward action. Therefore, the problem must be solved by modifying the feedforward action itself when the control signal saturates.

The approach taken in this thesis is to reduce the gain of the feedforward action during the time period when the control signal is saturated, looking for an improvement of the IAE value. In this way, the anti-windup action is reduced, and the control system performance will be improved. The approach is illustrated in Figure 3.14. The figure shows the same scheme as in Figure 3.12, except that a gain-reduction factor α has been added to the feedforward path. The factor α is one when the control signal is not saturated, which means that the original feedforward compensator is retained. However, when the control signal saturates, α will obtain a value smaller than one, making the desired control signal peak smaller so that the desired control signal is closer to the saturation limit. This will reduce the magnitude of the error e_{sat}, and therefore also the

modification of the integral term, contributing to reducing the impact of the anti-windup scheme on the feedforward control response.
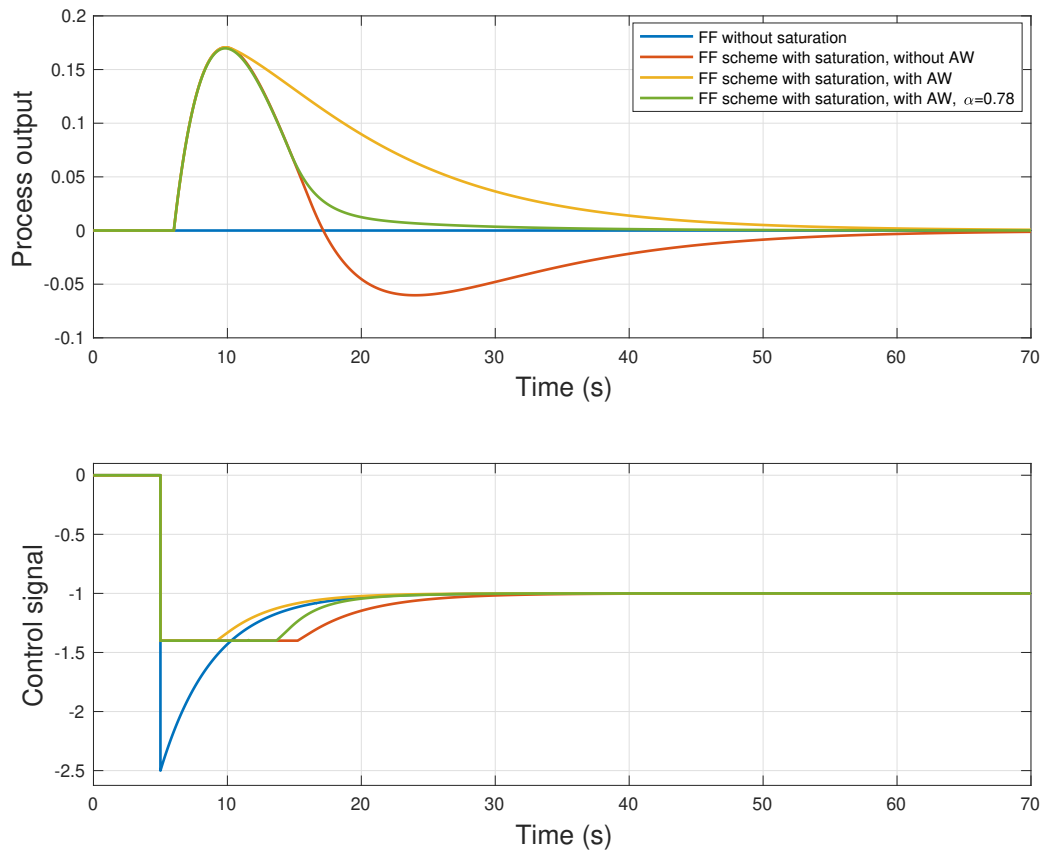

Figure 3.15. Comparison between different feedforward schemes.

To show the capabilities of the proposed idea, Figure 3.15 shows the same example as presented in Figure 3.13, but includes the new approach from Figure 3.14 with $\alpha = 0.78$. It can be seen that the time when the control signal is saturated has been increased in comparison with the case without gain reduction, i.e., when $\alpha = 1$, and the process output performance has been highly improved with a faster disturbance rejection without any overshoot.

However, the tuning of α is the key factor in the proposed scheme since it has a direct influence on the system performance. This can be seen in Figure 3.16, which shows the same example as before, but considering different α values. As observed, the new α parameter affects the control signal saturation and the performance of the process output.

Therefore, tuning rules for α should be defined within the proposed control approach according to a desired design objective. In this thesis, the calculation of α is performed based on a tradeoff between the amount of the control signal exceeding the saturation limits and the IAE of the control system. Notice that the aim of this approach is not focused on reducing the time that the system is in saturation (as typically pursued when saturation problem arises), but also to improve the control system performance. Therefore, the following three steps have been performed to obtain the proposed tuning rule for the α parameter:

1. The feedforward control signal is characterized and normalized based on the feedforward controller parameters and the saturation limits.

2. The previous control signal characterization is used within an optimization problem to find the optimal value of α that minimizes the IAE metric for a wide range of different scenarios.

3. Finally, a simple tuning rule for α is derived and generalized based directly on the feedforward control parameters and the saturation limits.

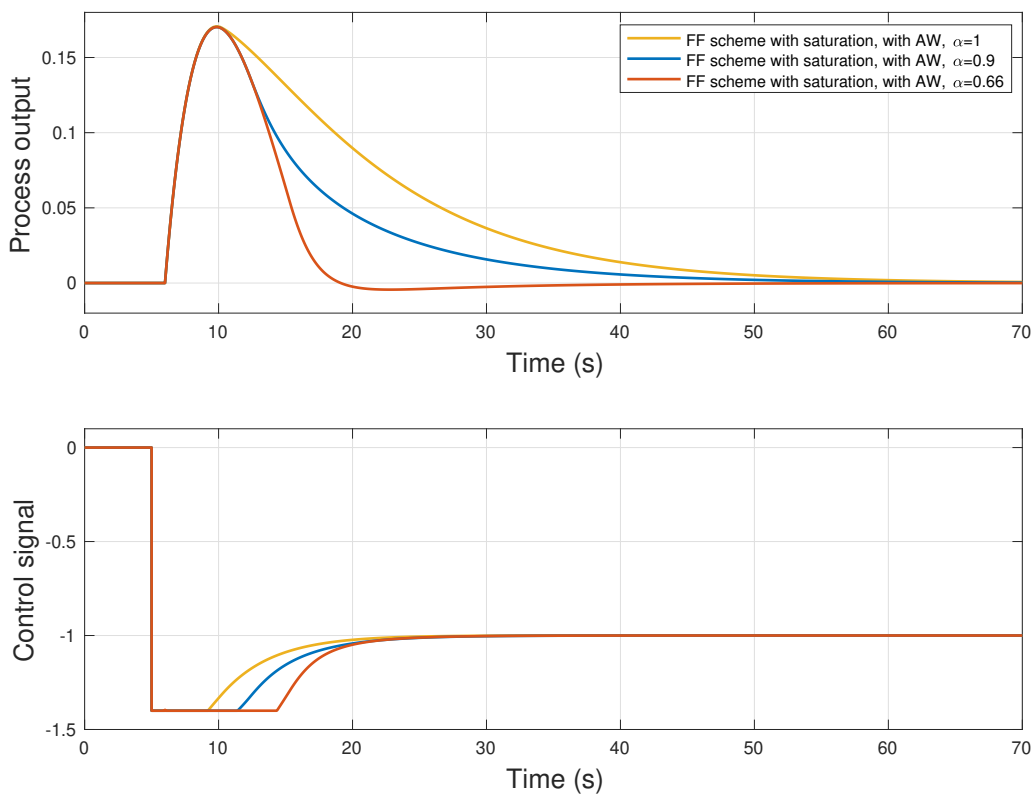All these steps are summarized in the following sections.

Figure 3.16. Comparison of the new scheme implementation with different values of the new gain-reduction factor α.

Step 1. Control signal characterization

An important piece of information in this study is to obtain a relationship between the peak value of the control signal when the system does not saturate, u_{peak}, and the distance to the saturation value, u_{limit}. This idea can be observed in Figure 3.17, which shows the responses to a load disturbance and some measures to characterize the control signal.

The values of these measures shown in Figure 3.17 can be obtained using the initial and the final value theorems on Equation (2.9), resulting in the initial peak value and the final value of the control signal at a step load disturbance of magnitude d:

$$u_{peak} = \lim_{t \to 0} u(t) = \lim_{s \to \infty} -sC_{ff}(s)\frac{d}{s} = \lim_{s \to \infty} -s\frac{K_d}{K_u}\frac{T_u s + 1}{T_d s + 1}\frac{d}{s} = -\frac{K_d}{K_u}\frac{T_u}{T_d}d$$

$$u_{final} = \lim_{t \to \infty} u(t) = \lim_{s \to 0} -sC_{ff}(s)\frac{d}{s} = \lim_{s \to 0} -s\frac{K_d}{K_u}\frac{T_u s + 1}{T_d s + 1}\frac{d}{s} = -\frac{K_d}{K_u}d \tag{3.12}$$

From Figure 3.17 and Equation (3.12), it can be seen that a peak will only occur when $|u_{peak}| > |u_{final}|$, and this will occur only when $T_z > T_p$. Therefore, we assume that this relation holds from now on. The ratio between T_z and T_p is important for the determination of the gain reduction factor α since it gives information about the control signal peak. Thus, the following time-constants ratio is defined

$$R_T = \frac{T_p}{T_z} \quad \text{where}: \ R_T \ \in \ (0,1) \tag{3.13}$$

The relation between the control signal and the saturation limits is of course, also important for the determination of α. The control signal saturation limits are u_{max} for the upper limit and u_{min} for the lower limit. To simplify, u_{limit} is used to refer to the saturation limit, applicable for
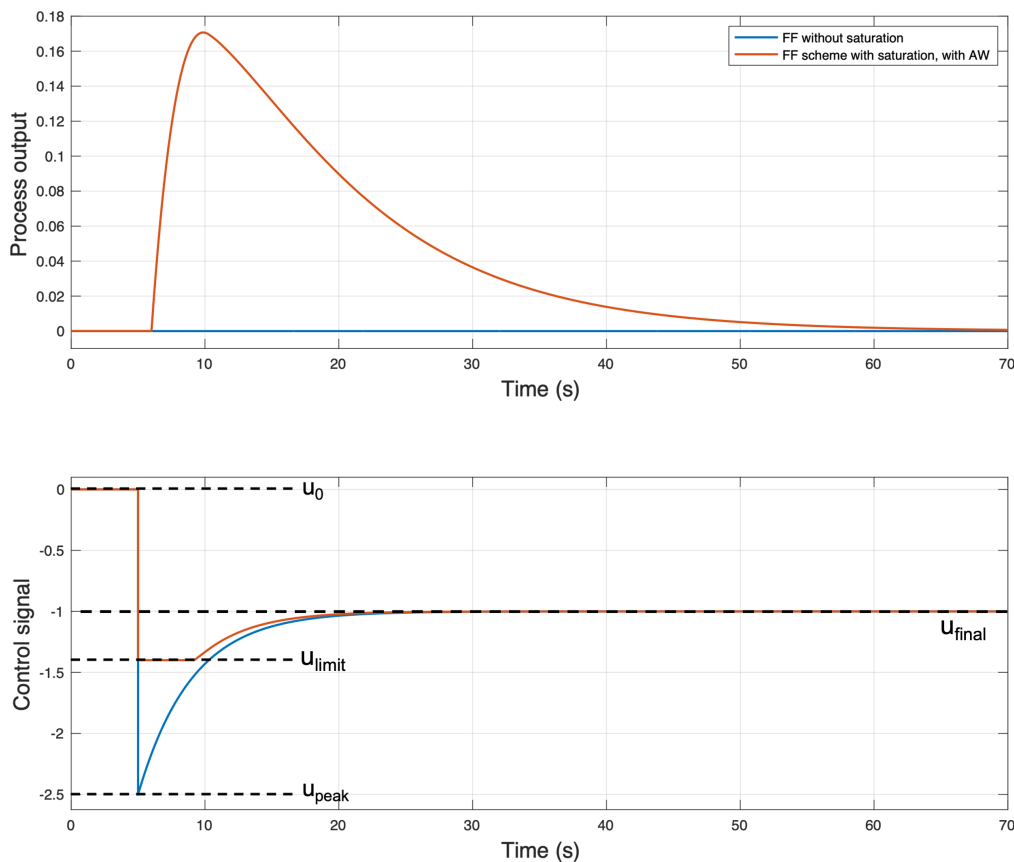

Figure 3.17. A load disturbance response and some measures to characterize the control signal behavior.

both control signal limits. Using notations defined in Figure 3.17, the saturation ratio is defined as:

$$R_S = \frac{u_{peak} - u_{limit}}{u_{peak} - u_0} \quad \text{where}: \ R_S \ \in \ (0,1) \tag{3.14}$$

The saturation ratio, R_S, represents the amount of control effort that is being lost due to saturation. Values of R_S close to 1 occur when the saturation is high, and values close to 0 when there is almost no saturation (we assume $|u_{peak}| > |u_{limit}|$).

Thus, two different ratios, R_T, and R_S, have been defined to characterize the feedforward control signal based on the compensator parameters and the saturation limits.

Step 2. Optimization of the α factor

In this thesis, suitable values of α have been found following an optimization procedure. The main objective is to find an α value to reduce the saturation effect while improving the control performance. Thus, a global optimization method has been applied to minimize the IAE at step load disturbances, as a metric to evaluate the performance. It is defined as

$$\min_{\alpha} \ \int_0^{T^*} |e(t)|\, dt \ \ \text{such that}: \quad 0 < \alpha \le 1 \tag{3.15}$$

where T^* is the simulation time for the optimization procedure.

The optimization problem was run through a wide range of tests by varying the ratios R_T and R_S in order to cope with an extensive range of combinations. The time-constant ratio R_T has been changed from 0.02 to 0.98 in steps of 0.02. For each value of R_T, different values of R_S are swept, using ten different values of the u_{limit} between u_{peak} and u_{final}. With each combination, the optimization problem defined in Equation (3.15) has been evaluated in order to find the optimal value of α in each simulation. The test parameters have been set as: $K_u = 1$, $L_u = 1$, $K_d = 1$, $L_d = 1$, and $u_0 = 0$. Notice that these values are not affecting to the feedforward saturation problem as observed from the equations derived in the previous section. On the other hand, it is important to mention that in order to separate the influence of the anti-windup control scheme and the tracking constant T_t, the tests have been performed without the anti-windup function.

Figure 3.18 shows the results of the optimization where the optimal value of α is shown versus R_S. Each line represents a separate R_T value. The one on the far right represents the smallest R_T value (0.02, largest difference between the time constants), and the one to the far left the highest R_T value (0.98, smallest difference between the time constants). It can be seen that when the saturation ratio R_S is small and the time-constant ratio R_T is large, the gain-reduction factor α is close to 1. However, when the control signal saturates more, this factor becomes smaller. It can also be observed that when R_T is small, u_{peak} is high and, therefore can have a larger R_S. On the other hand, when the time constants are close so that R_T is small, u_{peak} is small, and so is the R_S value. In these cases, the factor α is almost 1. Notice that a wider range of simulations could have been performed for the results shown in Figure 3.18. Nevertheless, these variations are enough for the approximations performed in the next section and the obtained tuning rule.

Step 3. Tuning rule for the α factor

Due to the complexity of the problem described above and the variation of the responses in Figure 3.18, this section presents a linear approximation to derive an equation for α. To find

the equation, the result of the optimization described above has been divided into five different regions. The mean value of each region has been calculated in order to estimate a linear function.
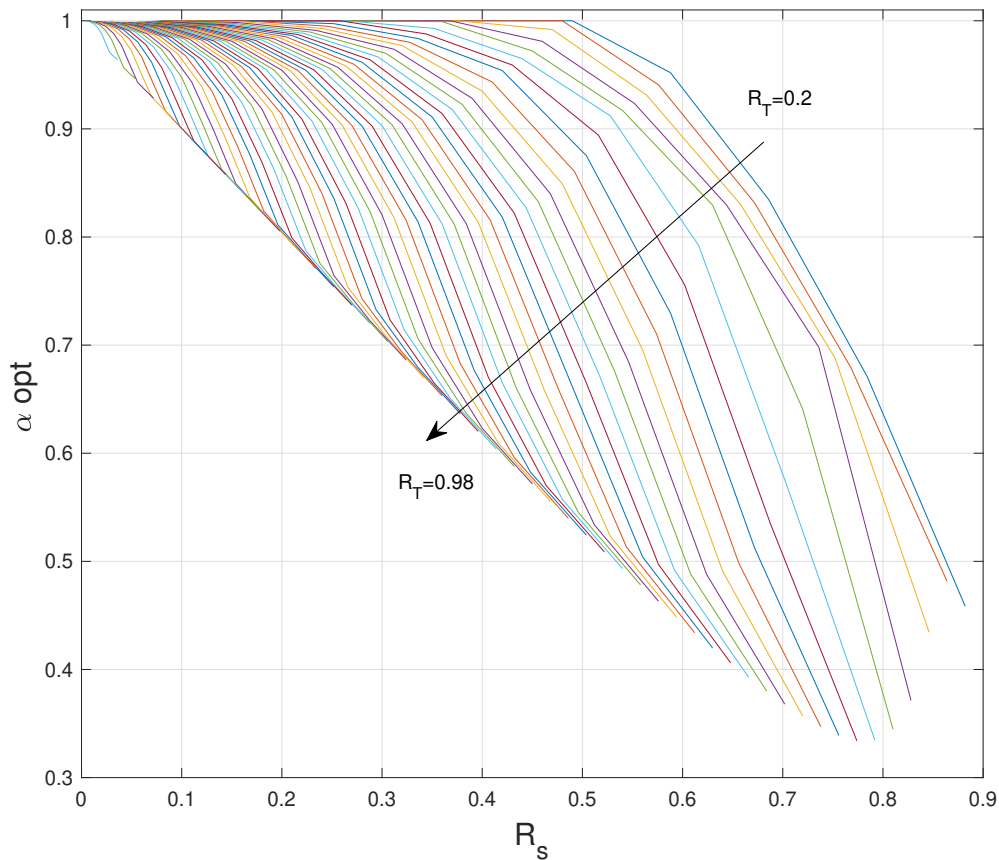

Figure 3.18. Result of the optimization tests.

Figure 3.19 shows these different regions where the solid highlighted curves represent the mean values of each R_T group. So, by analyzing these values, a general linear function can be obtained as defined in Equation (3.16).

$$\alpha = \begin{cases} f & 0 < f < 1 \\ 1 & \text{else} \end{cases}$$ (3.16)

$$f(R_S, R_T) = -1.6R_S - R_T + 1.9$$

In Figure 3.19, the dotted highlighted lines represent the approximation of the new function in each R_T region, showing an adequate fitting.

To show an example of the validation for Equation (3.16), a test has been carried out to compare the optimal and approximate values of α. The example parameters are: $K_u = 1$, $T_u = 10$, $L_u = 1$, $K_d = 1$, $T_d = 4$, $L_d = 1$, and $R_S = 0.51$ ($u_{limit} = -1.22$). The controller parameters are $K_p = 3.3$, $\tau_i = 10$ Figure 3.20 shows the simulation responses for this example. As observed, the α values obtained by applying the equation ($\alpha = 0.68$) and the optimal method ($\alpha = 0.61$) are very close, resulting in an almost identical response.
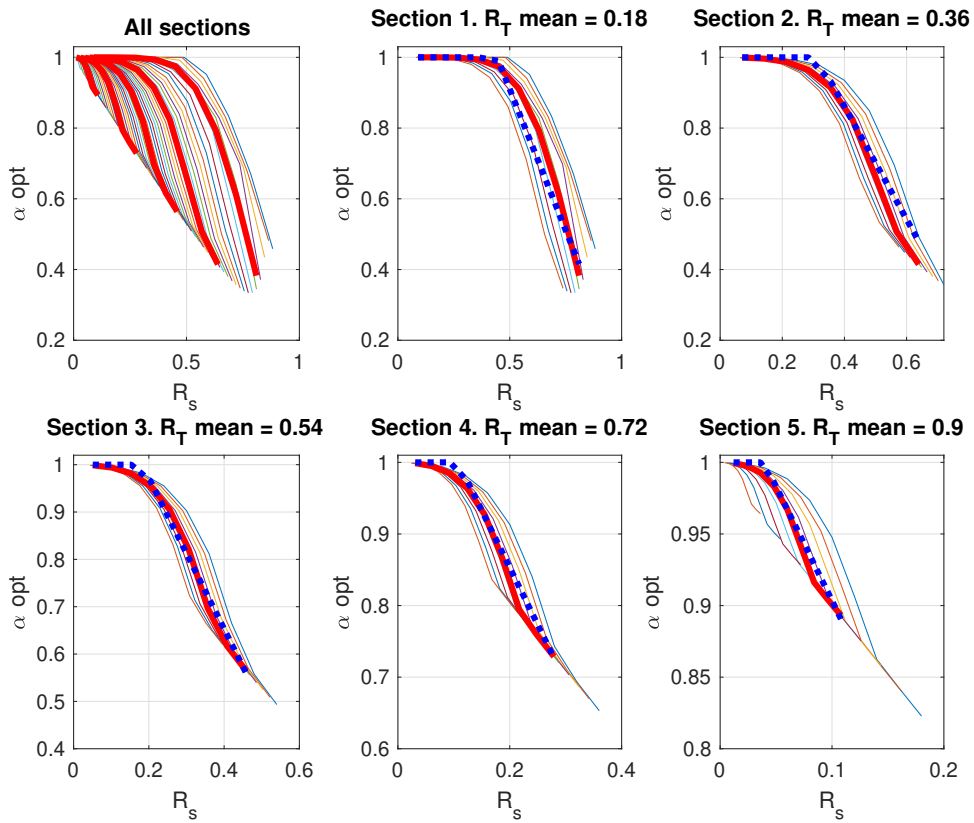
Figure 3.19. Optimization test sections. The highlighted continuous curves represent the mean values of each section. The dotted highlighted curves represent the linear approximation of the developed equation in each region.
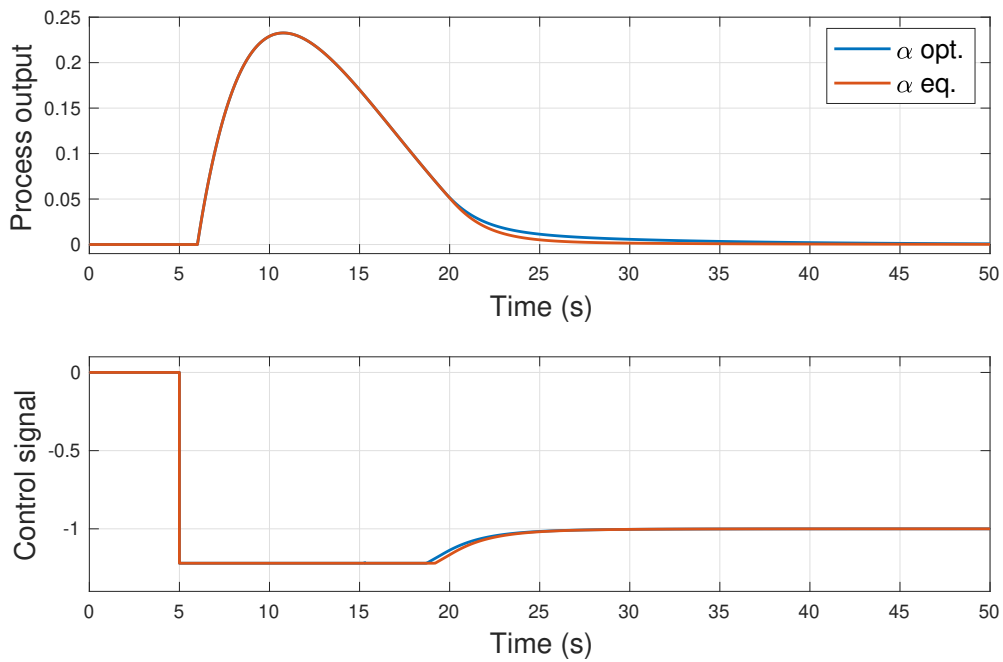

Figure 3.20. Comparison between α obtained by (3.16) and optimization method.

Thus, a new equation has been developed to calculate a new gain-reduction factor α to apply to the feedforward compensator in order to reduce its gain and improve its performance when the control signal saturates.

3.2.3 Examples

In this section, the use of the gain-reduction factor α, determined according to the method presented in the previous section, is applied to five different process models P_u and P_d with different relations between the process model parameters. The process models have the following characteristics:

- **Example 1:** $K_u = K_d$, $L_u = L_d$, small R_T and large R_S.

- **Example 2:** $K_u \neq K_d$, $L_u = L_d$, small R_T and medium R_S.

- **Example 3:** $K_u = K_d$, $L_u < L_d$ (no inversion problem), small R_T and medium R_S.

- **Example 4:** $K_u = K_d$, $L_u > L_d$ (inversion problem), small R_T and medium R_S.

- **Example 5:** $K_u = K_d$, $L_u = L_d$, small R_T and medium R_S. P_1 and P_2 are second-order transfers function with two real poles.

In the examples, performances of the classic feedforward scheme with anti-windup and the new scheme with gain reduction proposed in this contribution are compared. A step disturbance with amplitude $d = 1$ is applied at time $t = 5$ s, and $u_0 = 0$. The anti-windup scheme is applied in both schemes with $T_t = 0.3\tau_i$, and the controller has been tuned with the Lambda method (2.5), with $\lambda = 0.2T_u$.

	IAE_{norm}	$Imax_{norm}$
Example 1	0.63	0.31
Example 2	0.66	0.26
Example 3	0.68	0.62
Example 4	0.73	0.53
Example 5	0.26	0.53

Table 3.1. Normalized IAE and maximum integral values in the five examples.

Table 3.1 summarizes the comparisons. The IAE has been used as the metric to evaluate performance. To normalize it, in each example, it has been calculated as follows:

$$IAE_{norm} = \frac{IAE_{\alpha=eq}}{IAE_{\alpha=1}} \qquad (3.17)$$

The maximum value of the integral term has also been used in the comparison, and it has been normalized as:

$$Imax_{norm} = \frac{Imax_{\alpha=eq}}{Imax_{\alpha=1}} \qquad (3.18)$$

Notice in Equations (3.17) and (3.18) the subscripts $\alpha = eq$ means the use of the α tuning rule from Equation (3.16). As observed, in all cases, the indicators are below 1, which means that the proposed method is running better than the feedforward with $\alpha = 1$.

Example 1

The parameters in this example are: $K_u = 1$, $T_u = 10$, $L_u = 1$, $K_d = 1$, $T_d = 2$, $L_d = 1$, $R_S = 0.7$ $(u_{limit} = -1.5)$, $R_T = 0.2$. The PI controller parameters are $K_p = 3.3$, $\tau_i = 10$. The gains and the delays are the same in both transfer functions, but there is a large difference between the time constants. The parameters give a small R_T value and a large value of R_S.
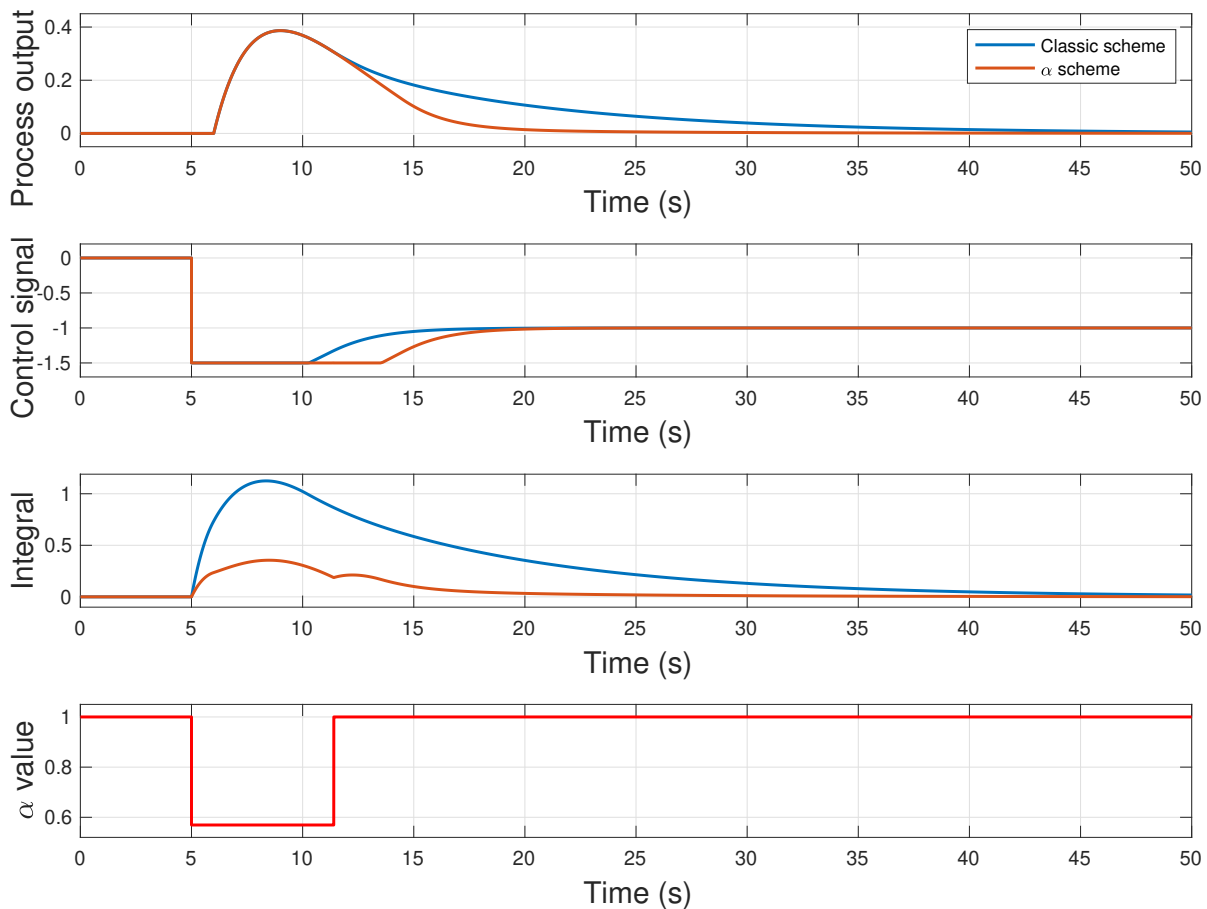

Figure 3.21. Example 1 simulation results comparing the proposed solution for the saturation problem and the classic feedforward control.

In Figure 3.21, the improvement of the new method compared to the classical scheme can be seen. The load disturbance response in the process output is rejected faster, and the control signal stays at the saturation limit for a longer time. Regarding the integral term, it can be seen that it has decreased because of the reduction in the feedforward gain. It can also be seen that at the time instant when α returns to 1, and therefore the feedforward gain comes back to its original value, the integral increases and makes the control signal continue to be saturated for a longer time. Looking at the IAE_{norm} value of Table 3.1, the new scheme has decreased the IAE value by a factor of 0.63 compared with the classical one. The integral maximum value has also been reduced by a factor of 0.31.

Example 2

The parameters in this example are: $K_u = 19$, $T_u = 10$, $L_u = 1$, $K_d = 80$, $T_d = 3$, $L_d = 1$, $R_S = 0.57 \, (u_{limit} = -6)$, $R_T = 0.3$. The PI controller parameters are $K_p = 0.17$, $\tau_i = 10$. The delays are the same, but the gains differ between the two models, and are very high.
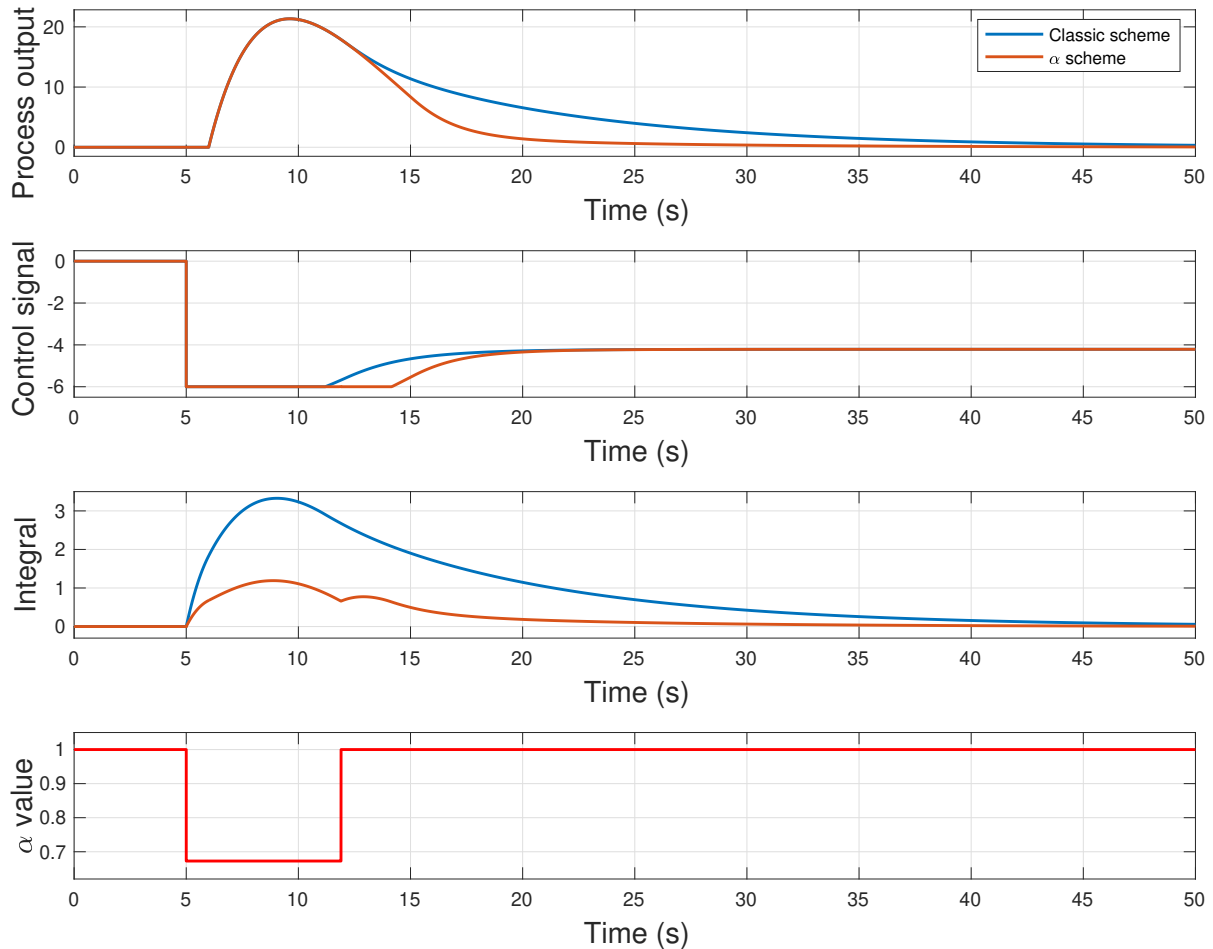

Figure 3.22. Example 2 simulation results comparing the proposed solution for the saturation problem and the classic feedforward control.

It can be seen in Figure 3.22 that the method works also in this case with high gains. The load disturbance is rejected faster with the new method, and the behavior of the integral is the same as in the previous example, allowing the control signal to saturate for a longer time. As shown in Table 3.1, the implementation of the new scheme improves the value of the IAE by a factor of 0.66 compared to the classic one, and the integral maximum value has been reduced by a factor of 0.26.

Example 3

The results for this example are shown in Figure 3.23. The parameters in this example are: $K_u = 1$, $T_u = 10$, $L_u = 3$, $K_d = 1$, $T_d = 3.5$, $L_d = 7$, $R_S = 0.47 \, (u_{limit} = -1.5)$, $R_T = 0.35$. The PI controller parameters are $K_p = 2$, $\tau_i = 10$. The gains are the same, but the delays are different in the two models. Since $L_u < L_d$, there is no delay inversion problem.

As in the previous examples, it can be seen in the process output plot that the disturbance is rejected faster when the new scheme is used. In this case, the saturation time of the control signal

is considerably longer for the new scheme compared with the classic one, and yet, unlike the previous examples, the time period when the feedforward gain is reduced is minor. Regarding the IAE index, from Table 3.1 an improvement by a factor of 0.68 is obtained, and the integral maximum value has been reduced by a factor of 0.62.
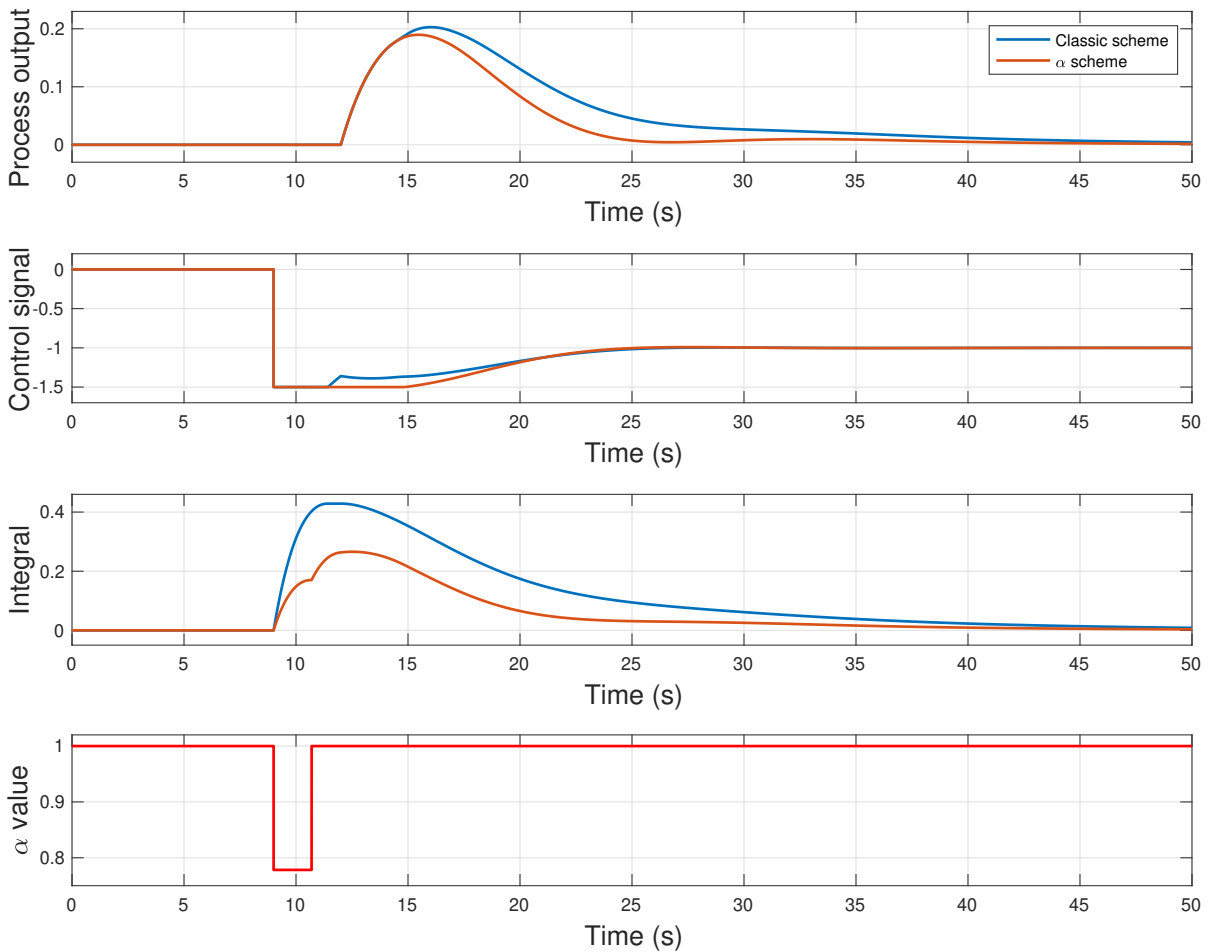

Figure 3.23. Example 3 simulation results comparing the proposed solution for the saturation problem and the classic feedforward control.

Example 4

The parameters in this example are: $K_u = 1$, $T_u = 10$, $L_u = 6$, $K_d = 1$, $T_d = 3$, $L_d = 4$. The PI controller parameters are $K_p = 1.25$, $\tau_i = 10$. The gains are the same, but the delays differ between the two models. In this example, $L_u > L_d$ results in a delay inversion problem. This means that the classic tuning rule can not be used. Instead, the tuning rule that takes the delay inversion problem into account presented in [36] has been used. This rule is based on setting the feedforward gain and time constant T_p in order to reduce the overshoot in the process output and minimize the IAE value. The compensator parameters are calculated as defined in Equations (2.11) and (2.12).

Figure 3.24 shows the results of this simulation, where the saturation and time-constant ratio parameters are: $R_S = 0.67$ ($u_{limit} = -1.5$), $R_T = 0.18$. It can be seen in the process output plot that the new gain-reduction factor α improves the load disturbance rejection. In this case, the time period when the control signal saturates with the new scheme is shorter than in the previous examples, and also the time when the compensator gain is reduced. From Table 3.1,

the IAE value is decreased by a factor of 0.73, and the maximum value of the integral term has been reduced by a factor of 0.53. This example shows that the use of the gain reduction factor is not restricted to the classical feedforward tuning rule, but can be applied to other tuning rules as well.
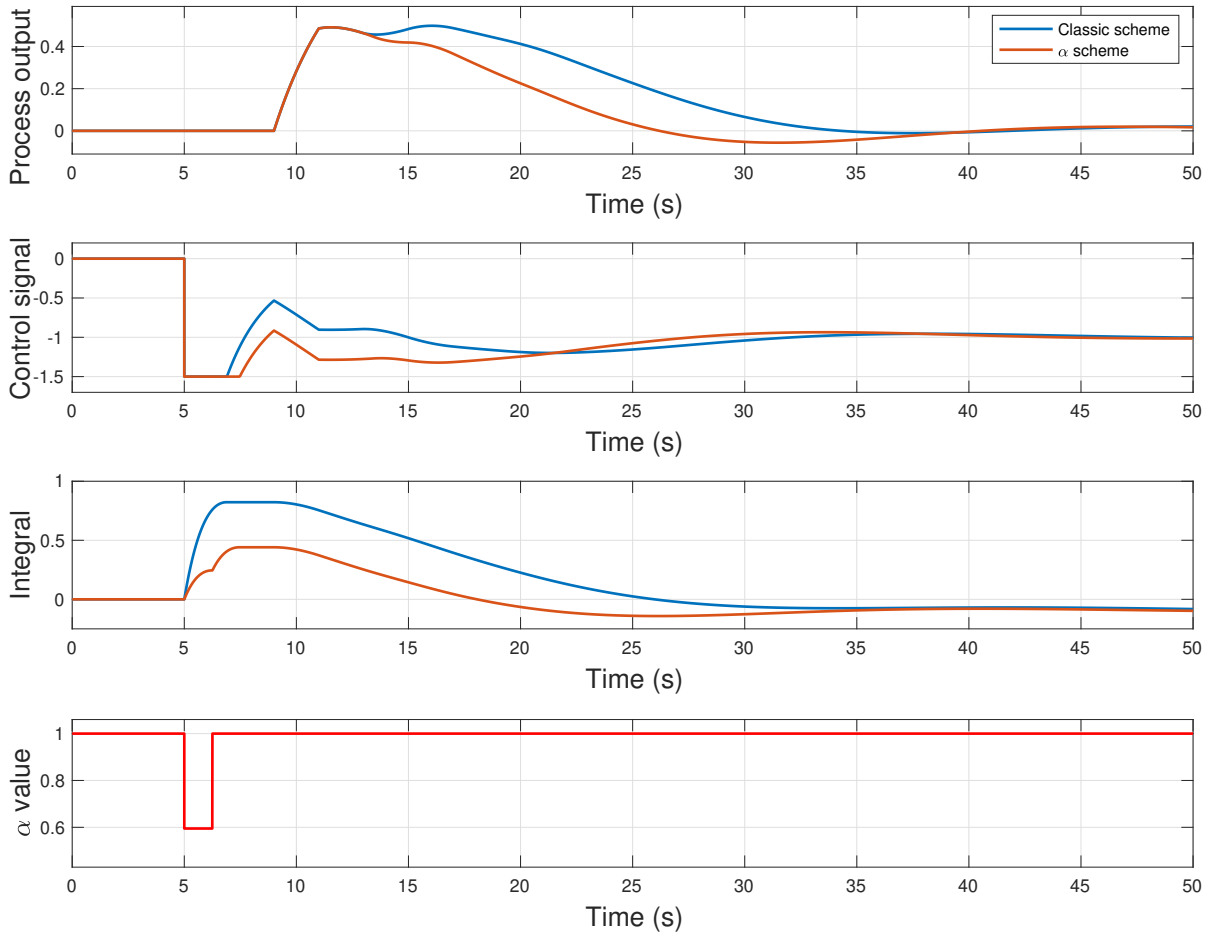

Figure 3.24. Example 4 simulation results comparing the proposed solution for the saturation problem and the classic feedforward control.

Example 5

In this example, two second-order transfer functions with two real poles, defined in Equation (3.19), have been selected. The parameters are: $K_u = 1$, $T_{u,1} = 10$, $T_{u,2} = 5$, $L_u = 0$, $K_d = 1$, $T_{d,1} = 3$, $T_{d,2} = 1$, and $L_d = 0$.

$$P_u(s) = \frac{K_u}{(T_{u,1}s + 1)(T_{u,2}s + 1)}e^{-L_u s}$$
$$P_d(s) = \frac{K_d}{(T_{d,1}s + 1)(T_{d,2}s + 1)}e^{-L_d s}$$

(3.19)

To apply the rule, the half-rule approximation to a first-order system with time delay has been applied [125]. So, the resulting first-order approximated models are shown in Equation (3.20), resulting in the parameters: $K_u = 1$, $T_{u,approx} = T_{u,1} + T_{u,2}/2 = 12.5$, $L_{u,approx} = L_{u,1} + L_{u,2}/2 = 2.5$, $K_d = 1$, $T_{d,approx} = T_{d,1} + T_{d,2}/2 = 3.5$, and $L_{d,approx} = L_{d,1} + L_{d,2}/2 = 0.5$. The PI controller parameters are $K_p = 2.5$, $\tau_i = 12.5$.

$$P_u(s) \approx \frac{K_u}{(T_{u,1} + \frac{T_{u,2}}{2})s + 1} e^{-(L_u + \frac{T_{u,2}}{2})s}$$

$$P_d(s) \approx \frac{K_d}{(T_{d,1} + \frac{T_{d,2}}{2})s + 1} e^{-(L_d + \frac{T_{d,2}}{2})s}$$

(3.20)

Once the approximation is made, $L_{u,approx} > L_{d,approx}$, which results in a delay inversion problem. As it has been done in Example 4, for designing the feedforward, the tuning rule that considers the delay inversion problem is used [36]. The new pole T_p and gain K_{ff} are calculated as defined in Equations (2.11) and (2.12). Hence, the new values of the time-constant and saturation ratio are $R_T = 0.19$ and $R_S = 0.66$.
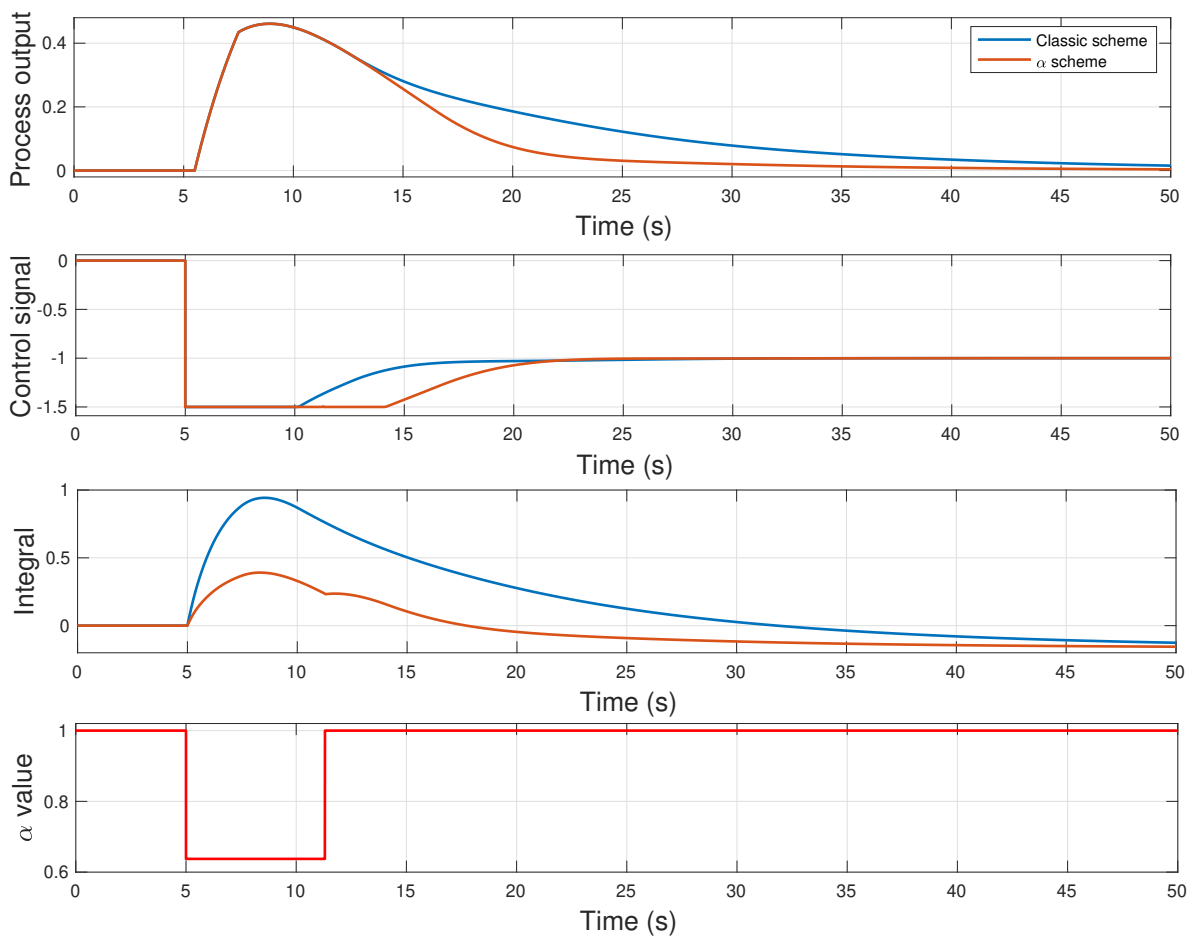

Figure 3.25. Example 5 simulation results comparing the proposed solution for the saturation problem and the classic feedforward control.

The simulation results are presented in Figure 3.25. The process output plot demonstrates the enhancement in load disturbance rejection achieved by the new gain-reduction factor α. The control signal saturates for a longer time than in the previous example, and the compensator gain reduction occurs within an increased time period. Analysis of Table 3.1 reveals a 0.71 decrease in the IAE value and a 0.26 reduction in the maximum integral term value.

This example illustrates the robustness of the gain reduction factor, even when approximating a second-order system as a first-order system with delay. As presented in Example 4,

it is demonstrated again that the proposed approach can be applied not only to the classical feedforward tuning rule but also to other existing tuning methods to deal with inversion problems.

3.2.4 Conclusions

This contribution treats a problem that has not been recognized before, namely the negative influence anti-windup functions may have on feedforward control actions. An efficient feedforward compensator will often give significant peaks in the control signal at step changes in the load disturbance, and these peaks may cause saturation of the control signal. The anti-windup function avoids integrator windup by modifying the integral term of the controller when the control signal saturates. It is shown that this modification of the integral term may cause sluggish load disturbance responses at feedforward control, which is the opposite of the intention with the use of feedforward.

In this contribution, it is suggested to overcome the problem by reducing the gain of the feedforward compensator during periods of control signal saturation, and in this way reduce the anti-windup effect on the load disturbance response. Therefore, a gain-reduction factor α is introduced in the feedforward path. The factor is one when the control signal is not saturated, but when the control signal becomes saturated, α gets a value less than one. An optimization-based method to determine α is presented based on the IAE criterion. The result of the optimization is approximated by a simple linear function that gives α as a function of the parameters of the compensator and the distance from the actual control signal peak to the saturation limit.

The proposed strategy to handle the feedforward saturation problem and the choice of gain-reduction factor α have been tested through simulations of different SISO process models. Nevertheless, this solution can be easily extrapolated to a MIMO system by considering decoupled control loops. The examples show that the strategy works well and gives significant improvements in the load disturbance responses.

This contribution has resulted in a scientific journal article, indexed in the Journal Citation Report (JCR), and is currently under review [58].

3.3 Double Feedforward Compensation for Cascade Control Schemes

Control schemes like feedback control may not always be adequate for effectively managing complex processes in the process industry. Alternative control strategies such as feedback plus feedforward, cascade control, and cascade control with feedforward components may be required to address the control challenges. Implementing these control schemes offers enhanced capabilities and flexibility, enabling better control system performance and handling of complexities in the process industry.

In some processes, adopting a cascade control structure is crucial for improving load disturbance rejection and system performance. This structure consists of two control loops: an inner loop nested within an outer loop. The inner loop must exhibit a faster dynamic response than the outer loop, specifically for handling load disturbances in the inner loop. By incorporating the intermediate process measurement, load disturbances affecting the inner loop can be mitigated

before propagating to the primary outer loop, enhancing the robustness of the control system and ensuring reliable operation even in challenging process conditions. In the literature, several studies can be found analyzing and implementing this control technique. In [104], a survey studying the cascade control strategies in which controller parameters are expressed in terms of known process model parameters is developed. In [78], two new two-degree-of-freedom control structures are proposed for cascade control systems, both of which are identical in the controller design procedure. In [68], a PI–PD Smith predictor scheme is used in the outer loop, and internal model control is in the inner loop of the cascade control in order to improve the performance.

Despite the power of cascade control to reject disturbances that affect the inner loop, there may be some disturbances that it can not take over efficiently, and they can substantially influence the operation and performance of industrial processes. When the disturbances are measurable, considering them in advance can aid the feedback controller in effectively mitigating their impact. Feedforward control is the mainly used solution to reject measurable load disturbances [37, 77]. Despite that, there is a limited number of studies in the literature that specifically address the rejection of measurable disturbances in a cascade control scheme. In [140], a feedforward–cascade controller for dissolved oxygen concentration in an activated sludge process is designed in order to meet stricter effluent quality standards at a minimum cost. In [82], a cascade control with a non-linear model-based feedforward is proposed to control a McKibben artificial muscle actuator. However, the combination and tuning of both control schemes have not been treated before.

In this thesis, a simple new method for rejecting measurable disturbances of the output outer loop in cascade control is presented. The solution is based on analyzing various designs and implementations of feedforward control within the cascade scheme. The proposed approach suggests the implementation of two static feedforward controllers, one entering the outer loop and the other entering the inner loop. The gain of the feedforward controller in the inner loop will be adjusted according to the proposed design rule to enhance the performance of the process output. The variation in process dynamics has been taken into account for the design. Several examples are proposed to validate the robustness of the proposed equation. All of them demonstrate how the performance at the output of the outer loop in rejecting the disturbance significantly improves while also reducing its control effort.

3.3.1 Preliminaries

In this section, the classical cascade control scheme described in Section 2.1.2 is used, but adding a load measurable disturbance at the process output (see Figure 3.26).

This contribution will focus on two nested loops for simplicity, but the concept can be extended to include more loops if needed. The scheme is composed by the inner loop process $P_2(s)$, the controller $C_2(s)$, the signals e_2 (inner error), r_2 (inner reference) and y_2 (inner process output). The outer loop is defined by the process P_1, the controller $C_1(s)$, and the signals e_1 (outer error), r_1 (system reference) and y_1 (system output). There is also a measurable load disturbance d, and the model $P_d(s)$ describes the dynamics between this disturbance and the process output.

It is assumed that the three process models ($P_1(s)$, $P_2(s)$ and $P_d(s)$) are first-order systems with time delay. They are defined in Equation (3.21), where K_1, K_2 and K_d are the static gains, T_1, T_2 and T_d are the time constants, and L_1, L_2 and L_d are the time delays:
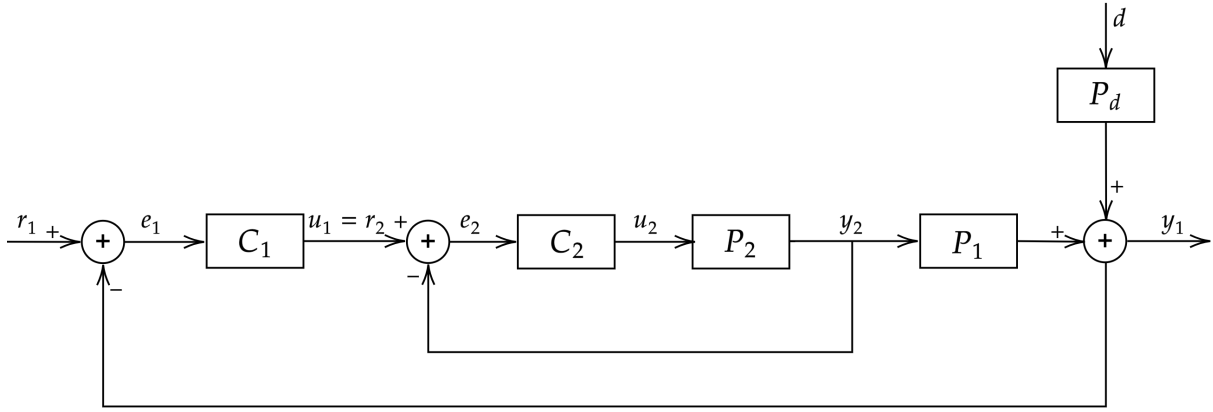
Figure 3.26. Cascade control scheme with measurable disturbances at the process output.

$$P_1(s) = \frac{K_1}{T_1 s + 1} e^{-L_1 s} \ , \quad P_2(s) = \frac{K_2}{T_2 s + 1} e^{-L_2 s} \ , \quad P_d(s) = \frac{K_d}{T_d s + 1} e^{-L_d s} \qquad (3.21)$$

The controllers $C_1(s)$ and $C_2(s)$ are PI with transfer functions defined by Equation (2.2), with $\tau_d = 0$. Note that this is only the basic structure.

The Lambda tuning method described in Section 2.1.1 is considered to calculate the PI controller parameters according to (2.5), where λ is the desired closed-loop time constant [131].

3.3.2 Feedforward on Cascade Control with Load Disturbances

As mentioned in Section 2.1.2, the main objective of cascade control is to minimize the impact of the non-linearities and disturbances that affect the inner loop, improving the performance of the outer loop. However, when measurable disturbances affect the output y_1, other control strategies, such as feedforward control, can be implemented to minimize their impact. In this section, two simple solutions found in the literature to solve the rejection-to-measurable-disturbances problem in cascade control schemes are analyzed.

Since d is measurable, feedforward can be used to improve the load disturbance rejection (Section 2.1.3). This is defined by Equation (2.9). Two possible solutions are studied based on the feedforward implementation to address load disturbances on cascade control. First, and as usually done in the literature, the feedforward is designed for $P_u = P_1 P_2$ and is added to the inner loop control signal (u_2). Secondly, the feedforward is designed with $P_u = P_1 P_{2cl}$, being added to the outer loop control signal (u_1), with P_{2cl} the closed-loop dynamics of the inner loop.

Solution 1

Based on the processes and the classical definition of feedforward, the first solution is to design a feedforward controller using an approximation of the product of both processes P_1 and P_2, introducing disturbance rejection with $C_{ff2}(s)$ to u_2, as shown on Figure 3.27. So, an approximation to a first-order system with time delay (Equation (3.22)) has been applied to the product $P_1 P_2$. Based on $T_1 > T_2$ and using the half-rule approximation [125], the first-order approximated model is:

$$P_u(s) = \frac{K_u}{T_u s + 1} e^{-(L_u s)} \tag{3.22}$$

where:

$$P_u(s) = P_1(s)P_2(s) = \frac{K_1 K_2}{(T_1 s + 1)(T_2 s + 1)} e^{-(L_1 + L_2)s} \approx \frac{K_1 K_2}{(T_1 + \frac{T_2}{2})s + 1} e^{-(L_1 + L_2 + \frac{T_2}{2})s} \tag{3.23}$$
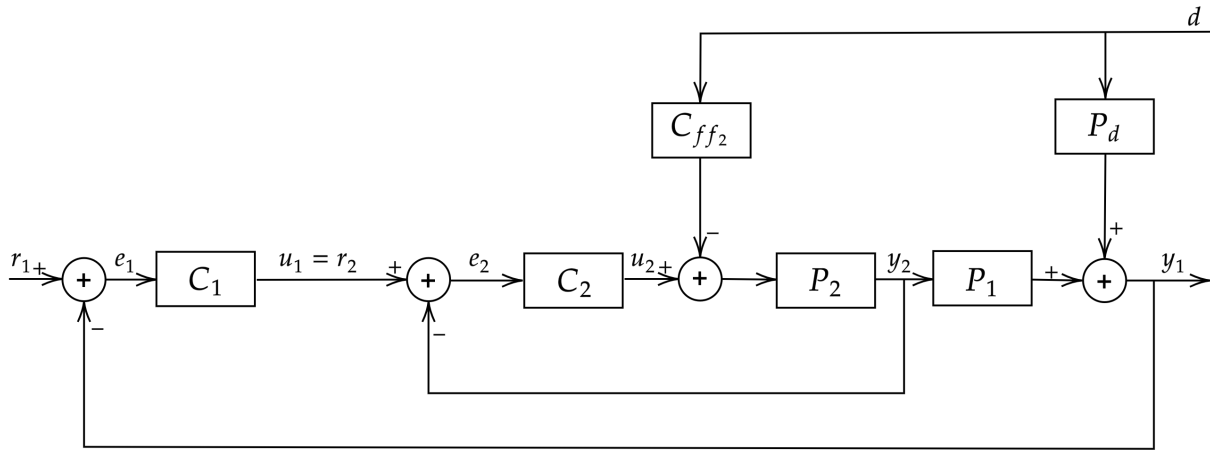

Figure 3.27. Cascade control scheme with feedforward controller C_{ff2}.

Simulations without feedforward and with both static gain and lead-lag feedforward have been implemented and compared. The parameters for the simulation are: $K_1 = 1$, $K_2 = 1$, $K_d = 1$, $T_1 = 30$, $T_2 = 10$, $T_d = 20$, $L_1 = 0$, $L_2 = 0$ and $L_d = 0$. Applying the previous approximation, the resulting processes parameters are $K_u = 1$, $T_u = 35$, and $L_u = 5$. For the static gain feedforward, there are no inversion problems, and it is calculated as:

$$C_{ff2}(s) = \frac{K_d}{K_1 K_2} = 1$$

When proceeding with the lead-lag calculation, inversion problems arise as $L_u > L_d$. Therefore, the rule defined in Equations (2.11) and (2.12) is applied, resulting in:

$$C_{ff2}(s) = K_{ff} \frac{T_z s + 1}{T_p s + 1} = 0.91 \frac{35s + 1}{17.06s + 1}$$

In Figure 3.28, the outer and inner loop outputs performance and control signals can be observed, without feedforward, with static compensator, and with lead-lag compensator, respectively. It can be seen that the feedforward contribution, in this case, is low, and the system output is practically the same as not including it. So, this solution is not recommendable to be used due to the low contribution to the system performance.

Solution 2

The second solution is to design a lead-lag feedforward controller with an approximation of the product of the outer process P_1 and the closed-loop inner loop transfer function P_{2cl}, introducing disturbance rejection with $C_{ff1}(s)$ in u_1, as shown on Figure 3.29. The controller C_2 has been designed with the Lambda method, giving a closed-loop time constant λ_2. An approximation to a first-order system with time delay has been applied to the product of $P_1 P_{2cl}$.
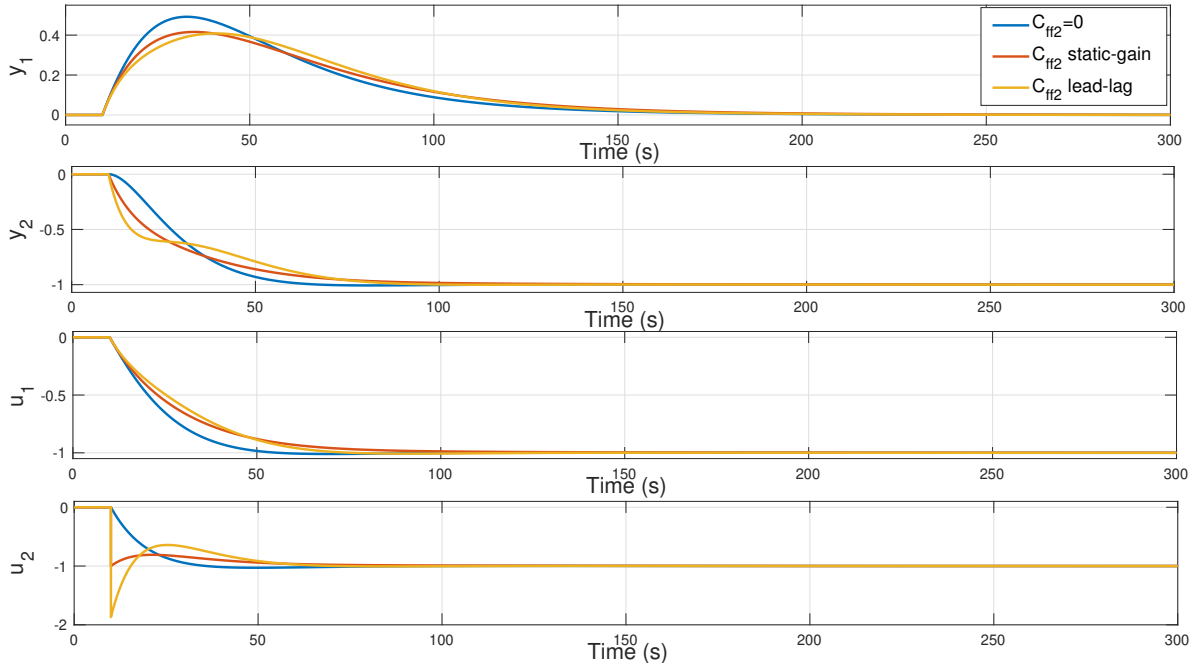
Figure 3.28. Simulation results for control scheme in Figure 3.27.

Based on $T_1 > \lambda_2$ and using again the half-rule approximation [125], first order with time delay approximated model P_u, defined in Equation (3.22), is:

$$P_u(s) = P_1(s)P_{2cl}(s) = \frac{K_1}{(T_1 s + 1)(\lambda_2 s + 1)} e^{-(L_1+L_2)s} \approx \frac{K_1}{(T_1 + \frac{\lambda_2}{2})s + 1} e^{-(L_1+L_2+\frac{\lambda_2}{2})s} \quad (3.24)$$
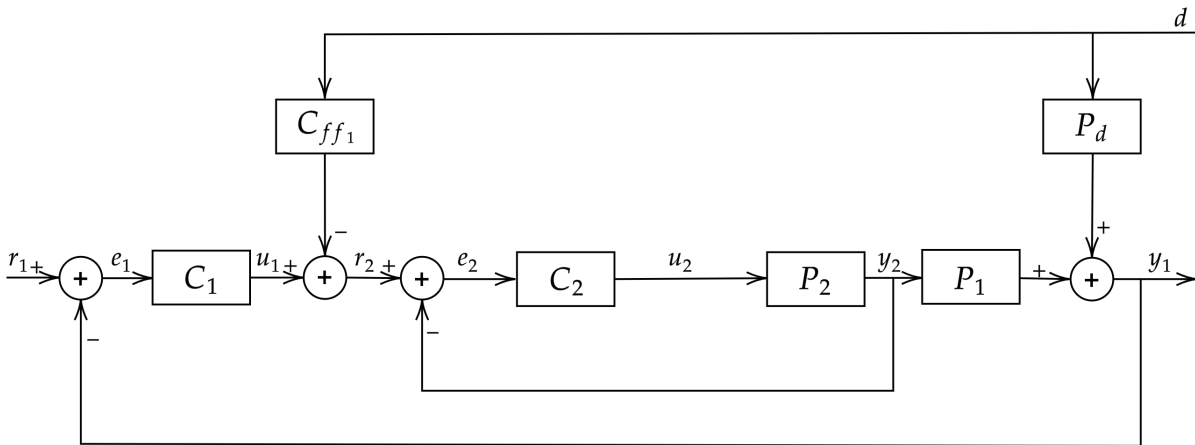

Figure 3.29. Cascade control scheme with feedforward controller C_{ff1}.

As done in the first solution, simulations have been done to compare the system performance without feedforward, with static gain compensator, and with lead-lag feedforwards. The simulation parameters used are: $K_1 = 1$, $K_2 = 1$, $K_d = 1$, $T_1 = 30$, $T_2 = 10$, $T_d = 20$, $L_1 = 0$, $L_2 = 0$ and $L_d = 0$. By applying the approximation mentioned above, the resulting process parameters are $K_u = 1$, $T_u = 32.5$, and $L_u = 2.5$. In the case of the static gain feedforward, there are no inversion problems, and its calculation is as follows:

$$C_{ff1}(s) = \frac{K_d}{K_1} = 1$$

Again, in the calculation of the lead-lag feedforward, inversion problems will arise due to the condition $L_u > L_d$. As a solution, the rules specified in Equations (2.11) and (2.12) are applied, giving:

$$C_{ff1}(s) = K_{ff}\frac{T_z s + 1}{T_p s + 1} = 0.95\frac{32.5s + 1}{18.53s + 1}$$
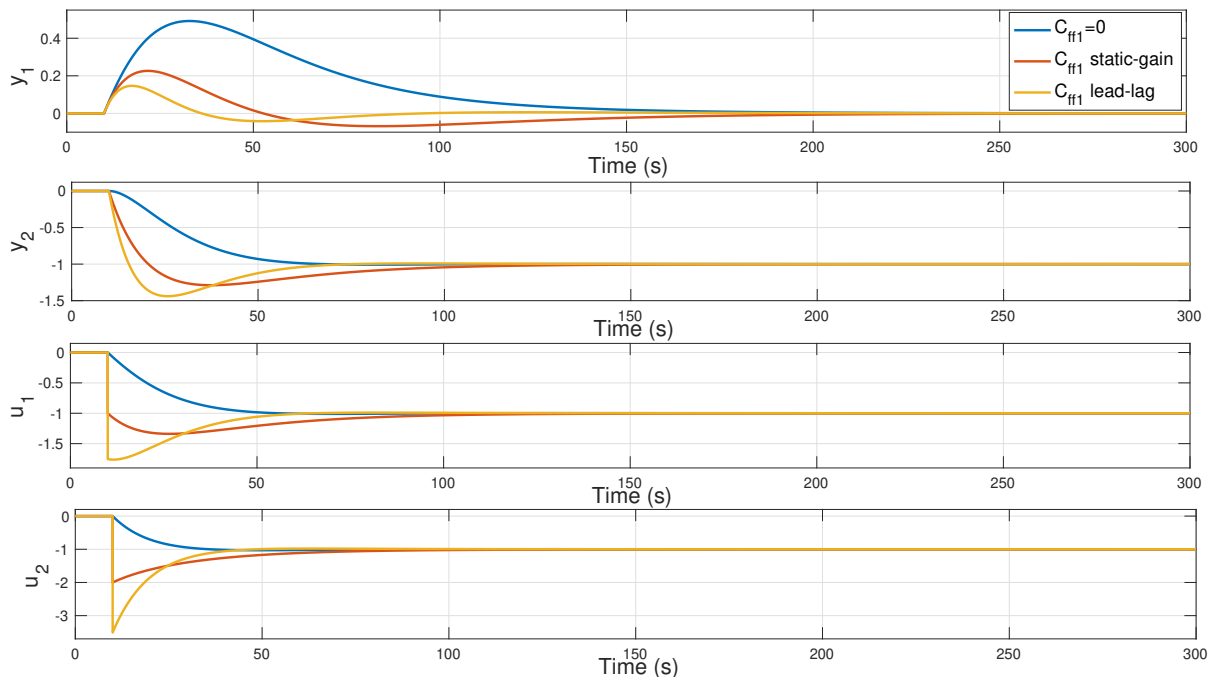

Figure 3.30. Simulation results for control scheme in Figure 3.29.

Figure 3.30 shows the simulation results. It can be observed that, in this case, the implementation of both static gain and lead-lag feedforwards improves the disturbance rejection performance at the system output. If the lead-lag response is analyzed in detail, mainly focusing on the control signal of the internal loop u_2, it can be seen that a similar response to the one obtained with $C_{ff2}(s)$ is achieved. However, implementing it in the external loop also helps reach the steady-state value faster, unlike first solution.

On the other hand, the static feedforward generates less accumulated value on the control effort in u_1. Due to the absence of the lead-lag peak, as observed from Equation (3.12), the steady-state value of the control signal is the value obtained by applying the static feedforward. Therefore, when the disturbance arrives, less error is generated in the control signal. From this analysis, the idea developed in the work emerges. The objective is to combine both feedforward $C_{ff1}(s)$ and $C_{ff2}(s)$ in such a way that a response in the control signal of the external loop u_1 similar to the one obtained with the static gain $C_{ff1}(s)$ is achieved, aiming to reach the steady-state value as quickly as possible and with minimal control effort. And for the control signal of the internal loop, the goal is to design a feedforward that accelerates the response as much as possible, obtaining a response similar to the signal obtained by the lead-lag $C_{ff1}(s)$.

3.3.3 Proposed Solution

Based on the analysis conducted above, this section proposes a simple solution based on static feedforward controllers, which are widely used in industry, and also simplifies the approximations made with lead-lag controllers. In this way, both controllers $C_{ff1}(s)$ and $C_{ff2}(s)$ work simultaneously, as shown on the scheme in Figure 3.31. The controller $C_{ff1}(s)$ is responsible for bringing the outer loop to the value of the new steady state to eliminate the steady-state error in the output as quickly as possible. The controller $C_{ff2}(s)$ provides a fast response to reject the disturbance.
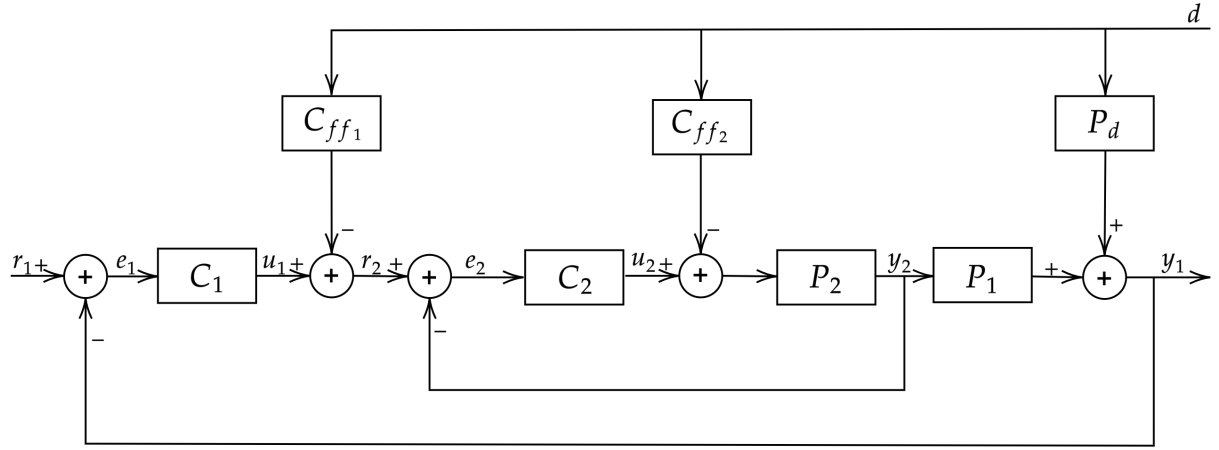

Figure 3.31. Proposed cascade with double feedforward control scheme.

The static feedforward controllers are calculated as follows:

$$C_{ff1} = \frac{P_d}{P_1 P_{2cl}} = \frac{K_d}{K_1}$$

$$C_{ff2} = \frac{P_d}{P_1 P_2}\alpha = \frac{K_d}{K_1 K_2}\alpha$$

A new term α has been included in the feedforward $C_{ff2}(s)$ in order to modify its gain to optimize the IAE value of the process output as performance criteria. The design of both PI controllers has been carried out using the Lambda method, described in section 2.1.1. The closed-loop time constants are λ_1 and λ_2 for the outer and inner loops, respectively.

To perform that, first, the time domain closed-loop response is derived for the scheme in Figure 3.31. The Laplace transform of system output, assuming r_1 and d as Laplace transform of reference and disturbance inputs, respectively, is given by:

$$y_1 = dP_d + \frac{P_1}{\lambda_2 s + 1}(C_1 r_1 - C_1 y_1 + C_{ff1} d) + \frac{P_1 P_2 C_{ff2}}{1 + P_2 C_2}d$$

where:

$$u_1 = C_1(r_1 - y_1), \quad \frac{P_2 C_2}{1 + P_2 C_2} = \frac{1}{\lambda_2 s + 1}$$

so:

$$y_1 = \frac{P_1 C_1}{\lambda_2 s + 1 + P_1 C_1}r_1 + \left(\frac{(\lambda_2 s + 1)P_d}{\lambda_2 s + 1 + P_1 C_1} + \frac{P_1 C_{ff1}}{\lambda_2 s + 1 + P_1 C_1}\frac{(\lambda_2 s + 1)P_1 P_2 C_{ff2}}{(\lambda_2 s + 1 + P_1 C_1)(1 + P_2 C_2)}\right)d$$

Developing, and substituting:

$$1 + P_2 C_2 = \frac{\lambda_2 s + 1}{\lambda_2 s}$$

$$\lambda_2 s + 1 + P_1 C_1 = \frac{\lambda_1 \lambda_2 s^2 + \lambda_1 s + 1}{\lambda_1 s}$$

$$y_1 = \frac{\lambda_1 s P_1 C_1}{\lambda_1 \lambda_2 s^2 + \lambda_1 s + 1} r_1 + \left(\frac{(\lambda_2 s + 1)\lambda_1 s P_d}{\lambda_1 \lambda_2 s^2 + \lambda_1 s + 1} + \frac{\lambda_1 P_1 s C_{ff1}}{\lambda_1 \lambda_2 s^2 + \lambda_1 s + 1} + \frac{\lambda_1 \lambda_2 s^2 P_1 P_2 C_{ff2}}{\lambda_1 \lambda_2 s^2 + \lambda_1 s + 1} \right) d$$

Now, the two real poles of the denominator are calculated:

$$p_{1,2} = \frac{-\lambda_1 \pm \sqrt{\lambda_1^2 - 4\lambda_1 \lambda_2}}{2\lambda_1 \lambda_2} = \frac{-\lambda_1 \pm \sqrt{\lambda_1(\lambda_1 - 4\lambda_2)}}{2\lambda_1 \lambda_2}$$

If a fixed ratio $\lambda_1 / \lambda_2 = 4$ is assumed to ensure that a response with two real poles is obtained:

$$p_{1,2} = \frac{-\lambda_1 \pm \sqrt{4\lambda_2(4\lambda_2 - 4\lambda_2)}}{24\lambda_2 \lambda_2} = -\frac{1}{2\lambda_2}$$

So, if $r_1 = 0$ is considered, and instantiating the values of P_1, P_2 and P_d from Equation (3.21), the following expression for y_1 is obtained:

$$y_1 = \frac{(\lambda_2 s + 1)\lambda_1 s K_d}{(2\lambda_2 s + 1)(2\lambda_2 s + 1)(T_d s + 1)} d + \frac{\lambda_1 K_1 s C_{ff1}}{(2\lambda_2 s + 1)(2\lambda_2 s + 1)(T_1 s + 1)} d +$$
$$+ \frac{\lambda_1 \lambda_2 s^2 K_1 K_2 C_{ff2}}{(2\lambda_2 s + 1)(2\lambda_2 s + 1)(T_1 s + 1)(T_2 s + 1)} d$$

Then, using the following approximation:

$$(2\lambda_2 s + 1)(2\lambda_2 s + 1) \approx (4\lambda_2 s + 1)$$

It is obtained:

$$y_1 = \left(\frac{(\lambda_2 s + 1)\lambda_1 s K_d}{(4\lambda_2 s + 1)(T_d s + 1)} + \frac{\lambda_1 K_1 s C_{ff1}}{(4\lambda_2 s + 1)(T_1 s + 1)} + \frac{\lambda_1 \lambda_2 s^2 K_1 K_2 C_{ff2}}{(4\lambda_2 s + 1)(T_1 s + 1)(T_2 s + 1)} \right) d$$

In the first transfer function, the time constants can be separated to cancel the zero, obtaining:

$$y_1 = \left(\frac{\lambda_1 s K_d}{(3\lambda_2 s + 1)(T_d s + 1)} + \frac{\lambda_1 K_1 s C_{ff1}}{(4\lambda_2 s + 1)(T_1 s + 1)} + \frac{\lambda_1 \lambda_2 s^2 K_1 K_2 C_{ff2}}{(4\lambda_2 s + 1)(T_1 s + 1)(T_2 s + 1)} \right) d$$

Now, using $\lambda_1 = 4\lambda_2$, $C_{ff1} = K_d / K_1$ and $C_{ff2} = \alpha K_d / (K_1 K_2)$, we have

$$y_1 = K_d 4\lambda_2 \left(\frac{s}{(3\lambda_2 s + 1)(T_d s + 1)} + \frac{s}{(4\lambda_2 s + 1)(T_1 s + 1)} + \frac{\lambda_2 s^2 \alpha}{(4\lambda_2 s + 1)(T_1 s + 1)(T_2 s + 1)} \right) d$$

Once the final expression is obtained, it is transformed into the time domain:

$$
\begin{aligned}
y(t) = K_d 4\lambda_2 \Bigg(& \frac{-e^{-\frac{t}{3\lambda_2}} + e^{-\frac{t}{T_d}}}{T_d - 3\lambda_2} + \frac{-e^{-\frac{t}{4\lambda_2}} + e^{-\frac{t}{T_1}}}{T_1 - 4\lambda_2} + \frac{\alpha_2\lambda_2 e^{-\frac{t}{T_2}}}{(T_1 - T_2)(T_2 - 4\lambda_2)} - \\
& - \frac{\alpha_2\lambda_2 e^{-\frac{t}{T_1}}}{(T_1 - T_2)(T_1 - 4\lambda_2)} - \frac{\alpha_2\lambda_2 e^{-\frac{t}{4\lambda_2}}}{(T_1 - 4\lambda_2)(T_2 - 4\lambda_2)} \Bigg)
\end{aligned}
$$

When attempting to analyze it, a problem of exponential sum arises, which does not have a direct analytical solution. Due to this, a numerical solution based on optimization is studied to calculate the optimal value of α. A global optimization method has been applied to minimize the IAE at step load disturbances, as a metric to evaluate the performance. It is defined as

$$
\min_{\alpha} \int_0^{t_f} |e_1(t)|\, dt \quad \text{such that} \quad 0 \le \alpha \tag{3.25}
$$

So, the optimization problem was run through a wide range of tests by varying the ratio between T_1 and T_2, with $T_2/T_1 < 1$. Also, the value of T_d has been modified, normalizing the ratio between the disturbance time constant and the time constant equivalent, where $T_u = (T_1 + 0.5\lambda_2)$. The time-constant ratio T_2/T_1 has been changed from 0.1 to 0.9 in steps of 0.1. For each value of T_2/T_1 different values of T_d/T_u are swept, using different values of T_d. Simulations with a ratio below 0.3 have not been taken into account due to the difference between the time constant of the external and internal loop being so large that the implementation of a cascade control loop would not be applicable. With each combination, the optimization problem defined in Equation (3.25) has been evaluated in order to find the optimal value of α in each simulation. The test parameters have been set as: $K_1 = 1$, $K_2 = 1$, $K_d = 1$, $L_1 = 0$, $L_2 = 0$, $L_d = 0$, and $u_0 = 0$.

Figure 3.32 shows the results of the optimization where the optimal value of α is shown versus T_d/T_u. Each line represents a different T_2/T_1 value. The ones on the upper side represent the smallest values, where $T_2/T_1 < 0.3$, the largest difference between the time constants. The ones that are on the lower side represent the highest values, where $T_2/T_1 < 0.9$, the smallest difference between the time constants.

Due to the complexity of the problem described above and the variation of parameter α observed in Figure 3.32, a piecewise linear approximation has been carried out to obtain an equation for the calculation of α. The obtained equation is a piecewise linear equation of first order (3.26).

$$
\alpha =
\begin{cases}
0.25\beta + \varphi & if\ x \le 0.25 \\
\beta x + \varphi & if\ 0.25 < x \le 1.15 \\
0 & if\ x > 1.15
\end{cases}
\tag{3.26}
$$

with

$$
x = \frac{T_d}{T_u} = \frac{T_d}{T_1 + 0.5\lambda_2}, \quad \beta = -1.91\left(\frac{T_2}{T_1}\right)^{-0.86}, \quad \varphi = 2.28\left(\frac{T_2}{T_1}\right)^{-0.84}
$$

The values of β and φ depend on the ratio between T_2/T_1, and x on the ratio between T_d/T_u. The developed equation has a constant value of $x = 0.25$ for the ratio of T_d/T_u smaller than 0.25. For values between $T_d/T_u > 0.25$ and $T_d/T_u \le 1.15$, the equation is linear, with a slope

depending on the value of T_d/T_u and the ratio between T_2/T_1. For values above $T_d/T_u > 1.15$, α will be 0, so no $C_{ff2}(s)$ will be needed.

In Figure 3.32, the validation of the equation represented by the circles is shown. It can be observed how the proposed rule fits accurately the results obtained from the optimization problem.
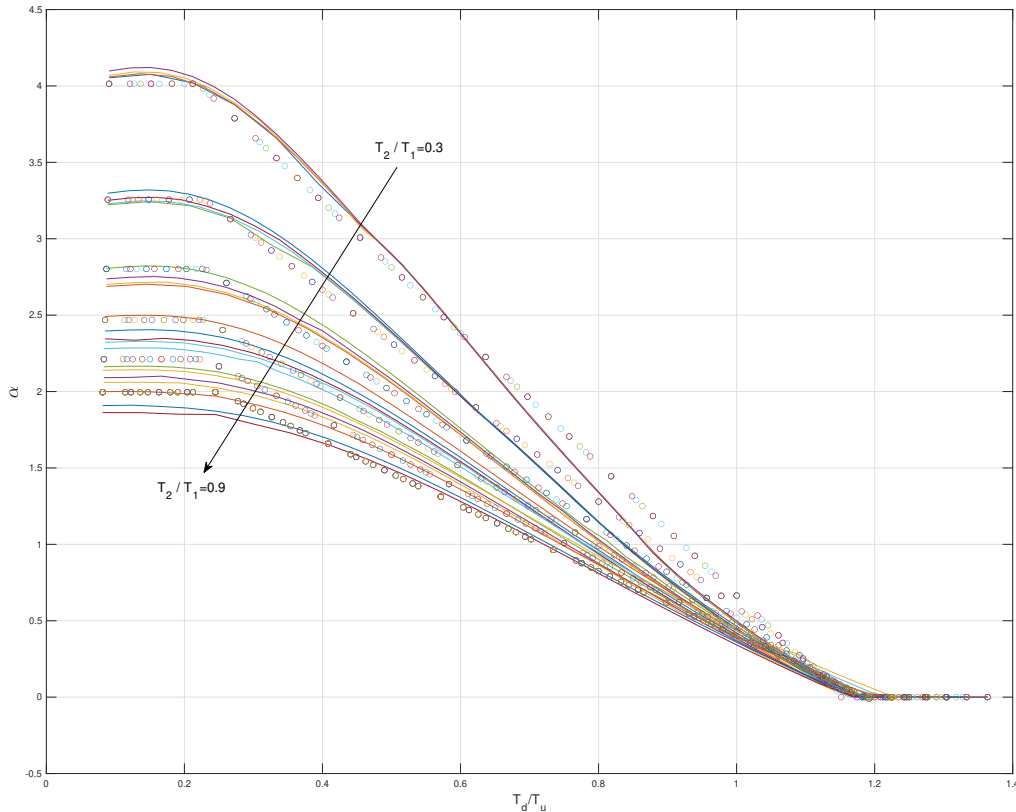

Figure 3.32. Optimization test. The continuous curves represent the values obtained by the optimizer. The dotted curves represent the validation of the developed equation.

Tuning Guideline

This section summarizes the proposed design rule for the new control scheme in Figure 3.31, including the tuning for the new gain of the feedforward controller $C_{ff2}(s)$ by a factor α. The different steps to design the compensator are:

1. Set the closed-loop time constants for the inner and outer PI controllers in such a way that the following relationship is fulfilled:

$$\frac{\lambda_1}{\lambda_2} \geq 4$$

2. Set the outer feedforward controller in the following way:

$$C_{ff1} = \frac{K_d}{K_1} e^{-L_{ff1}}$$

$$L_{ff1} = \max(0, L_d - (L_1 + L_2))$$

3. Set the inner feedforward controller in the following way:

$$C_{ff2} = \alpha \frac{K_d}{K_1 K_2} e^{-L_{ff2}}$$

$$\alpha = \begin{cases} 0.25\beta + \varphi & \text{if } x \le 0.25 \\ \\ \beta x + \varphi & \text{if } 0.25 > x \le 1.15 \\ \\ 0 & \text{if } x > 1.15 \end{cases}$$

with

$$x = \frac{T_d}{T_u}, \quad where: \ T_u = (T_1 + 0.5\lambda_2)$$

$$\beta = -1.91 \left(\frac{T_2}{T_1}\right)^{-0.86}$$

$$\varphi = 2.28 \left(\frac{T_2}{T_1}\right)^{-0.84}$$

and

$$L_{ff2} = \max(0, L_d - (L_1 + L_2))$$

3.3.4 Examples

In this section, the use of the gain-reduction factor α for the feedforward $C_{ff2}(s)$, determined according to the method presented in the previous section, is applied to processes with different relations between the processes model parameters. The processes models have the following characteristics:

- **Example 1:** $K_1 \neq K_2 \neq K_d$, $L_1 = L_2 = L_d$, $T_2/T_1 = 0.35$, $T_u > T_d > T_2$.

- **Example 2:** $K_1 = K_2 = K_d$, $L_1 = L_2 = L_d$, $T_2/T_1 = 0.65$, $T_d < T_2$.

- **Example 3:** $K_1 = K_2 = K_d$, $L_1 = L_2 = L_d$, $T_2/T_1 = 0.55$, $T_d > T_u$.

- **Example 4:** $K_1 = K_2 = K_d$, $L_1 < L_d, L_2 = 0$ (no inversion problem), $T_2/T_1 = 0.5$, $T_u > T_d > T_2$.

- **Example 5:** $K_1 = K_2 = K_d$, $L_1 > L_d, L_2 = 0$ (inversion problem), $T_2/T_1 = 0.5$, $T_u > T_d > T_2$.

- **Example 6:** $K_1 = K_2 = K_d$, $L_1 = L_2 = L_d$. $P_1(s)$, $P_2(s)$ and $P_d(s)$ are second-order transfers function with two real poles.

In each example, four cases are analyzed. The cascade control scheme only with $C_{ff1}(s)$, as shown in Figure 3.29, is simulated for the static gain and the lead-lag feedforwards. Then, the scheme in Figure 3.31 with $C_{ff1}(s)$ and $C_{ff2}(s)$ calculated as static gains with α obtained by

the optimization method and with the new equation proposed in this contribution are compared, to validate the proposed equation. In addition, values of T_2/T_1 outside the range selected for modelling have been chosen to demonstrate the robustness of the proposed solution. A step disturbance with amplitude $d = 1$ is applied at time $t = 5$ s. The controllers have been tuned with the Lambda method (2.5), fulfilling the condition $\lambda_1/\lambda_2 = 4$.

Moreover, two indices in order to objectively evaluate the control performance are proposed: the Integral Absolute Error for the outer loop error (IAE) and the Sum of Control Increments (SCI) of the outer control signal, given by:

$$IAE = \int_{t_0}^{t_f} |e_1(t)| \, dt \tag{3.27}$$

$$SCI = \int_{t_0^+}^{t_f} (u_1(t) - u_1(t^-))dt \tag{3.28}$$

where $t_o^+ = t_0 + dt$ and $t^- = t - dt$.

The SCI value has been used in the comparison to measure the outer control signal u_1 effort has been reduced with the proposed solution. It has been normalized as:

$$SCI_{norm} = \frac{SCI_\alpha}{SCI_{lead-lag}} \tag{3.29}$$

where SCI_α and $SCI_{lead-lag}$ denote the sum of control increments from the simulation of the proposed solution developed in this contribution and the classical feedforward scheme only with C_{ff1}, respectively. Table 3.2 summarizes the comparisons.

	$IAE(1)$	$IAE(2)$	$IAE(3)$	SCI_{norm}
Example 1	59.53	19.27	12.01	0.49
Example 2	20.78	5.28	9.45	0.44
Example 3	3.60	2.95	3.00	1.03
Example 4	14.25	6.54	4.90	0.49
Example 5	19.63	8.22	10.09	0.43
Example 6	13.72	6.47	6.32	0.56

Table 3.2. Normalized SCI and IAE values in all the examples. IAE(1): $C_{ff1} = Static\,gain$, IAE(2): $C_{ff1} = Lead - lag$, IAE(3): α from Equation (3.26).

Example 1

The parameters are: $K_1 = 10$, $K_2 = 15$, $K_d = 6$, $T_1 = 30$, $T_2 = 10.5$, $T_d = 20$, $L_1 = 0$, $L_2 = 0$ and $L_d = 0$. The controllers parameters are: $K_{p1} = 0.17$, $\tau_{i,1} = 32.10$, $\lambda_1 = 16.8$ for $C_1(s)$, and $K_{p2} = 0.17$, $\tau_{i,2} = 10.5$, $\lambda_2 = 4.2$ for $C_2(s)$. The gain values differ to see how the new implementation does not depend on them. The time constant of the disturbance model is in between the time constants of the inner and outer loops. There is no time delay, but when the approximation in Equation (3.24) is done to implement the lead-lag feedforward controller, an inversion problem will appear, and so the rules defined in Equations (2.11) and (2.12) are used.

Figure 3.33 shows the simulation results. The four evaluated cases previously commented can be observed. The static feedforward controller $C_{ff1}(s)$ provides a slow response with overshoot, whereas the lead-lag controller performs better with a faster response. The validation of the equation can also be observed, as the proposed solution and the optimizer yield almost identical responses. Furthermore, the performance of the proposed solution achieves very similar results in the output of the process y_1 compared to the lead-lag controller, resulting, in this case, a better IAE value. However, when examining the control signal u_1 and the SCI_{norm} value in Table 3.2, the control effort is reduced by a factor of 0.49 with the new solution compared to the lead-lag controller. Additionally, in the inner loop, it can be observed how the response of the controller u_2 accelerates due to the change in the value of α and the resulting control signal, which in this example is $\alpha = 3.33$.
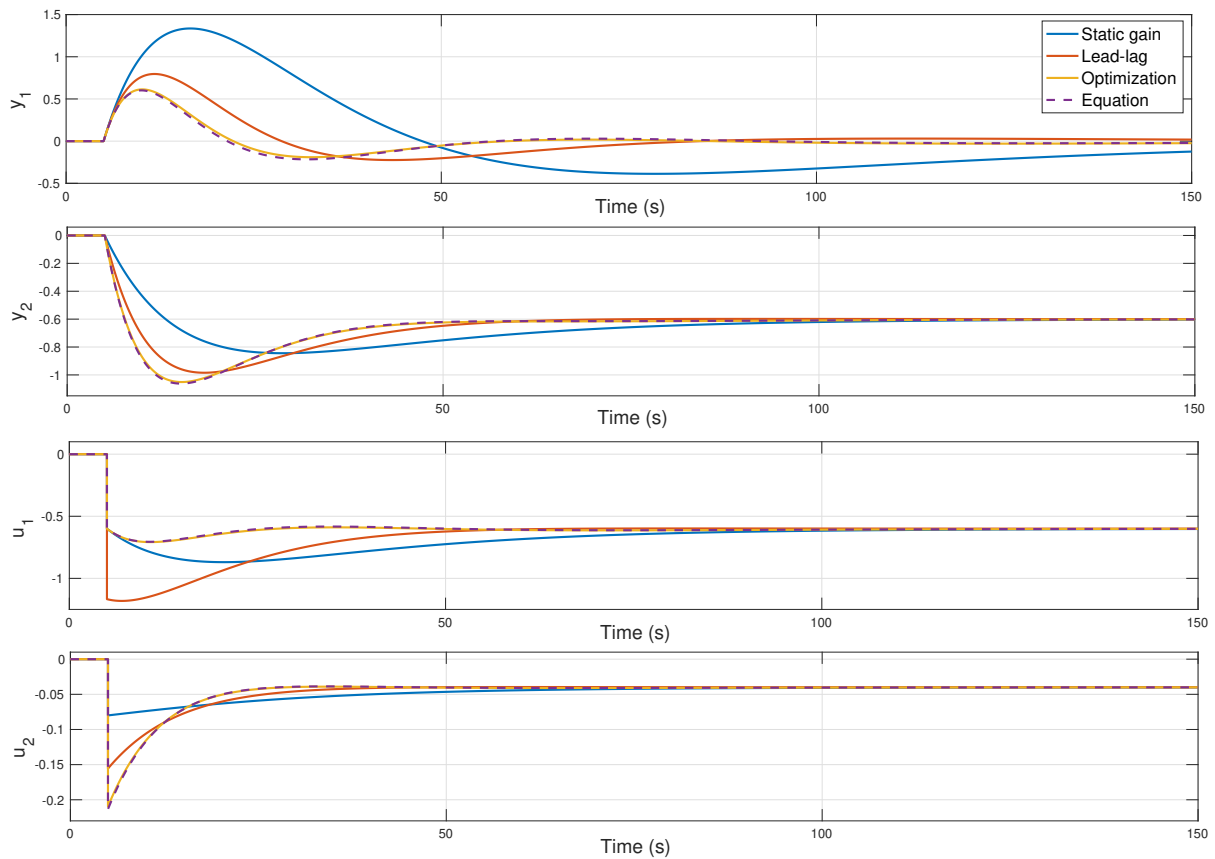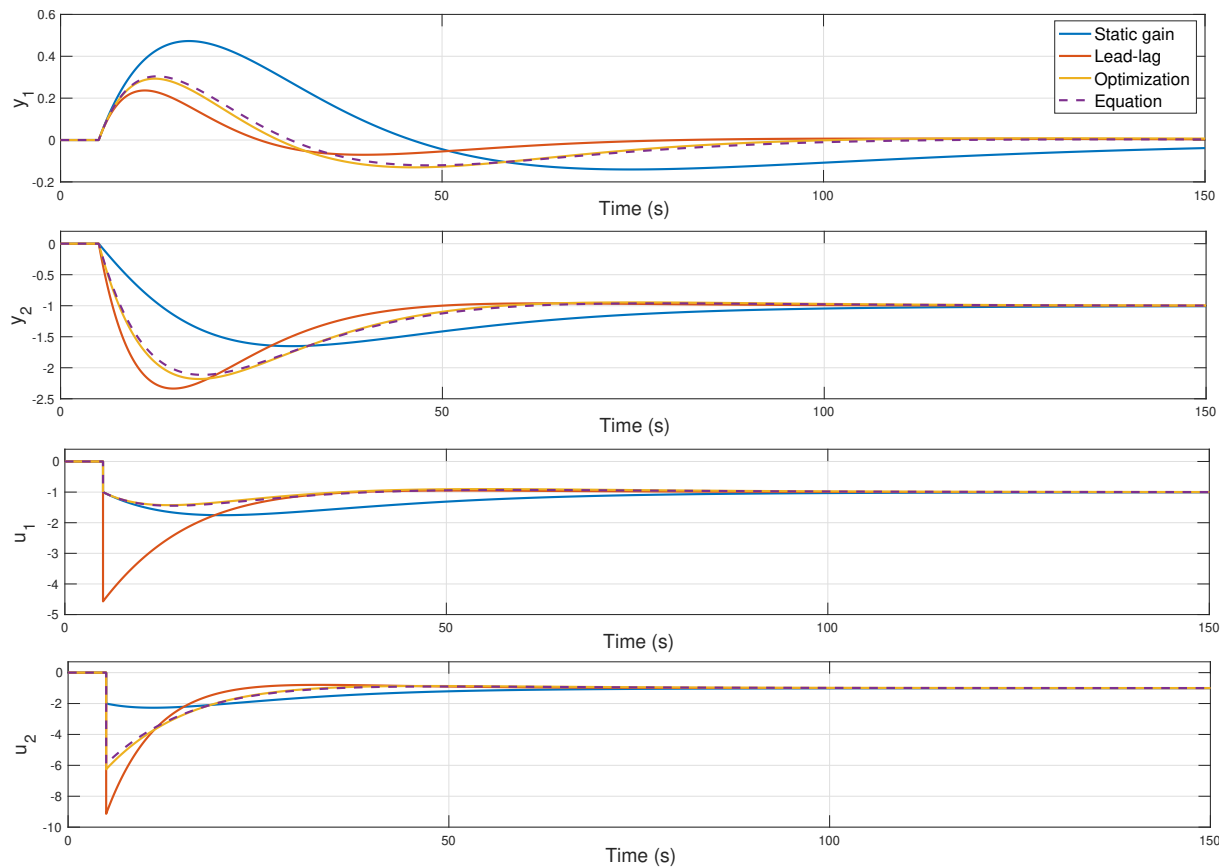

Figure 3.33. Simulation results in Example 1.

Example 2

The parameters are: $K_1 = 1$, $K_2 = 1$, $K_d = 1$, $T_1 = 35$, $T_2 = 13.5$, $T_d = 10$, $L_1 = 0$, $L_2 = 0$ and $L_d = 0$. The controllers parameters are: $K_{p,1} = 1.26$, $\tau_{i,1} = 38.75$, $\lambda_1 = 27$ for $C_1(s)$, and $K_{p,2} = 2$, $\tau_{i,2} = 13.5$, $\lambda_2 = 6.75$. In this example, all the gains are the same, and the time constant of the disturbance is smaller than the inner loop process time constant. As in the previous example, when implementing the lead-lag feedforward controller by approximating (3.24), an inversion problem arises, despite the absence of time delay. To address this, the rules defined in Equations (2.11) and (2.12) are employed.

By observing Figure 3.34, it can be seen that the static feedforward controller $C_{ff1}(s)$ yields a poorer response in disturbance rejection. Both the lead-lag controller and the proposed solution

achieve similar performance in the output of the process, with the lead-lag controller having a minor overshoot, as reflected in the IAE values obtained (see Table 3.2). However, when examining the control signal of the outer loop u_1, the control effort is highly reduced by a factor of 0.44 with the proposed solution. In this case, observing the control signal of the inner loop, the proposed solution also reduces the control signal peak, with the value obtained by the equation for reducing the gain of $C_{ff2}(s)$ being $\alpha = 3.89$.

Figure 3.34. Simulation results in Example 2.

Example 3

In this example, the models parameters are: $K_1 = 1$, $K_2 = 1$, $K_d = 1$, $T_1 = 35$, $T_2 = 14$, $T_d = 40$, $L_1 = 0$, $L_2 = 0$, $L_d = 0$. The controllers parameters are: $K_{p,1} = 1.22$, $\tau_{i,1} = 38.75$, $\lambda_1 = 28$ for $C_1(s)$, and $K_{p,2} = 2$, $\tau_{i,2} = 14$, $\lambda_2 = 7$ for $C_2(s)$. Similar to previous examples, implementing the lead-lag feedforward controller based on the approximation of (3.24) leads to an inversion problem, despite the absence of any time delay. To tackle this issue, the rules specified in Equations (2.11) and (2.12) are utilized again. In this case, all the gains are equal, and the time constant of the disturbance is larger than the approximated time constant T_u.

Analyzing the results in Figure 3.35, it can clearly be observed that, in this case, the three responses give similar output performances. Since $T_d > T_u$, implementing the lead-lag controller does not highly improve the static controller because there is no peak in control signal u_1. This behavior is also evident when analyzing the IAE values obtained in Table 3.2. Consequently, in this case, the proposed solution achieves a similar control effort of the output control signal u_1. Similar to previous examples, it is validated that the equation provides the same value as the optimizer, which is $\alpha = 0.51$.
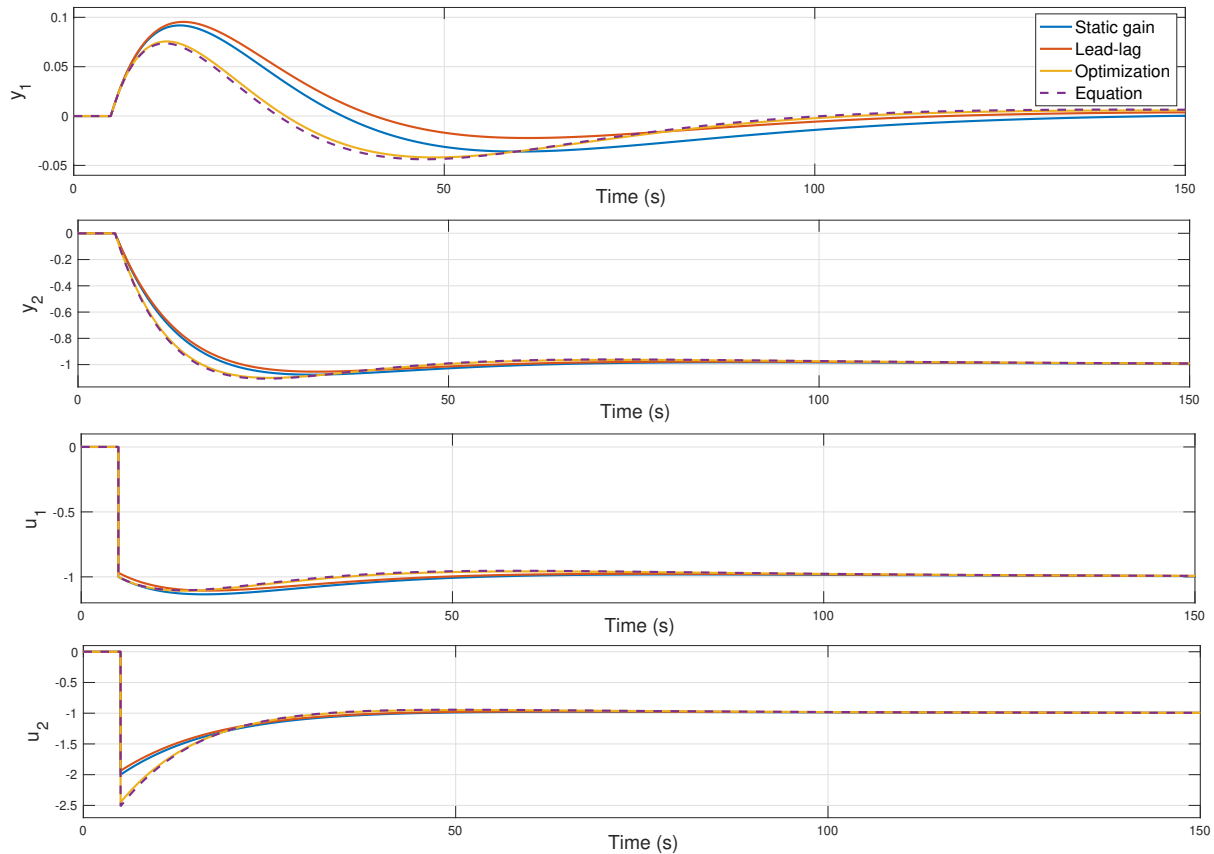
Figure 3.35. Simulation results in Example 3.

Example 4

The parameters in this example are: $K_1 = 1$, $K_2 = 1$, $K_d = 1$, $T_1 = 35$, $T_2 = 15$, $T_d = 20$, $L_1 = 2$, $L_2 = 0$ and $L_d = 8$. The controllers parameters are: The controller parameters are: $K_{p,1} = 1.08$, $\tau_{i,1} = 38.75$, $\lambda_1 = 30$ for $C_1(s)$, and $K_{p,2} = 2$, $\tau_{i,2} = 15$, $\lambda_2 = 7.5$ for $C_2(s)$. Gains are the same in all the models; the disturbance time constant is between T_2 and T_u, and in this case, time delay has been included in the disturbance and outer process model. $L_u < L_d$, so there are no inversion problems to calculate the lead-lag controller.

Figure 3.36 shows the results of this example. It can clearly be observed how the equation is validated again with the results of the optimization. It can also be seen that the contribution of the static feedforward, in this case, is limited. However, both the lead-lag feedforward and the proposed solution reduce the impact of the disturbance on the output y_1. From Table 3.2 it can bee seen that the new solution improves the output performance. Regarding the control effort of the external control signal u_1, once again, the proposed solution with $\alpha = 2.56$ has reduced it by a factor 0.49. This example demonstrates that the rule is independent to the time delay in the processes. Nevertheless, more examples with delay are analyzed in the following sections.

Example 5

In this example, the parameters of the processes are: $K_1 = 1$, $K_2 = 1$, $K_d = 1$, $T_1 = 30$, $T_2 = 12.5$, $T_d = 16$, $L_1 = 6$, $L_2 = 0$ and $L_d = 2$. The controllers parameters are: $K_{p,1} = 0.97$, $\tau_{i,1} = 33.12$, $\lambda_1 = 25$ for $C_1(s)$, and $K_{p,2} = 2$, $\tau_{i,2} = 12.5$, $\lambda_2 = 6.25$ for $C_2(s)$. Now, $L_d < L_u$, therefore, inversion problems on the calculation of the lead-lag controller will occur, so the rules defined in Equations (2.11) and (2.12) are used.
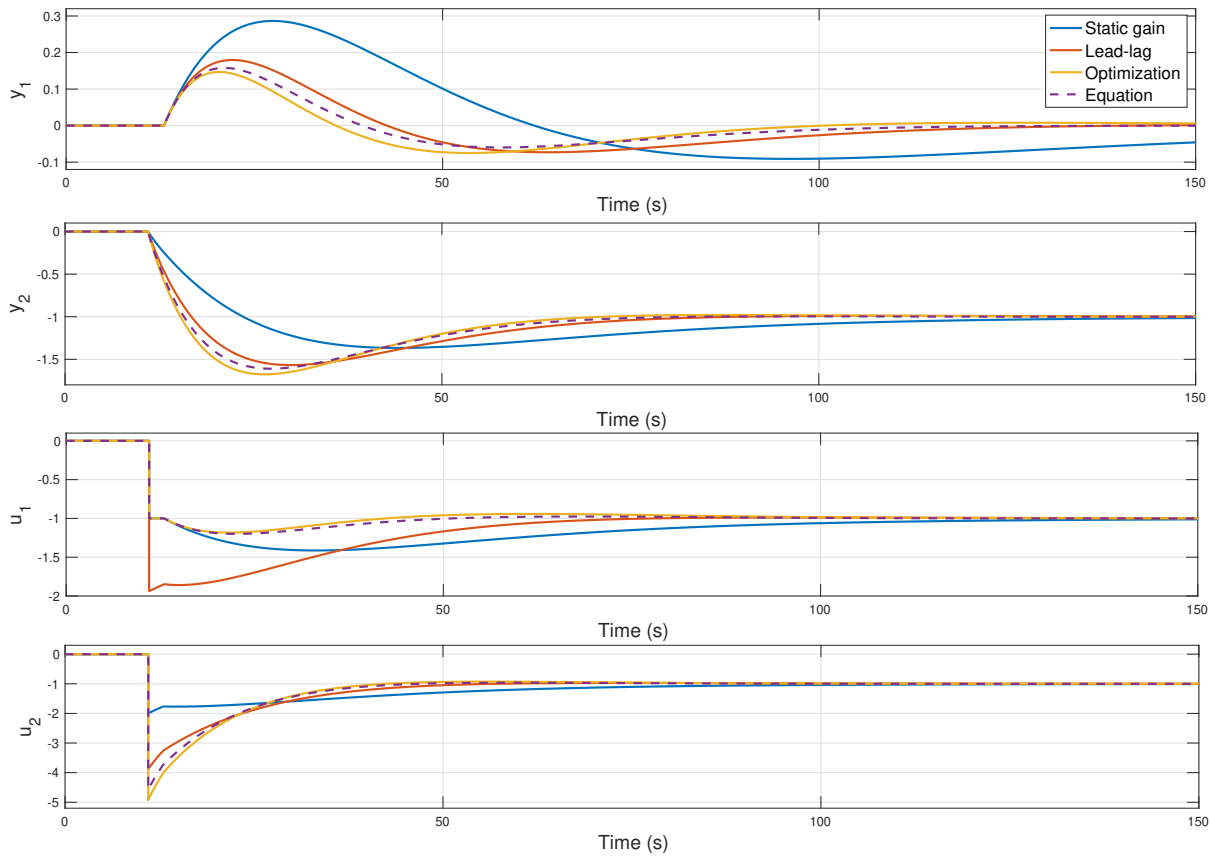
Figure 3.36. Simulation results in Example 4.

In this case, it is shown in Figure 3.37 how the proposed response with $\alpha = 2.75$ achieves a performance at the output y_1 that is similar to the case of $C_{ff1}(s)$ with lead-lag, but with a reduced control effort of u_1 by a factor of 0.43. Similarly to previous examples, the equation is validated by observing that the result with the equation is equal to what the optimizer provides. In this example, as can be observed from Table 3.2, the IAE index is very similar to the one obtained with the lead-lag controller. Once again, it is demonstrated that the proposed solution is independent of time delay and, in the case of inversion problems, employing two static feedforward controllers yields responses very similar to a lead-lag controller with design rules applied to enhance its performance.

Example 6

In this example, a second-order transfer function with two real poles, defined in Equation (3.30), has been selected. The parameters are: $K_1 = 1$, $K_2 = 1$, $K_d = 1$, $T_{1,1} = 25$, $T_{1,2} = 10$, $T_{2,1} = 10$, $T_{2,2} = 2$, $T_{d,1} = 15$ $T_{d,2} = 5$, $L_1 = 0$, $L_2 = 0$ and $L_d = 0$.

$$P_1(s) = \frac{K_u}{(T_{1,1}s + 1)(T_{1,2}s + 1)}e^{-L_1 s}$$

$$P_2(s) = \frac{K_u}{(T_{2,1}s + 1)(T_{2,2}s + 1)}e^{-L_2 s} \qquad (3.30)$$

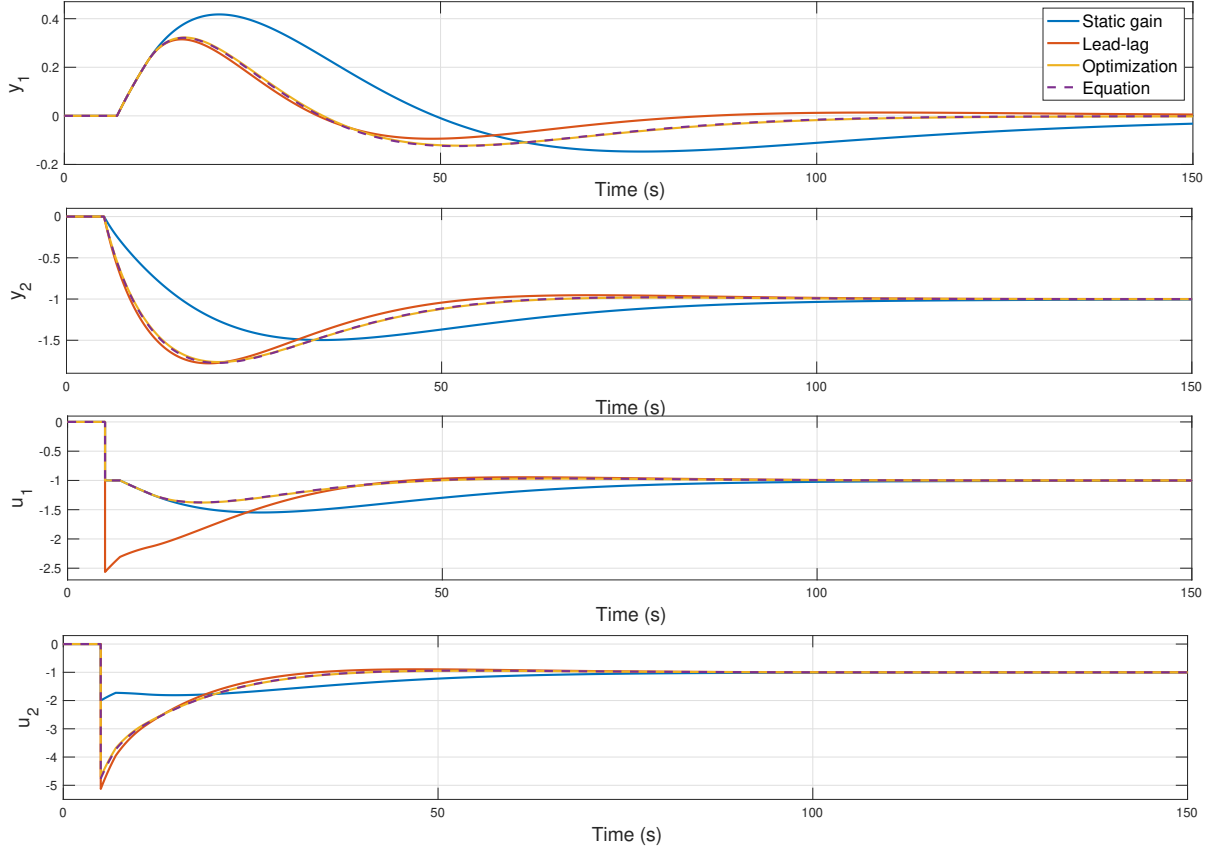$$P_d(s) = \frac{K_d}{(T_{d,1}s + 1)(T_{d,2}s + 1)}e^{-L_d s}$$

Figure 3.37. Simulation results in Example 5.

To apply the rule, an approximation to a first-order system with time delay has been applied, using the half-rule approximation [125]. So, first orders approximated models are shown in Equation (3.31), resulting in the parameters: $K_1 = 1$, $T_{1,approx} = 27$, $L_{1,approx} = 5$, $K_2 = 1$, $T_{2,approx} = 11$, $L_{2,approx} = 1$, $K_d = 1$, $T_{d,approx} = 17.5$ and $L_{d,approx} = 2.5$. The controllers parameters are: $K_{p,1} = 1$, $\tau_{i,1} = 29.75$, $\lambda_1 = 22$ for $C_1(s)$, and $K_{p,2} = 2$, $\tau_{i,2} = 11$, $\lambda_2 = 5.5$ for $C_2(s)$.

$$P_1(s) \approx \frac{K_1}{(T_{1,1} + \frac{T_{1,2}}{2})s + 1} e^{-(L_1 + \frac{T_{1,2}}{2})s}$$

$$P_2(s) \approx \frac{K_2}{(T_{2,1} + \frac{T_{2,2}}{2})s + 1} e^{-(L_2 + \frac{T_{2,2}}{2})s} \qquad (3.31)$$

$$P_d(s) \approx \frac{K_d}{(T_{d,1} + \frac{T_{d,2}}{2})s + 1} e^{-(L_d + \frac{T_{d,2}}{2})s}$$

Once the approximation is made, $L_{u,approx} = L_1 + L_2 > L_{d,approx}$, which results in a delay inversion problem. As it has been done in Example 5, for designing the feedforward, the tuning rule that considers the delay inversion problem is used [36]. The new pole T_p and gain K_{ff} are calculated as defined in Equations (2.12) and (2.11).

Results can be observed in Figure 3.38. In this example, the validation of the equation is once again observed. The response at the output of the static feedforward is the one that shows a minor improvement in disturbance rejection. However, the proposed solution and the static

feedforward exhibit similar responses, achieving faster disturbance rejection. Regarding the control effort of u_1, once again, a reduction of 0.56 is obtained. This example demonstrates that the proposed solution, with two static feedforward controllers, is robust against approximations in high-order models to first-order systems.
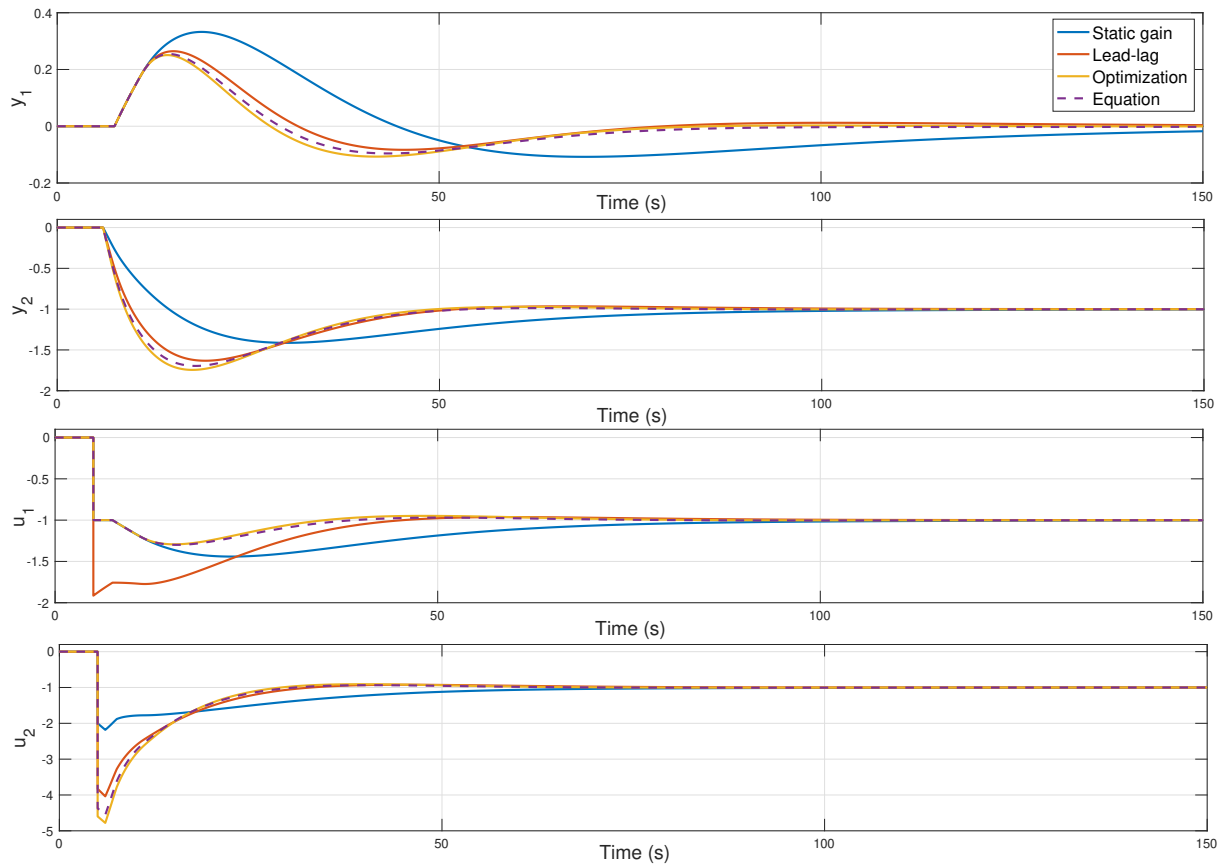

Figure 3.38. Simulation results in Example 6.

3.3.5 Conclusions

This contribution addresses the issue of measurable disturbances at the output of a cascade control system by introducing a novel solution. While the existing literature commonly adopts lead-lag or static feedforward control approaches to mitigate this problem, this study thoroughly examines these solutions, motivating the proposed control scheme. An alternative approach by implementing two static controllers, one in the outer loop and the other in the inner loop is presented. The gain of the outer feedforward controller is calculated using traditional methods. Similarly, the gain for the inner controller follows the conventional approach described in the literature but including a weighting factor, denoted as α, to minimize the IAE of the control error of the main process output.

To determine the optimal value of α, an optimization-based method is introduced, considering the relationship between the time constants of the inner and outer loop processes and the disturbance. The optimization process results are approximated using a simple piecewise linear function that defines α based on the process parameters. Through rigorous simulation experiments, the study demonstrates the effectiveness of this straightforward and solid approach. It not only enhances the performance of the process output but also reduces the overall control effort

required, highlighting the advantage of calculating and implementing static-gain feedforwards instead of lead-lags.

This contribution has led to a scientific journal article that is currently under the review process, and the journal is indexed in the Journal Citation Report (JCR) [59].

4. Contributions to the Automation of Industrial Processes

This chapter presents the simulation and experimental results on the evaluation of some of the control strategies summarized in this thesis for the facilities described in Chapter 2. In Section 4.1, three contributions are presented for a raceway reactor. In Section 4.1.1, a linear model predictive controller will be implemented in simulation. Additionally, in Section 4.1.2, a robust controller will be designed and implemented both in simulation and in the industrial plant. Lastly, in Section 4.1.3, an interactive tool will be introduced to facilitate the implementation of control strategies, enhance understanding of the complex model of photobioreactors, and provide training for both researchers and plant operators. In Section 4.2, the results of the combination of feedback linearization strategies with a robust controller for the temperature control problem in a greenhouse are presented. Finally, Section 4.3 shows the results of implementing the contribution presented in Section 3.2 for temperature control in a temperature control laboratory.

4.1 Microalgae Raceway Photobioreactors

Environmental sustainability and the need for new renewable and clean energy sources drive the search for more environmentally friendly solutions, such as microalgae cultivation in industrial photobioreactors. Microalgae biomass requires low water consumption, making it possible to cultivate them in any location [14, 34]. Additionally, due to their high lipid content, microalgae biomass can be transformed into biodiesel through the direct transesterification process [3, 73], providing an alternative solution to fossil fuels. Microalgae are also used in cosmetics, animal feed, and wastewater treatment [66].

As indicated in [24], and described in Chapter 2, the most important variables affecting microalgae growth are the temperature of the medium, solar radiation, pH, and dissolved oxygen. Additionally, the photosynthetic response of microalgae to solar radiation depends on many other variables, making the system highly complex [29]. For raceway reactors, the requirements for solar radiation exposure and operating temperature conditions are generally determined by the system's architecture and geographical location. Therefore, the variables to be controlled in

this type of reactor are pH and dissolved oxygen. Both variables have highly dynamic behavior strongly dependent on the photosynthesis process, and it is necessary to keep them close to desired set-points [100]. Between these two variables, pH is the most important to control as it directly influences the proper execution of photosynthesis. This variable exhibits a strongly nonlinear behavior, affected by the injection of CO_2 into the medium and the consumption of CO_2 during photosynthesis. Control of this variable has been approached in the literature from different perspectives. In [29], a linear control was implemented by combining a PI controller with a lead controller around the desired operating point. In [57], a robust PID controller based on QFT was used in a raceway reactor. To control the pH during the night without solar radiation and to achieve reduced CO_2 injection during the day, a control based on events combining daytime and nighttime dynamics was proposed in [112]. On the other hand, in [102], an event-based control using model predictive control was implemented, which was later improved and combined with selective and simultaneous dissolved oxygen control [101].

Furthermore, efficient simulator tools for complex industrial processes are crucial in training operators and enhancing their understanding of the system [30]. They provide a virtual environment where operators can simulate and practice different scenarios, gaining valuable hands-on experience without the risks and costs of operating the real system. One of the main advantages is that they allow operators to familiarize themselves with the process dynamics, equipment behavior, and control strategies in a safe and controlled environment. They can explore different operating conditions, observe the system's response to various disturbances, and learn how to handle abnormal situations without threatening production [11].

Simulators also enable engineers to test and validate different control techniques before implementing them in the real system [98]. They provide a platform for evaluating the performance of different control algorithms, tuning control parameters, and assessing the system's response to changes in set-points or disturbances. This iterative process of experimentation and optimization helps to identify the most effective control strategies and fine-tune them for optimal performance. They also visually represent the industrial process, allowing operators to visualize the interactions between different components and variables. This visual feedback enhances their understanding of the system's behavior and helps them identify potential bottlenecks, inefficiencies, or safety hazards. It also facilitates real-time troubleshooting and real-time decision-making by providing real-time data and visualizations. Overall, simulator tools for complex industrial processes offer a cost-effective and efficient way to train operators, understand system behavior, and optimize control strategies. They provide a virtual platform for experimentation, learning, and continuous improvement, ultimately leading to safer and more efficient industrial operations.

According to the previous review, in this section, three contributions applied to the reactors are presented. First, a linear predictive controller is implemented in simulation to regulate the pH in raceway reactors. Additionally, a robust controller for pH control will be designed and implemented both in simulation in the model and in the real facility. Lastly, an interactive tool is introduced to facilitate the implementation of control strategies, enhance understanding of the complex model of photoreactors, and provide training for both researchers and plant operators.

4.1.1 Generalized Predictive Control

This contribution presents the implementation of a Generalized Predictive Controller, defined in detail in Section 2.1.5 for pH control in a raceway photobioreactor for microalgae cultivation. The nonlinear dynamics of pH are directly and indirectly influenced by other system variables,

such as the supply of CO_2 to the culture medium, excess O_2 resulting from microalgae photosynthesis, solar radiation, and biomass concentration. Typically, these reactors are controlled using simple on/off controllers that do not consider the system model or CO_2 consumption. Given the importance of maintaining pH within specific ranges directly impacting productivity, this study opts for designing a linear predictive control strategy that constrains the system's output to optimal values, thereby increasing productivity while reducing CO_2 usage.

Process Model

From a theoretical perspective, pH control is a nonlinear problem that can only be linearized under certain circumstances [28]. As described in Section 2.2, considering that the process output is the pH of the culture, the opening of the CO_2 injection valve is the manipulated variable, and solar radiation is the major disturbance of the system. The behavior of the system can be highly simplified and be represented by the following differential equation [13], [124]:

$$\tau_r \frac{dpH}{dt} = \alpha u(t - L_u) + \beta(pH_0 - pH) + \gamma_r I \tag{4.1}$$

The pH_0 is the pH at the equilibrium point, β is a factor to adjust the system's time constant, α is the static gain of the system, u is the control signal representing CO_2 injections, L_u is the time delay, and γ_r and τ_r are parameters that depend on solar radiation, I, and the state of the culture, respectively.

This low-order linear model has been identified, taking into account the photobioreactor's structure, the pH sensor's location, and the dynamics observed in the data. Thus, the model mentioned above relating the pH output and CO_2 injection can be represented by the following transfer functions [13]:

$$pH = \frac{K_u}{1 + T_u s} e^{-L_u s} u_{CO_2} \tag{4.2}$$

where pH is the culture pH, u_{CO_2} is the valve opening percentage, K_u is the static gain, T_u the time constant and L_u time delay.

The models used in this study were obtained around pH values (operating point) where, as shown in Figure 4.1, the system productivity is maximum [101]. Thus, a pH of 7.8 was chosen as the operating point, according to the selected microalgae strain (see Chapter 2).

Different pulse trains have been applied to the CO_2 injection throughout the daylight period to obtain the model. The obtained model is based on the first-order transfer function of the first term in Equation (4.2). Figure 4.2 shows, as an example, the validation of the model for a specific testing day [61]. It is important to note that only the part of the model that depends on CO_2 injection has been used, and the radiation term has been disregarded due to its minimal effect on the pH (with small gain values, on the order of 10^{-4}). The oscillatory component of the dynamics is due to the continuous recirculation in the reactor. These dynamics could have been captured with a second-order term, as proposed in [13], but it is considered unmodeled dynamics in this work. The resulting model is given in seconds and is as follows:

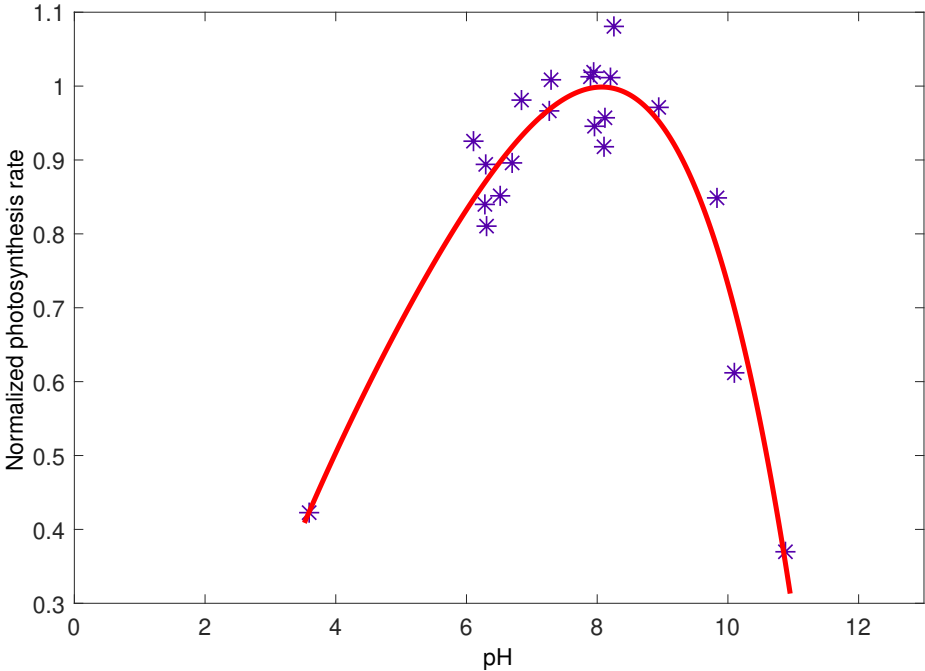$$pH = \frac{-1.65}{1 + 3390s} e^{-110s} u_{CO_2} \tag{4.3}$$

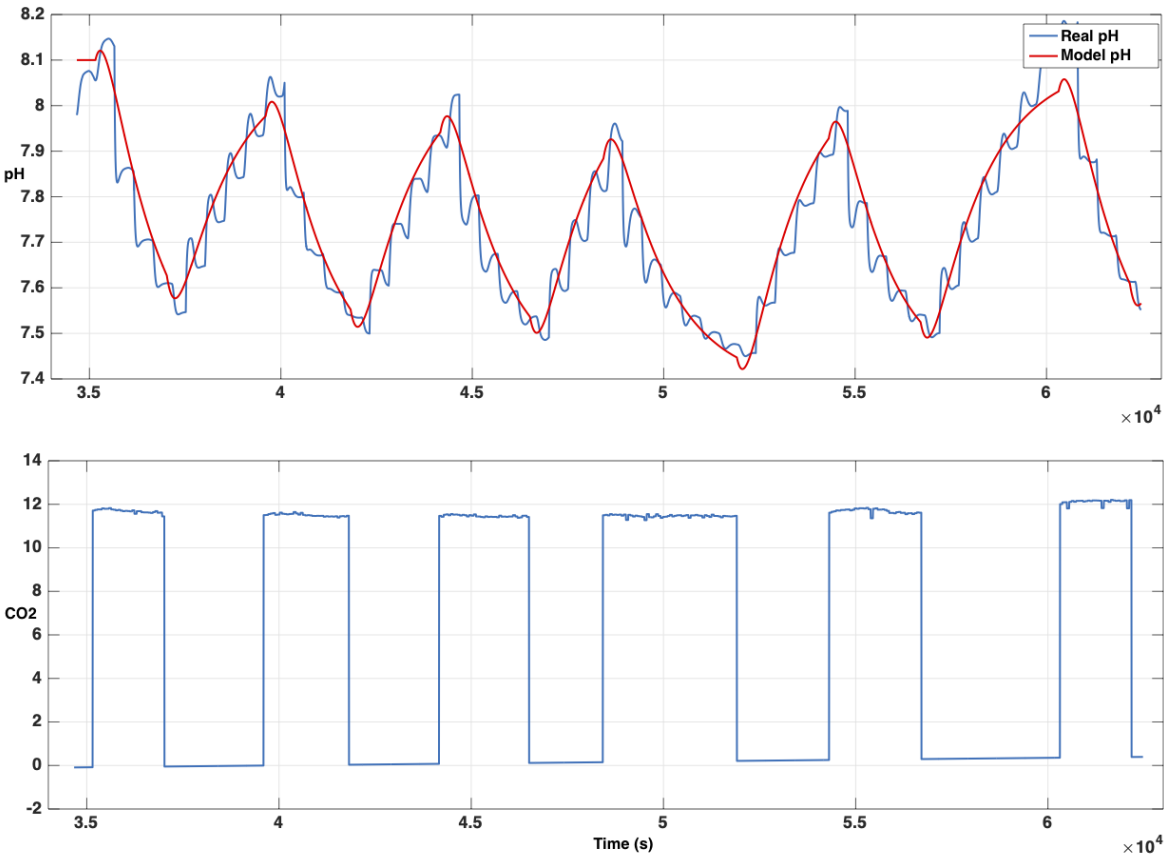Figure 4.1. Productivity and pH relation.

Figure 4.2. Model validation for the implementation of GPC in the reactors. The obtained model is represented in red.

GPC Implementation

The GPC involves applying a control sequence [22] that minimizes the cost function defined in Equation (2.32).

The minimum of J, assuming no constraints on the control signal, can be computed by setting the gradient of J equal to zero, such that the optimal solution can be obtained by minimizing the quadratic function expressed in vector form:

$$J(u) = (Gu + f - r)^\top (Gu + f - r) + \Lambda u^\top u \tag{4.4}$$

where G contains the step response coefficients of the process, f is the free response of the system, w is the future reference trajectory, and u represents the future increments of the control signal. Equation (4.4) can be rewritten as defined in Equation (2.35).

The quadratic function obtained is minimized subject to the system's constraints (Table 2.1) by solving a classical quadratic programming problem. In this case, the implemented constraints in the controller are those related to the amplitude and increment of the control signal, as well as the amplitude of the system output:

$$u_{min} \leq u(t) \leq u_{max}$$

$$\Delta u_{min} \leq \Delta u(t) \leq \Delta u_{max}$$

$$y_{min} \leq y(t) \leq y_{max}$$

Results

Two simulation tests are presented for a day with changing radiation conditions due to the passage of clouds in order to evaluate the proposed control strategy.

Both tests were conducted under the same external radiation conditions but with variations in the output constraint and appropriate limitations imposed on the control signal and its increments. The set-point for the pH at the output, y_{ref}, was fixed at 7.8. The main objective of this work is to evaluate the possibility of limiting pH variations through the constraint management capability of the GPC algorithm. Hence, the proposed tests focused on the same simulation day but considered two different allowable ranges for the output to analyze the achievement of this objective. The minimum and maximum prediction horizons were set with values of $N_1 = 1$ and $N_2 = 500$, respectively. The control horizon is $N_u = 3$, and the control effort weighting is set to $\Lambda = 200$ [115]. The sampling time was set to 5 seconds.

The constraints are set with the following values:

$$0 \leq u(t) \leq CO_{2max}$$

$$\Delta u_{min} \leq \Delta u(t) \leq \Delta u_{max}$$

$$y_{min} = y_{ref} - Y_{min} \leq y(t) \leq y_{max} = y_{ref} + Y_{max}$$

The control variable is limited to the values that the real system can provide, between 0 and the maximum CO_{2max} value of 12 L/min. The control signal increment was also set to a value of 12 L/min. Lastly, the system output is constrained to values very close to the reference value of $y_{ref} = 7.8$, as mentioned in Section 2.2.1; maintaining the pH value close to this reference will increase productivity. In this case, it is possible to limit the maximum and minimum values around the reference, y_{ref}, by setting values for Y_{min} and Y_{max}, respectively. The simulation activates the control algorithm once the radiation exceeds 100 $\mu E/m^2$s.

Figure 4.3 shows the first test where the output limits were imposed with $Y_{min} = 0.2$ and $Y_{max} = 0.2$. It can be observed that the GPC algorithm successfully keeps the output within the established bounds. It should be noted that in some instances, it exceeds these limits due to modelling errors existing at that operating point between the obtained linear model and the nonlinear model used as a simulator [29]. The use of CO_2 is minimized by only pulsing when necessary to maintain the reference within the desired values and also comply with the control signal constraints.
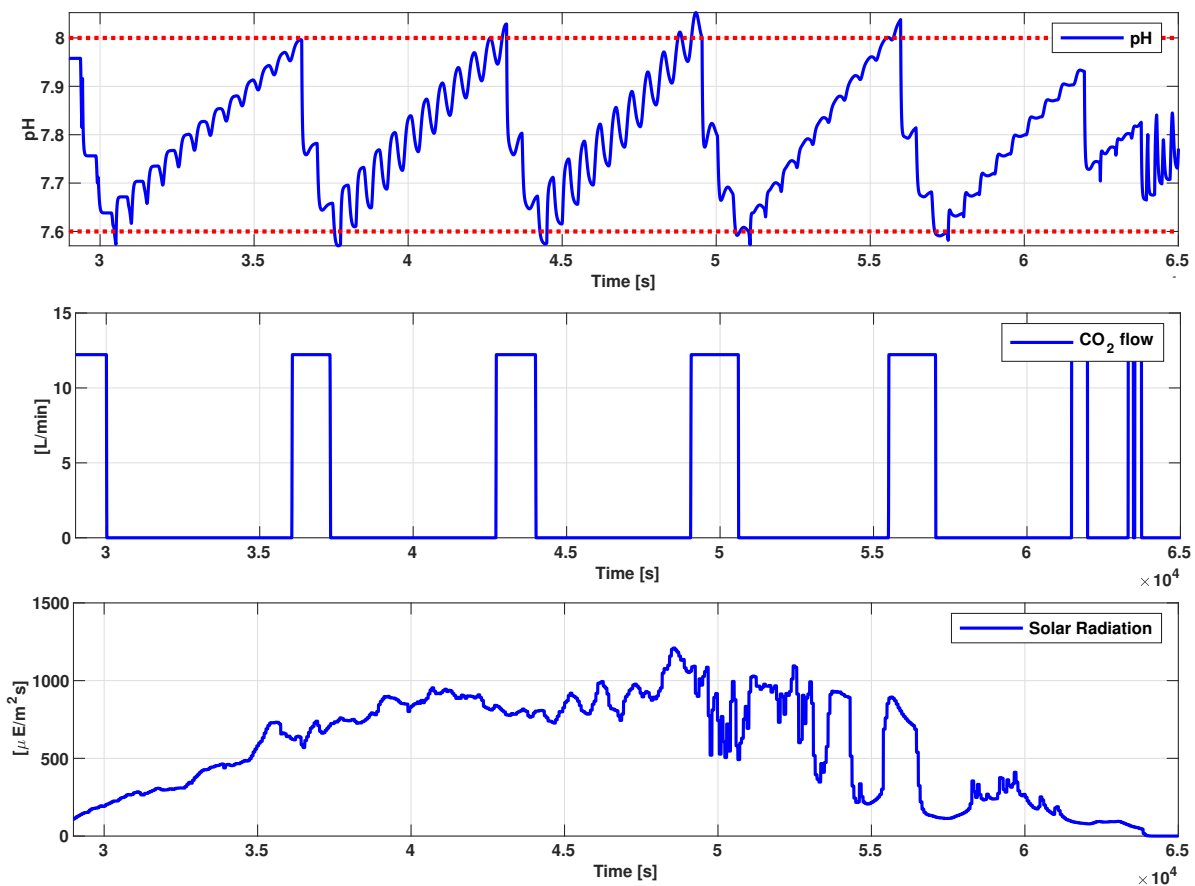

Figure 4.3. Control test with output constraint limits $Y_{min} = 0.2$ and $Y_{max} = 0.2$.

The second test is shown in Figure 4.4. In this case, the reference is the same as in the previous test. However, the output signal bounds have been reduced to $Y_{min} = 0.1$ and $Y_{max} = 0.1$ to achieve a lower pH variation and, therefore, have a more positive impact on the system's productivity. It can be observed that all the imposed constraints are still satisfied. However, a change in the CO_2 injection by the GPC algorithm can be observed compared to the previous test. The injection frequency is increased with smaller pulses to keep the pH within the established

limits. Therefore, it can be concluded that the GPC algorithm is a helpful solution for maintaining the pH at optimal values while reducing CO_2 consumption.
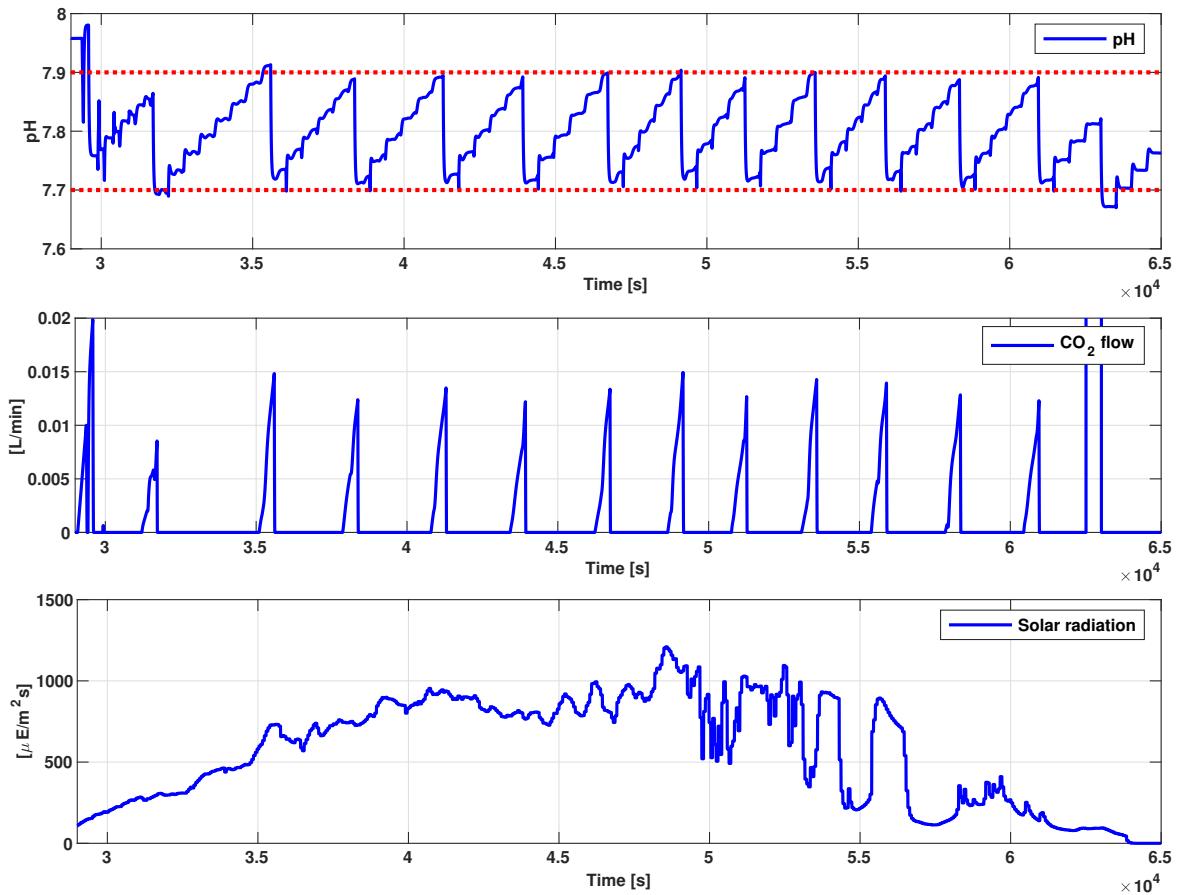

Figure 4.4. Control test with output constraint limits $Y_{min} = 0.1$ and $Y_{max} = 0.1$.

The proposed solution has achieved results very similar to other works obtained in [29, 61, 112]. These works address different control strategies in tubular and raceway photobioreactors, such as robust control with QFT or PI control based on events distinguishing between day and night. The main advantage of this strategy compared to the ones mentioned earlier is that it allows us to intrinsically manage the treatment of constraints and the issue of pH variability at the process output.

Unlike other similar works implementing predictive control in a raceway photobioreactor, such as in [101], where event-based predictive control is applied, this work made use of the constraints that the predictive controller allows to impose on the process output. The obtained result is satisfactory, as it can be observed that the system output is bounded within the established limits while the control signal also adheres to its constraints. This ensures that productivity is maximized as long as the pH value remains close to the set reference value while reducing the environmental impact due to the reduced CO_2 injection enabled by this control strategy.

Conclusions

This contribution presents the generalized linear predictive control of the pH in a raceway reactor. The obtained results are satisfactory, as it is observed that the system output stays within the established limits while the control signal also meets its constraints. This ensures that the

productivity is maximized as long as the pH remains as close as possible to the established reference value, reducing the environmental impact due to the decrease in CO_2 injection. It is planned to evaluate the behavior of the control algorithm over several consecutive weeks in simulation, conducting tests under different external conditions to observe its performance. After that, the proposed control can be implemented in an industrial reactor. The design and evaluation of new nonlinear versions of predictive control algorithms are also planned. Besides, this contribution has resulted in the publication of a scientific article in a national control conference [56].

4.1.2 Robust Control

Most of the control strategies mentioned above are based on a nominal plant model assuming that the pH is always close to the desired operating point. However, as previously mentioned, the solid nonlinear component of the system leads to modelling errors, requiring consideration of possible uncertainties in the control strategy design process. In this regard, this work presents a new solution for pH control by designing a robust controller using QFT [44]. In this approach, the nonlinear dynamics of the system and the different sources of error are captured in the form of a low-order model with parametric uncertainty. Once this model is obtained, a robust PID controller is designed to meet specific performance and stability specifications [61]. Similar to other methodologies, such as the one proposed in [132] for PID tuning, the sensitivity function is employed, but the controller structure is not restricted in this case. The results have been successfully evaluated in a nonlinear process simulator [29], analyzing the behavior at different operating points and under various external working conditions. Subsequently, the controller has been implemented in a real reactor described in Section 4.1, where several experiments have been conducted over consecutive days at different operating points.

In this contribution, a model of the system with parametric uncertainty covering the typical working ranges of pH has been developed, and later a robust controller with QFT is designed to achieve certain robust performance and stability requirements. The resulting control algorithm has been evaluated in simulation and real tests against different working conditions and at different operating points, obtaining satisfactory results.

Simplified Model

This section presents the low-order linear model identified, taking into account the structure of the photobioreactor, the sensor and actuator distribution, and the dynamics observed in the data. Considering that the output of the process is the pH of the culture, the opening of the CO_2 injection valve is the manipulated variable, and solar radiation is the major disturbance of the system, the behavior of the system can be represented by the transfer function defined in Equation (4.2), where pH is the pH of the culture, u_{CO_2} is the valve opening percentage, K_u is the static gain, T_u is the time constant, and L is the time delay [13].

These parameters, especially the system gain and time constant, exhibit considerable variation due primarily to the influence of solar radiation, which directly affects the photosynthesis process and thus causes changes in the process dynamics.

In order to capture the potential uncertainty of the process, various experiments have been conducted for different operating points around which the system productivity is maximized. [101]. In this way, operating points of pH=7, pH=8, and pH=9 were selected, covering a wide operation range. Different pulse trains in CO_2 injection were applied throughout the daylight

period around each operating point for 20 days under different environmental conditions. Figure 4.5 shows the model validation for a specific test day.
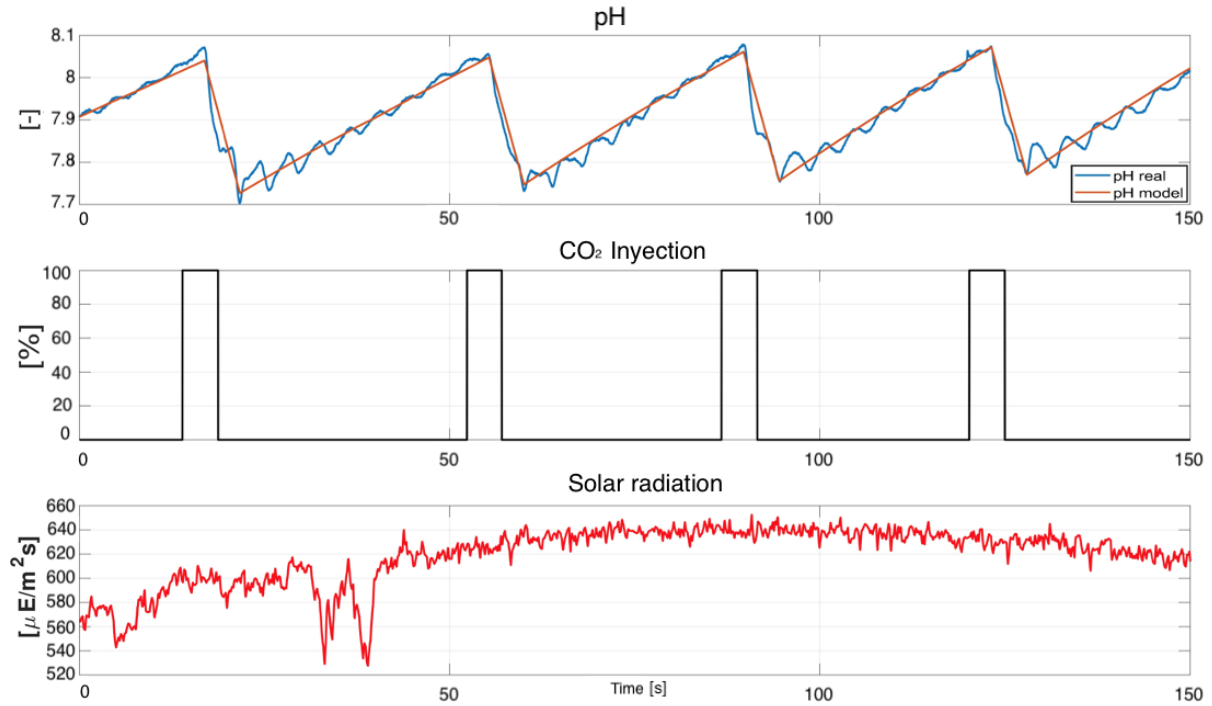

Figure 4.5. Model validation for pH in the contribution of a QFT controller in the raceway reators.

A total of 60 experiments were conducted, spanning 20 days for each of the three different operating points. Using the reaction curve method, models were obtained for each of these experiments. Uncertainty bounds were then calculated for the pH model, resulting in the following family of plants (time constants and delays in seconds):

$$P(s) \in \mathcal{P} = \left\{ \frac{K_u}{1 + T_u s} e^{-L_u s}, \text{ with} \right. \tag{4.5}$$

$$\left. K_u \in [-4.1, -0.35], \ T_u \in [3.4, 8] \cdot 10^3, \ L_u \in [1, 1.4] \cdot 10^2 \right\}$$

It is essential to highlight the significant parameter variability due to the diurnal effect of radiation on the photosynthesis process and the change in operating points. In addition to the parametric uncertainty in the models, it is important to consider the uncertainty introduced by the sensors and actuators, as well as external factors such as weather conditions (e.g., rain or wind), reactor temperature, etc.

Controller Design

This section presents the design of the proposed QFT robust controller using the model with uncertainty presented in the previous section. The objective is to design a controller C and a prefilter F if necessary, as shown in the diagram in Figure 2.8, where all the specifications are met for the plant family $\mathcal{P}$ [39]. A proprietary package developed in Matlab® has been used for the controller calculation [86].

The first step in QFT controller design is to define the set of design frequencies and the desired behavior and stability specifications for the closed-loop system, expressed as inequalities on the closed-loop transfer functions. Considering the model uncertainty shown in Equation (4.5), as well as the magnitude of the time constant and delay, a set of low frequencies has been selected to cover the system's operating range: $\Omega = \{0.0001, 0.0005, 0.001, 0.01\}$ rad/s. Additionally, the specifications are defined in the frequency domain. For this system, a stability specification with a phase margin greater than or equal to $S_{lim} = 45°$ for all operating points has been chosen, as defined by Equation (2.39).

For reference tracking, the specifications are given by Equations (2.41), (4.6) and (4.7), which correspond to a closed-loop time constant between 3500 and 8200 seconds.

$$B_l(s) = \frac{1}{(6400s + 1)(2600s + 1)(1000s + 1)} \tag{4.6}$$

$$B_u(s) = \frac{1}{3500s + 1} \tag{4.7}$$

It should be noted that, as shown in the closed-loop tests, the pH starts at a different initial value each day, so it is necessary to perform set-point tracking to ensure that the pH is close to the optimal value required by the cultivated microalgae strain.

Once the specifications are defined, the uncertainty is represented in the Nichols Chart for the frequencies in Ω, as shown in Figure 4.6. A plant from the set is chosen as the nominal plant, $P_0(s) \in \mathcal{P}$, defined in Equation (4.8). In each template, the nominal plant is marked with an asterisk.

$$P_0(s) = \frac{-4.1}{3390s + 1} e^{-100s} \tag{4.8}$$

Next, based on the specifications defined earlier and the templates, for each frequency ω in the set Ω, forbidden regions are obtained in the Nichols Chart for the open-loop transfer function [86].

$$L_0(j\omega) = C(j\omega)P_0(j\omega)$$

These bounded regions are defined as boundaries, with one for each frequency and specification defined. Figure 4.7 shows the boundaries corresponding to the stability specification of 2.32 dB and the reference tracking specification given by the difference in magnitude in dB between the bounds in Equations (4.6) and (4.7), evaluated for the frequencies in the set Ω.

Once all the boundaries are defined, the open-loop function $L_0(j\omega)$ must have a shape that satisfies all the limits for each frequency. Figure 4.7 also shows the fitting of the nominal open-loop function for the tuned PID controller in series form [1]. The controller $C(s)$ and the filter $F(s)$ are given by the following equations:

$$C(s) = -34.28 \left(1 + \frac{0.00035}{s}\right)\left(1 + 83.89s\right) \tag{4.9}$$

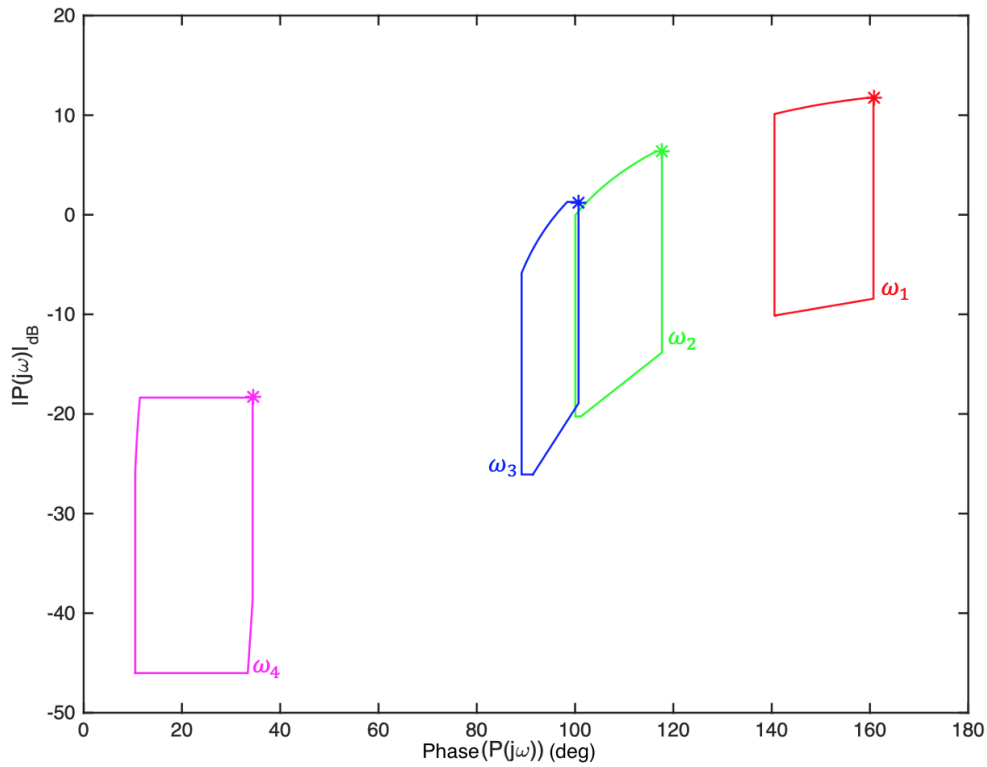$$F(s) = \frac{1}{4762s + 1} \tag{4.10}$$

Figure 4.6. Templates ($\omega_1 = 0.0001, \omega_2 = 0.0005, \omega_3 = 0.001, \omega_4 = 0.01$).
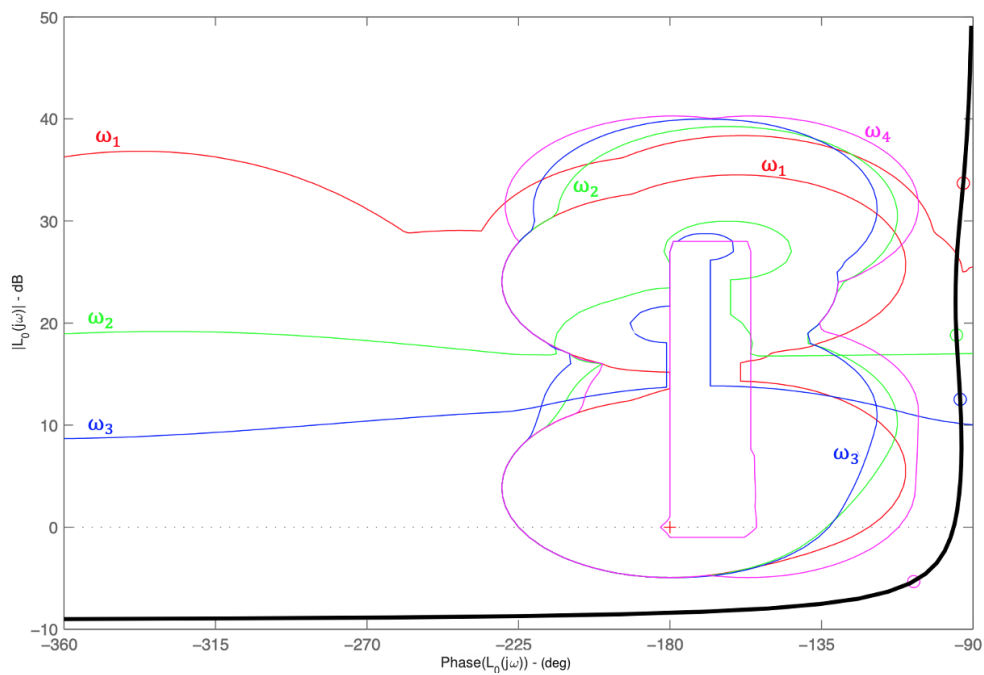

Figure 4.7. Adjustment of L_0, stability boundaries and tracking ($\omega_1 = 0.0001, \omega_2 = 0.0005, \omega_3 = 0.001, \omega_4 = 0.01$).

The final step in the controller design is to validate whether the specifications for frequencies outside the set Ω are met with the selected controller. Figures 4.8 and 4.9 show the validation of the design for the tracking and stability specifications in the frequency domain, respectively.
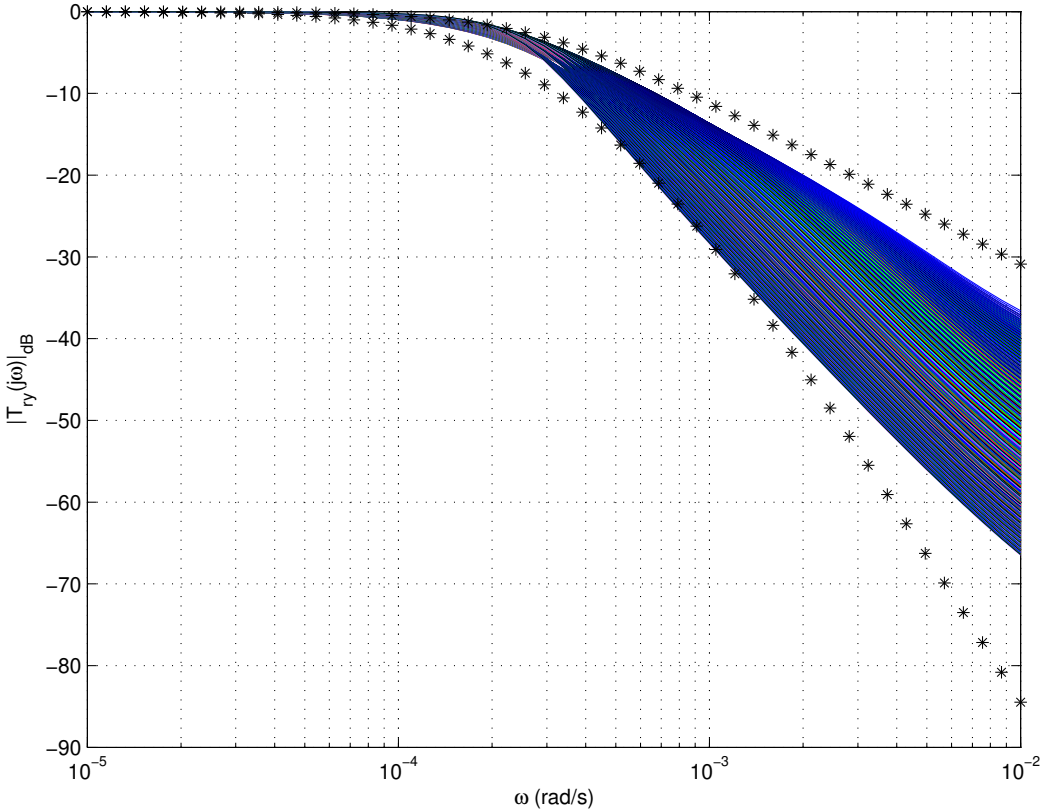
Figure 4.8. Validation of the reference tracking specifications.
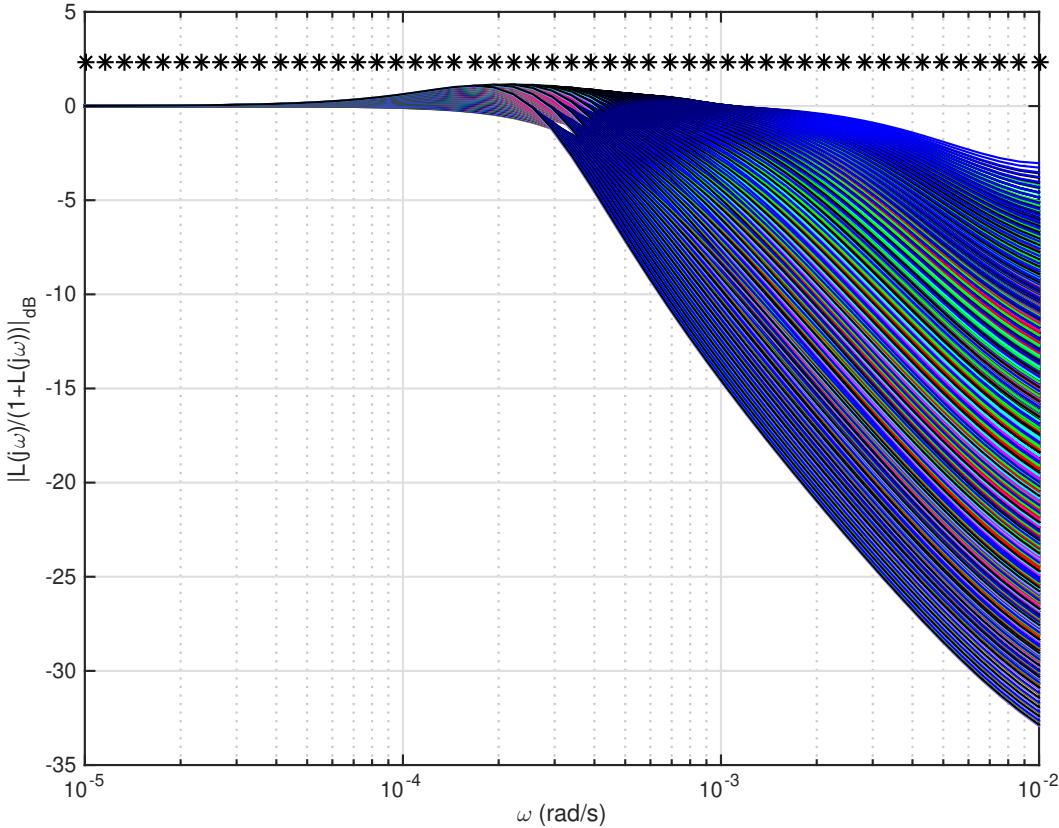
Figure 4.9. Validation of the stability specifications.

Results

In this section, the robust controller design is evaluated through simulation in different operating points, as well as its performance in the actual raceway reactor.

To evaluate the proper performance of the controller in simulation, several days with different weather conditions and operating points have been used as a reference to assess the controller's performance in the face of process dynamics variability. This allows for assessing its behavior before implementing it in the actual plant. The simulations have been carried out using the nonlinear model of the photobioreactor described in Section 2 and implemented in Simulink [28]. In order to analyze the system's behavior in different operating points and evaluate if it meets the designed specifications for reference tracking, downward step changes in pH have been applied at the beginning of the day. It is worth noting that these situations naturally occur in the daily operation of the process since pH values reach close to 9 during the night, and each morning it is necessary to bring the pH value close to the optimal values for the specific strain being cultivated.

Figures 4.10 and 4.11 show two example experiments for a sunny day and a cloudy day, each of them at different operating points, starting the step changes in pH at initial values of 8.3 and 7.9, respectively. In these figures, it can be observed that the system's behavior is consistent with the design specifications. It is nearly the same on both days despite starting from different operating points and being subjected to different weather conditions, demonstrating the proper functioning of the proposed robust controller. Notice that, the oscillations in the pH response are due to implementing the nonlinear model based on partial differential equations.

In Figure 4.12, the behavior of the reactor on a cloudy day can be observed. At the beginning of the day, the pH is in an open loop (no control during the night), reaching a pH value close to 8 in the early morning. When switching from manual to automatic mode, the system successfully reaches the reference, in this case, a pH of 7.4. It is worth noting how the controller quickly rejects disturbances caused by the passage of clouds, as can be observed shortly before 14:00 (2 PM).

Figure 4.13 shows a less cloudy day where the goal is to maintain a pH of around 7.8 during the day. To achieve this, the control is switched from manual to automatic once the radiation is sufficient for the microalgae to perform photosynthesis. The satisfactory response of the pH reaching the reference can be observed when the automatic mode is activated, around 9:30 AM. The control signal is smooth throughout the day, and disturbances due to changes in radiation are adequately rejected.

As observed in the experimental tests, the behavior of the robust controller is valid for the uncertainty introduced by different operating points, changes in set-points, and varying weather conditions.
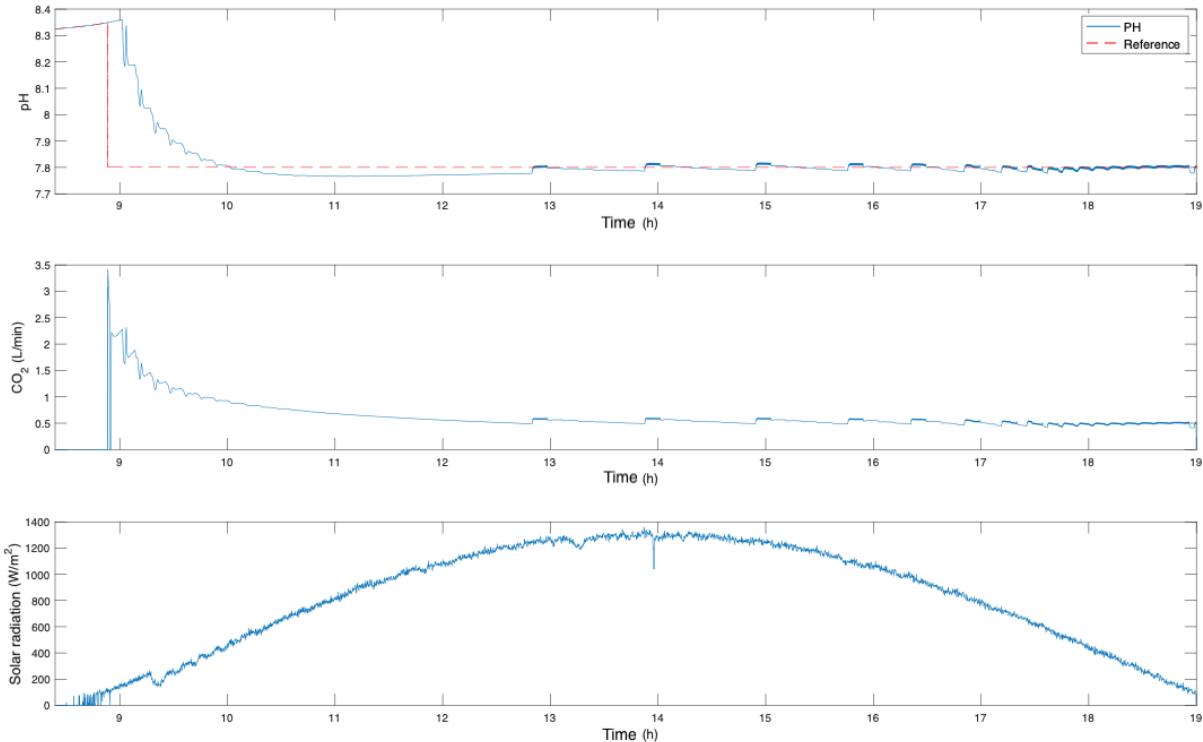
Figure 4.10. Simulation experiment on a sunny day with an initial pH value of 8.3.
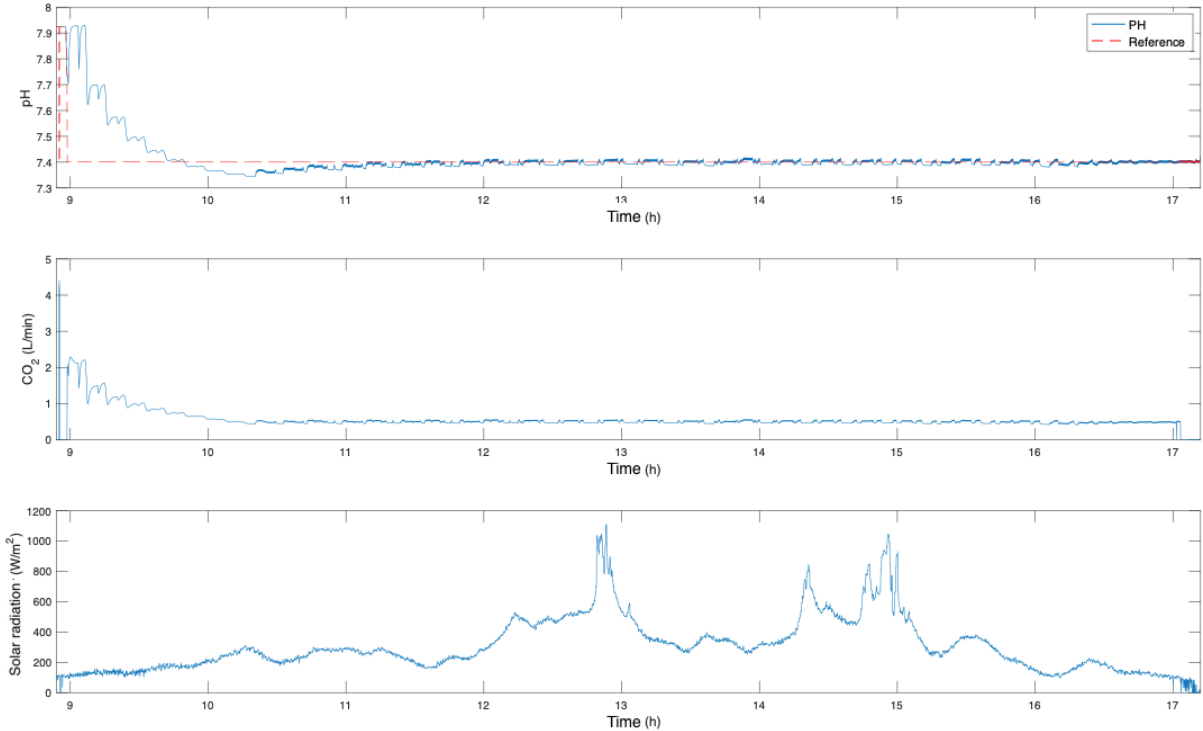

Figure 4.11. Simulation experiment on a cloudy day with an initial pH value of 7.9.
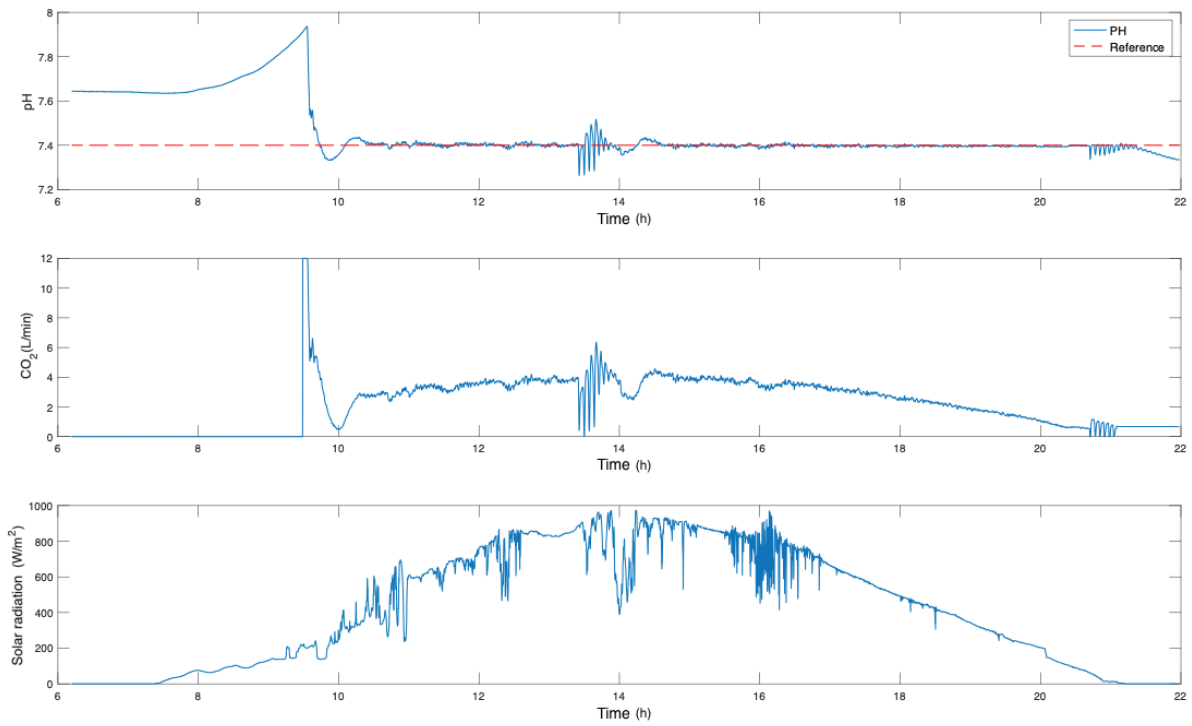
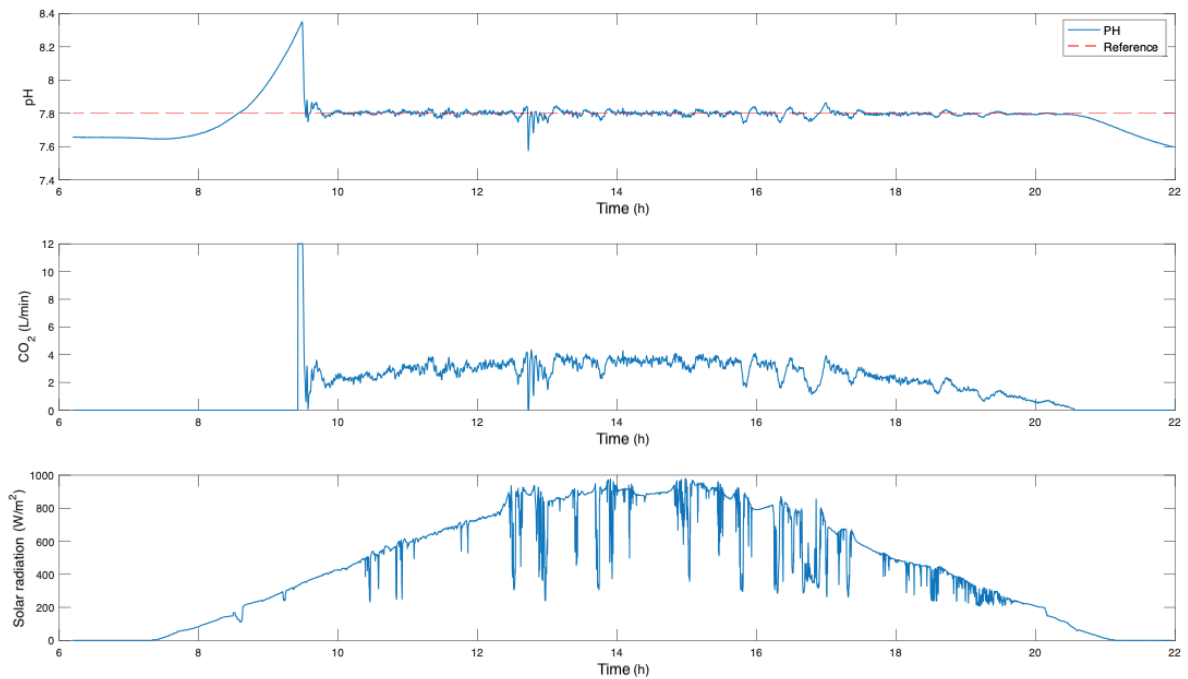Figure 4.12. Real raceway reactor implementation with a set-point of pH=7.4.

Figure 4.13. Real raceway reactor implementation with a set-point of pH=7.8.

Conclusions

This contribution presents the robust control with QFT of the pH in a raceway-type reactor. The experiments demonstrate the good performance of the controller for the different operating points and under the tested operating conditions. Overall, the proposed control strategy effectively regulates the pH levels in the reactor, providing stability and accurate tracking of reference values. The robustness of the controller allows it to handle uncertainties and disturbances, ensuring reliable operation even in the presence of external factors. These results highlight the effectiveness and practicality of the developed control approach, making it a promising solution for pH control in raceway reactors and similar industrial processes.

This contribution has led to a publication of a scientific journal article in *"Revista Iberoamericana de Automática e Informática industrial"*, Q4 in the Journal Citation Report (JCR) [55].

4.1.3 A Computer-Based Tool to Simulate Raceway Photobioreactors for Design, Operation, and Control Purposes

Given the intricate nature of the reactor model, as outlined in Section 2.2.1, the complexity of these processes becomes evident when considering aspects such as design, operation, modelling, and control [34]. In this sense, there is a need to develop tools that allow the user to easily simulate the behavior of the system and to modify the main parameters from biological, design, and operation perspectives. Therefore, in this work, a graphical tool for the simulation of the raceway reactor is presented. This tool includes the nonlinear models developed in [119], [29] and [113], and the control algorithms presented in [102] and [112]. It has been developed using M-code and the App Designer from Matlab® [81]. It allows to access and to modify the most important variables of the process, to simulate the system, and to observe the results in a straightforward and graphical way. Notice that the proposed tool also permits to modify the reactor structure and its design. Moreover, different strains can be studied by including their biological parameters. Real data related to the weather variables from a meteorological station of an industrial raceway reactor are used as inputs to the tool covering different seasons of the year. Furthermore, several control approaches can be analyzed for pH and DO variables in order to study the impact on biomass productivity [63].

There are two main control strategies implemented in the tool that can be used independently or jointly. The first one, as done in [102], a selective pH and dissolved oxygen control is implemented as shown in Figure 4.14. This control scheme allows addressing simultaneous pH and DO control, satisfying all requirements. In the diagram, it can be observed that pH and DO are controlled with their own controller (C_{pH} and C_{DO}, respectively), which provides two control signals (u_{pH} and u_{DO}). A selective mechanism determines the control signal to be used in the system (u_{SC}) using selective logic (P_{RW}). The pH controller will be prioritized when the pH value is outside of established limits around its pH set-point (SP_{pH}) (a dead band is used to have some control tolerance). When pH is inside the limits, the DO controller will be selected in order to try to achieve its DO set-point (SP_{DO}). In the developed tool, the dissolved oxygen is always implemented by using an On/Off controller, and for pH PI or On/Off controllers can be selected. The set-points are set by the user. The second control strategy is daytime/nighttime control. It has been demonstrated that by controlling the pH during the daytime and nighttime, important performance improvements can be achieved [112]. So, the pH is controlled 24 hours a day using a PI or an On/Off control for the daytime period and an On/Off control for the nighttime (notice that during the nighttime, microalgae do not perform photosynthesis).
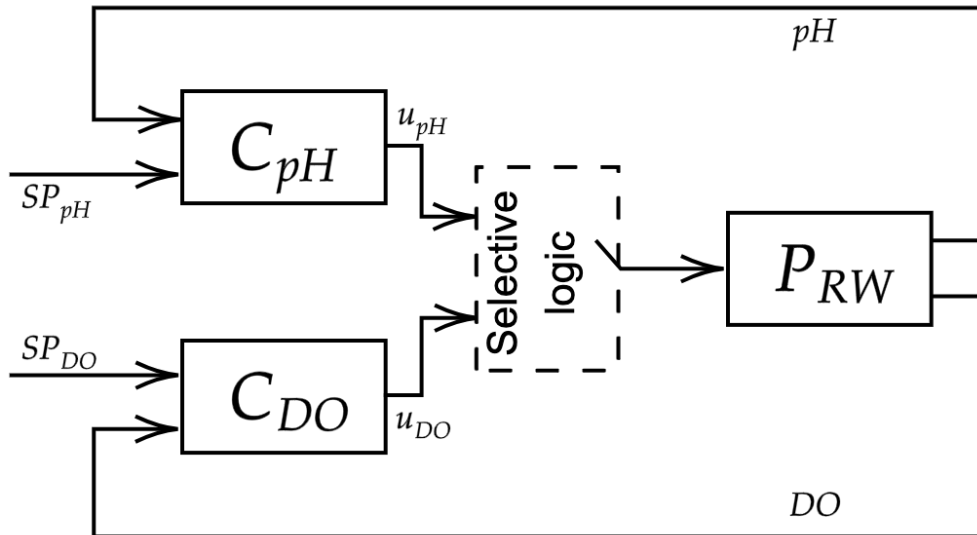
Figure 4.14. Selective control scheme for DO and pH [102].

The Tool

In this section, the functionality of the developed tool is described, which highlights the theoretical concepts exposed in the previous section. The tool is available through `http://www2.ual.es/sabana/data-center-2/` for both MacOS and Windows operating systems.

The software used for the design of the tool is the Matlab App Designer®, a tool for the development of graphical user interfaces (GUI) or user interfaces in general, that improves the accessibility of software applications, eliminating the need to learn a particular programming language to build them and avoiding the need to write commands in order to execute the different functionalities for an application. Matlab® Apps are stand-alone Matlab® programs with a GUI that automates a task or calculation. These App can be run under the Matlab environment (which is the recommendable option) or as stand-alone executable programs without Matlab® [81]. Notice that the tool only uses weather data as input. All system variables are simulated using the models and control approaches presented in the previous section.

Initialization and parameters configuration

The tool is designed in three different areas, as shown in Figure 4.15. Starting at the top, the Play and Stop buttons are observed, which allow running or stopping the simulation. Below these buttons, there is a box with text that gives information about the program's execution. On the right part, there is a group of radio buttons that allows running the simulation in open-loop (the Manual radio button) or in closed-loop (the Automatic radio button). The tab in which the control parameters can be configured will be explained later. In the middle area, there is a panel to configure and modify all the parameters of the reactor.

In the tool configuration area, there are four different tabs to modify the most important parameters of the process, as shown in Figure 4.16. In the first tab (Figure 4.16a), the initial values of the pH, dissolved oxygen, biomass concentration, and temperature can be set for the start of the simulation. When the manual model is selected, it is possible to modify the flow
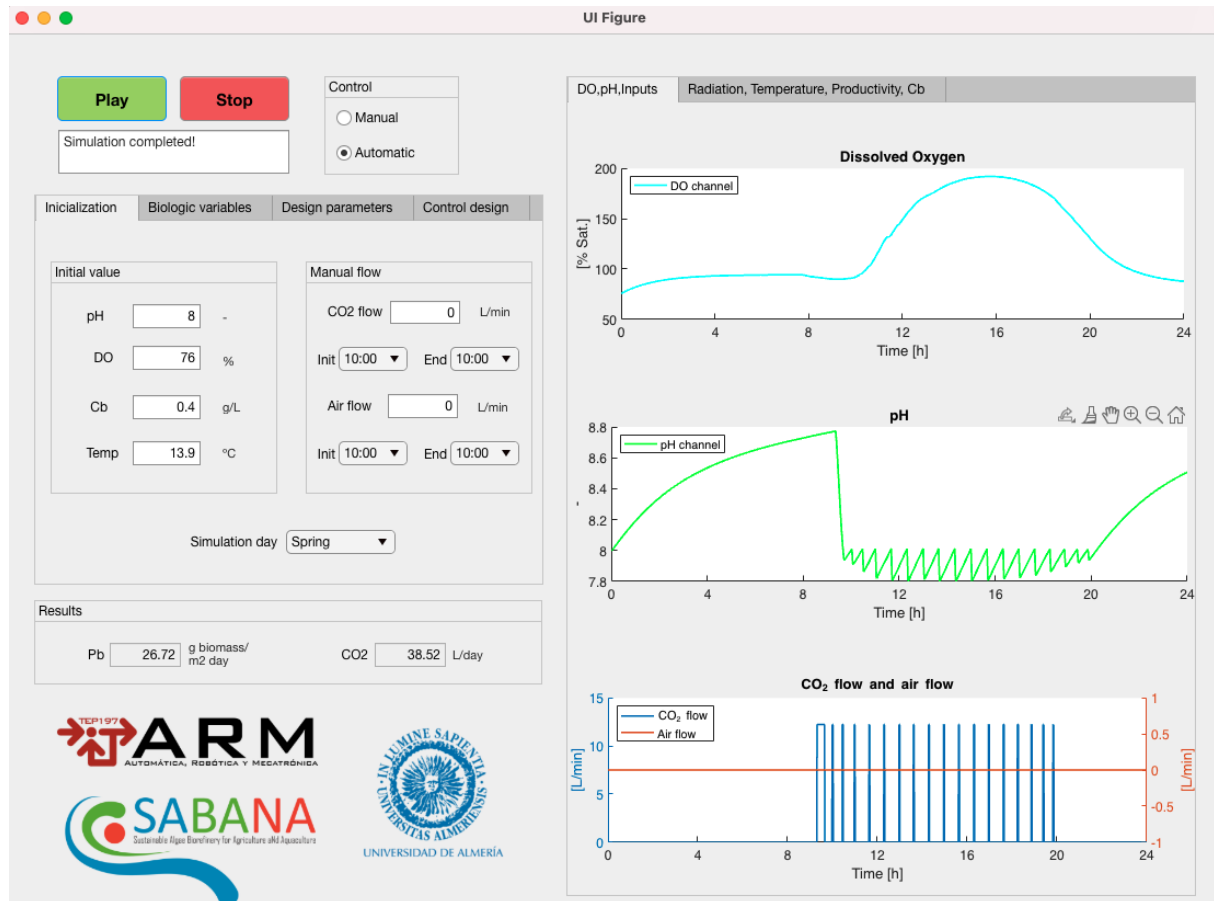
Figure 4.15. Main screen of the raceway reactor simulation tool.

value for the CO_2 and the air, and the start and end times, being able to select how much flow and for how long it is applied. At the bottom, a drop-down element is provided to choose the season of the year chosen for the simulation, spring, summer, autumn, or winter, where real weather data from the reactor described above are used as inputs to the model. The second tab (Figure 4.16b) is dedicated to the biological variables. It is possible to modify the biological parameters of the microalgae and thus be able to simulate different strains. From the design parameters tab (Figure 4.16c), it is possible to modify the physical dimensions of the reactor: length, height, and width. The last tab is focused on the control approaches (Figure 4.16d). These parameters are used when the automatic option is selected. As the main variables to control are pH and dissolved oxygen, the corresponding set-point values can be modified. Control can be done only on pH, only on dissolved oxygen, or on both variables at the same time by using the selective control approach discussed above. On the other hand, the reactor can also be controlled only during the day when there is solar radiation or during the day and night. For the control of dissolved oxygen, the On/Off method is used. To control the pH, On/Off or PI control strategies can be selected, being able to modify the design parameters (K_p and τ_i) for the last one.

After the simulation, the results are displayed in two areas. On one hand, at the left (Figure 4.17), quantitative results for productivity (P_b) and carbon dioxide (CO_2) consumption are given for the simulated day. On the other hand, the results can be seen graphically on the right part of the tool. In the first tab, Figure 4.18a displays the evolution of the dissolved oxygen and pH along the day. Below them, the plot shows two different variables, the CO_2 and air flows, that are used to control the pH and the dissolved oxygen, respectively. In manual mode, a specific
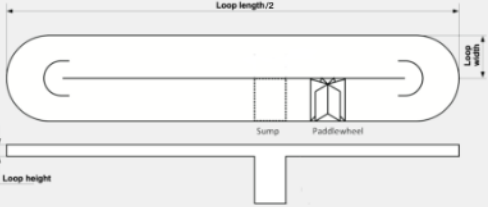
schedule is manually set. In the second tab, Figure 4.18b shows the evolution of the temperature and the solar radiation, the biomass productivity (P_b), and the microalgae biomass concentration (C_b) along the day.

(a) Initialization menu.

(b) Biologic variables menu.

(c) Design parameters menu.

(d) Control design menu.

Figure 4.16. Menu panel tabs.

Figure 4.17. Numeric simulation results.

Ilustrative Examples

Notice that there is a large number of possible scenarios to perform the simulation of the system. So, this section presents some of the most representative ones. It is important to note that all the results obtained are computational. The data required by the model to compute the simulation are taken from the real raceway reactor, described in Section 2. The first example is a simulation of two different seasons of the year with different climate conditions in order to
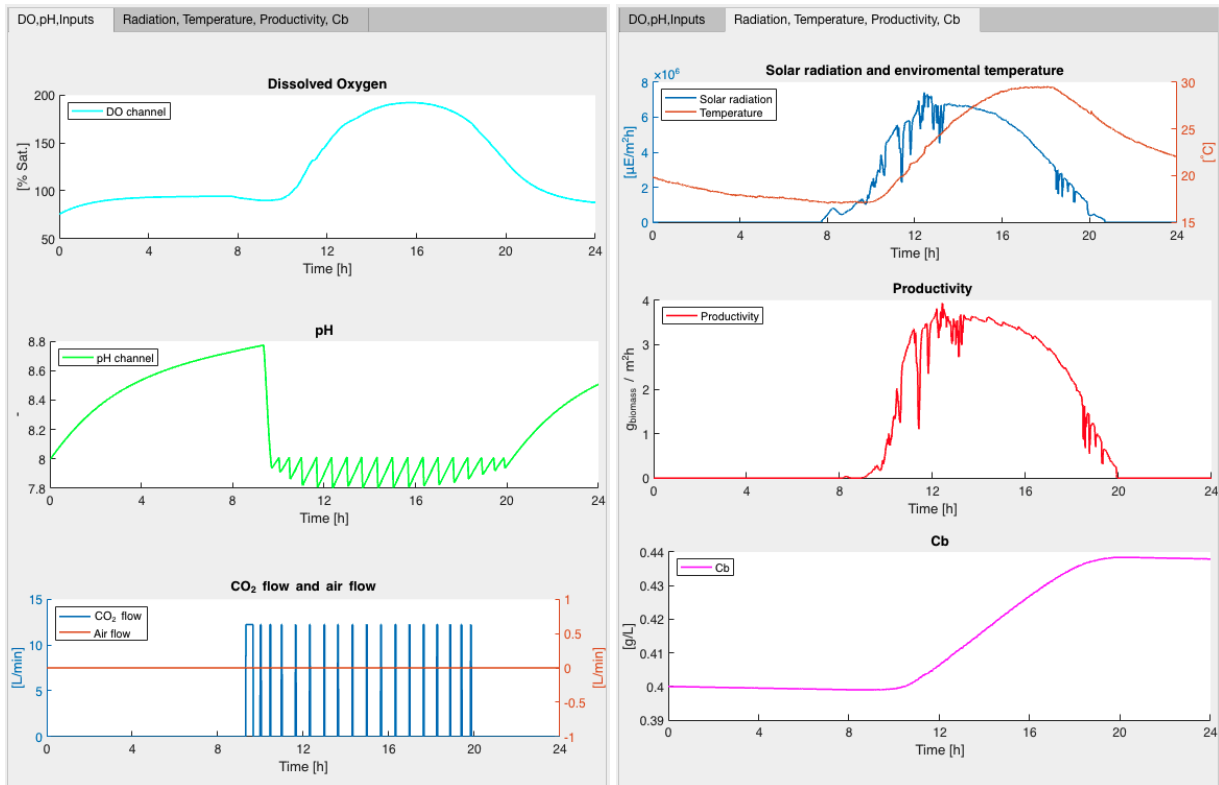
(a) Dissolved Oxygen, pH, carbon dioxide, and air flow graphics.

(b) Radiation, temperature, productivity, and biomass concentration graphics.

Figure 4.18. Graphical results.

analyze the weather effect. Then, in a second example, a comparison of the productivity is made, changing the culture depth of the reactor for the same weather conditions. After that, two different strains are simulated, the *Nannochloropsis gaditana* and the *Scenedesmus almeriensis*, to see their behavior in the same reactor and under the same operating conditions. Their characteristic parameters are defined in Table 4.1. Finally, two different control strategies are compared to control the culture pH.

Parameter	*Nannochloropsis gaditana*	*Scenedesmus almeriensis*	Units
$X_{r,max}$	41	48	$^\circ C$
$X_{r,min}$	4.6	9	$^\circ C$
$X_{r,opt}$	32	29	$^\circ C$
$PO_{2,max}$	139	350	$mg\,L^{-1}h^{-1}$
n	2	2	-
I_k	151	200	$\mu E\,m^{-2}s^{-1}$

Table 4.1. Strains characteristic parameters, [7, 15].

Season impact

The time of year in which the reactor is operated is a crucial factor for microalgae productivity. In order to show this effect, two extreme cases will be simulated, summer and winter, respectively. For this simulation, the *Scenedesmus almeriensis* strain was used (see Table 4.1 for the characteristic parameters).

In Figure 4.19, closed-loop simulations with an On/Off control for summer (Figure 4.19a) and winter (Figure 4.19b) seasons are shown. At the top of the figure, the numeric results can be observed. As expected, in summer the total production, $P_b = 24.74 \, [g_{biomass} \, m^{-2} \, day^{-1}]$, is higher than in winter, $P_b = 10.09 \, [g_{biomass} \, m^{-2} \, day^{-1}]$.

Observing the graphics results can also be seen the considerable difference in the radiation curve, being directly proportional to the productivity curve. The most significant differences in these two curves lie in the hours of solar radiation per day (12 hours in summer and 9 hours in winter), and its maximum value. On the other hand, the variation in the environmental temperature between these two days is relevant, as studied in [113], also affecting the growth of microalgae, being the maximum reached in winter $X_r = 18 \, [°C]$ and in summer $X_r = 34 \, [°C]$ and the minimum $X_r = 11 \, [°C]$ and $X_r = 24 \, [°C]$, respectively.
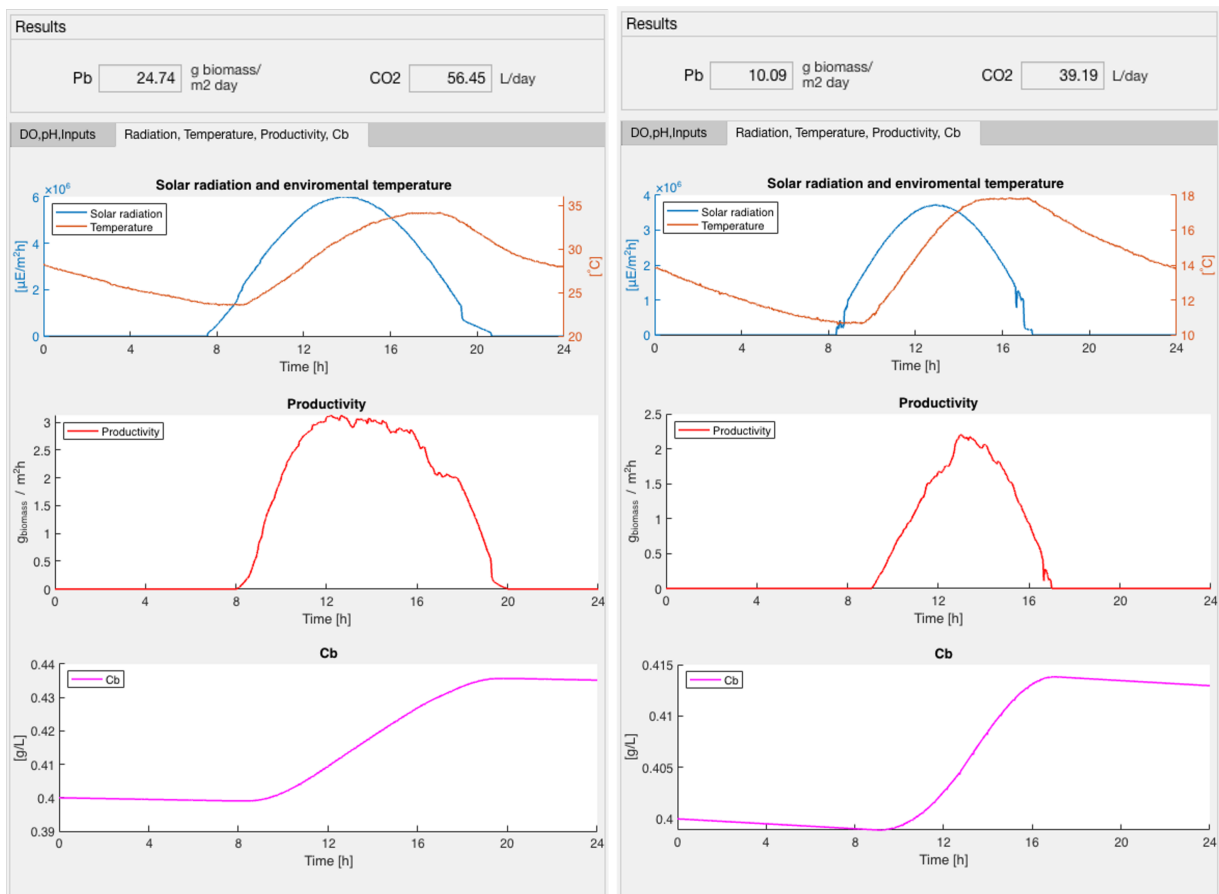
(a) Open loop simulation on summer.

(b) Open loop simulation on winter.

Figure 4.19. Summer and winter graphical results.

Moreover, the influence of solar radiation on the system through the pH can be also observed just by looking at the total carbon dioxide flow consumed each day. The microalgae pH increases with solar radiation, so to keep it on the desired set-point value, the system introduces CO_2 to lower it. In summer, this process is faster than in winter because there is much more sunlight, and thus the photosynthesis process increases. For that reason, the system requires more CO_2, being able to have a great difference between both seasons of the year. In the example, in summer the consumption value is $CO_2 = 56.45\,[L\,day^{-1}]$, and in winter $CO_2 = 39.19\,[L\,day^{-1}]$.

Culture depth influence

The culture depth can directly affect the productivity of the system. As studied in [112], the reactor temperature can be regulated in microalgae raceway reactors by modifying the culture depth. This study is important because an inadequate temperature strongly reduces biomass productivity even if there is enough sunlight. For this example, the depths $0.1\,[m]$ and $0.3\,[m]$ are chosen. Both simulations have been done in the same conditions, a closed-loop simulation with an On/Off control, using the *Scenedesmus almeriensis* strain, in spring and with the same initial values for variables in Figure 4.16a.

Figure 4.20 shows the configuration parameters, the performance results, and the graphical representations for both cases. The graphical results provide information about productivity throughout the day. The average value when culture depth is of $0.1\,[m]$, is $P_b = 22.44\,[g_{biomass}\,m^{-2}\,day^{-1}]$, lower than when is $0.3\,[m]$ that is $P_b = 28.24\,[g_{biomass}\,m^{-2}\,day^{-1}]$. It is shown that by increasing the volume of the reactor, the production of microalgae increases. Otherwise, in [9], it is shown that by increasing the culture depth, the photosynthetic light integration is reduced, and therefore, productivity decreases. This study will be included in the model in future versions to improve its behavior. It can also be observed how the curve keeps the maximum productivity for more time along the day for the case of a lower culture depth. As shown in this example, with this tool, it is possible to study which is the optimum culture depth for a given strain and for each season of the year in order to maximize the system productivity.

Strain selection

Two different strains are simulated as commented above, *Scenedesmus almeriensis* and *Nannochloropsis gaditana*. The values of the characteristic parameters are shown in Table 4.1 [7, 15]. The simulation conditions are the same for both strains. The analysis is done in spring and with an On/Off daily controller, where the pH set-point is set to 8. The results can be seen in Figure 4.21. At the top of the figure, the different biological configurations of both strains are set. Below, the graphical results are given, which are very similar for both cases. However, the numerical results provide very interesting information for each strain. It can be observed that there is a great difference between CO_2 consumption, $34.1\,[L\,day^{-1}]$ and $50.21\,[L\,day^{-1}]$, respectively. With the *Scenedesmus almeriensis* the average productivity along the day is $P_b = 18.89\,[g_{biomass}\,m^{-2}\,day^{-1}]$, but with the *Nannochloropsis gaditana* is $P_b = 9.48\,[g_{biomass}\,m^{-2}\,day^{-1}]$. So, it can be concluded that the best strain for this location and conditions would be the *Scenedesmus almeriensis*.

In the tool, other strains can be simulated in order to find which one is appropriate for any location and see how it grows for any season of the year.
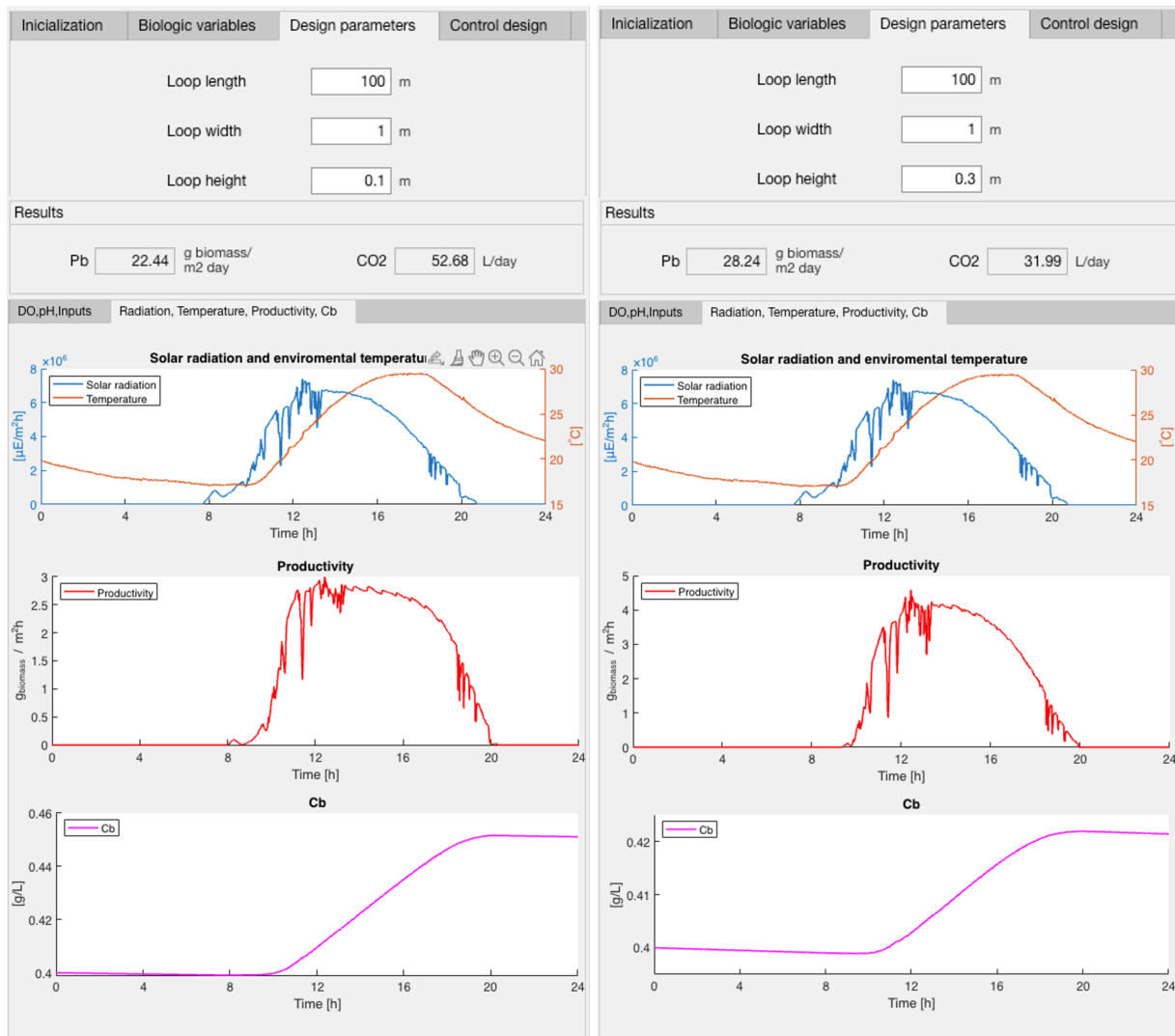
(a) Open loop simulation. Height 0.1m.

(b) Open loop simulation. Height 0.3m.

Figure 4.20. Graphical results changing the system height.

Control strategies

Another advantage of this simulation tool is to evaluate different control schemes to maintain the pH and the dissolved oxygen at a desired value. Traditionally, raceway reactors are operated by On/Off controllers during the daytime, but different studies have shown that other types of controllers, such as PI, are much more efficient [112]. Therefore, in this example, an On/Off controller for the pH during the day is compared with a PI controller with an anti-windup scheme [1]. Both simulations are run under the same conditions, in summer and with a pH set-point value of 7.5. For the PI control case, a low-order linear model is identified as shown in Equation (4.2), in which parameters are static gain $K_u = -1.74$, time constant $T_u = 3390\,[s]$ and time delay $L_u = 100\,[s]$. Lambda tuning rule (Section 2.1.1) has been selected to tune the PI controller, with a closed-loop time constant of $\lambda = 0.2T_u$. Thus, the resulting PI controller parameters are $K_p = -0.78$ and $\tau_i = 3390\,[s]$.

Figure 4.22 shows both simulations. It can be seen how the pH oscillates around the set-point, especially for the On/Off control with an important oscillatory behavior. With respect to the

115
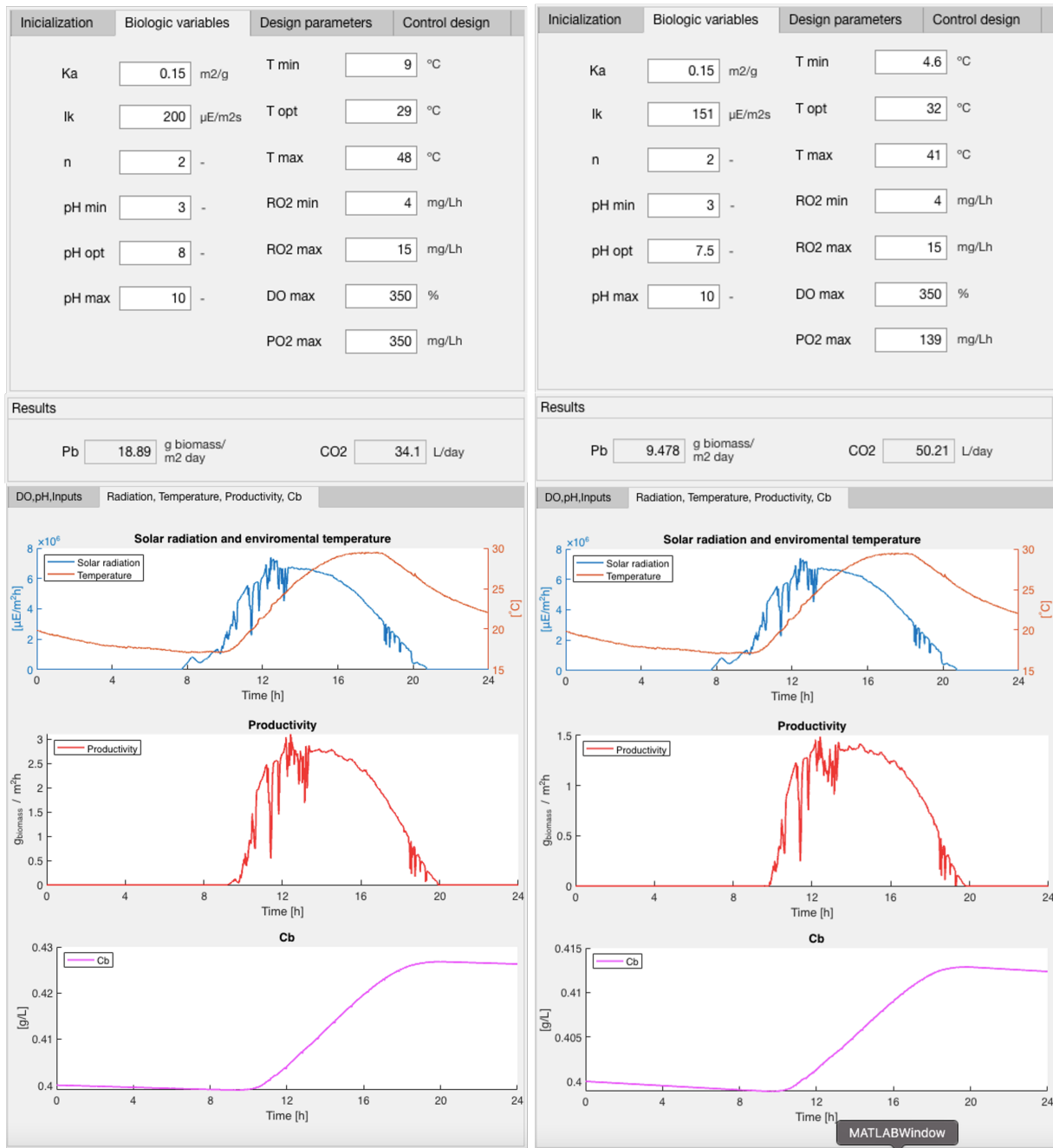
(a) Scenedesmus almeriensis results.

(b) Nannochloropsis gaditana results.

Figure 4.21. Strain change graphical results.

control effort, the On/Off controller provides a more aggressive control signal as expected. This is also observed in the CO_2 consumption, which is $90.69\,[L\,day^{-1}]$ and $23.65\,[L\,day^{-1}]$, for the On/Off and PI control, respectively. In the case of biomass productivity, both control approaches give similar results, being $P_b = 27.32\,[g_{biomass}\,m^{-2}\,day^{-1}]$ for On/Off control and $P_b = 25.44\,[g_{biomass}\,m^{-2}\,day^{-1}]$ for PI controller. The reason is that in spite of the oscillations, the pH value is kept very close to the optimum of 7.5. Thus, these results show how the PI control is more efficient than the On/Off control and highlight the importance of choosing a control strategy looking for a trade-off between performance and control effort (CO_2 injections).
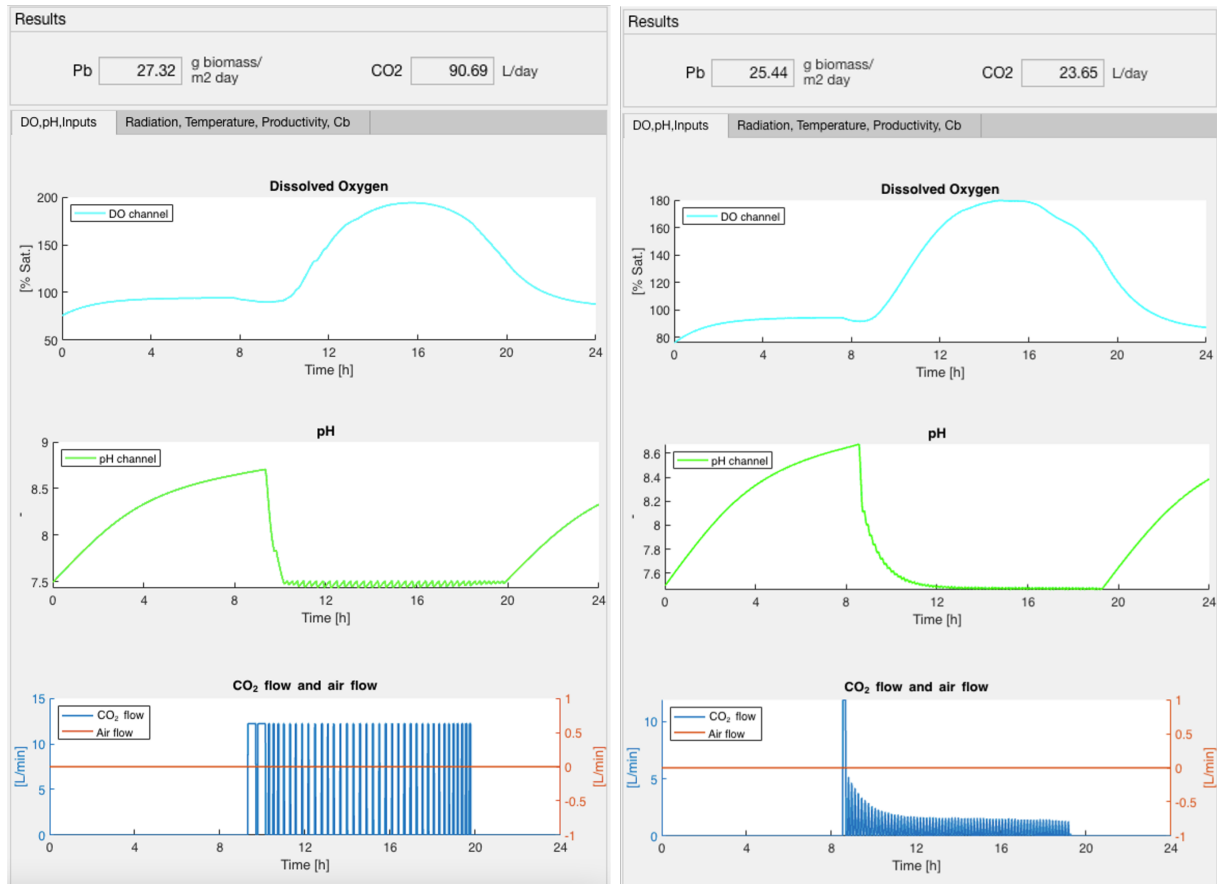
(a) On Off control. (b) PI control.

Figure 4.22. Graphical results for control strategies.

Conclusions

This contribution presents a novel software tool to simulate the performance of microalgae cultivation in raceway photobioreactors. It allows the user to evaluate these complex systems in a very simple way, helping to study, for example, the feasibility of its implementation at an industrial scale. The tool provides different functionalities, such as the possibility of modifying the biological variables of the model to use any strain. The reactor design parameters are also editable, letting to simulate the process using different reactors parameter values and test which configuration is the more adequate. The four seasons of the year are available to analyze the evolution of the microalgae under different weather conditions. Several control strategies can also be applied in order to analyze the performance improvements. This tool has been developed only for one location, Almería (Spain). Future versions will allow to configure any world location, introducing its representative climate parameters along the year. Furthermore, additional control strategies will be included, as well as the option to simulate several consecutive days when necessary.

This contribution has been published in a scientific journal article in *"Computers & Chemical Engineering"* journal, Q2 in the Journal Citation Report (JCR) [63].

4.2   Greenhouse

The main objective of greenhouses is to increment the economic benefits of the farmer looking for a balance between the cost of obtaining the optimal climate conditions for crop growth and the fulfillment of the regulations on agriculture and the environment, which are often based on obtaining a product suitable for human consumption, avoiding pollution and minimizing the impact on the environment. The automatic control strategies allow farmers to meet these objectives.

The microclimate provided by a greenhouse allows to obtain crop production in seasons that otherwise would not be possible. Furthermore, crop growth needs suitable environmental conditions to maximize its production. So, it is important to keep climatic variables inside the greenhouse in optimal conditions, in special temperature and humidity variables. This can be achieved using automatic control techniques. Therefore, over the years, the scientific community has been actively working on the modelling and control of greenhouses, trying to optimize the use of resources (water, energy, human worker hours,...) while minimizing the effects on the environment. A survey of the literature on greenhouse climate control is presented in [130]. In [75], for example, a hierarchical architecture is proposed where the lower layer consists of a linear quadratic optimal controller based on a linearized model for the greenhouse temperature. In this case, a heating system is used as a control actuator. However, the standard tool to obtain the necessary environmental conditions is the regulation of the natural ventilation of the greenhouse. In [141], a PSO-based MPC is used to control the temperature of a greenhouse using forced heating and natural ventilation. In [118], a Bayesian network is implemented to control the greenhouse indoor temperature, acting directly on the ventilation. This network learns from previous manual and automatic control actions for predefined set-points in the presence of changing outer environmental conditions. In [139], a two time-scales receding horizon optimal control system is implemented to control a greenhouse where forced heating, CO_2 supply, ventilation, and LED lighting are used to achieve the crop growth objectives. In [99], Symmetric Send-On-Delta event-based PI controllers are applied to control the inside air temperature using natural ventilation. In [33], the greenhouse temperature is controlled using natural ventilation by a nonlinear model predictive control strategy. The controller is based on a second-order Volterra series model obtained from experimental data. In [105], a multiobjective hierarchical control architecture is proposed for the greenhouse crop growth problem.

The control problem difficulty resides in the complexity of the greenhouse model. Its behavior is described in terms of a system of non-linear differential equations describing mass balances and energy transfer in the plastic cover, soil surface, one soil layer, and crop. These processes depend on the outside environmental conditions, greenhouse structure, type and state of the crop, and on the effect of the control actuators [111]. To deal with the greenhouse non-linearities, some classical methodologies based on non-linear control theory have been used for designing the controller. The feedback linearization control law [42] is a clear example. In [97], a model-based combined scheme of feedback with feedforward linearization is proposed to cope with the external disturbances, taking the constraints on the actuators into account to define feasible set-points. A PI feedback controller is used to cope with the uncertainty of the process but in an implicit form, without explicitly considering the uncertainty in the designing process. In [74], an adaptive feedback linearization-based predictive control is proposed in order to control the greenhouse temperature, and in [103], a non-linear model predictive control via feedback linearization of the greenhouse is proposed to control the inside temperature.

Nevertheless, classical feedback linearization control strategies rely on detailed system models, so they are not capable of coping with model uncertainties. Some robust control techniques have been applied to control greenhouses climate, considering the uncertainties of the model. In [87], robust control techniques based on the QFT are used to achieve adequate values of inside greenhouse temperature in spite of uncertainties and disturbances acting on the system.

In this contribution, the feedback linearization control technique (2.1.4) is used combined with QFT (2.1.6) in order to cope with the complex non-linear climate control problem. At first approach, feedback linearization control was implemented in the real system, taking the non-linear model for the greenhouse into account. The results obtained showed that the approximated greenhouse model using only feedback linearization was not a linear model with fixed parameters due to physical parameters variability and disturbances. Then a robust control technique complementing the feedback linearization law was used, aimed at achieving desired values of inside greenhouse temperature in spite of uncertainties and disturbances acting on the system. Experimental results are presented to validate the proposed control approach.

Feedback Linearization

In this section, the calculation of the controller is developed, combining feedback linearization and QFT control techniques. Due to the strong non-linearity and complexity of the system, FL is used first to simplify the controller design. So, a linearized FOPDT model of the plant can be obtained from the combination of FL with the greenhouse nonlinear model. Afterwards, this linear FOPDT model is calibrated by making tests on the real plant, where the FL non-linear block is placed in series with the greenhouse. Notice that due to the modelling errors and variability of the process disturbances, an uncertain FOPDT model is obtained. Then, for this reason, QFT is used to design a robust controller to control the combination of FL and the greenhouse. Figure 4.23 shows the control scheme implemented in the real system, and that will be described in detail in this section.
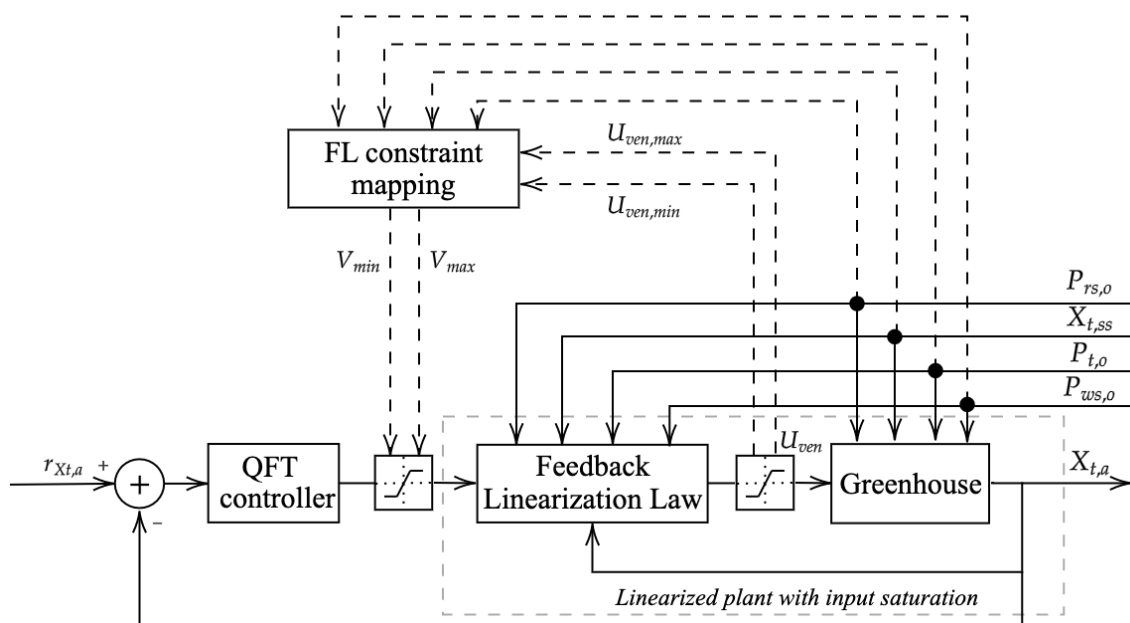

Figure 4.23. Feedback linearization and QFT control scheme for greenhouse temperature control problem.

In order to deal with the nonlinearities of the model, the feedback linearization technique is used. The main idea behind this technique [42] is the treatment of nonlinear systems as if they were linear by means of algebraic transformations and feedback [67]. Equation (2.58) can be rewritten as follows:

$$C_{sh,a}C_{den,a}\frac{C_{vol,a}}{C_{area,ss}}\frac{dX_{t,a}(t)}{dt} + (C_{cnv,ss-a} + C_{cnd-cnv,a-e} - C_{evap,2}ET)X_{t,a}(t) =$$

$$C_{aoc,a}V_{toc,cu}P_{rs,e}(t) + C_{cnv,ss-a}X_{t,ss}(t) + C_{cnd-cnv,a-e}P_{t,e}(t) - \frac{C_{den,a}C_{sh,a}}{C_{area,ss}}\phi_v(t) - C_{evap,1}ET$$

$$(4.11)$$

Then, this model is transformed into canonical form Equation (4.12) using functions g and b which depend on system disturbances, $\varrho = (P_{rs,e}, X_{t,ss}, P_{t,e}, ET)$ (references to t variable have been deleted in equations in order to obtain more compact expressions):

$$\begin{aligned} \dot{x} &= g(x, \varrho) + b(x, \varrho) \cdot v \\ y &= h(x) \end{aligned} \qquad (4.12)$$

where

$$x = X_{t,a} \qquad (4.13)$$

$$g(x, \varrho) = -\frac{C_{area,ss} \cdot (C_{cnv,ss-a} + C_{cnd-cnv,a-e} - C_{evap,2}ET) \cdot x}{C_{sh,a}C_{den,a}C_{vol,a}} \qquad (4.14)$$

$$b(x, \varrho) = \frac{C_{area,ss}}{C_{sh,a}C_{den,a}C_{vol,a}} \qquad (4.15)$$

$$\begin{aligned} v &= C_{aoc,a}V_{toc,cu}P_{rs,e} + C_{cnv,ss-a}X_{t,ss} + C_{cnd-cnv,a-e}P_{t,e} - \\ &\quad - \frac{C_{den,a}C_{sh,a}}{C_{area,ss}}\phi_v - C_{evap,1}ET \end{aligned} \qquad (4.16)$$

$$h(x) = x \qquad (4.17)$$

Then, the following first-order input-output relationship is found:

$$\begin{aligned} A\dot{\psi}(t) + B\psi(t) &= v(t) \\ \eta(t) &= \psi(t) \end{aligned} \qquad (4.18)$$

where $\psi = x = X_{t,a}$ and

$$\begin{aligned} A &= C_{sh,a}C_{den,a}\frac{C_{vol,a}}{C_{area,ss}} \\ B &= (C_{cnv,ss-a} + C_{cnd-cnv,a-e} - C_{evap,2}ET) \end{aligned}$$

So, FL makes it possible to use a linear controller to regulate the inside temperature $X_{t,a}$ by means of the virtual control signal $v(t)$ and according to (4.18). Then, once the virtual control signal is calculated, the real control signal U_{ven} is computed according to Equation (4.16).

To account for the actuator saturation (the window opening is limited between 0º and 45º), a standard anti-reset wind-up mechanism [1] has been implemented. Since anti-windup must be applied to the virtual signal, window opening limits are transformed into virtual signal limits using the inverse transformation of Equation (4.16). Thus, in this case, the limits on the virtual control signal ($v_{min}(t)$ and $v_{max}(t)$) (see Figure 4.23) are computed from Equations (2.60), (2.61) and (4.16). The maximum value of $v(t)$ is obtained when the variable U_{ven} has its minimum value, while the minimum value of $v(t)$ corresponds to the maximum value of U_{ven}, taking into account that U_{ven} varies between 0º and 45º.

In order to identify the characteristic parameters for the linear model, the FL block was implemented at the real plant input, and several open-loop step inputs were applied to the virtual control signal, $v(t)$. The open-loop tests were performed around noon and for 15 days with many different disturbance profiles. Figure 4.24 shows an example of four open-loop tests where different profiles of solar radiation and wind speed are observed. Figure 4.25 represents the first of these days. As it can be seen from the figure, an overdamped response was observed as expected, and thus a FOPDT model was used to capture the process dynamics relating to the greenhouse inside temperature, $X_{ta}(t)$, with respect to the virtual control signal, $v(t)$. Figure 4.25 shows also a validation of the FOPDT model obtained for this day. Therefore, different FOPDT models were obtained for all 15 open-loop tests, and it was observed that the FOPDT model parameters vary within a certain range, which results in the following uncertain model:

$$P(s) \in \mathcal{P} = \left\{ \frac{X_{t,a}(s)}{V(s)} = \frac{K_u}{T_u s + 1} e^{-L_u s}, \text{ with} \right. \tag{4.19}$$

$$\left. K_u \in [0.0021, 0.0084]^o C/\%, \ T_u \in [9, 32] min, \ L_u \in [2, 7] min \right\}$$

Notice that this variation in the linear model parameters is because of the complexity of the process and the modelling error coming from the coefficients in the nonlinear model from Equation (2.58). So, this uncertain model is used in the following section to design a robust PI controller for the control system.

QFT-Based PI Controller

Due to the uncertainty in the system observed in the previous section, a robust control technique must be used. QFT methodology [45] is chosen for this purpose. The first step in QFT is to choose performance and stability specifications. Notice that the final control scheme is given by Figure 4.23.

Considering the uncertain model given by Equation (4.19), and according to the magnitude of the time constant and the delay, the low-frequency range is of interest in this case. So, $\Omega = \{0.0001, 0.005, 0.01, 0.1\}$ rad/s is selected as the design frequencies set. A specification of phase margin greater or equal to 45º for all plants is considered. Due to the nature of the system, the main objective to take into account is the regulation problem. So, the following specification for input disturbances rejection is considered:

$$\left| \frac{P(j\omega)}{1 + C(j\omega)P(j\omega)} \right| \leq \left| \frac{K_{dr} j\omega}{(T_{dr} j\omega + 1)_r^n} \right| \forall \omega \in \Omega \tag{4.20}$$
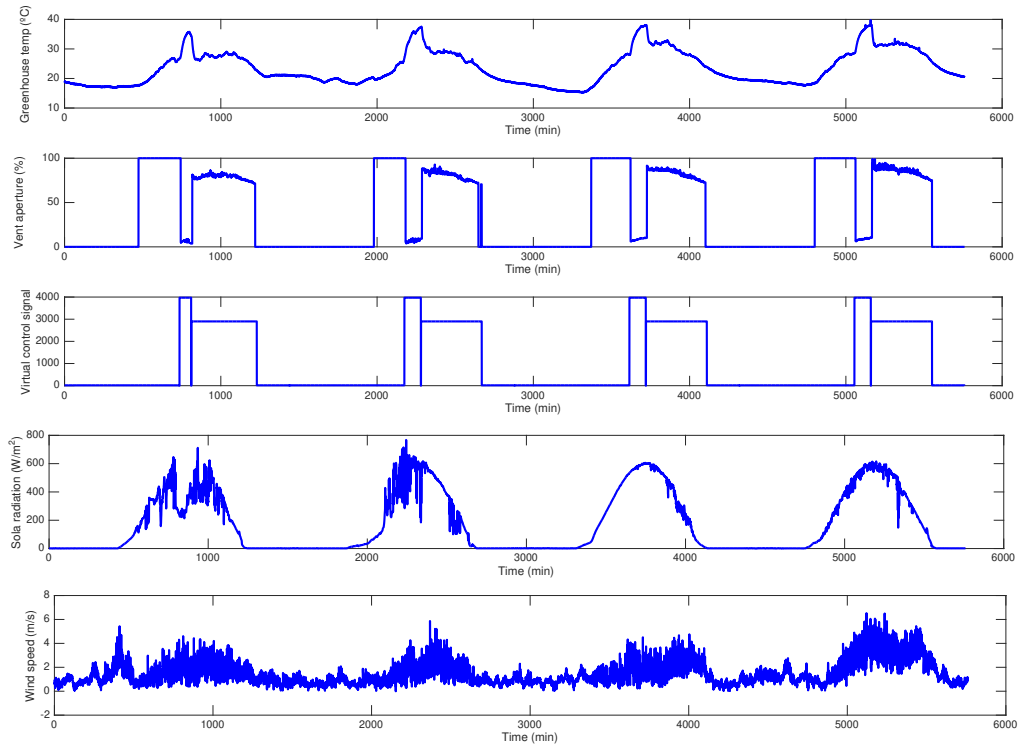
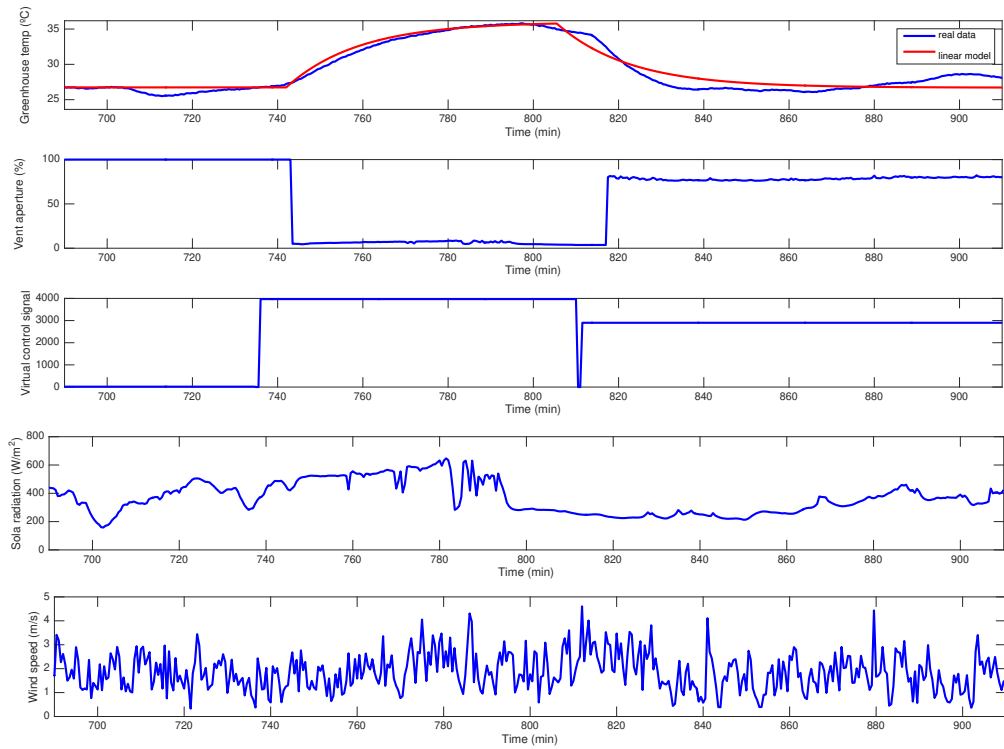Figure 4.24. Open-loop tests with the feedback linearization block for 4 days.

Figure 4.25. Greenhouse model validation.

where $T_{dr} = (0.95/n_r)T_{ol}$, with $K_{dr} = 9$, $n_r = 2$ and $T_{ol} = 9$ min. The parameter T_{ol} is chosen as the open loop time constant for the slowest plant. The nominal plant chosen for design is given by $K_u^0 = 0.0021$ ℃/%, $T_u^0 = 32$ min, and $L_u^0 = 2$ min.

In order to proceed with the design of the controller, the value sets or templates [10], which describe the system uncertainty in the Nichols Chart, are computed from Equation (4.19), and the design frequencies set Ω, resulting in the representation showed in the Figure 4.26.

Using the algorithm in [86], the performance and stability boundaries are computed as shown in Figure 4.27. Then, the nominal open loop transfer function is shaped to fulfill the required specifications [20]. Based on the resulting boundaries, a PI controller can be tuned to satisfy the specifications, resulting in the PI controller given by (4.21). Figure 4.27 shows the nominal open loop transfer function fulfilling all boundaries for frequencies in Ω.

$$C(s) = \frac{0.14(s/0.0007 + 1)}{s} \tag{4.21}$$
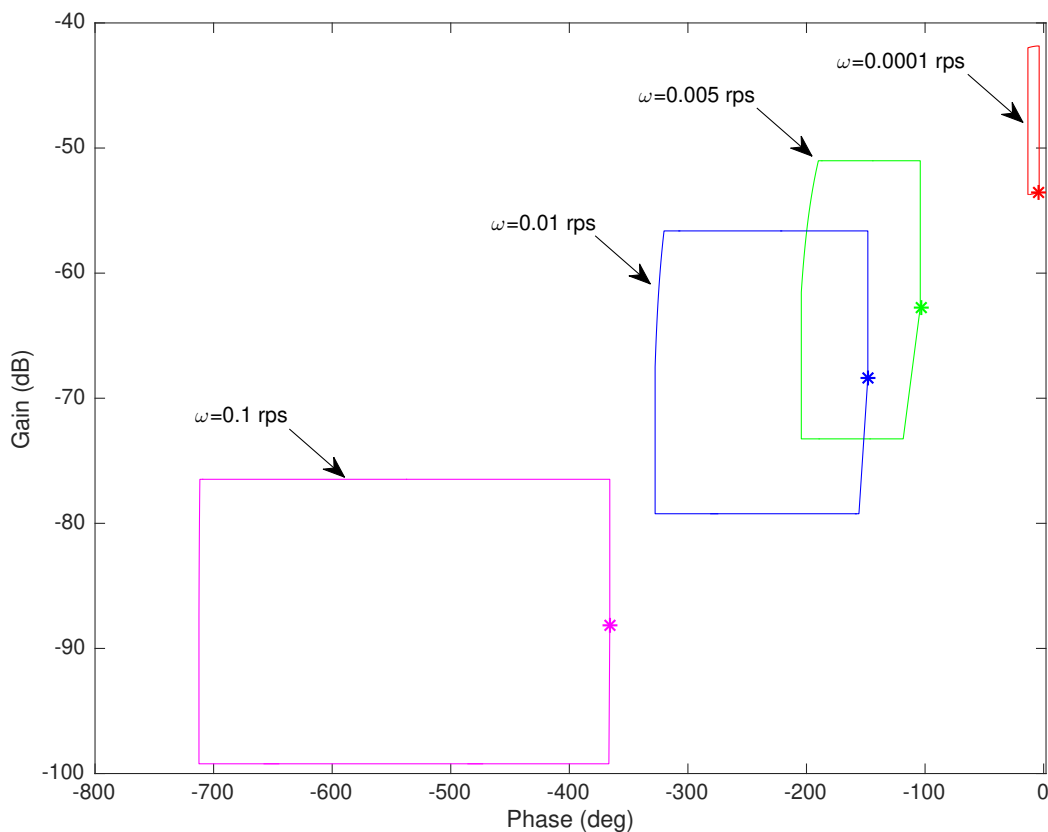
Figure 4.26. Templates for frequencies in Ω.

Figures 4.28 and 4.29 show the validation for the designed PI controller. All the specifications are satisfied.

As commented above, regarding the saturation problem, an anti-windup approach was used for the resulting PI controller, where the constraints in the vents were mapped to constraints in the virtual control signal.
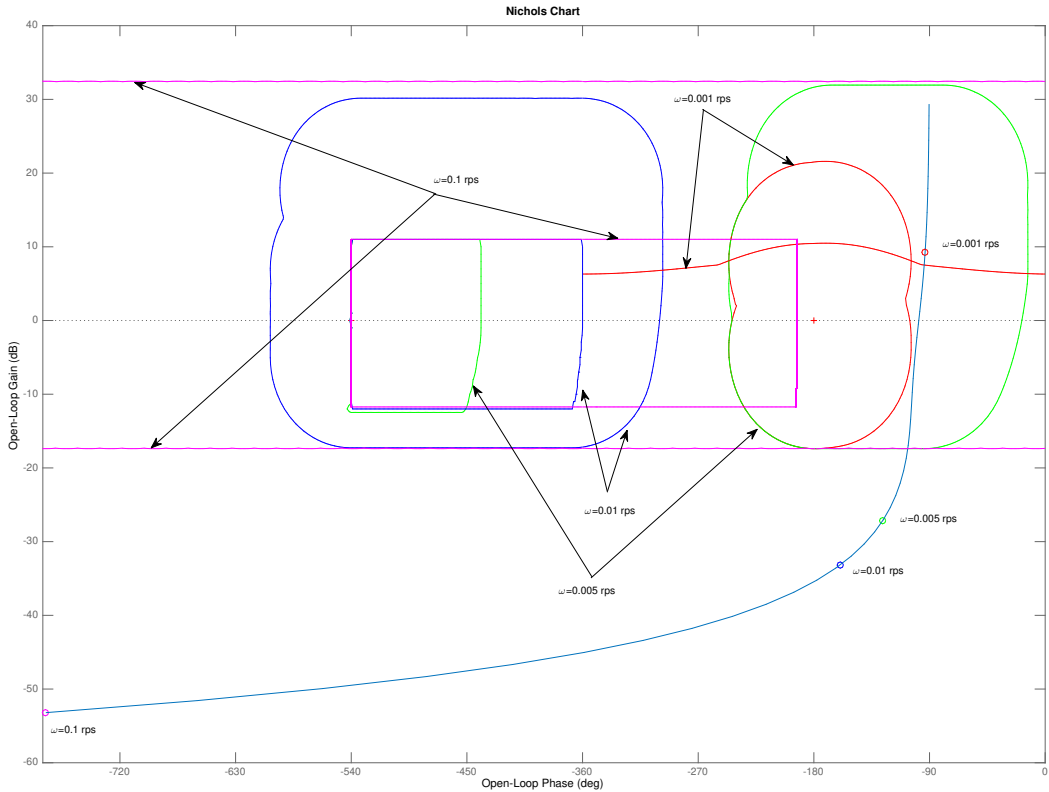
Figure 4.27. Stability and disturbances rejection bounds, and nominal open loop shaping.

Figure 4.28. Validation for stability specification (Phase Margin of 45 degrees).

Figure 4.29. Validation for input disturbances rejection specification.

Experimental Results

In this section, the results of performance at the real facilities are shown and discussed. Figures 4.30-4.32 show three different experimental tests for different weather and operating point conditions. The control signal, U_{ven}, is expressed in percentage for a clear understanding. Furthermore, in these experiments, diff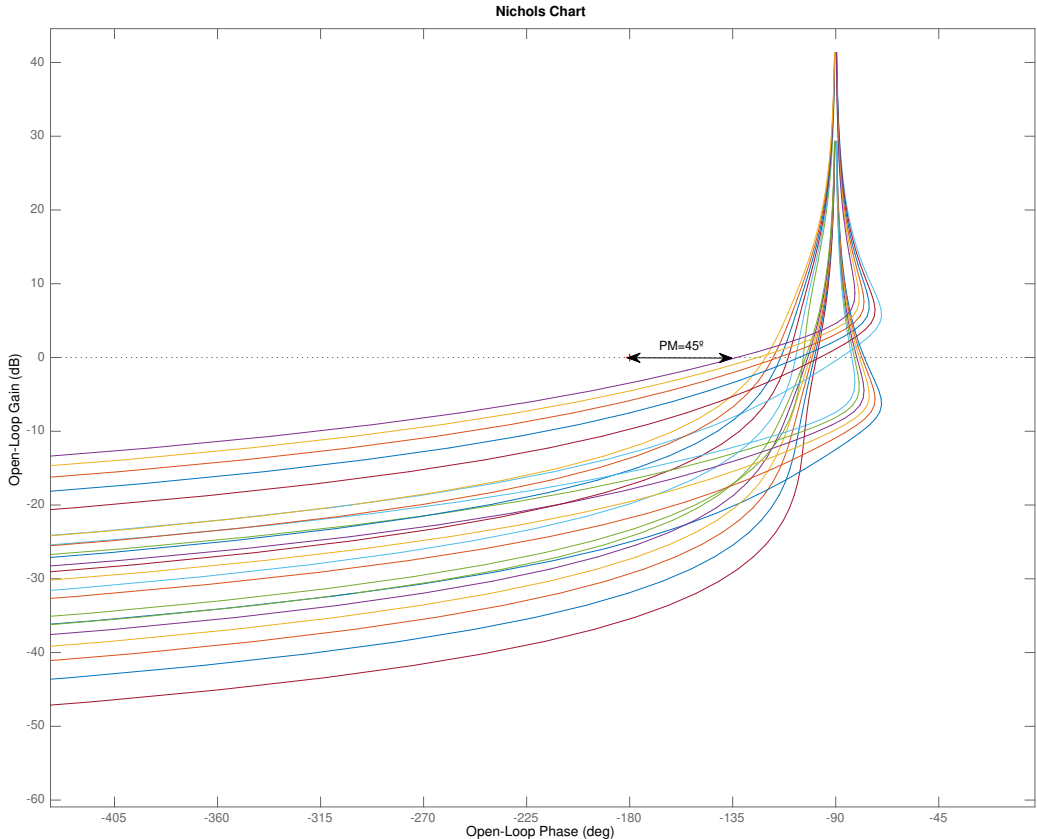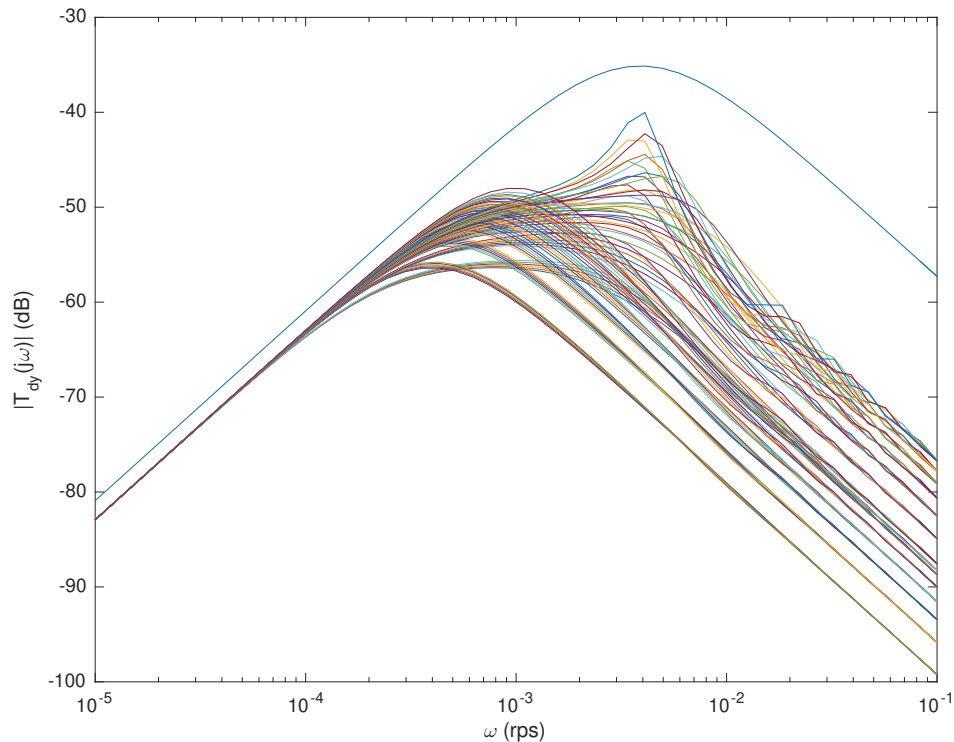erent set-point profiles are given to analyze the response of the proposed control approach. Figures 4.30a and 4.30b show the results for a cloudy day with important variations in the wind speed. As observed from Figure 4.30a, different step changes were performed for the inside temperature in order to show how the proposed control approach is able to follow the reference in spite of the disturbances variations. Moreover, from this figure, it is also observed that the virtual control signal is changing continuously to provide an adequate vent aperture in order to compensate for the disturbance variations. Notice that the main changes on the virtual control signal are mainly due to solar radiation variations, as observed in time instants 115, 155, and 285 min. On the other hand, the virtual control signal presents a high variability due to the wind speed disturbance. However, this variability is compensated by the feedback linearization, and thus it does not appear on the vent aperture.

Figures 4.31a and 4.31b show a second example for a clear day, but with a constant wind speed of around 4 m/s. Figure 4.31a shows how both the virtual control signal and the vent aperture from the robust PI controller and the feedback linearization block, respectively, softly vary in this case to keep the inside temperature close to the proposed reference. The higher changes in the ventilation control signal occur exactly where the changes in the temperature reference are applied. In the rest of the experiment, the ventilation aperture varies slowly due to soft variations in the system disturbances. However, it can be observed that from the time instant 875 to the end of the experiment, the virtual control signal starts to increase to compensate for the continuous decrease in solar radiation. On the other hand, again, the variability in the wind speed is translated to the virtual control signal but not to the ventilation aperture.
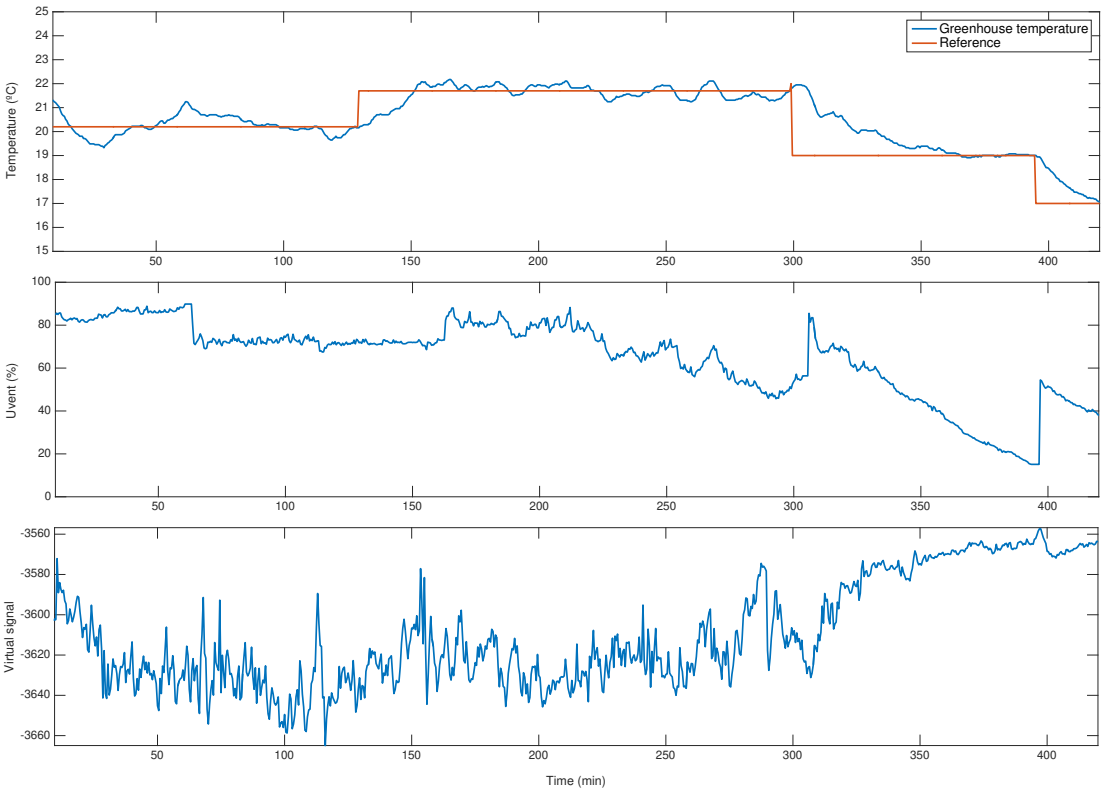
(a) Process output and the control signals.
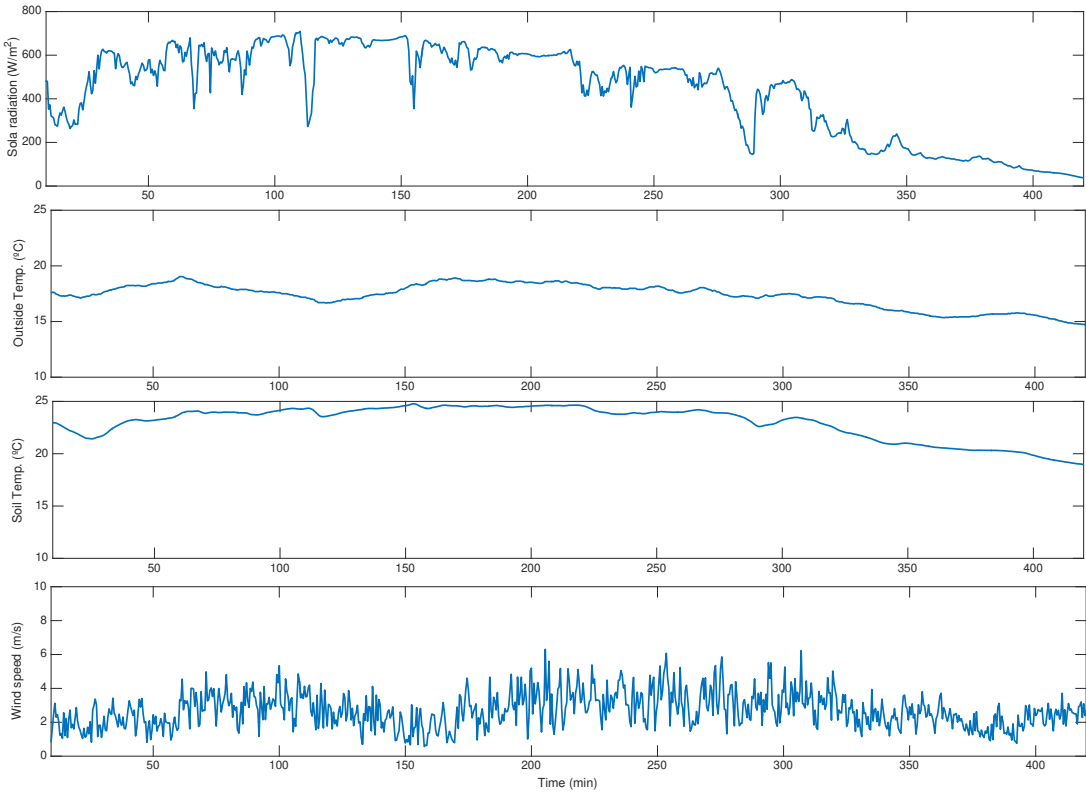
(b) Process disturbances: solar radiation, outside temperature, soil temperature, and wind speed.

Figure 4.30. Control results for test 1.

(a) Process output and the control signals

(b) Process disturbances: solar radiation, outside temperature, soil temperature, and wind speed.

Figure 4.31. Control results for test 2.
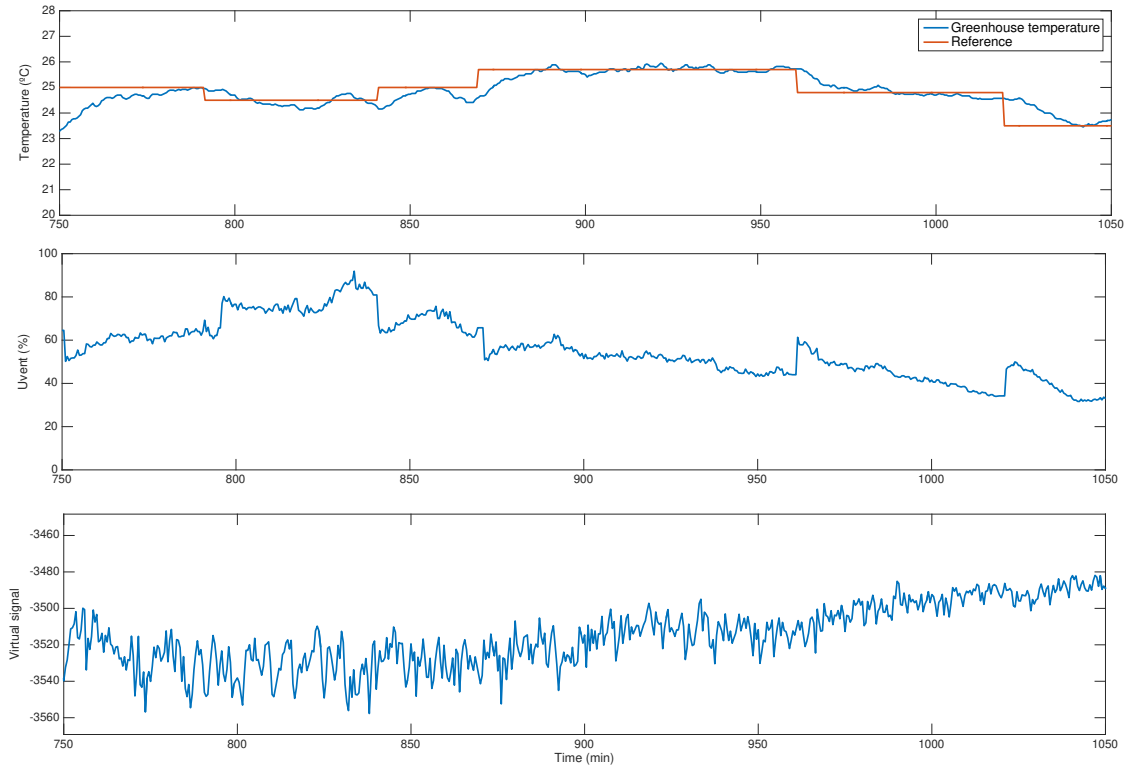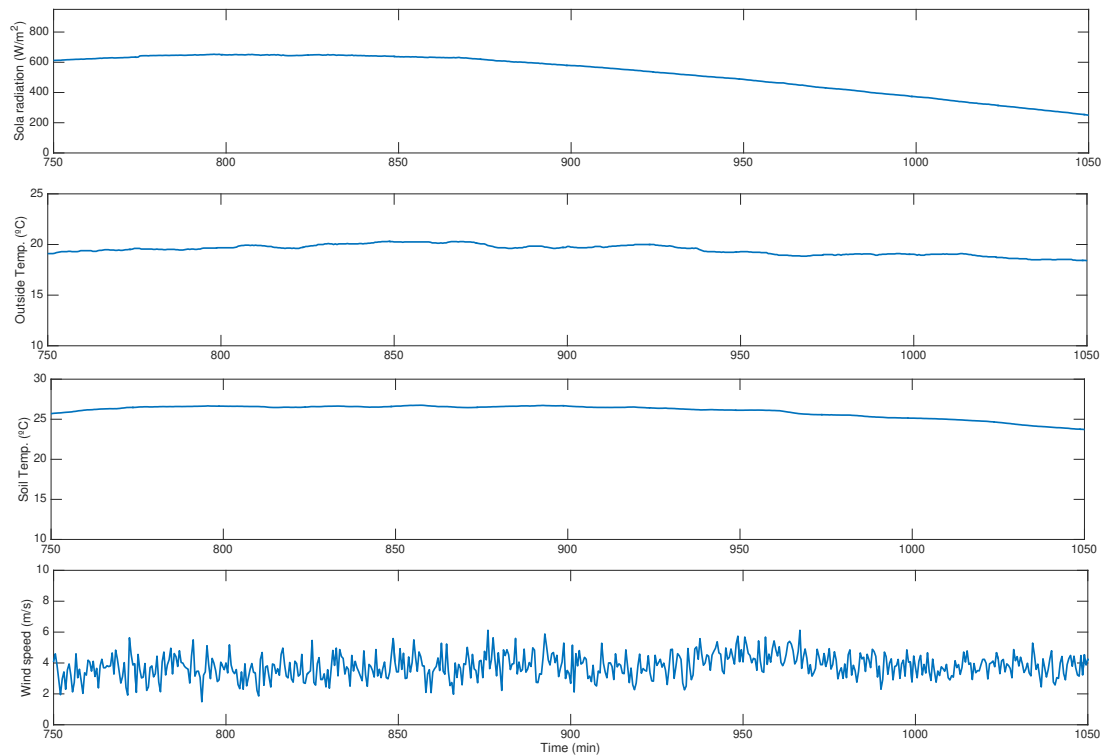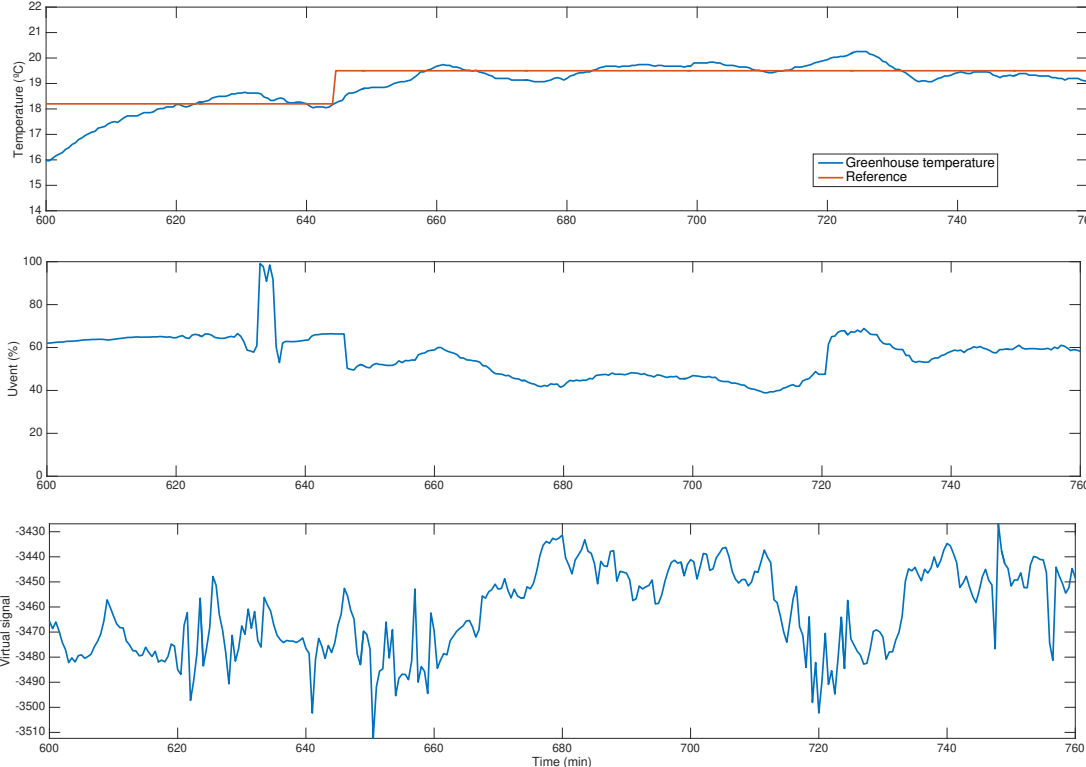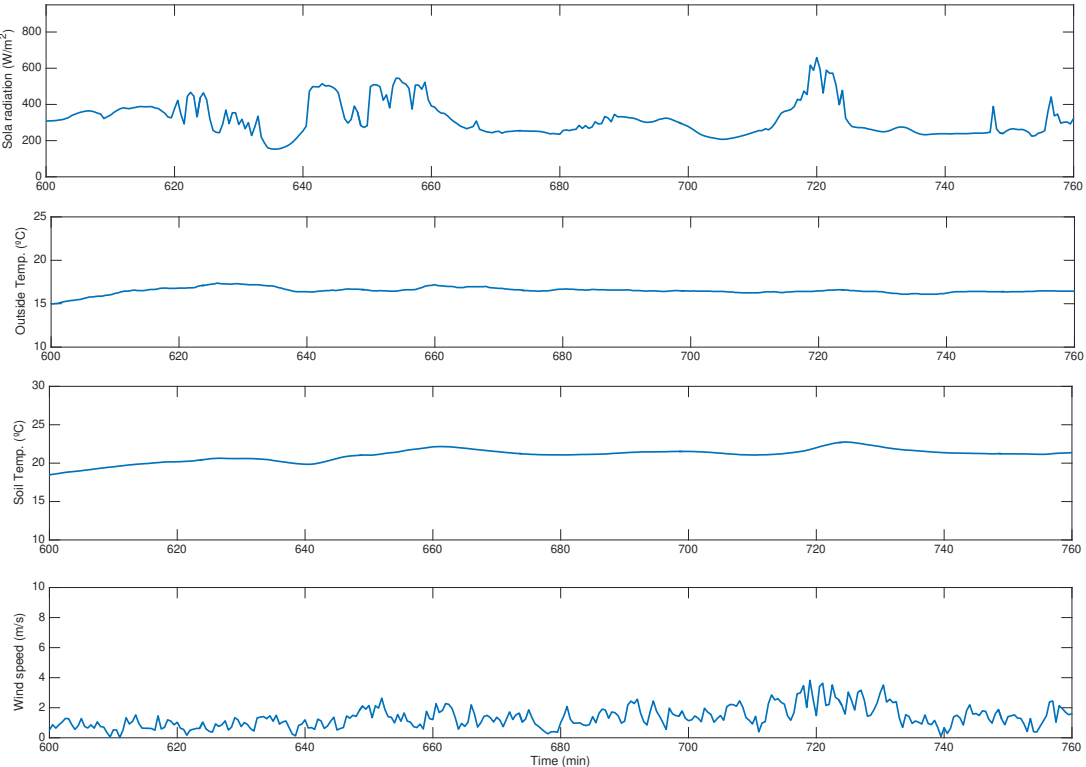
(a) Process output and the control signals

(b) Process disturbances: solar radiation, outside temperature, soil temperature, and wind speed.

Figure 4.32. Control results for test 3.

Figures 4.32a and 4.32b show a third example of a cloudy day with separated and intermittent passing clouds. In this case, a slow wind speed was observed, and for this reason, now the virtual control signal does not have too much variability. Figure 4.32a shows the control results where it can be seen how the virtual control signal and the vent aperture strongly vary around time instants $t = 620$ min and $t = 740$ min to compensate for the strong radiation changes. Thus, it is again observed how the proposed control approach attenuates the effect of the disturbances on the ventilation aperture. This is an important advantage for the actuator lifetime.

So, it has been observed how the proposed control approach is able to cope with the non-linear behavior of the system and the process variability due to important changes in the operating point and process disturbances. The control scheme was able to keep the proposed set-point values providing promising results for the greenhouse inside temperature control problem.

Conclusions

This contribution has presented the combination of two control techniques in order to approach the diurnal greenhouse climate control problem. First, a feedback linearization control strategy has been implemented and validated in the plant. Despite canceling the non-linearities of the model, discrepancies from the real system were observed being captured as parametric uncertainty. Then, a PI controller was designed using QFT and evaluated in the real system. The proposed control approach was tested on different days with different weather and operating conditions. The control system was able to reach the proposed setpoint changes in spite of the changes in the disturbances and in the operating points.

This research work has been published in a scientific journal article in the *"IEEE Access"* journal, which is recognized as a Q1 journal in the Journal Citation Report (JCR) [62].

4.3 TCLab

This section presents the real implementation of the proposed control approach described in Section 3.2 on a thermal system, defined in Section 2.2.3.

The TCLab platform is a commercial product of APMonitor [5], whose structure and appearance are shown in Figure 2.18, constituting an excellent testing field for multivariable control strategies at the industrial level (it can be observed that the actuators and sensors it incorporates are also illustrative of those used in chemical and industrial environments in general). As described in Section 2.2.3, the model consists of two transistors (actuators) that dissipate heat by passing an electric current through them, whose intensity is regulated by the Arduino board. It also has two thermistors (sensors) that vary their electrical resistance based on the temperature at which they are located. So, by measuring the voltage drop produced by a known current, it is possible to determine the temperature. Each thermistor is attached to one of the transistors using thermochromic adhesive, ensuring direct heat transmission between the actuator and the sensor. The adhesive is black and turns pink as the assembly heats up. A red LED is also used on the board to indicate if either of the transistors exceeds 40 ^{o}C.

Arduino can be directly used as a controller if its microcontroller is programmed for that purpose or the application is promoted by its manufacturer. Arduino can serve as an interface between the physical system and a computer control system. This is made possible by libraries that enable communication between Arduino and software such as Python or Matlab$^®$.

Note that the platform consists of a pair of sensors and actuators implies that it is a multi-variable system from a control perspective. However, for applying the contribution defined in Section 3.2 on it, a single transistor has been used, making it a single-variable system, and the second transistor is used only to introduce disturbances into the system, as can be seen in Figure 4.33. The heat transfer phenomena considered in the simplified model provided by the manufacturer for the platform are convection and radiation, as expressed in Equations (2.62) and (2.63).
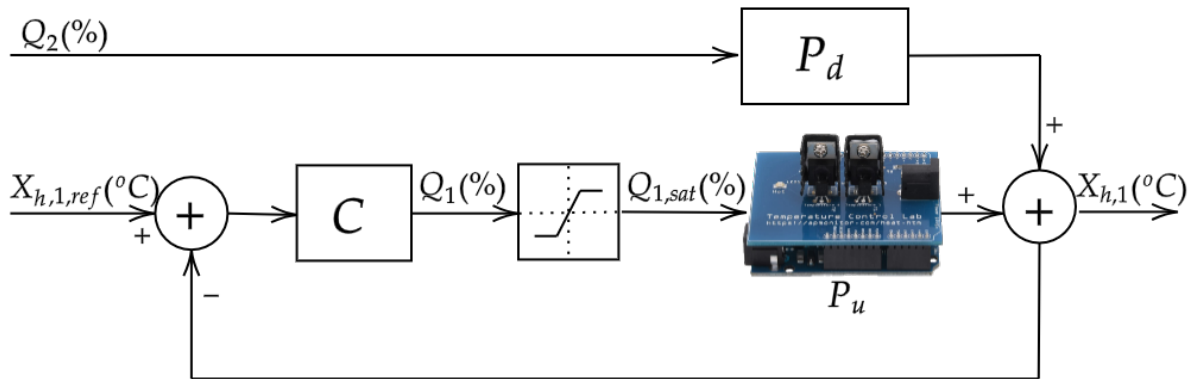
Figure 4.33. TCLab problem block diagram.

The suitability of TCLab as an experimental facility for automatic control has been studied in multiple recently published works in the scientific literature, as cited below. In [116], the advantages and disadvantages of using TCLab as a portable laboratory are presented, compared to other low-cost prototypes used for teaching purposes. In [89, 93], it is demonstrated that TCLab is an excellent platform for students in introductory control courses to identify models and test PID controllers. Furthermore, some studies have explored advanced control techniques with TCLab, such as feedforward control, cascade control [88], model predictive control [96], and sliding mode control (SMC) [43].

To get the output models regarding the input and the load disturbance, two tests on the real platform have been carried out. As can be seen in Figure 2.18, the controlled variable or process output is Temperature 1 ($^o C$), and the control signal is Heater 1 (%). The measurable disturbance is the Heater 2 (%), which affects the process output through the temperature effect from transistor 2. Heater 1 and 2 control signal limits are $0\% - 100\%$.

To obtain the linear models of the system around an operating point given by a Temperature 1 equal to $33\,^o C$ and a control signal of Heater 1 equal to $u_0 = 18.3\%$, several step-like open-loop tests have been carried out. Both process and disturbance models were approximated as first-order systems with delay, which parameters are:

$$P_u(s) = \frac{K_u}{T_u s + 1} e^{-L_u s} = \frac{0.51}{667 s + 1} e^{-12 s}, \quad P_d(s) = \frac{K_d}{T_d s + 1} e^{-L_d s} = \frac{0.08}{446 s + 1} e^{-76 s} \quad (4.22)$$

Figure 4.34 and 4.34 show the validation of the obtained models through a step test. Figure 4.34 depicts the validation of P_u, with a 5% step change in Heater 1. Figure 4.34 validate P_d, with a 20% step change in Heater 2.
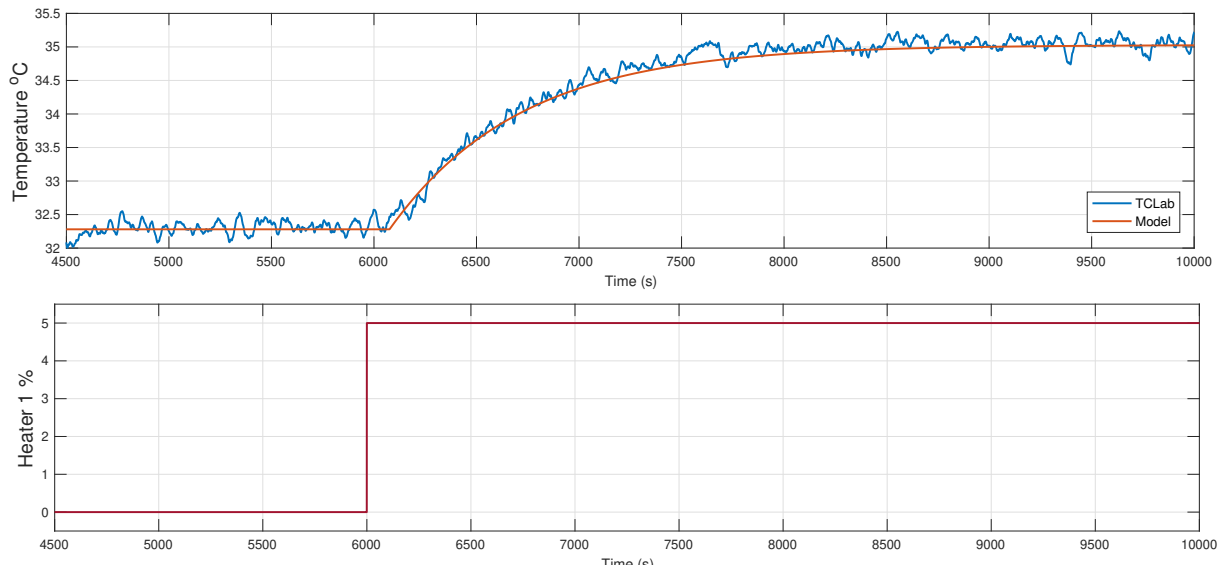
Figure 4.34. TCLab process model validation.
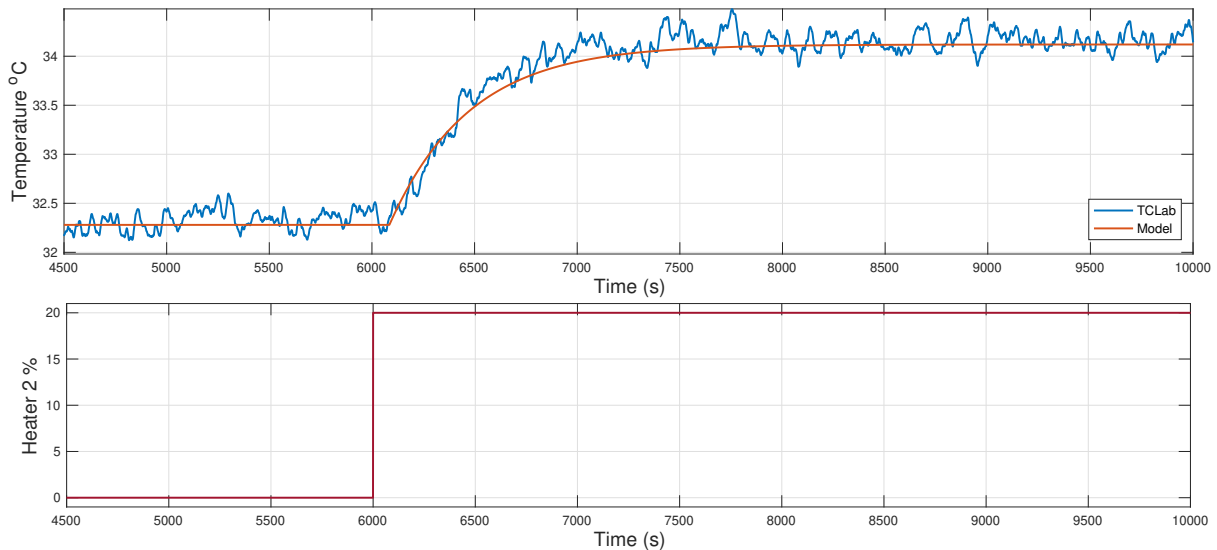
Figure 4.35. TCLab disturbance model validation.

Once the models are obtained, the solution presented in Section 3.2 is implemented. Two different closed-loop tests around the selected operating point are performed, one with the classic scheme and the other with the new solution. A step disturbance signal with an amplitude of $d = 100\%$ is applied using Heater 2 at time $t = 1040$ s. The PI controller was tuned with the Lambda method, with $\lambda = 0.6T_u$, and the anti-windup scheme is applied in both cases with $T_t = 0.3\tau_i$. The control signal peak and final value are $u_{peak} = -7.5$, $u_{final} = 2.31$, respectively. The parameters to apply the proposed solution are calculated from Equations (3.13), (3.14), and (3.16):

$$R_T = \frac{T_p}{T_z} = \frac{446}{667} = 0.67$$

$$R_S = \frac{u_{peak} - u_{limit}}{u_{peak} - u_0} = \frac{-7.5 - 0}{-7.5 - 18} = 0.3$$

131

$$\alpha = -1.6R_S - R_T + 1.9 = -1.6(0.3) - 0.67 + 1.9 = 0.7$$

First, a simulation test is done to validate the proposed solution, and subsequently, a test is done on the actual board. Figure 4.36 shows the simulation test, resulting in a value of $IAE_{norm} = 0.79$, and the maximum value of the integral has been reduced by $Imax_{norm} = 0.34$. The results confirm the validity of applying the solution in simulation, significantly improving system performance by 0.79. It can be seen how the new solution enhances disturbance rejection, leading to a notable 0.34 reduction in the maximum integral value. With the proposed solution successfully validated through simulation, the next step is implementing it in the real system.
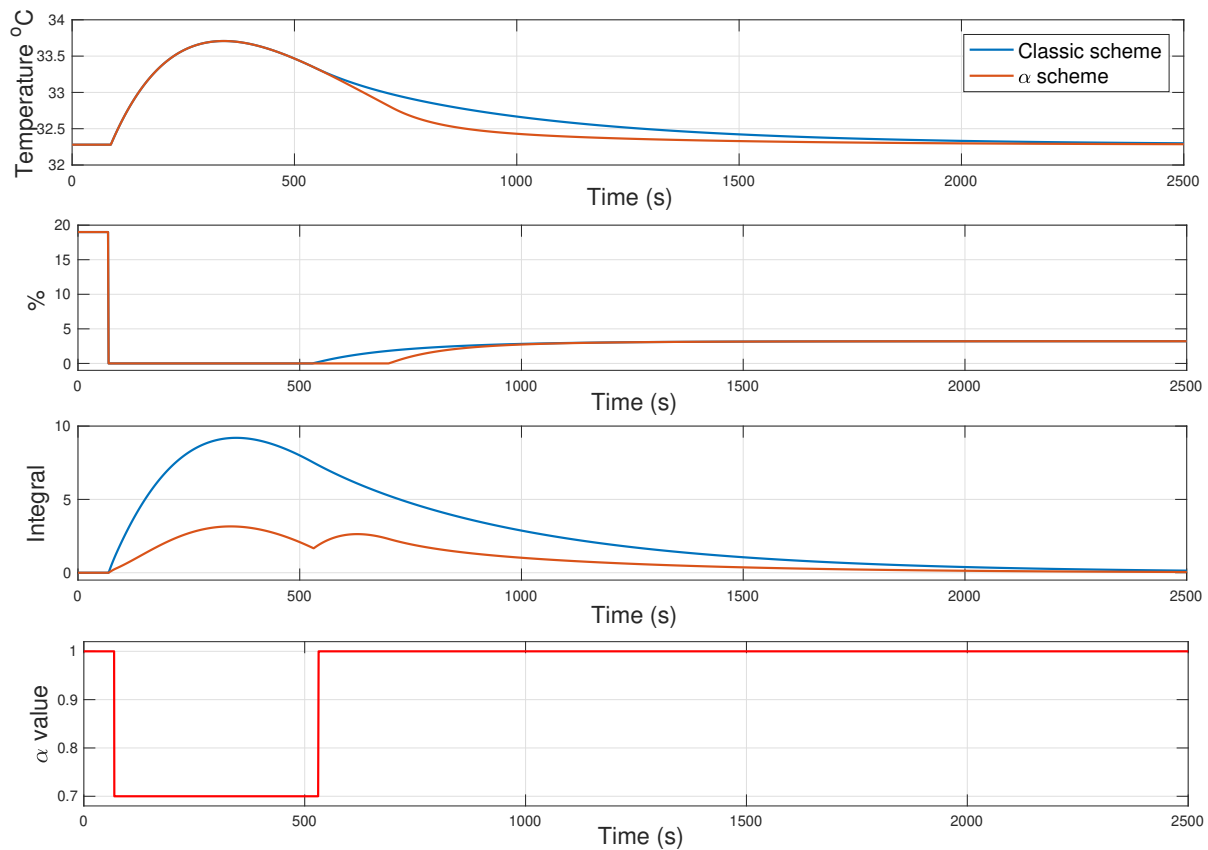
Figure 4.36. Simulation results.

Figure 4.37 shows the results obtained in the real temperature control platform. As happened in the simulation example presented before, it can be observed that the implementation of the new control scheme with $\alpha = 0.7$ significantly improves the performance of the process output, returning to the reference value faster than the classic scheme. The control signal remains at saturation for a longer time than the classic scheme owing to the change in the α value. The IAE value is considerably improved, resulting in a normalized IAE value of $IAE_{norm} = 0.64$. In addition, the maximum integral value is reduced by a factor $Imax_{norm} = 0.85$. This high value in the integral is due to the errors that can be observed in the experiment, and therefore, a value as low as in the simulation is not obtained.
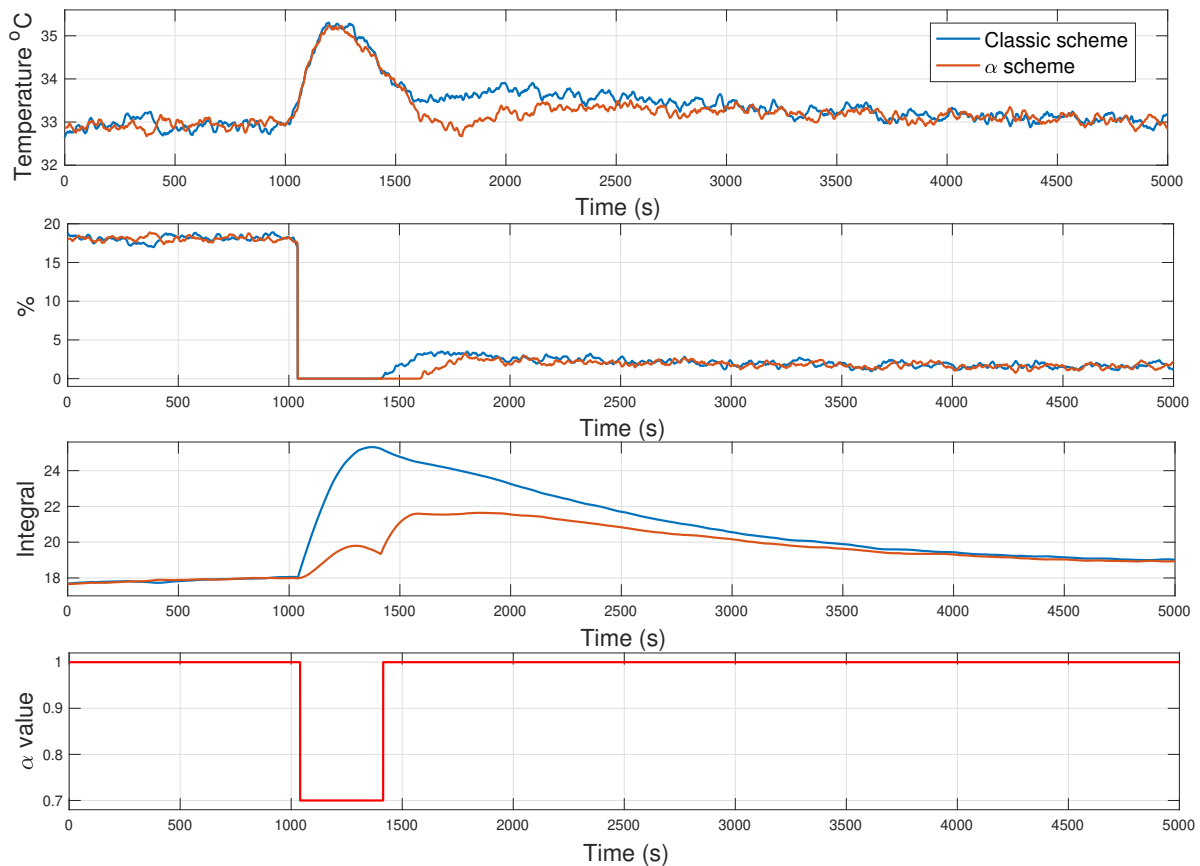
Figure 4.37. Experimental results in the TCLab.

Conclusions

Implementing the proposed solution from Section 3.2 in an experimental temperature control laboratory, the practical application of this approach is demonstrated. The experimental laboratory serves as a testbed for validating the effectiveness and performance of the proposed solution in a controlled environment. This validation process is essential to ensure that the solution's theoretical concepts can effectively translate into practical applications and other more complex plants, yielding similarly satisfactory results.

This contribution has resulted in a scientific journal article, indexed in the Journal Citation Report (JCR), and is currently under review [58].

5. Conclusions and Future Works

In this final chapter, the main ideas derived from the previous chapters serve to conclude this thesis. Section 5.1 discusses some of the topics covered within the thesis, analyzing their drawbacks and benefits, and reiterates the importance and originality of the contributions already presented in Chapter 1. Section 5.2 presents possible future research to continue working on these topics.

5.1 Conclusions

This thesis summarizes two major contributions. Firstly, classical control strategies have been studied, and modifications have been proposed for their improvement. Secondly, the validity of implementing these strategies and others in industrial systems, such as a microalgae reactor, a greenhouse, and a temperature control laboratory, have been demonstrated.

Regarding Chapter 3, three contributions are proposed. All of them share the common goal of studying different systems subjected to measurable disturbances. Section 3.1 has examined the classical feedforward control scheme in the presence of measured disturbances and uncertainties. A robust control design has been utilized. The analysis reveals that the introduction of a feedforward compensator alters the traditional QFT specification for the regulation problem. This leads to a solution that involves modifying the boundaries of the regulation problem within QFT to incorporate the presence of the feedforward controller. By adopting this approach, new boundaries are derived, and the QFT method is employed to design a robust PI controller that accounts for uncertainties. Furthermore, a new approach is proposed to deal with saturation problems when a measurable disturbance arrives. The effectiveness of the suggested approach in Section 3.2 for addressing the feedforward saturation problem and the selection of the gain-reduction factor α has been evaluated using simulations of various SISO process models. The simulation examples demonstrate that the strategy performs well and significantly enhances the response to load disturbances. Moreover, the solution has been implemented in a temperature control system, highlighting its applicability to real-world nonlinear systems, described in Section 4.3. The

results indicate substantial improvements in load disturbance rejection when saturation issues occur. In addition, the contribution from Section 3.3 addresses the challenge of measurable disturbances in cascade control systems by proposing a novel solution. Through rigorous simulation experiments, the study demonstrates the effectiveness of this straightforward and solid approach. This solution not only improves the process output but also reduces the overall control effort required.

All these contributions described above demonstrate that there is still research to be done in classical control, and many improvements for various problems need to be developed. Moreover, the continuous advancement of control theory and the application of classical control strategies in complex industrial systems highlight the ongoing relevance and potential for further exploration in this field. By studying deeper classical control techniques and identifying areas for enhancement, researchers and practitioners can continue to refine and optimize control systems, ultimately leading to more stable, efficient, and reliable operations in diverse applications. The study of classical control still needs to be continued, and there is ample opportunity for future research and innovation in this important discipline.

Regarding Chapter 4, three experimental plants, two of them industrial plants, have been studied. Firstly, the control of the main variables of a microalgae raceway photobioreactor has been investigated. Additionally, control strategies have been applied to address the climate control problem in a greenhouse. Lastly, one of the developed strategies has been implemented in a temperature control platform.

The proposed solution presented in Section 4.1.1 implements a GPC control algorithm in the simulation of a microalgae raceway photobioreactor. The results are highly satisfactory, as it is evident that the system output remains within the established limits while the control signal also adheres to its constraints. This ensures that productivity is maximized by maintaining the pH value close to the desired reference while simultaneously reducing the environmental impact through minimized CO_2 injection facilitated by this control strategy. The contribution presented in 4.1.2 introduces a robust control strategy with QFT for pH regulation in a raceway-type reactor. The experimental results demonstrate the remarkable performance of the controller across various operating points and under different testing conditions. The proposed control strategy effectively maintains the desired pH levels in the reactor, ensuring stability and accurate tracking of reference values. The robust nature of the controller enables it to handle uncertainties and disturbances, ensuring reliable operation even in the presence of external factors. These results emphasize the effectiveness and practicality of the developed control approach, making it a promising solution for pH control in raceway reactors and other similar industrial processes. The contribution of Section 4.1.3 introduces a new software tool for simulating the performance of microalgae cultivation in raceway photobioreactors. The tool offers a user-friendly interface that simplifies the evaluation of these complex systems, making it easier to study their feasibility for industrial-scale implementation. It provides various functionalities, including the ability to modify the biological variables of the model to accommodate different strains. Additionally, it allows users to adjust reactor design parameters, enabling simulations with different parameter values to determine the most suitable configuration. The tool covers all four seasons of the year, facilitating the analysis of microalgae evolution under different weather conditions. It also supports the application of various control strategies to assess performance improvements.

The contribution from Section 4.2 has presented the combination of two control techniques in order to approach the diurnal greenhouse climate control problem. First, a feedback linearization control strategy has been implemented and tested in the plant. Despite canceling the non-linearities of the model, discrepancies from the real system were observed being captured as parametric uncertainty. Then, a PI controller was designed using QFT and evaluated in the real system. The proposed control approach was tested on different days with different weather and operating conditions in a real greenhouse. The control system was able to reach the proposed setpoint changes in spite of the changes in the disturbances and in the operating points.

In Section 4.3, the solution proposed in Section 3.2 is implemented in an experimental laboratory to control the temperature, defined in detail in Section 2.2.3. First-order system models with time delay are obtained through open-loop tests for both the disturbance and the plant. Once these models are validated, a simulation test is conducted to verify the validity of the proposed method, followed by a test on the real platform. The results demonstrate how the new solution improves the rejection of the measurable disturbance by applying the proposed rule when the control signal is saturated. This showcases its applicability on an experimental scale.

These contributions provide valuable insights into the practical implementation of classical control strategies in industrial facilities. The successful operation of these strategies on complex systems highlights their robustness and effectiveness in controlling various processes and achieving desired outcomes. While simplifications may be necessary to facilitate implementation, the demonstrated correct functioning of these strategies underscores their reliability and suitability for industrial applications. These findings emphasize the importance and relevance of classical control techniques in addressing the control challenges faced by complex industrial systems. Furthermore, the importance of designing simulators for operator training and the implementation of control strategies for study purposes before applying them in the real plant is also demonstrated.

As stated in the previous Section 1.2, readers are referred to the contributions of this thesis with regard to the research objectives. These are recapped below and include the publications that support them:

- A robust QFT-based PI controller for a feedforward scheme has been studied [61].

- A practical solution to the saturation problem in feedforward control for measurable disturbance is presented and implemented in a temperature control lab [58].

- A new approach with double feedforward compensation for cascade control scheme is proposed [59].

- A linear model predictive control subject to constraints, is implemented in simulation to control the pH of a microalgae raceway photobioreactor [56].

- A robust control strategy is implemented in simulation and in real microalgae raceway photobioreactor [55].

- A computer-based tool to simulate raceway photobioreactors for design, operation, and control purposes is developed [63].

- Feedback linearization technique is implemented and combined with robust control to control the temperature of a real greenhouse [62].

5.2 Future Works

In terms of future work, the main perspectives include the issues discussed in this section.

As this thesis has demonstrated, there is still a significant amount of research and problem-solving that needs to be done in the field of classical control strategies. Research works in this direction should continue. The contributions presented in this thesis serve as a first step for further exploration and development in this area. The identified limitations, challenges, and unresolved issues provide a clear motivation to continue working on classical control methods. This includes improving existing techniques and algorithms and exploring novel approaches to address specific control problems. By addressing these gaps, researchers can further enhance the effectiveness, efficiency, and applicability of classical control strategies in various domains. The potential for innovation and improvement in this field is extensive, and the quest for refining and optimizing classical control techniques remains an ongoing and inspiring work.

It is crucial to recognize the industrial utility of these advancements and to perform further testing and validation of these new solutions in different experimental plants. This evaluation will help to demonstrate their viability and effectiveness in industrial scenarios. These new contributions to control strategies can be implemented in practical applications, such as photobioreactors, greenhouses, solar furnaces, and various laboratory setups, such as height control in tanks or temperature control laboratories. This iterative process of testing and refining ensures that the developed solutions are not only theoretically demonstrated but also applicable to real industrial environments. The goal is to bridge the gap between theory and practice, making significant contributions to classical control strategies and benefiting industrial processes and systems. Thus, some possible future works include:

- Continue studying cascade control schemes and find solutions to problems such as control signal saturation in both loops.

- Continue studying the effect of disturbances on different classical control schemes and seek new solutions to improve the performance of the process when disturbances occur.

- Investigate how uncertainty affects different classical control schemes and propose solutions based on the design of robust controllers that consider this uncertainty.

- Apply all these developed strategies in different industrial plants accessible to the University of Almería, such as microalgae photobioreactors, greenhouses, solar furnaces, a four-tank height control laboratory, or a temperature control laboratory.

Bibliography

[1] Åström, K.J., Hägglund, T., 2006. Advanced PID control. ISA - The Instrumentation, Systems and Automation Society.

[2] Abramovitch, D.Y.D., 2023. Daniel Y.(Danny) Abramovitch [People in Control]. IEEE Control Systems Magazine 43, 21–24.

[3] Acién, F.G., Fernández-Sevilla, J.M., Molina-Grima, E., 2017. Microalgae: The basis of mankind sustainability. Case Study of Innovative Projects-Successful Real Cases; Llamas, B., Ed , 123–140.

[4] Adam, E.J., Marchetti, J.L., 2004. Designing and tuning robust feedforward controllers. Computers & Chemical Engineering 28, 1899–1911.

[5] APMonitor, 2016. Temperature Control Lab. [Online] Available at: `http://apmonitor.com/pdc/index.php/Main/ArduinoTemperatureControl` (Accessed: 17 December 2021).

[6] Åström, K.J., 1999. Automatic control—the hidden technology, in: Advances in Control: highlights of ECC'99, Springer. pp. 1–28.

[7] Barceló-Villalobos, M., Gómez, C., Sánchez Zurano, A., García, L.A., Maldonado, S.E., Peña, J., Acién, F.G., 2019a. Variations of culture parameters in a pilot-scale thin-layer reactor and their influence on the performance of scenedesmus almeriensis culture. Bioresource Technology Reports 6, 190–197.

[8] Barceló-Villalobos, M., Hoyo, Á., Rodríguez-Miranda, E., Guzmán, J.L., Acién, F.G., 2022. A new control strategy to improve the mass transfer capacity and reduce air injection costs in raceway reactors. New Biotechnology 70, 49–56.

[9] Barceló-Villalobos, M., Fernández-del Olmo, P., Guzmán, J.L., Fernández-Sevilla, J.M., Acién, F.G., 2019b. Evaluation of photosynthetic light integration by microalgae in a pilot-scale raceway reactor. Bioresource technology 280, 404–411.

139

Bibliography

[10] Barmish, B.R., 1988. New tools for robustness analysis, in: Proceeding of the 27th Conference on Decision and Control, IEEE.

[11] Bauer, M., Horch, A., Xie, L., Jelali, M., Thornhill, N., 2016. The current state of control loop performance monitoring–a survey of application in industry. Journal of Process Control 38, 1–10.

[12] Bennett, S., 1996. A brief history of Automatic Control. IEEE Control Systems Magazine 16, 17–25.

[13] Berenguel, M., Rodríguez, F., Acién, F.G., García, J.L., 2004. Model predictive control of pH in tubular photobioreactors. Journal of Process Control 14, 377–387.

[14] Bernard, O., 2011. Hurdles and challenges for modelling and control of microalgae for CO2 mitigation and biofuel production. Journal of Process Control 21, 1378–1389.

[15] Bernard, O., Rémond, B., 2012. Validation of a simple model accounting for light and temperature effect on microalgal growth. Bioresource Technology 123, 520–527.

[16] Bertolini, M., Mezzogori, D., Neroni, M., Zammori, F., 2021. Machine learning for industrial applications: A comprehensive literature review. Expert Systems with Applications 175, 114820.

[17] Black, H.S., 1934. Stabilized feedback amplifiers. Bell System Technical Journal 13, 1–18.

[18] Blevins, T.L., 2012. PID advances in industrial control. IFAC Proceedings Volumes 45, 23–28.

[19] Borase, R.P., Maghade, D., Sondkar, S., Pawar, S., 2021. A review of PID control, tuning methods and applications. International Journal of Dynamics and Control 9, 818–827.

[20] Borghesani, C., Chait, Y., Yaniv, O., 1995. The quantitative feedback theory toolbox for matlab. The MathWorks Inc. USA .

[21] Bot, G.P., 1983. Greenhouse climate: from physical processes to a dynamic model. Wageningen University and Research.

[22] Camacho, E.F., Alba, C.B., 2013. Model predictive control. Springer science & business media.

[23] Clarke, D.W., Mohtadi, C., Tuffs, P.S., 1987. Generalized predictive control—Part I. The basic algorithm. Automatica 23, 137–148.

[24] Costache, T.A., Acién, F.G., Morales, M.M., Fernández-Sevilla, J.M., Stamatin, I., Molina-Grima, E., 2013. Comprehensive model of microalgae photosynthesis rate as a function of culture conditions in photobioreactors. Applied microbiology and biotechnology 97, 7627–7637.

[25] Dahlin, E., et al., 1968. Designing and tuning digital controllers. Instruments and Control systems 41, 77–83.

[26] Elso, J., Gil-Martínez, M., García-Sanz, M., 2013. Quantitative feedback–feedforward control for model matching and disturbance rejection. IET Control Theory & Applications 7, 894–900.

[27] Fernández, I., Acién, F.G., Berenguel, M., Guzmán, J.L., 2014. First principles model of a tubular photobioreactor for microalgal production. Industrial & Engineering Chemistry Research 53, 11121–11136.

[28] Fernández, I., Acién, F.G., Guzmán, J.L., Berenguel, M., Mendoza, J.L., 2016. Dynamic model of an industrial raceway reactor for microalgae production. Algal Research 17, 67–78.

[29] Fernández, I., Peña, J., Guzmán, J.L., Berenguel, M., Acién, F.G., 2010. Modelling and control issues of pH in tubular photobioreactors. IFAC Proceedings Volumes 43, 186–191.

[30] Fowler, J.W., Rose, O., 2004. Grand challenges in modeling and simulation of complex manufacturing systems. Simulation 80, 469–476.

[31] García-Sanz, M., 2017. Robust control engineering: practical QFT solutions. CRC press.

[32] González, J., Rodríguez-Miranda, E., Guzmán, J.L., Acién, F.G., Visioli, A., 2022. Optimización de temperatura en reactores raceway para la producción de microalgas mediante regulación de nivel. Revista Iberoamericana de Automática e Informática industrial 19, 164–173.

[33] Gruber, J.K., Guzmán, J.L., Rodríguez, F., Bordons, C., Berenguel, M., Sánchez, J.A., 2011. Nonlinear MPC based on a volterra series model for greenhouse temperature control using natural ventilation. Control Engineering Practice 19, 354–366.

[34] Guzmán, J.L., Acién, F.G., Berenguel, M., 2021. Modelling and control of microalgae production in industrial photobioreactors. Revista Iberoamericana de Automática e Informática Industrial 18, 1–18.

[35] Guzmán, J.L., García-Mañas, F., Hoyo, Á., Ramos-Teodoro, J., Donaire, J.G., 2022. Use of TCLab kits for control engineering curricula at the University of Almería. IFAC-PapersOnLine 55, 362–367.

[36] Guzmán, J.L., Hägglund, T., 2011. Simple tuning rules for feedforward compensators. Journal of Process Control 21, 92–102.

[37] Guzmán, J.L., Hägglund, T., 2021. Tuning rules for feedforward control from measurable disturbances combined with PID control: a review. International Journal of Control , 1–14.

[38] Guzmán, J.L., Hägglund, T., Veronesi, M., Visioli, A., 2015. Performance indices for feedforward control. Journal of Process Control 26, 26–34.

[39] Guzmán, J.L., Moreno, J.C., Berenguel, M., Rodríguez, F., Sánchez-Hermosilla, J., 2011. A frequency domain quantitative technique for robust control system design. Robust Control, Theory and Applications , 391–405.

[40] Guzmán, J.L., 2006. Interactive Control System Design. Ph.D. thesis. Universidad de Almería.

Bibliography

[41] Hast, M., Hägglund, T., 2014. Low-order feedforward controllers: Optimal performance and practical considerations. Journal of Process Control 24, 1462–1471.

[42] Henson, M.A., Seborg, D.E., 1997. Nonlinear process control. Prentice Hall PTR Upper Saddle River, New Jersey.

[43] Herrera, M., Camacho, O., Leiva, H., Smith, C., 2020. An approach of dynamic sliding mode control for chemical processes. Journal of Process Control 85, 112–120.

[44] Horowitz, I., 1988. Quantitative feedback theory (QFT), in: 1988 American Control Conference, IEEE. pp. 2032–2037.

[45] Horowitz, I., 1993. Quantitative Feedback Design Theory (QFT). QFT Publications, Boulder, Colorado.

[46] Hoyo, Á., 2019a. Contribuciones de control robusto para sistemas sometidos a perturbaciones, in: Proceedings of the II Annual Meeting of the PhD Programme in Informatics of the University of Almería, Almería, Spain. (in Spanish).

[47] Hoyo, Á., 2019b. Un simulador para la enseñanza de la producción de microalgas en fotobioreacotores raceway, in: En el camino de la investigación educativa: Encuentro de investigación del alumnado 2019 (EIDA 2019), Editorial University of Almería. pp. 63–65.

[48] Hoyo, Á., 2020. Contribuciones de control robusto para sistemas sometidos a perturbaciones, in: Proceedings of the III Annual Meeting of the PhD Programme in Informatics of the University of Almería, Almería, Spain. (in Spanish).

[49] Hoyo, Á., 2021. Contribuciones de control robusto para sistemas sometidos a perturbaciones, in: Proceedings of the IV Annual Meeting of the PhD Programme in Informatics of the University of Almería., Almería, Spain. (in Spanish).

[50] Hoyo, Á., 2022. Contribuciones de control robusto para sistemas sometidos a perturbaciones, in: Proceedings of the V Annual Meeting of the PhD Programme in Informatics of the University of Almería, Almería, Spain. (in Spanish).

[51] Hoyo, Á., 2023. Contribuciones de control robusto para sistemas sometidos a perturbaciones, in: Proceedings of the VI Annual Meeting of the PhD Programme in Informatics of the University of Almería, Almería, Spain. (in Spanish).

[52] Hoyo, Á., Guzmán, J.L., Acién, F.G., Moreno, J.C., 2019a. A graphical tool to simulate raceway photoreactors, in: 2nd IWA Conference on Algal Technologies for Wastewater Treatment and Resource Recovery. Valladolid, Spain.

[53] Hoyo, Á., Guzmán, J.L., Berenguel, M., 2018a. Use of the benchmark for PID control in engineering studies at the university of almería. IFAC-PapersOnLine 51, 456–461.

[54] Hoyo, Á., Guzmán, J.L., Moreno, J.C., 2018b. Control robusto de procesos industriales no lineales con compensación de perturbaciones, in: Proceedings of the XVI CEA Symposium on Control Engineering, Almería, Spain. (in Spanish).

[55] Hoyo, Á., Guzmán, J.L., Moreno, J.C., Baños, A., 2022a. Control robusto del pH en un fotobiorreactor raceway. Revista Iberoamericana de Automática e Informática industrial 19, 274–283.

[56] Hoyo, Á., Guzmán, J.L., Moreno, J.C., Berenguel, M., 2019b. Control predictivo lineal del pH en un fotobiorreactor raceway, in: XL Jornadas de Automática, Universida de da Coruña, Servizo de Publicacións. pp. 414–420.

[57] Hoyo, Á., Guzmán, J.L., Moreno, J.C., Berenguel, M., et al., 2017. Control robusto con QFT del pH en un fotobiorreactor raceway. Actas de las XXXVIII Jornadas de Automática .

[58] Hoyo, Á., Hägglund, T., Guzmán, J.L., Moreno, J.C., 2023a. A practical solution to the saturation problem in feedforward control for measurable disturbances. Control Engineering Practice. (Under review).

[59] Hoyo, Á., Hägglund, T., Guzmán, J.L., Moreno, J.C., 2023b. Double feedforward compensation for cascade control schemes. (Under review).

[60] Hoyo, Á., Mañas-Álvarez, F.J., Rodríguez-Miranda, E., Gil, J.D., Castilla, M., Guzmán, J.L., 2022b. Bringing automatics and robotics closer to pre-university students. IFAC-PapersOnLine 55, 85–90.

[61] Hoyo, Á., Moreno, J.C., Guzmán, J.L., Hägglund, T., 2018c. Robust QFT-based PI controller for a feedforward control scheme. IFAC-PapersOnLine 51, 262–267.

[62] Hoyo, Á., Moreno, J.C., Guzmán, J.L., Rodríguez, F., 2019c. Robust QFT-based feedback linearization controller of the greenhouse diurnal temperature using natural ventilation. IEEE Access 7, 64148–64161.

[63] Hoyo, Á., Rodríguez-Miranda, E., Guzmán, J.L., Acién, F.G., Berenguel, M., Moreno, J.C., 2022c. A computer-based tool to simulate raceway photobioreactors for design, operation and control purposes. Computers & Chemical Engineering 156, 107572.

[64] Ippoliti, D., Gómez, C., del Mar Morales-Amaral, M., Pistocchi, R., Fernández-Sevilla, J.M., Acién, F.G., 2016. Modeling of photosynthesis and respiration rate for isochrysis galbana (T-Iso) and its influence on the production of this strain. Bioresource Technology 203, 71–79.

[65] Isermann, R., 2011. Perspectives of automatic control. Control Engineering Practice 19, 1399–1407.

[66] Jebali, A., Acién, F.G., Gómez, C., Fernández-Sevilla, J.M., Mhiri, N., Karray, F., Dhouib, A., Molina-Grima, E., Sayadi, S., 2015. Selection of native tunisian microalgae for simultaneous wastewater treatment and biofuel production. Bioresource Technology 198, 424–430.

[67] de Jesús Rubio, J., 2018. Robust feedback linearization for nonlinear processes control. ISA Transactions 74, 155–164.

[68] Kaya, I., Tan, N., Atherton, D.P., 2007. Improved cascade control structure for enhanced performance. Journal of Process Control 17, 3–16.

[69] Krishnaswamy, P.R., Rangaiah, G.P., Jha, R.K., Deshpande, P.B., 1990. When to use cascade control. Industrial & Engineering Chemistry Research 29, 2163–2166.

Bibliography

[70] Le, Q., Miralles-Pechuán, L., Kulkarni, S., Su, J., Boydell, O., 2020. An overview of deep learning in industry. Data Analytics and AI , 65–98.

[71] Leal, M., 2019. Análisis y sintonía de esquemas de control en cascada .

[72] Leal, M., Hoyo, Á., Guzmán, J.L., Hägglund, T., 2021. Double back-calculation approach to deal with input saturation in cascade control problems, in: CONTROLO 2020: Proceedings of the 14th APCA International Conference on Automatic Control and Soft Computing, July 1-3, 2020, Bragança, Portugal, Springer. pp. 200–209.

[73] Lee, D., Logan, B.E., 2011. Biofuels-II: Algal Biofuels and Microbial Fuel Cells. Bioresource Technology 102.

[74] Lijun, C., Shangfeng, D., Meihui, L., Yaofeng, H., 2018a. Adaptive feedback linearization-based predictive control for greenhouse temperature. IFAC-PapersOnLine 51, 784–789.

[75] Lijun, C., Shangfeng, D., Yaofeng, H., Meihui, L., 2018b. Linear quadratic optimal control applied to the greenhouse temperature hierarchal system. IFAC-PapersOnLine 51, 712–717.

[76] Liu, C., Arnon, T., Lazarus, C., Strong, C., Barrett, C., Kochenderfer, M.J., et al., 2021. Algorithms for verifying deep neural networks. Foundations and Trends® in Optimization 4, 244–404.

[77] Liu, L., Tian, S., Xue, D., Zhang, T., Chen, Y., 2019. Industrial feedforward control technology: a review. Journal of Intelligent Manufacturing 30, 2819–2833.

[78] Liu, T., Gu, D., Zhang, W., 2005. Decoupling two-degree-of-freedom control strategy for cascade control systems. Journal of Process Control 15, 159–167.

[79] Maciejowski, J.M., Huzmezan, M., 2007. Predictive control, in: Robust Flight Control: A Design Challenge. Springer, pp. 125–134.

[80] Markaroglu, H., Guzelkaya, M., Eksin, I., Yesil, E., 2006. Tracking time adjustment in back calculation anti-windup scheme, in: Proceedings 20th European Conference on Modelling and Simulation.

[81] MathWorks, 2021. App designer Matlab. URL: `https://www.mathworks.com`.

[82] Meller, M., Kogan, B., Bryant, M., García, E., 2018. Model-based feedforward and cascade control of hydraulic mckibben muscles. Sensors and Actuators A: Physical 275, 88–98.

[83] Mendoza, J.L., Granados, M.R., De Godos, I., Acién, F.G., Molina-Grima, E., Banks, C., Heaven, S., 2013. Fluid-dynamic characterization of real-scale raceway reactors for microalgae production. Biomass and Bioenergy 54, 267–275.

[84] Molina-Grima, E., Camacho, F.G., Pérez, J.A.S., Fernández-Sevilla, J.M., Acién, F.G., Gomez, A.C., 1994. A mathematical model of microalgal growth in light-limited chemostat culture. Journal of Chemical Technology & Biotechnology: International Research in Process, Environmental AND Clean Technology 61, 167–173.

144

[85] Molina-Grima, E., Fernández-Sevilla, J.M., Pérez, J.A.S., Camacho, F.G., 1996. A study on simultaneous photolimitation and photoinhibition in dense microalgal cultures taking into account incident and averaged irradiances. Journal of Biotechnology 45, 59–69.

[86] Moreno, J.C., Baños, A., Berenguel, M., 2006. Improvements on the computation of boundaries in QFT. International Journal of Robust and Nonlinear Control 16, 575–597.

[87] Moreno, J.C., Berenguel, M., Rodríguez, F., Baños, A., 2002. Robust control of greenhouse climate exploiting measurable disturbances. IFAC Proceedings Volumes 35, 271–276.

[88] de Moura Oliveira, P.B., Hedengren, J.D., Boaventura-Cunha, J., 2020a. Bridging theory to practice: Feedforward and cascade control with TCLab Arduino kit, in: Portuguese Conference on Automatic Control, pp. 23–32.

[89] de Moura Oliveira, P.B., Hedengren, J.D., Rossiter, J.A., 2020b. Introducing digital controllers to undergraduate students using the TCLab Arduino kit. IFAC-PapersOnLine 53, 17524–17529. doi:`10.1016/j.ifacol.2020.12.2662`.

[90] Muresan, C.I., Ionescu, C.M., 2020. Generalization of the FOPDT model for identification and control purposes. Processes 8, 682.

[91] Nian, R., Liu, J., Huang, B., 2020. A review on reinforcement learning: Introduction and applications in industrial process control. Computers & Chemical Engineering 139, 106886.

[92] Nisenfeld, A.E., Miyasaki, R.K., 1973. Applications of feedforward control to distillation columns. Automatica 9, 319–327.

[93] Oliveira, P.M., Hedengren, J.D., 2019. An APMonitor temperature lab PID control experiment for undergraduate students, in: 2019 24th IEEE International Conference on Emerging Technologies and Factory Automation (ETFA), pp. 790–797. doi:`10.1109/ETFA.2019.8869247`.

[94] Oswald, W.J., Golueke, C.G., 1960a. Biological transformation of solar energy, in: Advances in Applied Microbiology. Elsevier. volume 2, pp. 223–262.

[95] Oswald, W.J., Golueke, C.G., 1960b. Biological transformation of solar energy. Advances in Applied Microbiology 2, 223–262.

[96] Park, J., Martin, R.A., Kelly, J.D., Hedengren, J.D., 2020. Benchmark temperature microcontroller for process dynamics and control. Computers & Chemical Engineering 135, 106736.

[97] Pasgianos, G., Arvanitis, K., Polycarpou, P., Sigrimis, N., 2003. A nonlinear feedback technique for greenhouse environmental control. Computers and Electronics in Agriculture 40, 153–177.

[98] Patle, D.S., Ahmad, Z., Rangaiah, G.P., 2014. Operator training simulators in the chemical industry: review, issues, and future directions. Reviews in Chemical Engineering 30, 199–216.

[99] Pawlowski, A., Beschi, M., Guzmán, J.L., Visioli, A., Berenguel, M., Dormido, S., 2016. Application of SSOD-PI and PI-SSOD event-based controllers to greenhouse climatic control. ISA Transactions 65, 525–536.

[100] Pawlowski, A., Fernández, I., Guzmán, J.L., Berenguel, M., Acién, F.G., Normey-Rico, J.E., 2014a. Event-based predictive control of pH in tubular photobioreactors. Computers & Chemical Engineering 65, 28–39.

[101] Pawlowski, A., Mendoza, J.L., Guzmán, J.L., Berenguel, M., Acién, F.G., Dormido, S., 2014b. Effective utilization of flue gases in raceway reactor with event-based pH control for microalgae culture. Bioresource Technology 170, 1–9.

[102] Pawlowski, A., Mendoza, J.L., Guzmán, J.L., Berenguel, M., Acién, F.G., Dormido, S., 2015. Selective pH and dissolved oxygen control strategy for a raceway reactor within an event-based approach. Control Engineering Practice 44, 209–218.

[103] Piñón, S., Peña, M., Soria, C., Kuchen, B., 2000. Nonlinear model predictive control via feedback linearization of a greenhouse. IFAC Proceedings Volumes 33, 191–196.

[104] Raja, G.L., Ali, A., 2017. Series cascade control: An outline survey, in: 2017 Indian Control Conference (ICC), IEEE. pp. 409–414.

[105] Ramírez-Arias, A., Rodríguez, F., Guzmán, J.L., Berenguel, M., 2012. Multiobjective hierarchical control architecture for greenhouse crop growth. Automatica 48, 490–498.

[106] Ribeiro, J.M., Santos, M.F., Carmo, M., Silva, M., 2017. Comparison of PID controller tuning methods: analytical/classical techniques versus optimization algorithms, in: 2017 18th international Carpathian control conference (ICCC), IEEE. pp. 533–538.

[107] Roca, L., 2009. Contribuciones al modelado y control de una planta de desalación solar. Ph.D. thesis. Universidad de Almería.

[108] de Rocquigny, E., Devictor, N., Tarantola, S., 2008. Uncertainty in industrial practice: a guide to quantitative uncertainty management. John Wiley & Sons.

[109] Rodríguez, C., Guzmán, J.L., Berenguel, M., Hägglund, T., 2013. Generalized feedforward tuning rules for non-realizable delay inversion. Journal of Process Control 23, 1241–1250.

[110] Rodríguez, C., Guzmán, J.L., Berenguel, M., Hägglund, T., 2014. Optimal feedforward compensators for systems with right-half plane zeros. Journal of Process Control 24, 368–374.

[111] Rodríguez, F., Berenguel, M., Guzmán, J.L., Ramírez-Arias, A., 2015. Modeling and control of greenhouse crop growth. Springer.

[112] Rodríguez-Miranda, E., Beschi, M., Guzmán, J.L., Berenguel, M., Visioli, A., 2019. Daytime/nighttime event-based PI control for the pH of a microalgae raceway reactor. Processes 7, 247.

[113] Rodríguez-Miranda, E., Guzmán, J.L., Acién, F.G., Berenguel, M., Visioli, A., 2021. Indirect regulation of temperature in raceway reactors by optimal management of culture depth. Biotechnology and Bioengineering 118, 1186–1198.
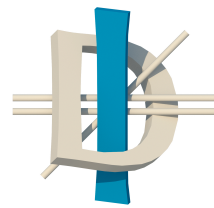
[114] Rodríguez Rubio, F., López, M., 1996. Control Adaptativo y Robusto. Universidad de Sevilla.

[115] Rossiter, J.A., 2003. Model-based predictive control: a practical approach. CRC press.

[116] Rossiter, J.A., Pope, S.A., Jones, B.L., Hedengren, J.D., 2019. Evaluation and demonstration of take home laboratory kit. IFAC-PapersOnLine 52, 56–61. doi:`10.1016/j.ifacol.2019.08.124`.

[117] Rundqwist, L., 1990. Anti-reset windup for PID controllers. IFAC Proceedings Volumes 23, 453–458.

[118] del Sagrado, J., Sanchez, J., Rodríguez, F., Berenguel, M., 2016. Bayesian networks for greenhouse temperature control. Journal of Applied Logic 17, 25–35.

[119] Sánchez Zurano, A., Gómez Serrano, C., Acién-Fernández, F.G., Fernández-Sevilla, J.M., Molina-Grima, E., 2021. Modeling of photosynthesis and respiration rate for microalgae–bacteria consortia. Biotechnology and Bioengineering 118, 952–962.

[120] Seborg, D., Edgar, T., Mellichamp, D., 1989. Process dynamics and control. Wiley. New York.

[121] Seborg, D.E., 1994. A perspective on advanced strategies for process control .

[122] Shinde, P.P., Shah, S., 2018. A review of machine learning and deep learning applications, in: 2018 Fourth international conference on computing communication control and automation (ICCUBEA), IEEE. pp. 1–6.

[123] Shinskey, F.G., 1996. Process control systems. Application, design, and tuning. 4th ed., McGraw-Hill. New York.

[124] Sierra, E., Acién, F.G., Fernández, J.M., García, J.L., González, C., Molina-Grima, E., 2008. Characterization of a flat plate photobioreactor for the production of microalgae. Chemical Engineering Journal 138, 136–147.

[125] Skogestad, S., 2003. Simple analytic rules for model reduction and PID controller tuning. Journal of Process Control 13, 291–309.

[126] Soroush, M., Muske, K.R., 2000. Analytical model predictive control, in: Nonlinear model predictive control, Springer. pp. 163–179.

[127] Sutton, R.S., Barto, A.G., 2018. Reinforcement learning: An introduction. MIT press.

[128] Tarbouriech, S., Turner, M., 2009. Anti-windup design: an overview of some recent advances and open problems. IET Control Theory & Applications 3, 1–19.

[129] Van Henten, E., Bontsema, J., 2009. Time-scale decomposition of an optimal control problem in greenhouse climate management. Control Engineering Practice 17, 88–96.

[130] Van Straten, G., van Willigenburg, G., van Henten, E., van Ooteghem, R., 2010. Optimal control of greenhouse cultivation. CRC press.

[131] Veronesi, M., Visioli, A., 2020. On the selection of lambda in lambda tuning for PI (D) controllers. IFAC-PapersOnLine 53, 4599–4604.

Bibliography

[132] Vilanova, R., Alcántara, S., Pedret, C., 2021. Sintonía de controladores PID: un enfoque analítico basado en el moldeo de la función de sensibilidad. Revista Iberoamericana de Automática e Informática industrial 18, 313–326.

[133] Vilanova, R., Arrieta, O., Ponsa, P., 2009. IMC based feedforward controller framework for disturbance attenuation on uncertain systems. ISA Transactions 48, 439–448.

[134] Vilanova, R., Visioli, A., 2012. PID control in the third millennium. Springer.

[135] Visioli, A., 2006. Practical PID control. Springer Science & Business Media.

[136] Visioli, A., 2012. Research trends for PID controllers. Acta Polytechnica 52.

[137] Weissman, J.C., Goebel, R.P., 1987. Design and analysis of pond systems for the purpose of producing fuels. Solar Energy Research Institute (SERI), Golden, Colorado. Grant number SERI/STR-231-2840 .

[138] Weng, C.K., Ray, A., 1997. Robust wide-range control of steam-electric power plants. IEEE Transactions on Control Systems Technology 5, 74–88.

[139] Xu, D., Du, S., van Willigenburg, L.G., 2018. Optimal control of chinese solar greenhouse cultivation. Biosystems Engineering 171, 205–219.

[140] Zhang, P., Yuan, M., Wang, H., 2008. Improvement of nitrogen removal and reduction of operating costs in an activated sludge process with feedforward–cascade control strategy. Biochemical Engineering Journal 41, 53–58.

[141] Zou, Q., Ji, J., Zhang, S., Shi, M., Luo, Y., 2010. Model predictive control based on particle swarm optimization of greenhouse climate for saving energy consumption, in: 2010 World Automation Congress, IEEE. pp. 123–128.

Science makes people reach selflessly for truth and objectivity.
It teaches people to accept reality, with wonder and admiration,
not to mention the deep awe and joy that the natural
order of things brings to the true scientist.

Lise Metiner

UNIVERSIDAD DE ALMERÍA